Upscaling of enzyme enhanced CO2 capture

Gladis, Arne Berthold

Publication date:
2017

Document Version
Publisher's PDF, also known as Version of record

Upscaling of enzyme enhanced CO_2 capture

Arne Berthold Gladis

PhD Thesis

April 2017

Center for Energy Resources Engineering

Department of Chemical and Biochemical Engineering

Technical University of Denmark

Kongens Lyngby

Denmark

Preface

This thesis is submitted to the Technical University of Denmark (DTU) as a partial fulfillment of the requirements for obtaining the degree of Doctor of Philosophy (PhD). This work has been carried out at the Center for Energy Resources Engineering (CERE), Department of Chemical and Biochemical Engineering, Technical University of Denmark (DTU) under the supervision of Associate professor Nicolas von Solms as main supervisor and Professor John M Woodley as well as Associate Professor Philip L Fosbøl as co-supervisors.

The present thesis "Upscaling of enzyme enhanced CO_2 capture" represents a contribution European research project for INnovaTive Enzymes and polyionic-liquids based membRAnes as CO_2 Capture Technology (INTERACT).

The project was financially supported by the European Commission under the Seventh Framework under grant agreement n° 608535 and by the Technical University of Denmark.

Arne Berthold Gladis
Kongens Lyngby, Denmark
28. April, 2017

Acknowledgements

I would like to thank everyone who supported me on the way to complete this thesis. My very special thanks belong to my supervisors Nicolas von Solms, John M Woodley and Philip L Fosbøl, who all contributed significantly in their own way to this thesis.

Nicolas, I am very grateful, that you gave me the opportunity to come to DTU and provided me with freedom and trust to conduct my PhD in my way while still supporting me whenever I needed help or advice. John, many thanks for your perceptive comments and advices throughout my study and providing me with the viewpoint from the biochemical engineering side, this helped me really a lot. Philip, your fascination and drive in CO_2 capture motivated me throughout the PhD and I really appreciated the many successful student collaborations that significantly contributed to this thesis, thank you very much.

The experimental work in this study would not have been possible without the support of all technicians and affiliated staff members. I thank, Zacharias Tecle, Povl Valdemar Andersen and Thoung Dang for their continuous support in the laboratory by keeping the setups running. Ingelis Larsen and Ann Marie Andersson, I am very grateful for your assistance in the pilot hall. Lars Kiørboe, thank you very much for your support and advice on how to upgrade the pilot plant absorber. I appreciate the great work on all the changes on the different setups by DTU Kemiteknik's workshop.

I would like to thank the INTERACT consortium, firstly for providing funds and secondly for all the nice and fruitful meetings we had all over Europe. It has always been a pleasure to collaborate with so many nice people with different scientific backgrounds on such an interesting topic.

Thanks to all coworkers at CERE and KT that made the daily life at DTU enjoyable and pleasant be it eating cakes or discussing the importance of science at the coffee machine. Special thanks to Louise, Patricia and Hanne for solving all non-science related problems at DTU for me. Kaj, I am very thankful for your help and assistance with the extended UNIQUAC model. Thank you very much Maria for introducing me into the topic of carbonic anhydrase enhanced CO_2 capture and providing good input and ideas over the years. Jozsef, thank you so much for helping me out with the CAPCO2 model as well as the GM model, the frequent discussions about mass transfer with reactions helped me also a lot in understanding this difficult topic. Carolina, it was a pleasure sharing office with you and thank you that you could bear my complaints about the PhD life. I would also like to thank all the students that did their master's or bachelor's project with me for contributing to this research: Jeppe, Morten, Randi, Jiangui, Niels and Sebastian.

I would like to thank my family for the unconditional support and love throughout my life.

Laura, thank you for your care, patience, understanding and love, without you I could have never completed this work.

In loving memory of my mother, Gisela Dorothea Gladis (1960-2016).

Abstract

Fossil fuels are the backbone of the energy generation in the coming decades for USA, China, India and Europe, hence high greenhouse gas emissions are expected in future. Carbon capture and storage technology (CCS) is the only technology that can mitigate greenhouse gas emissions from fossil fuel fired power by selectively capturing CO_2 from flue gases. High capital and high operational costs of this process are the major obstacles of industrial implementation. In the field of CCS the chemical absorption process is the most mature technology. The use of kinetic rate promoters that enhance the mass transfer of CO_2 with slow-capturing but energetically favorable solvents can open up a variety of new process options for this technology.

The ubiquitous enzyme carbonic anhydrase (CA), which enhances the mass transfer of CO_2 in the lungs by catalyzing the reversible hydration of CO_2, is one very promising mass transfer rate promoter for CCS. This process has been previously been tested successfully in lab scale and in some rare cases in pilot scale, but no validated process model for this technology has been published yet.

This PhD thesis presents an investigation of the feasibility of enzyme enhanced CO_2 capture technology by identifying the potentials and limitations in lab and in pilot scale and benchmarking the process against proven technologies. The main goal was to derive a realistic process model for technical size absorbers with a wide range of validity incorporating a mechanistic enzyme kinetic model and validating it against in-house pilot plant experiments.

The work consisted of identifying a suitable enzyme-solvent system and the ideal process conditions by comparing mass transfer rates of different solvents and enzyme enhanced solvents in a lab scale wetted wall column. A kinetic model for the mechanistic enzyme reactions was developed for MDEA (N-methyl-diethanolamine) solutions capable of describing the mass transfer of CO_2 for absorption and desorption. It incorporates the influence of all relevant process conditions for technical absorbers, such as: temperature, solvent concentration, enzyme concentration, CO_2 concentration in the gas and liquid phase, as well as bicarbonate concentration in the liquid phase.

The process with enzyme enhanced MDEA was scaled up, and absorption experiments were carried out on a 10 m high pilot absorber column. The influence of enzyme concentration, column height, as well as solvent flow rates were determined for 30 wt% MDEA in over 50 runs and compared to over 30 pilot plant runs with the industrial standard solvent 30 wt% MEA (monoethanolamine) under the same process conditions. The mass transfer performance of enzyme enhanced solutions was found to be close to the industrial standard.

The pilot plant experiments could be accurately predicted with the in-house absorber column model CAPCO2 after the kinetic enzyme model from the lab experiments was implemented. The model can very accurately simulate the influence of each process parameter tested.

For targeting the thermal stability of the enzyme in desorption, an alternative low temperature process without reboiler was presented. A stripping gas carrier is utilized in this process to avoid thermal deactivation of the enzymes in the solvent regeneration; its technical feasibility was successfully tested in pilot scale desorption experiments.

The experiments at lab and pilot scale have clearly proven CA's potential in CCS. The presented validated absorber column model together with the low temperature regeneration process can be used to simulate and optimize the enzyme enhanced CO_2 capture process and benchmark this novel technology against conventional processes.

Résumé på dansk

Indfangning og lagring af kuldioxid (CCS – ”carbon capture and storage”) er den eneste teknologi, der kan mindske drivhusgasemissioner fra kraftværker baseret på fossile brændsler. Disse kraftværker – med CCS – kommer til at være vores vigtigste energiforsyning i de kommende årtier. Omkostningerne forbundet med CCS er dog en hindring for, at det implementeres bredt og i stor skala. Udgifterne kan mindskes ved brug af katalysatorer. De fremmer transporten og kinetikken i relevante lav-energi opløsningsmidler, som normalt ikke kan anvendes, da de reagerer for langsomt. Et eksempel på en katalysator er enzymet carbonisk anhydrase (CA).

CA er en katalysator som gør, at vi mennesker og dyr kan komme af med CO_2 fra lungerne. CA er blevet foreslået som en mulig industriel optimering af CCS, men der foreligger kun få forsøg i laboratorie- og pilotskala og ingen procesmodeller, som kan forudsige de forbedrede muligheder.

Denne afhandling præsenterer en undersøgelse af enzymet i lab- og pilotskala med henblik på at udvikle en detaljeret model, som kan anvendes til procesdesign i industriel skala, for eksempel i en processimulator.

Der er blevet udviklet en kinetisk model for de grundlæggende enzymreaktioner i MDEA- (N-methyl-diethanolamin) opløsninger, som er i stand til at beskrive masseoverføring af CO_2 for absorption og desorption i laboratorieskala.

Processen med enzymforbedret MDEA er blevet opskaleret, og absorptionseksperimenter er blevet udført i en 10 meter høj pilot-absorberkolonne ved forskellige kolonnehøjder, gennemløbshastigheder og temperaturer. De enzymforbedrede opløsninger viste sig at være konkurrencedygtige sammenlignet med den industrielle standard, 30 wt% MEA (monoethanolamin).

Resultaterne fra laboratoriemålinger blev inkluderet i DTU’s CAPCO2 model, og resultatet er, at modellen kan forudsige pilotanlæggets målinger for enzymblandinger med stor nøjagtighed.

Enzymer kan have en tendens til at degradere ved høj temperatur. Derfor blev en ny proces udviklet og afprøvet i pilotskala, hvor solvent-regenereringen foregår uden opvarmning.

Forsøgene i lab- og pilotskala har klart vist CA’s potentiale i CO_2-indfangning og -lagring. Den validerede absorberkolonnemodel, som præsenteres i afhandlingen, kan benyttes til simulering og optimering af den enzymforbedrede CO_2-indfagningsproces samt benchmark af denne nye teknologi op imod konventionelle CCS processer.

Table of Content

Theory

Lab scale

Pilot scale

1. Introduction

"Energy is the only universal currency."
Vaclav Smil

It is easy to underestimate the value of energy in times where it seems abundant in many parts of the world. The availability of energy to humans was not always the same in world's history. Two fundamental energy shifts, first the agricultural revolution then the industrial revolution, changed the human society [1]. Before the agricultural revolution the humans had to rely on their hunting skills and the accessibility of tubers, seeds and berries for their energy supply. The primary energy source was solar energy transformed into biomass by plants through photosynthesis process and also further via digestion and metabolism of organisms. With cultivating their own grains and crops in the agricultural revolution the humans could provide their own food which also allowed them to domesticate animals as source of food and additional work power. Food or fodder remained the primal source of energy at this time as between 80 and 85 % of all mechanical energy came from human or animal muscle power. The rest could be delivered by wind and water flows [2]. Household needs like heating and cooking were covered by burning fuels, which were crop residues, charcoal, dried dung, but mainly wood. The progress in that time was limited on how efficiently solar energy could be converted to muscle power and on how muscle power could be applied with the material and technology available [3].

Due to regional wood shortage induced by the metallurgy process and ships building [2] fossil coal was introduced and used as a substitute fuel even before the industrial revolution [4]. Coal had an advantage compared to renewable timber: it provided a higher energy density and could be moved easily to places where it was needed [3]; though the extraction of coal remained a muscle based labor work in the beginning. Later the need of power outside the physical constraints of muscles for the exploitation of coal mines led to the invention of the steam engine [4]. In the following years coalmining and steam engines reinforced each other [3]. By 1890 coal surpassed biomass as main contributor to primary energy supply. Improvement in metallurgy helped designing more efficient and more robust steam engines, machines and tools. This opened up access to the other fossil fuels crude oil and natural gas, which increasingly gained attention after 1870 and 1880 [3]. The following fossil fuel fired technology evolution revolutionized the agricultural, transportation and communication sector completely. In summary the main shift in industrial revolution can be seen from solar induced muscle work to fossil fuel powered machines. This resulted in inexpensive and reliable energy which due to electrification could be distributed even better and could be applied to the need.

The intensive use of fossil fuels also brought several negative side effects to the burden of nature. Over time the pollution and devastation of the fossil fuel production process as well as the emission of harmful side products in badly controlled combustion processes could be reduced with more advanced technologies in the field of production and power generation. In recent years the concentration level of

carbon dioxide in the atmosphere has become the most alarming side effect. Its contribution on the earth temperature was first addressed to the greenhouse gas effect by Arrhenius [5]. The greenhouse effect describes that the sunlight which is reflected on the earth's surface gets partially absorbed by the greenhouse gases in atmosphere and then gets re-emitted in every direction. A part of it is send back to earth, thus providing an additional heating source. The coherency between increase in atmospheric greenhouse gas concentration and global temperature rise could be observed over the last 150 years. A further increase in global temperature could bring devastating and unforeseen consequences to life on earth. In recent years the aim became to limit the damage by reducing the emission of greenhouse gases in future.

From today's perspective it is hard to believe that the energy demand will decrease in the future, the opposite is much more likely [6]. The International Energy Outlook 2016 from EIA assumes an overall increase in energy consumption of 48 % between 2012 and 2040, with fossil fuels still levering 78 % of the total energy in 2040 [7], BP's Energy Outlook assumes a rise in primary energy of 34 % between 2014 and 2035 with a share from fossil fuels of approximately 80 % (down from 86 % in 2014) [8]. In these two scenarios the share of renewable energies should rise with the years, but the total increase can hardly make up with the total increase in energy demand. Fossil fuels are planned to be the "backbone" of the energy systems for the European union in the coming decades [9]. The consumption of fossil fuels is also expected to rise in that time frame in China and India [7]. Unless the Clean Power Plan comes into action the coal consumption of USA will also rise in the next years [7]. During that timeframe the emission of carbon dioxide will continue unless advanced technologies for exhaust gas cleaning will be applied to the process of power generation.

The carbon capture and storage technology (CCS) separates CO_2 from other flue gas components either before (pre-combustion) or after (post-combustion) the combustion of carbon containing fuels. The captured CO_2 will then be compressed and stored in saline aquifers beneath the surface. This is an energy intensive process, thus the power output of a power plant will be reduced if this technology is applied. Besides there are high capital costs needed for construction of the unit operations. The actual capital costs for this process remain unknown as this technology is not yet applied commercially in industrial scale. It therefore seems a contradiction to invest money into the CCS technology when it could be used instead to support "clean" energies which can offer greenhouse gas emission free energy in the future. If a strict greenhouse gas emission reduction is required then there is no alternative to CCS.

1.1. Post-combustion CCS technology

Only the CCS technology can target the emissions of carbon dioxide linked to the projection of the future energy generation. With a lifetime of more than 25 years for coal fired power plants, the now existing plants will be emitting large amounts of CO_2 for a long time, unless they are forced to shut down [10]; which although is a very costly move. The post-combustion technology offers the potential

to immediately reduce the greenhouse gas emission as it can be retrofitted to existing plants and does not interfere with current energy generation. In the post combustion technology the exhaust gas which is normally vented through the chimney is treated and large amounts of CO_2 are separated from other flue gas components. The CO_2 can then be compressed and stored beneath the surface and is thus prevented to influence the global temperature. The technology can be applied also on other large greenhouse gas point sources in industry such as natural gas cleaning, iron or cement production that together with power generation account for 60 % of the total greenhouse gas emissions [11]. Several processes can be used for that application, such as membranes or adsorption but just a solvent-based absorption/desorption process has the maturity to be applied on large scales like coal fired power plants [12]. The CCS technology comprises the whole route from capturing carbon dioxide to compression, transport in pipeline, and injection as well as long term geological storage of CO_2. This study just deals with the optimization of the most expensive step in post-combustion CCS, the carbon dioxide capture [13]. Interested reader are referred to excellent reviews on all aspects of carbon capture and storage [13][14].

1.2. Critical factors for chemical absorption

The separation of CO_2 from flue gases of coal fired power plants is challenging, because the gas volume streams that need to be treated are in the range of several million norm cubic meter per hour with a gas CO_2 concentration of around 12 vol % and close to ambient pressure. This results in very low driving forces for the process. Unless CO_2 is pumped to a reservoir for enhanced oil recovery, sold as food grade supplement to food industry or used as raw material in chemical synthesis there is no real value in the product, thus no financial incentive for the process. A process flow diagram of a solvent-based CCS process is shown in Figure 1.

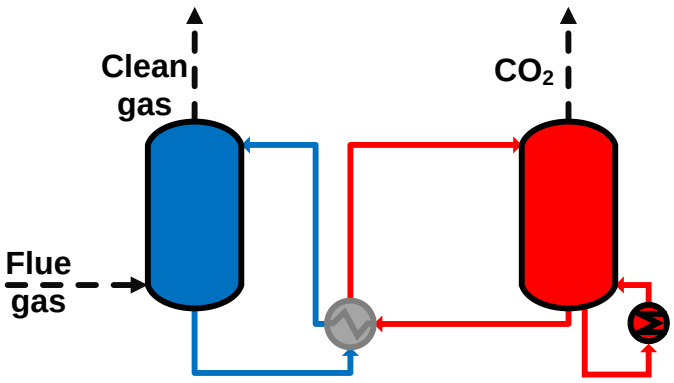

Figure 1: Flow diagram for a solvent based absorption/desorption process for CO_2 recovery from a flue gas stream

The flue gas is brought in contact with the liquid solvent in the absorber (blue); CO_2 is selectively absorbed into the solvent and the flue gas is cleansed running through the absorber upwards and exiting

on the top. The liquid solvent coming from the top of the absorber is capturing CO_2 on its way down. A chemical reaction between the solvent and CO_2 enhances the mass transfer of CO_2 into the liquid phase. The CO_2 loaded solvent is pumped into the desorber (red). On its way it is heated up against the warm solvent coming from the bottom of the desorber in a cross heat exchanger. Inside the desorber CO_2 is released from the solvent under input of thermal energy in the reboiler. After regeneration the CO_2-lean solvent is pumped back into the top of the absorber. The CO_2 coming from the desorber is compressed above supercritical conditions [14] (>31.1 °C & 74 bar) and can be injected into geological storages, like saline aquifers or depleted oil and gas fields in more than 1 km depth [13]. The depicted process flow diagram of the solvent-based absorption/desorption is a very simplified version of the capture process; in a real process the outline might be much more complex [16].

In order to make CCS economically competitive the capital investment and operational costs have to be brought down. It is very difficult to give estimates on the capital costs as the equipment size is very dependent on the scale of the process and the process itself. The main attributors to the capital costs for a chemical absorption process are the absorber and desorber towers, the cross heat exchanger as well as the compression unit [16][17]. The compression unit will be needed in every process, thus changes in the setup will influence the different processes equally. The size of the absorber and desorber towers are dependent on the mass transfer rates that are linked to the reaction rates between the solvent and CO_2 in the chemical absorption process. Thus high reaction rates for the solvents are needed. The liquid circulation rates determine the size of the cross heat exchanger, which can be influenced by using solvent with high CO_2 capacity.

Between 80 % and 90 % of the total process energy for the solvent-based absorption/desorption is needed for the solvent regeneration in the desorber [19], [20] making this the most importance parameter on the operational costs. The energy in the desorber is needed to heat up the solution, to generate stripping steam and reverse CO_2 reactions (heat of desorption) [20]. The magnitude of the different contributions depends on the process conditions and the solvent.

The total energy requirement of the best available technologies reduce the power output of an coal fired power plant by 9-16 % [10], [21]. One obvious approach for a cost efficient process would be to choose a solvent with high reaction kinetics and low heat of desorption and optimize the process. Unfortunately the heat of desorption and the kinetics are interrelated [19]. Solvents with high reaction rates like primary or secondary amines need more energy in the desorber reversing the reactions. Solvents that would require substantially less energy like tertiary amine or carbonate salt solutions result in absorber tower heights of several hundred meters for the same separation task [22].

1.3. Enzyme enhanced CO_2 capture

A catalyst can speed up the reaction rate between the solvent and CO_2 without changing the thermodynamic or chemical equilibrium of the solution. The enzyme carbonic anhydrase (CA)

(EC.4.2.1.1) catalyzes the reversible hydration of CO_2 forming bicarbonate and a proton and can be used in carbonate salt solutions and tertiary amines as kinetic rate promoter as their main reaction product of the CO_2 reaction is bicarbonate:

$$CO_2 + H_2O \xrightleftharpoons{CA} HCO_3^- + H^+ \tag{1.1}$$

The idea is to overcome the kinetic limitations of these solvents with a biocatalyst and enable their use in large scale processes where their beneficial energy requirements in the desorber might result in a cost and energy efficient process.

The feasibility of the enzyme enhanced CO_2 mass transfer has been proven in lab scale in a variety of solvents at different process conditions [23]–[28]. Even successful absorption experiments at pilot scale [29]–[31] and demonstration scale [32] have been carried out.

The application of CA in the CCS imposes some restrictions on the process as enzymes are temperature sensitive and might denature in the harsh environment of a conventional desorber. It is therefore important to exactly know the limits and the behavior of the enzyme at different process conditions and use this knowledge to design an innovative process in which the enzyme can sustain.

In order to benchmark the enzyme enhanced CO_2 capture technology against conventional solvent technologies precise process models and comparable experiments are required. These models preferably with mechanistic basis need to be able to describe the mass transfer of CO_2 in a wide range of process conditions and should be validated against experimental pilot plant data.

1.4. Motivation

This study aims to give a solid basis for the evaluation of the enzyme enhanced CO_2 capture processes, providing an experimental benchmark in lab and pilot scale by showing the potential and the limits of this process and giving the assets for a precise process simulation model.

Four main areas of work are identified:

a) Experimental benchmark in lab scale:
   - Experimental comparison of CO_2 mass transfer into different enzyme enhanced solvents in a wetted wall column lab setup
   - Determining the influence of solvent type, solvent concentration, solvent loading and temperature on the mass transfer
   - Identifying ideal process conditions for the enzyme in different solvents
   - Choosing one solvent for further investigation on pilot scale

b) Experimental benchmark in pilot scale
   - Preparation and characterization of a pilot absorber (10 m height*0.1 m diameter)

- Experimental campaigns with the industrial standard 30 wt% MEA
- Experimental campaigns with a selected enzyme solvent system
- Identification of relevant process parameters

c) Process modelling and model validation
- Derivation of a mechanistic kinetic model for the enzyme reactions from lab results
- Implementation of kinetic model into inhouse CAPCO2 absorber column model and model validation against pilot plant results

d) Process design for desorption
- Low temperature desorption process development
- Evaluation of technical feasibility with pilot scale experiments

1.5. Outline

This thesis has three different theory chapters (Chapter 2-4). Chapter 2 (Mass transfer and kinetics) provides the theory for a mass transfer process between two phases in a reactive system. Chapter 3 (Chemical solvents) gives an overview over the chemistry and reaction mechanisms of solvents applied for CO_2 absorption. The CO_2 solubility of solvents used in later experiments are explained in more detail. Chapter 4 (Enzymes) explains the principles of enzyme reactions in general and of the CA reaction in detail. It also provides a small literature review on enzyme enhanced CO_2 capture.

The next three chapters deal with the lab experiments on the wetted wall column: chapter 5 (Wetted wall column) describes the setup and explains the experimental procedure as well as the method to derive kinetic data from experiments; chapter 6 (Solvent comparison) summarizes the comparison of mass transfer for different enzyme enhanced and chemically enhanced solvents. Chapter 7 (Kinetic model for CA in MDEA) describes the kinetic enzyme model derivation from lab scale experiments.

The following chapters are linked to the pilot plant experiments: chapter 8 (Pilot scale absorber column setup) describes the pilot plant setup and explains the different phenomena and characteristics in packed columns; chapter 9 (Absorption experiments in pilot scale) shows the results from the different experimental campaigns in pilot scale. In Chapter 10 (Absorber column modelling) CAPCO2 with the implemented kinetic model derived in Chapter 7 is validated against the experimental results from Chapter 9. Chapter 11 (Desorption) gives an overview over the stripgas desorption experiments.

Chapter 12 summarizes the main findings from this work together with recommendations for future work in that field.

BIBLIOGRAPHY

[1] M. T. Huber, "Energizing historical materialism: Fossil fuels, space and the capitalist mode of production," *Geoforum*, vol. 40, no. 1, pp. 105–115, 2009.

[2] F. Cottrell, *Energy and Society*. McGraw-Hill, 1970.

[3] V. Smil, *Energy in World history*, 1st ed. Westwood Press, 1994.

[4] M. K. Hubbert, "Energy From Fossil Fuels," *Science*, vol. 108, no. 2813, pp. 589–590, 1948.

[5] S. Arrhenius, "On the Influence of Carbonic Acid in the Air upon the Temperature of the Ground," *Philos. Mag. J. Sci.*, vol. 41, no. page 270, pp. 237–279, 1896.

[6] Y. Kaya, "The role of CO_2 removal and disposal," *Energy Convers. Manag.*, vol. 36, no. 6–9, pp. 375–380, 1995.

[7] (EIA) U.S. Energy Information Administration, *International Energy Outlook 2016*, vol. 484, no. May. 2016.

[8] British Petroleum, "BP energy outlook 2016," *Br. Pet.*, vol. 53, no. 9, p. 98, 2016.

[9] K. Kavouridis and N. Koukouzas, "Coal and sustainable energy supply challenges and barriers," *Energy Policy*, vol. 36, no. 2, pp. 693–703, 2008.

[10] P. H. M. Feron, "Exploring the potential for improvement of the energy performance of coal fired power plants with post-combustion capture of carbon dioxide," *Int. J. Greenh. Gas Control*, vol. 4, no. 2, pp. 152–160, 2010.

[11] K. a. Mumford, Y. Wu, K. H. Smith, and G. W. Stevens, "Review of solvent based carbon-dioxide capture technologies," *Front. Chem. Sci. Eng.*, vol. 9, no. 2, pp. 125–141, 2015.

[12] G. T. Rochelle, "Amine scrubbing for CO_2 capture.," *Science*, vol. 325, no. 5948, pp. 1652–1654, 2009.

[13] J. Gibbins and H. Chalmers, "Carbon capture and storage," *Energy Policy*, vol. 36, no. 12, pp. 4317–4322, 2008.

[14] M. E. Boot-Handford, J. C. Abanades, E. J. Anthony, M. J. Blunt, S. Brandani, N. Mac Dowell, J. R. Fernández, M.-C. Ferrari, R. Gross, J. P. Hallett, R. S. Haszeldine, P. Heptonstall, A. Lyngfelt, Z. Makuch, E. Mangano, R. T. J. Porter, M. Pourkashanian, G. T. Rochelle, N. Shah, J. G. Yao, and P. S. Fennell, "Carbon capture and storage update," *Energy Environ. Sci.*, vol. 7, p. 130, 2014.

[15] E. S. Rubin, H. Mantripragada, A. Marks, P. Versteeg, and J. Kitchin, "The outlook for improved carbon capture technology," *Prog. Energy Combust. Sci.*, vol. 38, no. 5, pp. 630–671, 2012.

[16] Y. Le Moullec, T. Neveux, and L. Moullec, "Process modifications for CO_2 capture," in

Absorption-Based Post-Combustion Capture of Carbon Dioxide, 2016.

[17] M. O. Schach, R. Schneider, H. Schramm, and J. U. Repke, "Techno-economic analysis of postcombustion processes for the capture of carbon dioxide from power plant flue gas," *Ind. Eng. Chem. Res.*, vol. 49, pp. 2363–2370, 2010.

[18] M. Karimi, M. Hillestad, and H. F. Svendsen, "Capital costs and energy considerations of different alternative stripper configurations for post combustion CO_2 capture," *Chem. Eng. Res. Des.*, vol. 89, no. 8, pp. 1229–1236, 2011.

[19] H. F. Svendsen, E. T. Hessen, and T. Mejdell, "Carbon dioxide capture by absorption, challenges and possibilities," *Chem. Eng. J.*, vol. 171, no. 3, pp. 718–724, 2011.

[20] R. Notz, I. Tönnies, H. P. Mangalapally, S. Hoch, and H. Hasse, "A short-cut method for assessing absorbents for post-combustion carbon dioxide capture," *Int. J. Greenh. Gas Control*, vol. 5, no. 3, pp. 413–421, 2011.

[21] R. J. Notz, I. Toennies, N. McCann, G. Scheffknecht, and H. Hasse, "CO_2 Capture for Fossil Fuel-Fired Power Plants," *Chem. Eng. Technol.*, vol. 34, no. 2, pp. 163–172, 2011.

[22] N. Penders-van Elk, E. Hamborg, P. S., J. A. Carley, S. Fradette, and G. F. Versteeg, "Kinetics of absorption of carbon dioxide in aqueous amine and carbonate solutions with carbonic anhydrase," *Int. J. Greenh. Gas Control*, vol. 12, pp. 259–268, 2013.

[23] N. J. M. C. Penders-van Elk, P. W. J. Derks, S. Fradette, and G. F. Versteeg, "Kinetics of absorption of carbon dioxide in aqueous MDEA solutions with carbonic anhydrase at 298 K," *Int. J. Greenh. Gas Control*, vol. 9, pp. 385–392, 2012.

[24] X. Ye and Y. Lu, "CO_2 absorption into catalyzed potassium carbonate–bicarbonate solutions: Kinetics and stability of the enzyme carbonic anhydrase as a biocatalyst," *Chem. Eng. Sci.*, vol. 116, pp. 567–575, 2014.

[25] G. Hu, K. H. Smith, N. J. Nicholas, J. Yong, S. E. Kentish, and G. W. Stevens, "Enzymatic carbon dioxide capture using a thermally stable carbonic anhydrase as a promoter in potassium carbonate solvents," *Chem. Eng. J.*, vol. 307, pp. 49–55, 2016.

[26] S. Salmon and A. House, "Enzyme-catalyzed Solvents for CO_2 Separation", in *Novel Materials for Carbon Dioxide Mitigation Technology*, Elsevier B.V., 2015.

[27] M. Vinoba, M. Bhagiyalakshmi, A. N. Grace, D. H. Kim, Y. Yoon, S. C. Nam, I. H. Baek, and S. K. Jeong, "Carbonic anhydrase promotes the absorption rate of CO_2 in post-combustion processes," *J. Phys. Chem. B*, vol. 117, no. 18, pp. 5683–5690, 2013.

[28] A. Gladis, M. T. Gundersen, P. L. Fosbøl, J. M. Woodley, and N. von Solms, "Influence of temperature and solvent concentration on the kinetics of the enzyme carbonic anhydrase in carbon capture technology," *Chem. Eng. J.*, 2017.

[29] A. Kunze, G. Dojchinov, V. S. Haritos, and P. Lutze, "Reactive absorption of CO_2 into enzyme

accelerated solvents : From laboratory to pilot scale," *Appl. Energy*, vol. 156, pp. 676–685, 2015.

[30] O. Alvizo, L. J. Nguyen, C. K. Savile, J. a Bresson, S. L. Lakhapatri, E. O. P. Solis, R. J. Fox, J. M. Broering, M. R. Benoit, S. a Zimmerman, S. J. Novick, J. Liang, and J. J. Lalonde, "Directed evolution of an ultrastable carbonic anhydrase for highly efficient carbon capture from flue gas.," *Proc. Natl. Acad. Sci. U. S. A.*, vol. 111, no. 46, pp. 16436–41, 2014.

[31] A. Gladis, N. F. Lomholdt, P. L. Fosbøl, J. M. Woodley, and N. von Solms, "Pilot absorption experiments with carbonic anhydrase enhanced MDEA," *Energy Procedia*, 2016.

[32] L. Fradette, S. Lefebvre, and J. Carley, "Demonstration Results of Enzyme-Accelerated CO_2 Capture," *Energy Procedia*, vol. 0, pp. 14–18, 2017.

Theory

2. Mass transfer and kinetics

This chapter aims to provide understanding on the principles of mass transfer between two phases accompanied by a chemical reaction. The principles are explained here in the context of absorption of compound A (CO_2) from the gas phase into a liquid phase, but are also valid for other mass transfer operations. The mass transfer phenomena will be explained in detail using the two film model and the effects of irreversible and reversible first order reactions as well as accurate approximations for irreversible and reversible second order reactions and parallel reactions on the mass transfer will be described.

2.1. Principles of diffusion and reaction

Isolated systems are approaching equilibrium [1], thus if two phases are brought in contact they will equilibrate over time.

2.1.1. Diffusion

Molecule transfer, called diffusion, is one option to equilibrate between regions with higher and with lower concentration. It is caused by random thermal movement of the molecules which end up redistributing uniformly in the media after a certain time [2]. The observation that the molecular flux due to diffusion is proportional to the concentration gradient, with the proportionality factor being the Diffusion coefficient D_i^j for compound *i* in media *j*, lead to the following mathematical description of the diffusional flux J_i^j [3]:

$$N_i^j = J_i^j = -D_i^j \frac{dC_i}{dx} \tag{2.1}$$

The minus describes that the flux occurs in the direction of lower concentrations. This equation is also known as Fick's first law which describes steady-state diffusion as principles of mass transfer between two phases.

In an unsteady process, composition and mass transfer changes with time and position. For continuity the change in diffusional mass transfer in a small element must be equal to the change in concentration over time [3]:

$$\frac{dJ_i^j}{dx} = -\frac{dC_i}{dt} \tag{2.2}$$

Inserting the diffusional flux from Eq. (2.1) leads to:

$$\frac{dC_i}{dt} = D_i^j \frac{\partial^2 C_i}{\partial x^2} \tag{2.3}$$

This is known as Fick's second law which describes the evolution of the concentration due to diffusion over time [4].

2.1.2. Reaction kinetics

A system can also be equilibrated due to reaction. The reaction rate equation for compound A with a compound B forming the products P and Q can be written as:

$$\nu_A \cdot A + \nu_B \cdot B \underset{k_{-A}}{\overset{k_A}{\rightleftharpoons}} \nu_P \cdot P + \nu_Q \cdot Q \tag{2.4}$$

The factors ν_i describe the stoichiometry of each reactant in the reaction. The reaction rate of each compound can be expressed as change in compound *i* per volume and time:

$$r_i = \frac{1}{V} \frac{dN_i}{dt} \tag{2.5}$$

Due to the mass balance the rates of reaction of each compound are linked:

$$-\frac{r_A}{\nu_A} = -\frac{r_B}{\nu_B} = \frac{r_P}{\nu_P} = \frac{r_Q}{\nu_Q} \tag{2.6}$$

Considering just the forward reaction, the reaction rate r_A (mol s^{-1}) can be described as a function of concentration of A and B and rate constant k_{AB}:

$$-r_A = k_{AB} \cdot C_A^{\alpha} \cdot C_B^{\beta} \tag{2.7}$$

The exponents α and β are called reaction order of component A and B respectively. The overall reaction order is $\alpha + \beta$. In case the reaction can be considered as an elementary reaction, the reaction order of the component is equal to its stoichiometric coefficient ($\alpha = \nu_A$ and $\beta = \nu_B$). Since the reaction order is based on the observed concentration dependency of reaction rates, values can differ from being integer [5]. This can be explained, because mostly in more complex reactions not all elementary steps and intermediates are known and a reaction mechanism based on experimentally determined concentration changes is chosen [6]. The unit for the rate constant is dependent on the overall reaction order, so that the expressions for r_A results in concentration change per time.

Reaction (2.7) describes an irreversible reaction where no back reaction of the products is considered, which is a good approximation for a reaction far away from equilibrium. The closer the reaction approaches equilibrium the more profound the back reaction becomes. For an elementary reaction as described in Eq. (2.4) the reaction rate for A becomes:

$$-r_A = k_{AB} \cdot C_A^{\nu_A} \cdot C_B^{\nu_B} - k_{-AB} \cdot C_P^{\nu_P} \cdot C_Q^{\nu_Q} \tag{2.8}$$

The rate constant for the back reaction is k_{-AB}, which can be expressed in terms of forward reaction rate constant k_{AB} and the equilibrium constant K_{eq} with the following correlation, as there is no net reaction at chemical equilibrium:

$$\frac{k_{AB}}{k_{-AB}} = \frac{C_P^{*\nu_P} \cdot C_Q^{*\nu_Q}}{C_A^{*\nu_A} \cdot C_B^{*\nu_B}} = K_{eq} \tag{2.9}$$

The notification * symbolizes the concentration at equilibrium. Equation (2.8) and (2.9) lead to:

$$-r_A = k_{AB} \cdot C_A^{\nu_A} \cdot C_B^{\nu_B} - \frac{k_{AB}}{K_{eq}} \cdot C_P^{\nu_P} \cdot C_Q^{\nu_Q} = k_{AB} \left(C_A^{\nu_A} \cdot C_B^{\nu_B} - \frac{C_A^{*\nu_A} \cdot C_B^{*\nu_B} \cdot C_P^{\nu_P} \cdot C_Q^{\nu_Q}}{C_P^{*\nu_P} \cdot C_Q^{*\nu_Q}} \right) \approx k_{AB} \left(C_A^{\nu_A} \cdot C_B^{\nu_B} - C_A^{*\nu_A} \cdot C_B^{*\nu_B} \right) \tag{2.10}$$

The reaction rate can be thus described with a single rate constant and the distance from equilibrium[7].

2.2. Mass transfer theories

The mass transfer process between two phases can be described with simple models that incorporate all process parameters which can be solved mathematically. Currently the two-film theory, the penetration theory and the surface renewal theory are the most common theories for mass transfer between two phases. Their assumptions and differences will be briefly explained in the next section.

Even though the assumptions of these models seem quite simple and maybe even far from reality, over the years they have proven to be applicable in designing mass transfer equipment. The models themselves are quite different, when comparing two film with penetration/surface renewal theory, although they lead to similar results when describing mass transfer with reactions [5].

2.2.1. Two-film theory

The two-film theory originally proposed by Whitman and Lewis in 1923 [8] is the most simplified model. It assumes that two stagnant films exist parallel to the interface, one in each phase, through which mass transfer occurs purely through molecular diffusion. The bulk phase is well mixed and has a

uniform composition. The occurring mass transfer is a stationary operation. The mass transfer through the film without any reaction can be described as:

$$D_A \frac{d^2 C_A}{dx^2} = 0 \tag{2.11}$$

together with Fick's first law from Eq.(2.1) and the boundary conditions, $C_A = C_A^{int}$ at $x = 0$ as well as $C_A = C_A^{bulk}$, at $x = \delta$:

$$J_A = -D_A \frac{dC_A}{dx} = \frac{D_A}{\delta}(C_A^{int} - C_A^{bulk}) . \tag{2.12}$$

This can be regarded as the physical mass transfer equation for the two-film theory. From mass transfer theory a flux can be described with a mass transfer coefficient and a driving force. Therefore the physical mass transfer coefficient in the two film theory is the ratio between the diffusivity and the hypothetical film thickness:

$$k_{transfer}^{Film} = \frac{D_A}{\delta_{Film}} \tag{2.13}$$

2.2.2. Penetration theory/surface renewal theory

The penetration theory assumes, that the interface in a mass transfer operation is frequently exchanging. Every fluid element which participates in mass transfer comes from the well mixed bulk and stays at the surface for the exact same exposure time τ. At the beginning of the exposure time the fluid element has the same composition as the liquid bulk. Once at the surface the absorbent CO_2 starts diffusing into the liquid phase. The mass transfer is a non-steady state diffusion as described with the Fick's second law, thus the transferred amount and the concentration profile are dependent on time. The mass transfer coefficients as a function of τ in penetration theory are defined as:

$$k_{transfer}^{PT} = 2\sqrt{\frac{D_A}{\pi \cdot \tau}} \tag{2.14}$$

The surface renewal theory is a modification of the penetration theory proposed by Danckwerts [9]. In this model the exposure time of each fluid element on the interface is not the same but the renewal of the surface follows a probability distribution [3]. For surface renewal theory the mass transfer coefficient is defined as

$$k_{transfer}^{SR} = \sqrt{D_A \cdot s} \tag{2.15}$$

with s (s^{-1}) being the fractional surface renewal rate.

2.3. Mass transfer between two phases

Two phases can be equilibrated through the transfer of mass from one phase to the other. For absorption/desorption a difference in chemical equilibrium of a compound A between the gas and the liquid phase is responsible for mass transfer, i.e. the fugacity in the gas phase is different from the activity in the liquid phase. For practical reasons the state of compound A in the gas phase is often expressed in partial pressure P_A (Pa) rather than fugacity and in liquid phase in concentration C_A (mol m^{-3}) rather than activity. The link between the activity/fugacity and the partial pressure/concentration can be described with thermodynamic equilibrium models.

The partial pressure and concentration profiles of a physical and chemical CO_2 absorption process according to the two-film theory are shown in Figure 2.

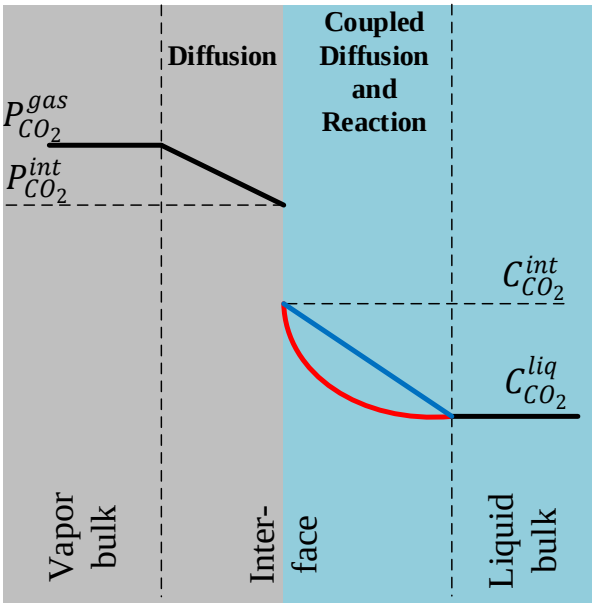

Figure 2: Mass transfer of CO_2 in absorption according to the two-film theory [8]; blue line indicates concentration profile of a physical absorption and red line of a chemical absorption process.

CO_2 coming from the well mixed gas bulk with a partial pressure of $P_{CO_2}^{gas}$ is diffusing through a laminar film to the gas-liquid interface. The transferred molar flux of CO_2 $N_{CO_2}^{gas}$ (mol s^{-1}) divided by the mass transfer area a_{eff} (m^2) can be described by the product of the gas side mass transfer coefficient $k_{CO_2}^{gas}$ (mol Pa^{-1} m^{-2} s^{-1}) and the driving force for mass transfer through the gas film, which is the difference between the partial pressures in the gas bulk $P_{CO_2}^{gas}$ (Pa) and at the interface $P_{CO_2}^{int}$ (Pa):

$$\frac{N_{CO_2}^{gas}}{a_{eff}} = k_{CO_2}^{gas} \cdot \left(P_{CO_2}^{gas} - P_{CO_2}^{int} \right) \tag{2.16}$$

At the interface CO_2 is dissolved into the liquid phase resulting in the CO_2 concentration $C_{CO_2}^{int}$. The correlation between CO_2 partial pressure in the gas phase and the CO_2 concentration in the liquid phase at the interface can be expressed with Henry's law assuming equilibrium at the interface:

$$P_{CO_2}^{int} = H_{CO_2} \cdot C_{CO_2}^{int} \tag{2.17}$$

The wording Henry's coefficient is just valid if the liquid phase is not reacting with CO_2. In most cases in chemical absorption a partition coefficient is used, which is also described as apparent Henry's coefficient H_{CO_2} (Pa m^3 mol^{-1}). This partition coefficient correlates the gas partial pressure of CO_2 to the interfacial CO_2 concentration as in Eq. (2.17).

The concentration profile of CO_2 in the liquid film is nonlinear in case of chemical absorption and linear in case of physical absorption according to the two-film theory. The reason for the bulge in chemical absorption is that CO_2 is additionally consumed by chemical reaction of CO_2 with the solvent. CO_2 is diffusing from the interface into the liquid bulk with a CO_2 concentration of $C_{CO_2}^{liq}$ that represents the equilibrium concentration of CO_2 in the liquid bulk. The mass transfer through the interface into the liquid bulk can be described in a similar manner as the mass transfer from the gas bulk to the interface:

$$\frac{N_{CO_2}^{liq}}{a_{eff}} = k_{CO_2}^{liq} \cdot \left(C_{CO_2}^{int} - C_{CO_2}^{liq} \right) = k_{CO_2}^{liq\ '} \cdot \left(P_{CO_2}^{int} - P_{CO_2}^{liq} \right) \tag{2.18}$$

The difference between the chemical liquid side mass transfer coefficients $k_{CO_2}^{liq}$ (m s^{-1}) and $k_{CO_2}^{liq\ '}$ (mole Pa^{-1} m^{-2} s^{-1}) is just the unit of the driving force, which is either described as differences in concentrations or partial pressures, thus they are linked with the partition coefficient. This expression is valid for physical and chemical absorption as long as the respective liquid side mass transfer coefficients for physical or chemical mass transfer are used.

The overall mass transfer from the gas into the liquid phase can be described with an overall gas mass transfer coefficient $K_{CO_2}^{ovG}$ (mole Pa^{-1} m^{-2} s^{-1}).

$$\frac{N_{CO_2}^{ov}}{a_{eff}} = K_{CO_2}^{ovG} \cdot \left(P_{CO_2}^{gas} - P_{CO_2}^{liq} \right) \tag{2.19}$$

The notation overall "gas" mass transfer coefficient declares that the driving force is expressed in units of the gas phase, e.g. partial pressure. The flux can also be described with an overall liquid side mass transfer coefficient $K_{CO_2}^{ovL}$ (m s^{-1}) as:

$$\frac{N_{CO_2}^{ov}}{a_{eff}} = K_{CO_2}^{ovL} \cdot \left(\frac{P_{CO_2}^{gas}}{H_{CO_2}} - C_{CO_2}^{liq} \right). \tag{2.20}$$

As the flow through the gas film $N_{CO_2}^{gas}$ to the interface is equal to the flow from the interface into the liquid $N_{CO_2}^{liq}$ and the overall flux from the gas into the liquid $N_{CO_2}^{ov}$, the following relation between $K_{CO_2}^{ovG}$, $k_{CO_2}^{liq}$ and $k_{CO_2}^{gas}$ can be derived:

$$\frac{1}{K_{CO_2}^{ovG}} = \frac{1}{k_{CO_2}^{gas}} + \frac{H_{CO_2}}{k_{CO_2}^{liq}} = \frac{1}{k_{CO_2}^{gas}} + \frac{1}{k_{CO_2}^{liq\,'}} \tag{2.21}$$

Accordingly for the overall liquid side mass transfer coefficient $K_{CO_2}^{ovL}$:

$$\frac{1}{K_{CO_2}^{ovL}} = \frac{1}{H_{CO_2} \cdot k_{CO_2}^{gas}} + \frac{1}{k_{CO_2}^{liq}} = \frac{1}{H_{CO_2} \cdot k_{CO_2}^{gas}} + \frac{1}{H_{CO_2} \cdot k_{CO_2}^{liq\,'}} \tag{2.22}$$

The reciprocal value of the mass transfer coefficient describes the mass transfer resistance in the phase. The overall mass transfer resistance is the sum of the gas side and liquid side mass transfer resistance.

During the diffusion CO_2 is reacting with the solvent; the CO_2 concentration is decreasing near the interface and the CO_2 gradient is increasing which will raise the driving force for diffusion and enhance the mass transfer. The mass transfer in absorption is dependent on the driving force, thus how far the chemical equilibria in the gas and liquid phase are apart from each other, and on the mass transfer resistances, the steepness of the partial pressure or concentration profiles in the films.

The following expression is often used to describe the mass transfer of a compound from the gas phase into a liquid accompanied by a chemical reaction [6], [10]:

$$\frac{N_{CO_2}}{a_{eff}} = \frac{\left(P_{CO_2}^{gas} - H_{CO_2} \cdot C_{CO_2}^{liq} \right)}{\frac{1}{k_{CO_2}^{gas}} + \frac{H_{CO_2}}{k_{CO_2}^{liq0} \cdot E}} \tag{2.23}$$

The product $H_{CO_2} \cdot C_{CO_2}^{liq}$ is the equilibrium partial pressure of the solvent; in some cases it is described as the backpressure of CO_2 in the solvent. The physical liquid side mass transfer coefficient $k_{CO_2}^{liq0}$

(m s^{-1}) is multiplied by the Enhancement factor E (-) describing the intensification of the mass transfer due to chemical reaction.

2.4. Mass transfer with reactions

The extent of mass transfer enhancement is dependent on the reaction kinetics, the diffusivity of the reaction educts as well as physical mass transfer coefficient $k_{CO_2}^{liq0}$ for that operation.

2.4.1. Irreversible first order reactions

When the concentration of A is changed due to diffusion and consumed through reaction the transfer through the film described in Eq. (2.21) has to be extended by the reaction term

$$D_A \frac{d^2 C_A}{dx^2} + R_A = 0\,. \tag{2.24}$$

Considering that compound A is undergoing an irreversible chemical reaction with first order kinetics this reaction term can be described as:

$$R_A = -k_A \cdot C_A \tag{2.25}$$

When the differential equation in Eq. (2.24) is solved, the molar Flux at the interface can be described as [11]:

$$N_A = \frac{D_A}{\delta} C_A^{int} \frac{\phi}{\tanh \phi} \tag{2.26}$$

The dimensionless parameter ϕ is defined as [5]:

$$\phi = \delta \sqrt{\frac{k_A}{D_A}} \tag{2.27}$$

From the convention of the physical mass transfer coefficient k_{liq0} for the two-film theory [8] in Eq. (2.23) , this term can be expressed as:

$$\phi = \sqrt{\frac{k_A D_A}{k_{liq0}^{\ 2}}} \tag{2.28}$$

The reaction modulus ϕ is the Hatta number Ha; the squared value ϕ^2 is equal to the ratio of maximum conversion of A due to reaction in the film to maximum diffusional stream through the film

in absence of chemical reaction. It can be derived for first order reactions from definition as the maximum conversion r_A (mol s^{-1}) in the film is the volumetric reaction rate R_A (mol m^{-3} s^{-1}) times the reaction volume V (m^3):

$$r_A = R_A \cdot V_r = k_A \cdot C_A \cdot \delta \cdot a \tag{2.29}$$

a being the interfacial area and δ (m) being the film thickness. The maximum diffusional stream j_A (mol s^{-1}) can be calculated from the diffusion flux per unit area J_A (mol m^{-2} s^{-1}) from Eq. (2.22) by multiplying with the surface area a (m^2):

$$j_A = J_A \cdot a = \frac{D_A}{\delta} \cdot a \cdot \left(C_A^{int} - C_A^{bulk} \right) \tag{2.30}$$

Considering a concentration of compound A in the liquid bulk of zero ($C_A^{bulk} = 0$) the Hatta number Ha becomes:

$$Ha^2 = \frac{r_A}{j_A} = \frac{k_A \cdot C_A \cdot \delta \cdot a}{\frac{D_A}{\delta} \cdot a \cdot C_A} = \frac{k_A \cdot D_A}{\frac{D_A^{\,2}}{\delta^2}} = \frac{k_A \cdot D_A}{k_{liq0}^{\,2}} \tag{2.31}$$

The square root of expression in Eq. (2.31) is equal to Eq. (2.28). The value is referred to as Hatta number for first order irreversible reactions. The mass transfer described in Eq. (2.26) is just valid for irreversible first order reactions.

2.4.2. Reversible first order reactions

The reactions in the chemical absorption process cannot always be regarded irreversible, especially in cases where the solvent loading is high, like in the bottom of the absorber, or in the desorber where the reverse reaction takes place. In the simple case of a first order reversible reaction the reaction rate described in Eq. (2.8) can be simplified to:

$$A \underset{k_{-A}}{\overset{k_A}{\rightleftharpoons}} P \tag{2.32}$$

with:

$$-r_A = k_A \cdot C_A - k_{-A} \cdot C_P = k_A \cdot C_A - k_A \frac{C_P}{K_{eq}} = k_A \left(C_A - C_A^* \right) \tag{2.33}$$

At chemical equilibrium the forward and reverse reaction need to be equal:

$$\frac{k_A}{k_{-A}} = \frac{C_P^*}{C_A^*} = K_{eq} \tag{2.34}$$

Considering that the liquid bulk is in equilibrium ($C_A^* = C_A^{bulk}$), which holds for fast reactions, the reversible Hatta number can be expressed as:

$$Ha^2 = \frac{\left(k_{1A} \cdot C_A - k_{-A} \cdot C_P\right) \cdot \delta \cdot a}{\frac{D_A}{\delta} \cdot a \cdot \left(C_A^{int} - C_A^{bulk}\right)} = \frac{k_{1A}\left(C_A^{int} - C_A^{bulk}\right) \cdot \delta \cdot a}{\frac{D_A}{\delta} \cdot a \cdot \left(C_A^{int} - C_A^{bulk}\right)} = \frac{k_{1A} \cdot D_A}{\frac{D_A{}^2}{\delta^2}} \tag{2.35}$$

The reversible Hatta number is the same as for the irreversible Hatta number from Eq. (2.31).

Huang and Kuo (1965)[12] derived the following expression for the mass transfer accompanied by first order reversible reaction:

$$N_A = \frac{D_A}{\delta}\left(\frac{K_{eq} \cdot D_{AP} + 1}{1 + K_{eq} \cdot D_{AP} \dfrac{\tanh \mu_1 \cdot Ha}{\mu_1 \cdot Ha}}\right) \cdot \left(C_A^{int} - C_A^{bulk}\right) \tag{2.36}$$

with:

$$D_{AP} = \frac{D_A}{D_P} \; and \; \mu_1 = \left(\frac{K_{eq} \cdot D_{AP} + 1}{K_{eq} \cdot D_{AP}}\right)^{0.5} \tag{2.37}$$

The mass transfer with a first order reversible reaction differs from the case of irreversible reaction described in Eq. (2.26). The differences are most profound in the regions near the equilibrium. Danckwerts [2] derived a similar expression for the case of equal diffusivity of educt and product ($D_{AP} = 1$).

2.5. Enhancement factors

Instead of solving the differential equations for reaction and diffusion of all reactions and for every stage in a mass transfer unit, an Enhancement factor model is often used. This Enhancement factor E is a scalar multiplier to the physical mass transfer that occurs in absence of a chemical reaction and describes the “Enhancement” effect of chemical reaction on the mass transfer.

$$J_A = \frac{D_A}{\delta} \cdot E \cdot \left(C_A^{int} - C_A^{bulk}\right) = k_{liq} \cdot E \cdot \left(C_A^{int} - C_A^{bulk}\right) \tag{2.38}$$

The Enhancement factor is therefore the ratio of the chemical and physical mass transfer coefficient:

$$E = \frac{k_{liq}^{'}}{k_{liq}} \tag{2.39}$$

The Enhancement factor gives information on the concentration gradient of the absorbed compound at the interface; it is therefore related to the conditions at the interface and the reaction rate taking place in the close vicinity of the interface.

2.5.1. Single second order reactions

The Enhancement factor for a first order reaction can be calculated from Eq. (2.26) describing mass transfer with first order chemical reactions and from Eq. (2.12) describing purely physical mass transfer by taking the ratio of these two values for the same driving force according to Eq. (2.39); consequently $E = Ha / \tanh Ha$. This can be simplified to $E = Ha$ for higher Hatta numbers as these two expressions differ less than 2% for Ha greater 2 and less than 1% for Ha greater 3. The Enhancement factor for second order reactions where one reactant is absorbed and the other reactant is diffusing from the liquid bulk is more complex. Mass transfer of a gas compound like CO_2 into a solvent with coupled reaction and diffusion into the bulk is dependent on the reaction rate between solvent and CO_2 at the interface. This reaction rate is the product of CO_2 concentration and solvent concentration at the interface and second order reaction rate constant for a single reaction occurring. The interfacial CO_2 concentration is known or can at least be calculated whereas the interfacial solvent concentration remains unknown and is a function of the reaction rate and diffusion of solvent molecules from the liquid bulk. The only known solvent concentration in mass transfer operations is the liquid bulk concentration as it is assumed that the liquid bulk is well mixed and in chemical equilibrium.

The Enhancement factor for a second order reaction can be described as function of the Hatta number. The second order Hatta number can be derived from the first order one in Eq. (2.31) by substituting the first order reaction rate constant by a second order reaction rate constant multiplied by the solvent concentration (B).

$$R_A = -k_{2B} \cdot C_A \cdot C_B = -k_{1A} \cdot C_A \tag{2.40}$$

The expression becomes thus:

$$Ha = \frac{\sqrt{k_{2B} \cdot C_B \cdot D_A}}{k_{liq}^0} = \frac{\sqrt{k_{sol} \cdot C_{sol} \cdot D_{CO_2}}}{k_{liq}^0} \tag{2.41}$$

The Enhancement factor of a second order reaction as a function of the Hatta number is shown in Figure 3.

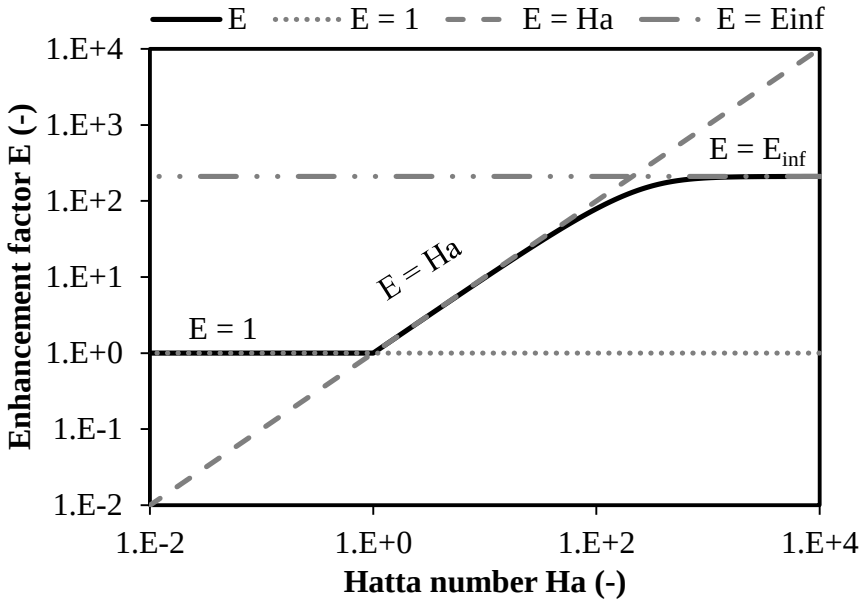

Figure 3: Correlation between Hatta number Ha and Enhancement factor E for a second order reaction together with asymptotic lines mode, modified from Westerterp et al. [5] and Levenspiel [6].

The Enhancement factor is constant and equal to one for small Hatta numbers indicating that no increase in mass transfer due to reaction occurs in that region. Then the Enhancement factor rises linearly with the Hatta number until it comes to a maximum value where it levels off. Three asymptotic lines can describe the behavior of the Enhancement factor in a wide region. First is the region of no enhancement, typically at Ha lower than 0.3, where the mass transfer is equal to the physical mass transfer [5]. The second asymptotic line is the linear increase of the Enhancement factor where the Enhancement factor is equal to the Hatta number. This region is referred to as pseudo-first order region, as the Enhancement Factor in that region is the same as that for a first order reaction. The last asymptotic line represents the maximum achievable Enhancement under these conditions. The Enhancement factor for a second order reaction between CO_2 and solvent according to the two-film theory is dependent on the diffusivity of the solvent and CO_2 in solution as well as their respective concentrations in the bulk and at the interface and the stoichiometric factor for the reaction γ_{sol}:

$$E_{\infty}^{film} = 1 + \frac{D_{sol} \cdot C_{sol}^{bulk}}{\gamma_{sol} \cdot D_{CO_2} \cdot C_{CO_2}^{int}} \tag{2.42}$$

The Hatta number cannot be changed at will in a process, but is resulting from the process conditions. A change in reaction kinetics and a change in physical mass transfer influence the Hatta number. To get a better understanding of the influence of chemical reaction on the mass transfer two cases are considered where the Hatta number is either changed by altering the physical mass transfer coefficient

and keeping the solvent reaction rate constant or by changing the solvent kinetics and keeping the physical mass transfer coefficient constant.

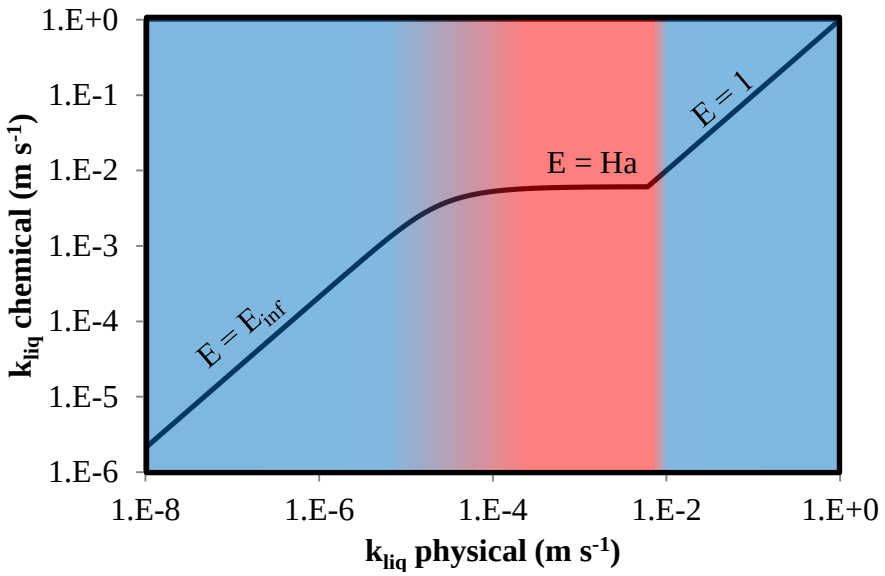

Figure 4: Chemical mass transfer coefficient as a function of physical mass transfer coefficient for 30 wt% MEA at 25 °C and 15 kPa CO_2 partial pressure.

The first case describes the absorption of CO_2 with a gas partial pressure of 15 kPa into 30 wt% MEA solution at 25 °C, where the physical mass transfer coefficient is changed. The effect of changing the physical mass transfer k_{liq0} on the chemical mass transfer ($k_{liq} = k_{liq0} \cdot E$) is shown in Figure 4. The blue areas are regions where the mass transfer is dependent on physical parameters and the red area, where the mass transfer is dependent on chemical parameter (reaction kinetics). The physical mass transfer coefficient in columns can be changed with the liquid flowrate. A higher liquid flowrate results in higher liquid velocities which increase the physical mass transfer coefficient. On film theory basis this can be explained as the laminar film thickness at the interface becomes smaller at higher velocities.

Starting at very low k_{liq0} values the physical and chemical mass transfer coefficients are rising equally. The mass transfer is thus dependent on the physical parameters in that region. The solvent reaction is only indirectly influencing the mass transfer, because the reaction rate is so high that the Enhancement factor is at its maximum value described in Eq. (2.42). Thus the mass transfer in this area becomes:

$$\frac{N_{CO_2}^{\infty}}{a_{eff}} = \frac{\left(P_{CO_2}^{gas} - H_{CO_2} \cdot C_{CO_2}^{liq}\right)}{\frac{1}{k_{CO_2}^{gas}} + \frac{H_{CO_2}}{k_{liq0} \cdot E_{\infty}^{film}}} \tag{2.43}$$

When the physical mass transfer coefficient is further increased there will be no increase in chemical mass transfer anymore. The mass transfer becomes solely dependent on the reaction kinetics of the solvent with CO_2. This is the pseudo-first order reaction regime. The pseudo-first order reaction region occurs in CO_2 absorption when the concentration of solvent is not changed in the film and the bulk solvent concentration is equal to the interface solvent concentration. The Enhancement factor for the pseudo-first order reaction regime is equal to the Hatta number. Inserting this expression into the mass transfer equation leads to:

$$\frac{N_{CO_2}^{ps.1}}{a_{eff}} = \frac{\left(P_{CO_2}^{gas} - H_{CO_2} \cdot C_{CO_2}^{liq}\right)}{\frac{1}{k_{CO_2}^{gas}} + \frac{H_{CO_2}}{\sqrt{k_{sol} \cdot C_{sol} \cdot D_{CO_2}}}} \tag{2.44}$$

The mass transfer under these conditions becomes independent from the physical mass transfer coefficient k_{liq0}, and is kinetically controlled. The liquid side mass transfer can then just be changed by influencing the reaction rate or diffusivity of CO_2. When further increasing the physical mass transfer, at some point the chemical mass transfer coefficient increases again. In that area the chemical and physical mass transfer coefficient are equal and the Enhancement factor has the value one. The highest mass transfer can be achieved theoretically at very high k_{liq0} values, but the range of physical mass transfer coefficients is limited, as the column will flood at some point and the liquid velocity might not be increased further. The range in which k_{liq0} can be varied in a real feasible process is much more narrow. Most of the processes are carried out in the area between infinite fast reaction and pseudo-first order reaction, thus are influenced by the physical and chemical parameters.

Considering another case of a very slow absorbing solvent like 30 wt% MDEA at 25 °C with 15 kPa CO_2 gas partial pressure and looking at the effect of a catalyst addition a different trend is obtained as shown in Figure 5. At a very low catalyst concentration the chemical liquid side mass transfer coefficient is not influenced by the physical liquid side mass transfer coefficient, as the Enhancement factor is around one and the solvent behaves like a physical solvent. When the catalyst concentration is increased at some point the chemical mass transfer coefficient rises and becomes linearly dependent on the catalyst concentration. This is the pseudo-first order regime, and the slope of the increase is the square root of the catalyst concentration. At some point a further increase in catalyst concentration does not influence the mass transfer anymore. The reaction is then close to instantaneous and the Enhancement factor has its maximum value. The mass transfer in that region is again dependent on the physical parameters.

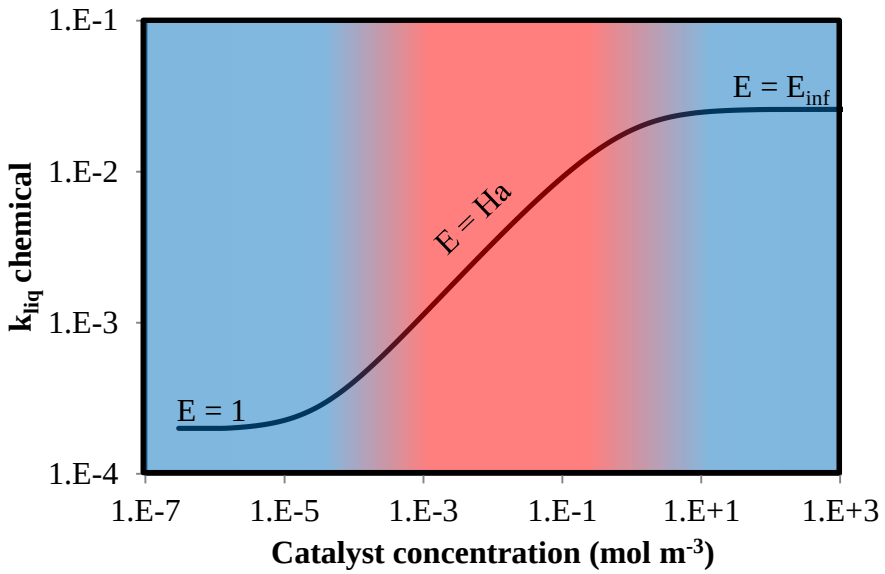

Figure 5: Chemical mass transfer coefficient as a function of catalyst concentration coefficient for 30 wt% MDEA at 25 °C and 15 kPa CO_2 partial pressure for k_{liq0} of 0.0001 m s^{-1}.

The mass transfer leaves the area of pseudo-first order behavior, when the reaction is so fast or the diffusion of solvent molecules from the bulk is so slow that the bulk and interface solvent concentration differs.

The pseudo-first order approximation is just valid for Ha lower than $0.2 \cdot E_{\infty}^{film}$ [6]. The Enhancement factor for the transition zone between pseudo-first order reaction and instantaneous reaction zone needs to be solved numerically, because the bulk and interface concentration of the solvent are different, but the interface value remains unknown.

Van Krevelen and Hoftijzer [13] derived an implicit approximation of the Enhancement factor of a second order irreversible reaction by:

$$E = \frac{Ha\sqrt{\frac{E_{\infty}^{film} - E}{E_{\infty}^{film} - 1}}}{\tanh\left(Ha\sqrt{\frac{E_{\infty}^{film} - E}{E_{\infty}^{film} - 1}}\right)} \tag{2.45}$$

This equation needs to be solved iteratively. A good starting point for the iteration is using the Ha number as Enhancement factor similar to pseudo first order reaction.

Gaspar and Fosbøl [14] derived a general model for the Enhancement factor, called GM model, which is set up for reversible (m+n) order reactions. This model was applied to the reversible CO_2-MEA-H_2O

second order system for absorption, desorption and reversible pinch/non-pinch conditions and showed that it was capable of describing the rigorous two film model within 2 % accuracy with an average deviation of less than 0.5 %. They set up several bridging relations between the interfacial and the bulk concentration for the reactants A and B, as well as the products C and D and deduced the system to a single algebraic equation:

$$E = Ha\sqrt{y_B^{int}}\,\frac{1-y_A^*}{1-y_A^b} \tag{2.46}$$

with y_A^*, y_A^b and y_B^{int} being dimensionless compositions defined as:

$$y_A^* = \frac{y_A^b \cdot y_C^{int} \cdot y_D^{int}}{y_B^{int}}; y_A^b = \frac{C_A^b}{C_A^{int}}; y_B^{int} = \frac{C_B^{int}}{C_B^b} \tag{2.47}$$

The ratio of interfacial and bulk solvent concentration y_B^{int} can be calculated from:

$$\left(1-E_{film}^{\infty}\right) y_B^{int} + Ha\left(y_A^* - 1\right)\sqrt{y_B^{int}} + E_{film}^{\infty} - y_A^b = 0 \tag{2.48}$$

The Enhancement factor E can be calculated by iteratively solving Eq. (2.46) and (2.48) [14].

2.5.2. Parallel reactions

The cases explained above assumed that only a single reaction with CO_2 occurs in the liquid film. An overall reaction in the aqueous media of an amine solutions consists of several parallel reactions, but in most cases a dominating reaction can be identified and an apparent reaction rate constant can be derived for this reaction incorporating the other reactions. In activated solvents with promoters and in highly loaded solvents these assumptions might be inaccurate; therefore expressions of the Enhancement factor for parallel reactions are needed. Most suitable is an expression of the overall Enhancement factor as a function of two or more single Enhancement factors for each reaction [15].

Due to the complexity and number of influencing parameters only Enhancement factors for parallel non-interacting reactions can be derived. The different reactions can be linked with thermodynamic relations but no kinetics in the interaction can be accounted for. For the reversibility of parallel reactions up to now just one expression for the Enhancement factor for first order reactions can be found in literature [16].

Three asymptotic behaviors can be seen for parallel non interacting second order reactions. The first treats the case of very low kinetics and is therefore of no interest for this study. The second case treats the case of first order approach where both reactions are in pseudo-first order. The Enhancement factor

for the overall mass transfer can be calculated under these conditions from the single Enhancement factors as [17]:

$$E_{ov}^{ps.1} = \sqrt{\sum_i E_i^2} \tag{2.49}$$

In the third case the reactions are instantaneous, the overall Enhancement factor can be calculated according to [18]:

$$E_{ov}^{\infty} = \sum_i \left(E_i^{\infty} - 1 \right) + 1 \tag{2.50}$$

For the latter cases in this work the expression from Eq. (2.49) will be used, when parallel reactions are considered as it is assumed that the pseudo first order approach is closer to the experimental case than the instantaneous reaction.

Nomenclature

Symbols:	
a_{eff}	Mass transfer area (m^2)
C_i^j	Concentration of i in position j (mol m^{-3})
D_A	Diffusivity (m^2 s^{-1})
E	Enhancement factor E (-)
H_{CO_2}	Partition coefficient (Pa m^3 mol^{-1})
Ha	Hatta number
J_A	Diffusion flux of compound A per unit area (mol m^{-2} s^{-1})
j_A	Diffusion flux of compound A total (mol s^{-1})
k_{AB}	Second order reaction rate constant for reaction A+B (m^3 mol^{-1} s^{-1})
K_{eq}	Equilibrium constant
$k_{CO_2}^{gas}$	Gas side mass transfer coefficient (mol Pa^{-1} m^{-2} s^{-1})
$k_{CO_2}^{liq}$	Liquid side mass transfer coefficient (m s^{-1})
$k_{CO_2}^{liq\ '}$	Liquid side mass transfer coefficient (mol Pa^{-1} m^{-2} s^{-1})
$k_{CO_2}^{liq0}$	Physical liquid side mass transfer coefficient (m s^{-1})
$K_{CO_2}^{ovG}$	Overall gas mass transfer coefficient (mol Pa^{-1} m^{-2} s^{-1})
$K_{CO_2}^{ovL}$	Overall liquid mass transfer coefficient (m s^{-1})
P_i^j	Partial pressure of i at position j (Pa)
R_A	Reaction rate per volume (mol m^{-3} s^{-1})
r_A	Reaction rate total (mol s^{-1})
s	Propability distribution for the fluid elements in surface renewal theory (s^{-1})
V_r	Reaction volume (m^3)
Greek symbols:	
γ_{sol}	Reaction stoichiometric coefficient for CO_2 reaction (-)
ϕ	Hatta modulus, Hatta number Ha (-)
τ	Penetration time in Penetration theory (s)
δ	Film thickness in film theory (m)
ν_i	Reaction stoichiometric coefficient (-)
Super-subscripts:	
Bulk	Fluid bulk
Ps.1	Pseudo-first order
int	Interface

BIBLIOGRAPHY

[1] M. L. Michelsen and J. M. Mollerup, *Thermodynamic Models: Fundamentals & Computational Aspects*. Tie-line publications, 2007.

[2] P. V. Danckwerts, *Gas-Liquid Reactions*, 1st ed. McGraw-Hill, 1970.

[3] T. K. Sherwood, R. L. Pigford, and C. R. Wilke, *Mass Transfer*, 1st ed. McGraw-Hill, 1975.

[4] B. Bird, W. E. Stewart, and E. N. Lightfoot, *Transport Phenomena*, 2nd ed. Wiley & Sons, 2000.

[5] K. R. Westerterp, W. P. M. van Swaaij, and A. A. C. M. Beenackers, *Chemical Reactor Design and Operation*, 2nd ed. John Wiley & Sons Ltd., 1987.

[6] O. Levenspiel, *Chemical Reaction Engineering*, 3rd ed. John Wiley & Sons Ltd., 1999.

[7] E. Y. Kenig, L. Kucka, and A. Gorak, "Rigorous modeling of reactive absorption processes," *Chem. Eng. Technol.*, vol. 26, no. 6, pp. 631–646, 2003.

[8] W. K. Lewis and W. G. Whitman, "Absorption symposium," *Ind. Eng. Chemnisty*, vol. 16, no. 12, pp. 1215–1220, 1924.

[9] P. V. Danckwerts, "Significance of Liquid-Film Coefficients in Gas Absorption," *Ind. Enguneering Chem.*, vol. 43, no. 6, pp. 1460–1467, 1951.

[10] G. F. Versteeg, L. A. J. . van Dijck, and W. P. M. van Swaaij, "On the Kinetics between CO_2 and Alkanolamines both in aqueous and non-aqueous solutions. An overview," *Chem. Eng. Commun.*, vol. 144, pp. 113–158, 1996.

[11] C. Huang and C. Kuo, "General Mathematical Model for Mass Transfer Accompanied by Chemical Reaction," *AIChE J.*, vol. 9, no. 2, pp. 161–167, 1963.

[12] C. Huang and C. Kuo, "Mathematical Model for Mass Transfer Accompanied by Reversible Chemical Reaction," *AIChE J.*, vol. 9, no. 2, pp. 161–167.

[13] D. W. van Krevelen and P. J. Hoftijzer, "Kinetics of Gas-Liquid reaction-Part1. General Theory," *RECUIL*, vol. 47, pp. 563–586, 1948.

[14] J. Gaspar and P. L. Fosbøl, "A general enhancement factor model for absorption and desorption systems: A CO_2 capture case-study," *Chem. Eng. Sci.*, vol. 138, pp. 203–215, 2015.

[15] J. Gaspar and P. L. Fosbøl, "Practical Enhancement Factor Model based on GM for Multiple Parallel Reactions: Piperazine (PZ) CO_2 Capture," *Chem. Eng. Sci.*

[16] K. Y. Li, H. Kuo, and J. L. jr. Weeks, "Mass Transfer Accompanied By Parallel Reversible Chemical Reactions," *Can. J. Chem. Eng.*, vol. 52, 1974.

[17] W. P. M. van Swaaij and G. F. Versteeg, “Mass transfer accompanied with complex reversible chemical reactions in gas-liquid systems: an overview,” *Chem. Eng. Sci.*, vol. 47, no. 13–14, pp. 3181–3195, 1992.

[18] C. S. Chang and G. T. Rochelle, “Mass transfer enhanced by equilibrium reactions,” *Ind. Eng. Chem. Fundam.*, vol. 21, no. 4, pp. 379–385, 1982.

3. Chemical solvents

This chapter gives as brief introduction into the topic of carbon capture solvents in chemical absorption processes. The solvent is referred to be the water soluble substance whereas the mixture of solvent and water is referred to as liquid phase or solution. The characteristics of the different solvent types are compared and physical properties relevant to mass transfer of the liquid phase are discussed. The CO_2 solubility in the solution for relevant solvents at different process conditions are compared and evaluated applying the extended UNIQUAC thermodynamic model.

3.1. Properties for an ideal solvent for CCS

In chemical absorption processes carbon dioxide is physically absorbed by the solution and then undergoes a quick chemical reaction with the solvent. In a normal process outline the solvent enters the column in the top and leaves it of the bottom. Sometimes it already contains some amount of CO_2 or CO_2 reaction products before entering; this amount is generally referred to the lean loading of the solvent and is mostly depending on the regeneration conditions. After absorbing CO_2 in the column the liquid leaves the column with a CO_2 "rich" loading. As the reaction between solvent and CO_2 are stoichiometric the loading is generally expressed as mole of CO_2 bound, by any reaction product, per mole of solvent. The difference between rich and lean loading is determining the amount of solvent needed for the capture process because it describes the amount of CO_2 the solvent takes up once it is running through the column; this value is called solvent capacity, which can be either referenced to the amount of solvent in mol or the mass of solution in kg. A high capacity results in a low solvent circulation rate. The actual amount of circulated liquid is dependent on the molecular weight of the solvent, and a low molecular weight is favorable as the molar concentration is higher for the same weight fraction. For comparison in an aqueous solution the molar concentration of the solvent in solution of 30 wt% MEA is almost double that of 30 wt% MDEA. The lean and rich loading of the solvent and thus the capacity are dependent on the thermodynamics of the solution which define the speciation of CO_2 and CO_2 reaction products as well as the bubble pressure of the different compounds. In general the "chemical" solubility of CO_2 in the solution (not to be mistaken with the physical solubility described by the Henry's law) describing the amount of CO_2 and all various reaction products thereof dissolved in the solution is increasing with the partial pressure of CO_2 in the gas phase and decreasing with higher temperature.

The solvent should provide high mass transfer and thus requires high reaction kinetics in order to keep the size of the equipment small. As these reactions need to be reversed in the regeneration step (desorption) the heat of absorption should be low[1]. A high heat of absorption also increases the

[1] Even though the energy is needed for desorption of CO_2, it is mostly referred to as heat of absorption, which describes the heat needed or heat generated for CO_2 to change between gas and liquid phase.

temperature inside the absorber column during the absorption, which will lead to a decrease in chemical CO_2 solubility and solvent capacity. Although some authors claim that a high heat of absorption is favorable [1], [2]. The main point for their argument is that the energy input in the desorber is needed for three different reasons: reversing of the reactions, generating water vapor to increase the driving force and heating up of the liquid from the inlet to boiling conditions in the reboiler. While the last energy requirement is the smallest and might be roughly similar for different solutions, as it depends on the ΔT in the cross heat exchanger, the other two are strongly interrelated [3]. The focus should not be solely put on the heat of absorption, leaving the latent heat loss, due to CO_2 and water vapor leaving the absorber out. According to van't Hoff's equation, the change in the equilibrium constant is linked to the enthalpy of absorption. Thus a higher enthalpy or heat of absorption results in a larger change of CO_2 equilibrium partial pressure with temperature, which means less water vapor exiting the desorber and reducing latent heat loss. The overall conclusion is not clear, as the energy demand is very closely linked to the process itself and process conditions [4]. In general solvents with high heat of reaction should be stripped at higher pressures whereas desorption for solvents with low heat of reaction should be carried out at lower pressure [2].

The solvent should also have a low viscosity which reduces the pumping costs and increases heat transfer in the cross heat exchanger [5]. Low viscosity is also beneficial to the diffusivity of CO_2 as the diffusion of CO_2 relies on the solvent viscosity [6].

Solvent losses can be minimized choosing a solvent with a low degradation tendency and low volatility. Therefore the solvents should be thermally stable and not produce volatile organic compounds (VOC) or react with fluegas impurities.

3.2. Solvent types for CO_2 absorption

Solutions in chemical absorption processes are generally mixtures of organic compounds or alkaline salts with water. The group of alkanolamines, chemical derivates of ammonia containing an alcohol group, stands out as solvents, as the hydroxyl reduces the vapor pressure and increases the water solubility whereas the amine groups are active for reacting with the carbon dioxide [7]. The name of this group is often shortened and referred to as amines. The chemical structures of different solvent molecules that are applied in gas cleaning are shown in Figure 6. The group of amines is distinguished by the number of substituents on the nitrogen. monoethanolamine (MEA) is a primary amine, piperazine (PZ) a secondary (di-)amine and N-methyldiethanolamine (MDEA) is a tertiary amine. 2-amino-2-methylpropan-1-ol (AMP) is also considered a primary amine, but because of the substituent on the α-C-atom, this amine belongs to the group of sterically hindered amines [8].

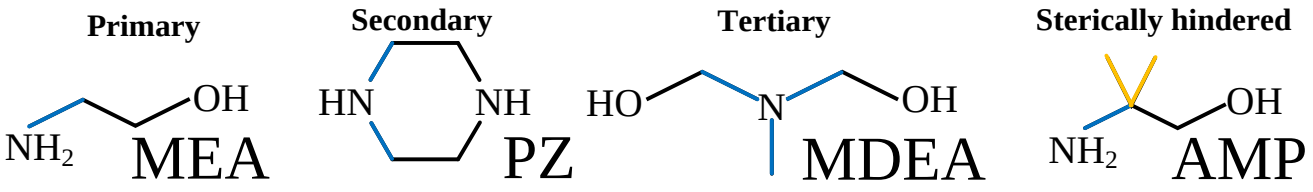

Figure 6: Chemical structure of different amine types

3.2.1. Primary/secondary amines

Primary amines and secondary amines have either one (primary) or two (secondary) substituent(s) on their nitrogen group. This allows these groups of amines to attack the physically bound CO_2 directly forming a covalent bond. The reaction mechanism is not totally clear on molecular basis [9], as there are two possibilities: a ter-molecular mechanism involving two amine molecules and CO_2 or a two-step mechanism as described in Eqs. (3.1) and (3.2). In the first reaction of the two step mechanism the amine is reacting directly with the carbon dioxide forming an instable zwitterion (3.1). A buffer molecule from the solution, which can be either water, hydroxide or another amine, withdraws the proton from the zwitterion in the second step, described in Eq. (3.2).

Nonetheless which mechanism is taking place on molecular level, both suggested mechanisms result in the same product: a carbamate ion and a protonated buffer. The protonated buffer molecule is mainly another amine molecule as the alkaline nature makes the amine a perfect proton acceptor.

$$CO_2 + AmH \underset{k_{-Am}}{\overset{k_{Am}}{\rightleftharpoons}} AmH^+COO^- \tag{3.1}$$

$$AmH^+COO^- + B \underset{k_{-B}}{\overset{k_B}{\rightleftharpoons}} AmCOO^- + BH^+ \tag{3.2}$$

The overall forward reaction rate of the amine can be described with k_{Am} and k_B (m^3 mol^{-1} s^{-1}), the second order rate constant of the amine and the buffer, as well as the concentrations of amine, CO_2 and buffer C_{Am}, C_{CO_2} and C_B (mol m^{-3}) respectively:

$$r_{CO_2} = \frac{k_{Am} \cdot C_{Am} \cdot C_{CO_2}}{1 + \frac{k_{-Am}}{k_B \cdot C_B}} \tag{3.3}$$

If the zwitterion formation is the rate-limiting step and the deprotonation reaction is much faster than the reverse reaction, which is the case for aqueous MEA solution [10] the second term in the denominator becomes very small the forward reaction rate can be expressed as:

$$r_{CO_2} = k_{Am} \cdot C_{Am} \cdot C_{CO_2} \tag{3.4}$$

The direct reaction mechanism of the primary/secondary amines results in higher reaction rates compared to other groups [11]. High reaction rates are linked to high heats of reaction [12] that have to be reversed in the desorption step. The most prominent representatives of these groups are monoethanolamine (MEA) and piperazine (PZ).

The two-step mechanism can explain to some extent why the maximum loading of primary/secondary amines is considered to be limited to 0.5 mol CO_2 per mol amine. When the zwitterion is deprotonated by the amine, all amine molecules have reacted at a loading of 0.5. This is valid for a 30 wt% MEA solution at 40 °C and a partial pressure of CO_2 in the gas of about 10 kPa. But as the partial pressure in the gas rises, higher loadings can be achieved. Then the carbamate is then hydrolyzed producing bicarbonate and restoring the amine. In highly diluted amine solutions loadings higher than 0.5 can be achieved even at 10 kPa CO_2 partial pressure [13].

3.2.2. Tertiary amines

Contrary to primary/secondary amines, tertiary amines with their three substituents on the nitrogen group cannot react directly with the CO_2 molecule. Experiments with non-aqueous MDEA proved that there is no direct mechanism [14]. The reaction rate in solutions with tertiary amine solvents is higher than just the reaction of OH^- ions present. Therefore a base catalysis from the tertiary amine is assumed, leading to the following reaction mechanism [10]:

$$CO_2 + Am + H_2O \rightleftarrows HCO_3^- + AmH^+ \tag{3.5}$$

This indirect reaction mechanism is the reason why the reaction kinetics of tertiary amines is much slower than that of primary/secondary amines [11]. The reaction rate of a tertiary amine with CO_2 can be expressed with the same equation as for primary amine in Eq. (3.4). Several studies have shown that solutions containing bicarbonate can be stripped to a higher extent and need less energy input for regeneration [12][15].

3.2.3. Sterically hindered amines

Sterically hindered amines are characterized by their substituent on the α-C-atom. They follow a reaction mechanism according to their amine structure whether they are primary/secondary amines or tertiary amines. Their steric hindrance results in unstable carbamates that are subsequently hydrolyzed [15]. A primary sterically hindered amine such as AMP (2-amino-2-methyl-1-propanol) reacts as described in Eqs. (3.1) and (3.2) following a hydrolyzing step of the unstable carbamate to regain a solvent molecule and from a bicarbonate:

$$AmCOO^- + H_2O \rightleftarrows HCO_3^- + AmH \tag{3.6}$$

3.2.4. Carbonate salt solutions

The most prominent representatives of the group of carbonate salt solutions are Na_2CO_3 and K_2CO_3. The absorption kinetics into carbonate salt solutions is generally lower than that of primary and secondary amines [16]. The non-volatility and thermal and chemical stability together with the low heat of absorption are some of the advantages carbonate solutions [7].

The overall reaction in a carbonate salt solution can be described as [17]:

$$CO_3^{2-} + H_2O + CO_2 \rightleftarrows 2HCO_3^- \tag{3.7}$$

This overall reaction can be divided into the following two reactions:

$$CO_2 + OH^- \rightleftarrows HCO_3^- \tag{3.8}$$

$$HCO_3^- + OH^- \rightleftarrows CO_3^{2-} + H_2O \tag{3.9}$$

As the second of these reactions (Eq. (3.9)) is a simple proton transfer its reaction speed is much faster making Eq. (3.8) the rate limiting step [17]. The kinetics of this reaction can be described with a second order reaction rate for the forward reaction:

$$r_{CO_2} = k_{OH^-} \cdot C_{OH^-} \cdot C_{CO_2} \tag{3.10}$$

The second order rate constant k_{OH^-} (m^3 $kmol^{-1}$ s^{-1}) itself is a function of the ionic strength of the solution and can be described with a rate constant for infinite dilution $k_{OH^-}^{\infty}$ (m^3 $kmol^{-1}$ s^{-1}) and an ion contribution term [18] dependent on the ion concentration [19] according to:

$$\log \frac{k_{OH^-}}{k_{OH^-}^{\infty}} = \sum b_{ion} \cdot I_{ion} \tag{3.11}$$

with:

$$\log k_{OH^-}^{\infty} = 11.916 - \frac{2382}{T} \tag{3.12}$$

and b_{ion} (m^3 $kmol^{-1}$) being the ion specific contribution parameter that is reported by Pohorecki and Moniuk[19].

3.2.5. Reactions in aqueous media

The solvents are mixed with water, resulting in a more complex reaction mechanism as water and its ionic species also react with CO_2 according to the following steps:

$$CO_2 + H_2O \rightleftarrows H_2CO_3 \tag{3.13}$$

$$CO_2 + OH^- \rightleftarrows HCO_3^- \tag{3.14}$$

The contribution of reaction (3.13) to the overall reaction can be neglected for aqueous amine solutions according to Pinsent et al.[20].

In an absorption process into an aqueous solvent solution the different compounds are reacting with CO_2 in parallel, the overall reaction rate can be described as:

$$r_{CO_2} = k_{OH^-} \cdot C_{OH^-} \cdot C_{CO_2} + k_{Am} \cdot C_{Am} \cdot C_{CO_2} + k_{H_2O} \cdot C_{H_2O} \cdot C_{CO_2} \tag{3.15}$$

3.3. Solvent properties

The most important solvent properties are density, viscosity and physical solubility of solvents. Kinetic constants can be derived from absorption data just when the experimental data is treated with the valuable solvent properties.

3.3.1. Density

The density of a solution, which relates the mass of a body to its volume, is needed to convert mass/molar fractions to molar concentration units. Weiland et al.[21] measured the density of unloaded and partially loaded amine solutions and correlated the density in the following form as ratio of average molecular weight and total volume:

$$\rho = \frac{x_{Am} \cdot M_{Am} + x_{H_2O} \cdot M_{H_2O} + x_{CO_2} \cdot M_{CO_2}}{x_{Am} \cdot V_{Am} + x_{H_2O} \cdot V_{H_2O} + x_{CO_2} \cdot V_{CO_2} + x_{Am} \cdot x_{H_2O} \cdot V^* + x_{Am} \cdot x_{CO_2} \cdot V^{**}} \tag{3.16}$$

With x_i being the molar-fraction, and V_i the molar volume of the different solvent compounds. The non-ideality of the density is accounted for with an interaction parameter for water-amine interaction V^* and for CO_2-amine interaction V^{**}. The molar volume and amine-CO_2 interaction parameter can be calculated from constants given by Weiland [21]:

$$V_A m = M_A m / (aT^2 + bT + c); V^{**} = d + e x_A m \tag{3.17}$$

These constants were determined for MEA, DEA and MDEA. This method can be used to determine solvent loading by measuring density when the solvent concentration is known. For the density of carbonate salt solutions a electrolyte model as proposed by Laliberte and Cooper can be used [22].

3.3.2. Viscosity/Diffusivity

The diffusivity of CO_2 in the solvents cannot be determined experimentally because the reactions are influencing the mass transfer. A widely applied method for estimating the diffusivity is the use of the N_2O analogy [23]. Therefore the diffusion of N_2O, a molecule with a similar shape but non-reacting in solutions is measured in water and the solvent mixture at the desired temperature. The diffusivity of CO_2 in the solution can then be related to the diffusivity of CO_2 in water with the following expression [10]:

$$D_{CO_2}^{sol} = D_{N_2O}^{sol} \frac{D_{CO_2}^{H_2O}}{D_{N_2O}^{H_2O}} \tag{3.18}$$

Ko et al. measured the diffusivity of N_2O in several amine solvent solutions among them MEA, MDEA and AMP and derived a temperature and solvent concentration dependent correlation for the diffusivity [24].

In case N_2O diffusivity data is not available for that solution, the CO_2 diffusivity can be correlated by the solvent's viscosity, based on a modified Einstein-Stokes type relation:

$$D_{CO_2}^{sol} = D_{N_2O}^{sol} \left(\frac{\mu_{H_2O}}{\mu_{sol}} \right)^{0.8} \tag{3.19}$$

In case no literature values are available for the diffusivity of solvent molecules in solution, it can also be calculated with a modified Einstein Stokes type equation [6]:

$$D_{Am}^{sol} = D_{Am}^{H_2O} \left(\frac{\mu_{H_2O}}{\mu_{sol}} \right)^{0.6} \tag{3.20}$$

The water viscosity can be taken from literature [25], the solvent viscosity can be either measured in a viscositymeter, or a literature correlation like the on by Weiland et al. [21] can be used. Literature correlation of $D_{CO_2}^{sol}$ and $D_{N_2O}^{sol}$ are listed in Versteeg, van Dijck, and van Swaaij [10].

3.3.3. Physical solubility

The solubility correlates the equilibrium between the gas phase and liquid phase at the interface. This value cannot be determined experimentally in reacting systems similar to the diffusivity. A similar N_2O analogy for solubility is used [26]:

$$H_{CO_2}^{sol} = H_{N_2O}^{sol} \frac{H_{CO_2}^{H_2O}}{H_{N_2O}^{H_2O}} \tag{3.21}$$

Some authors argue that the use of this analogy might be limited to much more dilute solutions than that of industrial interest [23], other claim that the values do not vary much from water [27]. Applying this analogy to derive kinetic constants and model mass transfer definitely influences the value of the kinetic constant. The kinetic constant should be therefore just be used together with the physical solubility as well as diffusivity used for the kinetic constant determination.

3.4. Solubility in solvents

The reaction rates are depending on the concentrations of the different educts in the solvent solution. The composition of the solutions is changing with the process conditions such as temperature or gas CO_2 partial pressure. In order to be able to set up the mass transfer equation detailed information of the composition of the phases are needed, which can be provided by a thermodynamic model for the solution.

3.4.1. Extended UNIQUAC model

A reaction is happening spontaneously when the Gibbs free energy of the products becomes lower than the one of the educts. At chemical equilibrium the net reaction rate is zero, thus the Gibbs free energy of product and educt are equal. The van't Hoff equation relates the chemical equilibrium constant, thus the composition of a system, to the temperature:

$$R \cdot T \cdot \ln K = \Delta G^0 = \Delta H_R^0 - T \Delta S^0 \tag{3.22}$$

With ΔG^0 being the change in Gibbs free Energy, ΔH_R^0 being the change in Enthalpy and S^0 the Entropy change. In case the overall reaction of MDEA, a tertiary amine which reacts as described in Eq. (3.5) is considered the overall equilibrium constant can be written as [3]:

$$K = \left(\frac{x_{HCO_3^-} \cdot x_{MDEAH^+}}{\left(p_{CO_2} / p^0 \right) \cdot x_{H_2O} \cdot x_{MDEA}} \right) \cdot \left(\frac{\gamma_{HCO_3^-} \cdot \gamma_{MDEAH^+}}{\phi_{CO_2} \cdot \gamma_{H_2O} \cdot \gamma_{MDEA}} \right) \tag{3.23}$$

In general several reactions take place in aqueous solvents. The reactions are influencing each other as some compounds are present in several possible reactions. For speciation modeling of solvents the main reactions involving all ionic species need to be considered. In case of CO_2 reaction with MDEA in aqueous solution, the following 4 reactions can be considered [28]:

$$\begin{aligned}
&(\mathrm{I}) H_2O \rightleftarrows OH^- + H^+ \\
&(\mathrm{II}) CO_2 + OH^- \rightleftarrows HCO_3^- \\
&(\mathrm{III}) HCO_3^- + OH^- \rightleftarrows CO_3^{2-} + H_2O \\
&(\mathrm{IV}) MDEA + H_2O \rightleftarrows MDEAH^+ + OH^-
\end{aligned} \tag{3.24}$$

Equilibrium is achieved when the chemical potential of the products and educts are equal. Thus the following requirements have to be fulfilled for equilibrium:

$$\begin{aligned}
&(\mathrm{I}) \mu_{H_2O} = \mu_{OH^-} + \mu_{H^+} \\
&(\mathrm{II}) \mu_{CO_2} + \mu_{OH^-} = \mu_{HCO_3^-} \\
&(\mathrm{III}) \mu_{HCO_3^-} + \mu_{OH^-} = \mu_{CO_3^{2-}} + \mu_{H_2O} \\
&(\mathrm{IV}) \mu_{MDEA} + \mu_{H_2O} = \mu_{MDEAH^+} + \mu_{OH^-}
\end{aligned} \tag{3.25}$$

With the chemical potential μ_i of component i defined by its standard state chemical potential μ_i^0 and the components activity a_i, thus the molefraction x_i (-) and symmetrical activity coefficient γ_i or infinite dilution activity coefficient γ_i^∞ and rational unsymmetrical activity coefficient γ_i^* :

$$\mu_i = \mu_i^0 + RT \ln a_i = \mu_i^0 + RT \ln\left(x_i \cdot \gamma_i\right) = \mu_i^0 + RT \ln \gamma_i^\infty + RT \ln\left(x_i \cdot \gamma_i^*\right) \tag{3.26}$$

In case one component is considered to be volatile the following equilibrium between gas and liquid phase has also to be considered for this component:

$$\mu_i^{liq} = \mu_i^{gas} \tag{3.27}$$

For reaction number (IV) this can be expressed as:

$$-\left(\mu_{MDEAH^+} + \mu_{OH^-} - \mu_{MDEA} - \mu_{H_2O}\right) = RT \ln\left(\frac{a_{MDEAH^+} \cdot a_{OH^-}}{a_{MDEA} \cdot a_{H_2O}}\right) = RT \ln\left(\frac{x_{MDEAH^+} \cdot \gamma_{MDEAH^+} \cdot x_{OH^-} \cdot \gamma_{OH^-}}{x_{MDEA} \cdot \gamma_{MDEA} \cdot x_{H_2O} \cdot \gamma_{H_2O}}\right) \tag{3.28}$$

The other reactions (I-III) can be written in a similar way. This might be rewritten as [29]:

$$-\frac{\Delta G_j^0}{RT} = \sum_i v_i^j \ln a_i \tag{3.29}$$

ΔG_j^0 being the increment in standard state Gibbs energy of formation for the process *j* and v_i^j is the stochiometric coefficient for the process j with products having positive and educts having a negative value. When comparing with Eq. (3.22) it can be seen, that the right-hand part of Eq. (3.29) describes the Equilibrium constant. A thermodynamic model for the activity coefficients is needed to describe the influence of temperature, composition and pressure on the equilibrium constant. The extended UNIQUAC model has shown great results in describing the vapor-liquid equilibrium of carbon dioxide capture solvents like MEA [30], MDEA [28] and NH_3 [31]. Even solid-liquid-vapor equilibria (K_2CO_3+PZ) [32] and liquid-liquid-vapor equilibria (MAPA-DEEA) [33] could be modelled.

The basis for that model is the UNIQUAC model, a local composition model proposed by Abrams and Prausnitz [34] which was later extended by a Debye-Hueckel term to be applicable to electrolyte thermodynamics. In the current framework of the Extended UNIQUAC model as described by Thomsen [35], the Excess Gibbs energy, which states deviation from the ideal Gibbs energy for real solutions, consists of three terms: a combinatorial term, an residual term and a electrostatic term:

$$\frac{G^E}{RT} = \left(\frac{G^E}{RT}\right)_{Combinatorial} + \left(\frac{G^E}{RT}\right)_{Residual} + \left(\frac{G^E}{RT}\right)_{Electrostatic} \tag{3.30}$$

The combinatorial excess Gibbs energy, which relates to the entropy, is dependent on relative volume and relative surface area of each component. These values are considered temperature independent and are used in parameter fitting.

The residual excess Gibbs energy term is considering the enthalpy. Temperature dependent energy interaction parameter are regressed from data fitting, the relative surface area from the combinatorial term is also used in the residual term.

The electrostatic excess Gibbs energy, which is a term that is added to the original Uniquac model describes the ion-ion interaction. The extended Debye Hueckel law is used for the long-range interaction between the ions. By partial molar differentiations of the excess Gibbs energy, the activity coefficients are obtained.

3.4.2. CO_2 solubility in MEA

The partial pressure of CO_2 in the exhaust gases from coal fired power plants is between 12-15 kPa. It is therefore of interest how much CO_2 a potential solvent solution can theoretically capture. This value is dependent on the solutions thermodynamics as it can take CO_2 until the equilibrium partial pressure of CO_2 over the solution is as high as the gas CO_2 partial pressure. The equilibrium partial pressure of

CO_2 and thus the solvents' capture capability itself is a function of solvent concentration and temperature. The amount of CO_2 MEA solutions can store when it is in equilibrium with a gas CO_2 partial pressure of 15 kPa is shown in Figure 7. The results are shown as solvent loading, describing the mole of CO_2 per mole of MEA molecule for different solvent concentrations as well as solvent capacity, describing the amount of mole captured per kilogram of solvent solution, where the solution just comprises of solvent and water and does not account for the CO_2 in the liquid phase. It can be seen in Figure 7, that the solvent loading is decreasing with temperature as well as with solvent concentration in a low temperature range, whereas the solvent capacity is decreasing with temperature, but increasing with solvent concentration. This figure shows clearly, that the often reported maximum solvent loading of MEA of 0.5 mol CO_2 per mol MEA is just valid for a 30 wt% MEA solution at 313 K and around 15 kPa CO_2. Whereas a change in one of these process conditions results in higher or lower solvent loading. The solvent capacity is a more crucial process parameter than the solvent's loading, as this value is linked to the liquid's circulation rates. The solutions thermodynamic would suggest a very high solvent concentration for high solvent capacity. This is although not feasible for a real process, as MEA is very corrosive, which makes solvent concentrations above 30 wt% not practicable for the process [7].

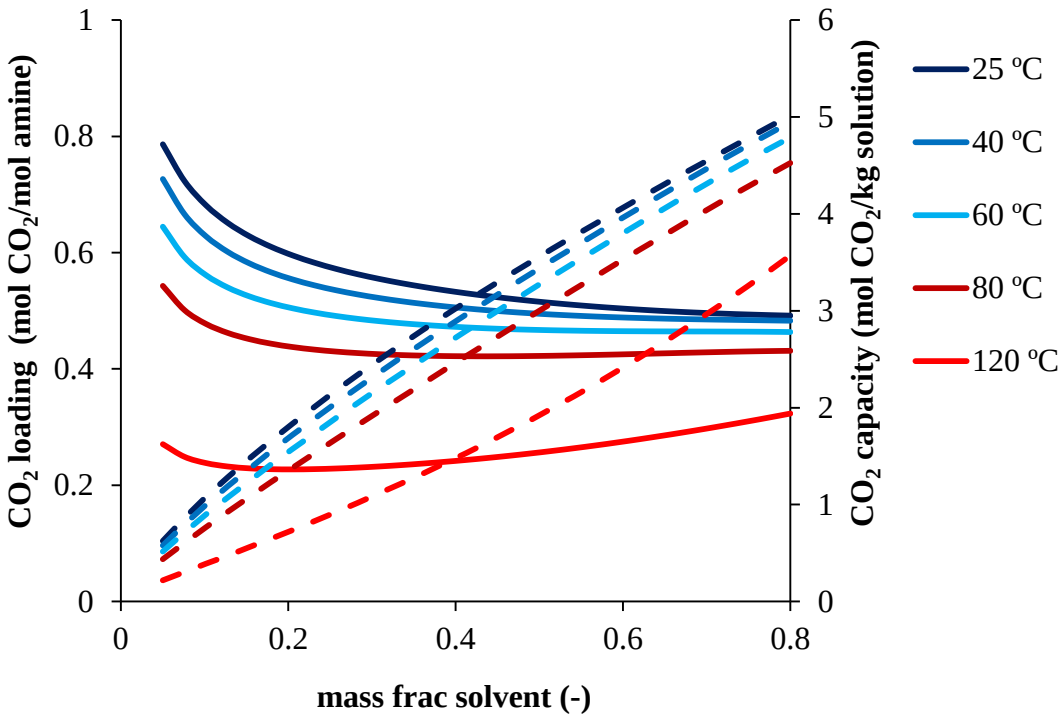

Figure 7: CO_2 loading and CO_2 capacity for MEA solutions at different solvent concentrations for 15 kPa CO_2 gas partial pressure; continuous lines refer to CO_2 loading, dashed lines to CO_2 capacity [30].

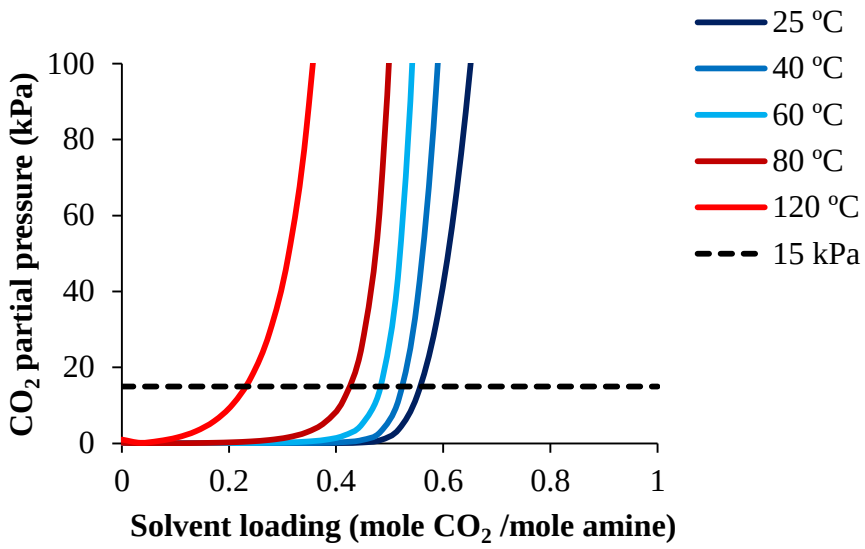

Figure 8: CO_2 loading in 30 wt% MEA solutions as function of CO_2 partial pressure for temperatures between 25 and 120 ºC [30].

Up to now the industrial standard for CCS applications is a 30 wt% MEA solution [1]. The thermodynamics of this solution described as solvent loading as function of equilibrium CO_2 partial pressure are shown in Figure 8. The equilibrium partial pressure of 30 wt% MEA solutions is very dependent on the temperature and rises very fast once a certain solvent loading is reached. The solvent loading of a solution with an equilibrium partial pressure of 100 kPa is just slightly higher than the loading of a solution with 15 kPa equilibrium partial pressure. This means that in order to regenerate that solvent a temperature swing is needed. A pressure swing would not provide benefits unless it would be at complete vacuum. This graph also shows why the lean loading of a 30 wt% MEA solutions is around 0.2-0.25 mole CO_2 per mol MEA. The maximum regeneration temperature of MEA is around 110-120 °C in the desorber otherwise the solvent is degraded rapidly [36]. At this temperature no lower solvent loading can be achieved in the regeneration for 30 wt% MEA.

3.4.3. CO_2 solubility of MDEA

The solvent thermodynamics of the tertiary amine MDEA are very different compared to MEA. The solvent loading and solvent capacity as a function of solvent concentration and temperature are shown in Figure 9. The solvent loading is clearly decreasing with higher temperature and higher solvent concentration. The solvent capacity is peaking at a medium solvent concentration, the maximum is moving towards a lower solvent concentration once the temperature is increased. The solvent capacity of MDEA seems to be much lower than MEA solutions, but cutting out the solution with higher solvent concentrations than 30 wt% which are impracticable will lead to results in the same order of magnitude. The highest solvent capacity can be found for a 45 wt% MDEA solution at 25 °C. At 40 °C

the maximum is around 40 wt% and at 60 °C 35 wt%. Several sources claim the maximum loading for MDEA solutions to be one, because it is a tertiary amine and use this as an argument on how MDEA is a more suitable solvent than MEA with a maximum loading of 0.5. This argumentation is completely wrong for CCS applied to coal fired power plants. A 30 wt% MDEA solution at 40 °C has a lower solvent loading (0.44) than a 30 wt% MEA solution (0.52) at the same temperature when it is in equilibrium with a gas phase with a CO_2 partial pressure of 15 kPa. The solvent capacities between these two solutions are even further apart, as MDEA has a higher molecular weight.

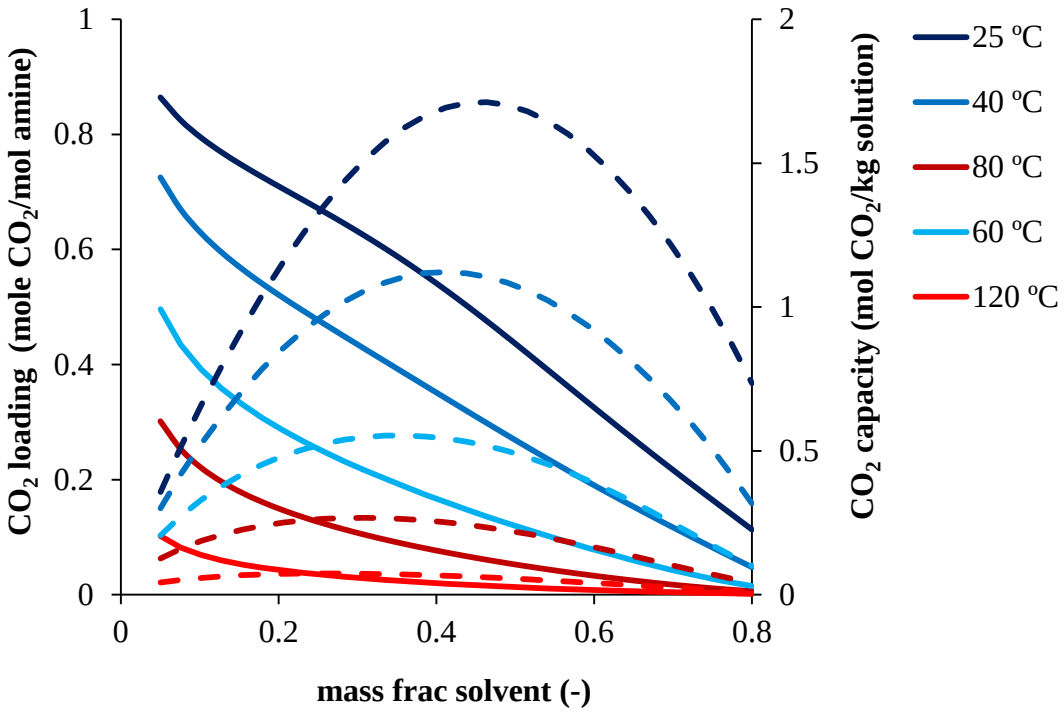

Figure 9: CO_2 loading and CO_2 capacity for MDEA solutions at different solvent concentrations for 15 kPa CO_2 gas partial pressure; continuous lines refer to CO_2 loading, dashed lines to CO_2 capacity [28].

When trying to find arguments for replacing MEA with MDEA rather the possibility to achieve very lean loadings in MDEA solutions should be brought up. The equilibrium partial pressure of CO_2 in MDEA as a function of solvent loading and temperature is shown in Figure 10. The equilibrium loading at 15 kPa is very temperature sensitive for MDEA solutions. At 25 °C almost 0.65 mol CO_2 per mol MDEA can be dissolved in the solution; at 40°C the equilibrium loading is just around 0.44.

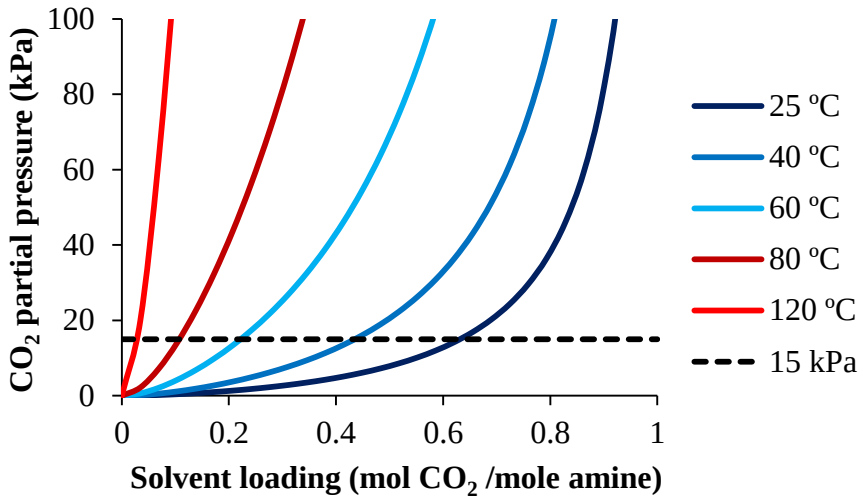

Figure 10: CO_2 loading in 30 wt% MDEA solutions as function of CO_2 partial pressure for temperatures between 25 and 120 °C

Unlike MEA where the solvent loading is not much changing with the equilibrium partial pressure of CO_2, MDEA is showing an influence of solvent loading on equilibrium partial pressure in the range of 0 to 100 kPa especially for low temperatures. Thus a pressure change in the desorber for MDEA solutions can influence the lean loading. The effect of pressure change in the desorber on the energy demand cannot be simply explained by a solubility diagram as shown Figure 8 and Figure 10, as the desorber pressure comprises of the vapor pressure of all volatile compounds inside the desorber, which are mainly water vapor and gaseous CO_2. The solubility diagram of 30 wt% MDEA shows that MDEA solutions can be stripped to very low lean loadings at high temperatures. This is a clear advantage of 30 wt% MDEA over 30 wt% MEA, where the lean loading is limited to around 0.2-0.25 (mol CO_2/ mol amine).

3.4.4. CO_2 solubility of K_2CO_3

The solvent loading profiles and solvent capacities of K_2CO_3 solutions as a function of solvent concentration with an equilibrium partial pressure of 15 kPa at different temperatures are shown in Figure 11. Carbonate salt solutions such as K_2CO_3 form solid precipitates. The trend lines in Figure 11 show just the region without precipitation. When the lines are stopping it is an indication that in that region precipitation occurs. The precipitating region decreases with higher temperature. At around room temperature precipitation might occur somewhere above 20 wt% K_2CO_3. The precipitation limits the range of suitable solvent concentrations especially at lower temperatures. Even though the solvent loadings are high for K_2CO_3 solutions, the capacity is lower than for MDEA and MEA solutions.

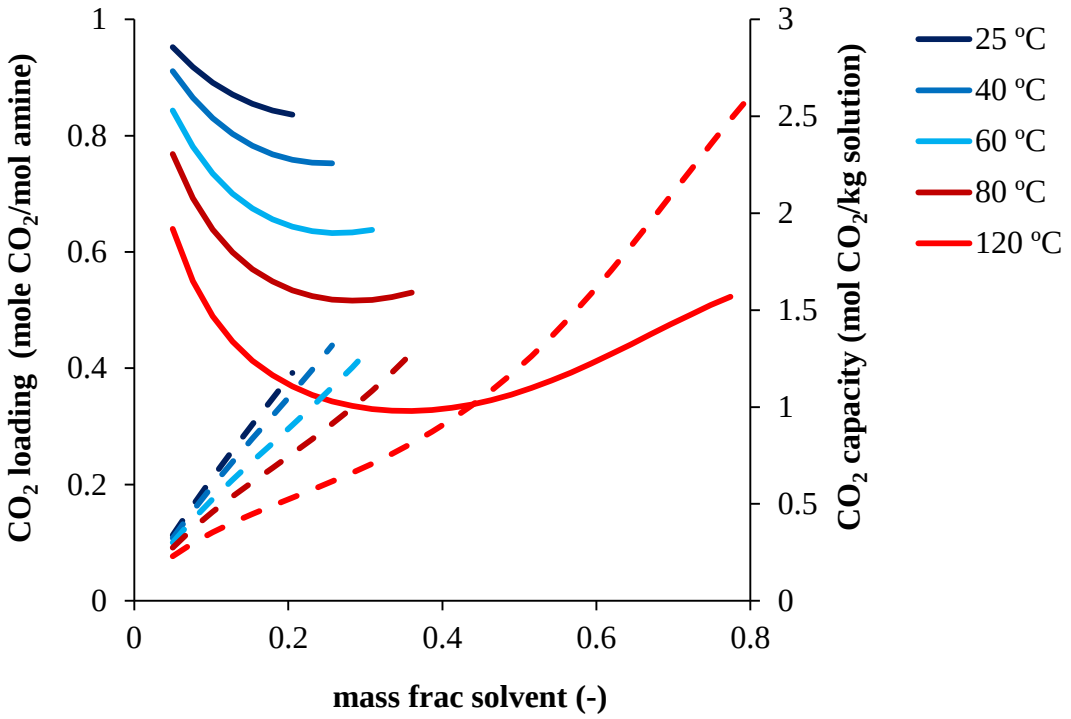

Figure 11: CO_2 loading and CO_2 capacity for K_2CO_3 solutions at different solvent concentrations for 15 kPa CO_2 gas partial pressure; continuous lines refer to CO_2 loading, dashed lines to CO_2 capacity [32]

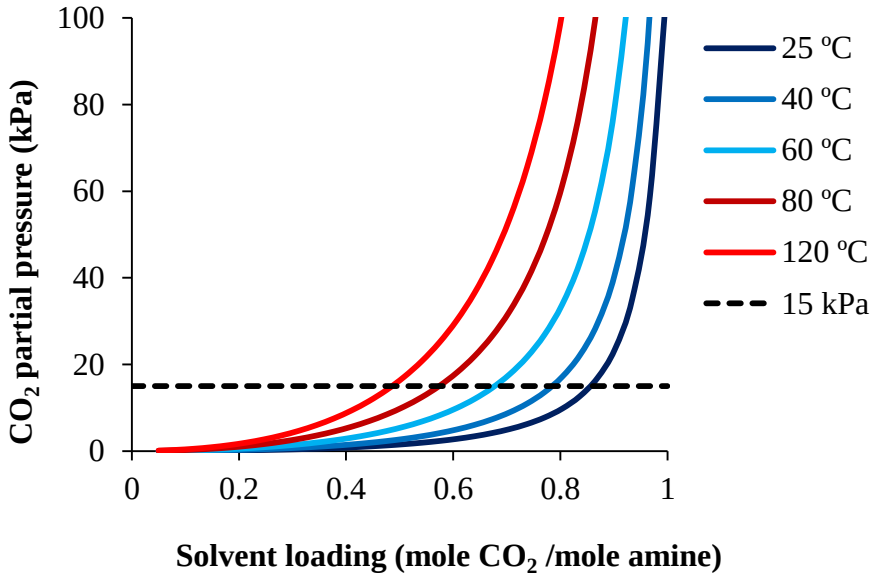

Figure 12: CO_2 loading in 15 wt% K_2CO_3 solutions as function of CO_2 partial pressure for temperatures between 25 and 120 ºC [32].

The equilibrium partial pressures of 15 wt% K_2CO_3 solutions as a function of solvent loading at different temperatures are shown in Figure 12. Even at high temperatures the solvent cannot be regenerated to very low solvent loadings. In the lower pressure range below 30 kPa the solvent loading is influenced by the equilibrium partial pressure. Thus for K_2CO_3 low pressure or vacuum regeneration is an option.

Nomenclature

Symbols:	
C_i	Concentration of i (mol m^{-3})
D_i^{sol}	Diffusion coefficient for i in solutions
G^0	Gibbs free energy
$H_{CO_2}^{sol}$	Partition coefficient (Pa m^3 mol^{-1})
H_R^0	Enthalpy
k_{Am}	Second order rate constant for amines (m^3 mol^{-1} s^{-1})
K	Equilibrium constant
R	Gas constant (J mol^{-1} K^{-1})
r_{CO_2}	Reaction rate of CO_2 (mol s^{-1})
S^0	Entropy
Abbreviations:	
Am	Amine
AMP	2-amino-2-methylpropan-1-ol
DEA	Diethanolamine
MDEA	N-methyldiethanolamine
MEA	Monothethanolamine
PZ	Piperazine
sol	Solution
Greek symbols:	
ρ	Density
μ	Viscosity
μ	Activity
ϕ_{CO_2}	Fugacity coefficient
γ_{H_2O}	Activity coefficient

BIBLIOGRAPHY

[1] G. Rochelle, E. Chen, S. Freeman, D. Van Wagener, Q. Xu, and A. Voice, "Aqueous piperazine as the new standard for CO_2 capture technology," *Chem. Eng. J.*, vol. 171, no. 3, pp. 725–733, 2011.

[2] J. Oexmann and A. Kather, "Minimising the regeneration heat duty of post-combustion CO_2 capture by wet chemical absorption: The misguided focus on low heat of absorption solvents," *Int. J. Greenh. Gas Control*, vol. 4, no. 1, pp. 36–43, 2010.

[3] H. F. Svendsen, E. T. Hessen, and T. Mejdell, "Carbon dioxide capture by absorption, challenges and possibilities," *Chem. Eng. J.*, vol. 171, no. 3, pp. 718–724, 2011.

[4] J. H. Meldon, "Amine screening for flue gas CO_2 capture at coal-fired power plants: Should the heat of desorption be high, low or in between?," *Curr. Opin. Chem. Eng.*, vol. 1, no. 1, pp. 55–63, 2011.

[5] M. E. Boot-Handford, J. C. Abanades, E. J. Anthony, M. J. Blunt, S. Brandani, N. Mac Dowell, J. R. Fernández, M.-C. Ferrari, R. Gross, J. P. Hallett, R. S. Haszeldine, P. Heptonstall, A. Lyngfelt, Z. Makuch, E. Mangano, R. T. J. Porter, M. Pourkashanian, G. T. Rochelle, N. Shah, J. G. Yao, and P. S. Fennell, "Carbon capture and storage update," *Energy Environ. Sci.*, vol. 7, p. 130, 2014.

[6] E. D. Snijder, M. J. M. te Riele, G. F. Versteeg, and W. P. M. van Swaaij, "Diffusion coefficients of several aqueous alkanolamine solutions," *J. Chem. Eng. Data*, vol. 38, no. 3, pp. 475–480, 1993.

[7] A. Kohl and R. Nielsen, *Gas Purification*, 5th ed. Gulf Publishing Company, 1997.

[8] G. Sartori, W. S. Ho, D. W. Savage, G. R. Chludzinski, and S. Wlechert, "Sterically-Hindered Amines for Acid-Gas Absorption," *Sep. Purif. Rev.*, vol. 16, no. November, pp. 171–200, 1983.

[9] D. Eimer, *Gas Treating: Absorption Theory and Practice*, 1st ed. John Wiley & Sons Ltd., 2014.

[10] G. F. Versteeg, L. A. J. . van Dijck, and W. P. M. van Swaaij, "On the Kinetics between CO_2 and Alkanolamines both in aqueous and non-aqueous solutions. An overview," *Chem. Eng. Commun.*, vol. 144, pp. 113–158, 1996.

[11] P. D. Vaidya and E. Y. Kenig, "CO_2-Alkanolamine Reaction Kinetics: A Review of Recent Studies," *Chem. Eng. Technol.*, vol. 30, no. 11, pp. 1467–1474, 2007.

[12] I. Kim and H. F. Svendsen, "Comparative study of the heats of absorption of post-combustion CO_2 absorbents," *Int. J. Greenh. Gas Control*, vol. 5, no. 3, pp. 390–395, 2011.

[13] U. E. Aronu, S. Gondal, E. T. Hessen, T. Haug-Warberg, A. Hartono, K. a. Hoff, and H. F. Svendsen, "Solubility of CO_2 in 15, 30, 45 and 60 mass% MEA from 40 to 120 °C and model representation using the extended UNIQUAC framework," *Chem. Eng. Sci.*, vol. 66, no. 24, pp. 6393–6406, 2011.

[14] G. F. Versteeg and W. P. M. van Swaaij, "On the kinetics between CO_2 and alkanolamines both in aqueous and non-aqueous solutions—II. Tertiary amines," *Chem. Eng. Sci.*, vol. 43, no. 3, pp. 587–591, 1988.

[15] R. J. Hook, "An Investigation of Some Sterically Hindered Amines as Potential Carbon Dioxide Scrubbing Compounds," *Ind. Eng. Chem. Res.*, vol. 36, no. 5, pp. 1779–1790, 1997.

[16] G. Hu, N. J. Nicholas, K. H. Smith, K. A. Mumford, S. E. Kentish, and G. W. Stevens, "Carbon dioxide absorption into promoted potassium carbonate solutions: A review," *Int. J. Greenh. Gas Control*, vol. 53, pp. 28–40, 2016.

[17] H. Knuutila, O. Juliussen, and H. F. Svendsen, "Kinetics of the reaction of carbon dioxide with aqueous sodium and potassium carbonate solutions," *Chem. Eng. Sci.*, vol. 65, no. 23, pp. 6077–6088, 2010.

[18] L. Kucka, E. Y. Kenig, and A. Górak, "Kinetics of the gas-liquid reaction between carbon dioxide and hydroxide ions," *Ind. Eng. Chem. Res.*, vol. 41, no. 24, pp. 5952–5957, 2002.

[19] R. Pohorecki and W. Moniuk, "Kinetics of reaction between carbon dioxide and hydroxyl ions in aqueous electrolyte solutions," *Chem. Eng. Sci.*, vol. 43, no. 1959, pp. 1677–1684, 1988.

[20] B. R. W. Pinsent, L. Pearson, and F. J. W. Roughton, "The Kinetics of Combination of Carbon Dioxide with Hydroxide Ions," *Trans. Faraday Soc.*, vol. 53, no. 1512, p. 160, 1956.

[21] R. H. Weiland, J. C. Dingman, D. B. Cronin, and G. J. Browning, "Density and viscosity of some partially carbonated aqueous alkanolamine solutions and their blends," *J. Chem. Eng. Data*, vol. 43, no. 3, pp. 378–382, 1998.

[22] M. Laliberte and W. E. Cooper, "Model for calculating the density of aqueous electrolyte solutions," *J. Chem. Eng. Data*, vol. 49, no. 5, pp. 1141–1151, 2004.

[23] J. G. M.-S. Monteiro and H. F. Svendsen, "The N_2O analogy in the CO_2 capture context: Literature review and thermodynamic modelling considerations," *Chem. Eng. Sci.*, vol. 126, pp. 455–470, 2015.

[24] J. J. Ko, T. C. Tsai, C. Y. Lin, H. M. Wang, and M. H. Li, "Diffusivity of nitrous oxide in aqueous alkanolamine solutions," *J. Chem. Eng. Data*, vol. 46, no. 1, pp. 160–165, 2001.

[25] J. Kestin, M. Sokolov, and W. A. Wakeham, "Viscosity of liquid water in the range −8 °C to 150 °C," *J. Phys. Chem. Ref. Data*, vol. 7, no. 3, p. 941, 1978.

[26] G. J. Browning and R. H. Weiland, "Physical Solubility Of Carbon Dioxide In Aqueous Alkanolamines Via Nitrous Oxide Analogy," *J. Chem. Eng. Data*, vol. 39, no. 4, pp. 817–822, 1994.

[27] G. Puxty and M. Maeder, "The fundamentals of post-combustion capture," in *Absorption-Based Post-Combustion Capture of Carbon Dioxide*, 1st ed., P. H. M. Feron, Ed. Elsevier Ltd, 2016, p. 814.

[28] N. Sadegh, E. H. Stenby, and K. Thomsen, "Thermodynamic modeling of CO_2 absorption in aqueous N-Methyldiethanolamine using Extended UNIQUAC model," *Fuel*, vol. 144, pp. 295–306, 2015.

[29] K. Thomsen and P. Rasmussen, "Modeling of vapor - liquid - solid equilibrium in gas - aqueous electrolyte systems," *Chem. Eng. Sci.*, vol. 54, pp. 1787–1802, 1999.

[30] L. Faramarzi, G. M. Kontogeorgis, K. Thomsen, and E. H. Stenby, "Extended UNIQUAC model for thermodynamic modeling of CO_2 absorption in aqueous alkanolamine solutions," *Fluid Phase Equilib.*, vol. 282, no. 2, pp. 121–132, 2009.

[31] V. Darde, W. J. M. Van Well, E. H. Stenby, and K. Thomsen, "Modeling of Carbon Dioxide Absorption by Aqueous Ammonia Solutions Using the Extended UNIQUAC Model," *Ind. Eng. Chem. Res.*, vol. 49, no. 24, pp. 12663–12674, 2010.

[32] P. L. Fosbøl, B. Maribo-Mogensen, and K. Thomsen, "Solids Modelling and Capture Simulation of Piperazine in Potassium Solvents," *Energy Procedia*, vol. 37, pp. 844–859, 2013.

[33] M. W. Arshad, N. von Solms, and K. Thomsen, "Thermodynamic modeling of liquid-liquid phase change solvents for CO_2 capture," *Int. J. Greenh. Gas Control*, vol. 53, pp. 401–424, 2016.

[34] D. S. Abrams and J. M. Prausnitz, "Statistical Thermodynamics of Liquid-Mixtures - New Expression for Excess Gibbs Energy of Partly or Completely Miscible Systems," *Aiche J.*, vol. 21, no. 1, 1975.

[35] K. Thomsen, "Modeling electrolyte solutions with the extended universal quasichemical (UNIQUAC) model," *Pure Appl. Chem.*, vol. 77, no. 3, pp. 531–542, 2005.

[36] J. Davis and G. Rochelle, "Thermal degradation of monoethanolamine at stripper conditions," *Energy Procedia*, vol. 1, no. 1, pp. 327–333, 2009.

4. Enzymes

This chapter provides an overview of the general principles of enzyme reactions and describes in detail the mechanism for carbonic anhydrase. It also gives an up to date literature review on comparable mass transfer experiments for enzyme enhanced CO_2 capture in lab and in pilot scale.

4.1. Enzyme mechanism and kinetics

Enzymes are biological catalysts that reduce the activation energy of (bio-)chemical reactions. Their function is dependent on the amino acid sequence and their three dimensional structure forming an active site with a catalytic activity into which a certain reactant (substrate) can bind. The main advantages for enzyme based catalysis compared to conventional catalysts are the high regio- and stereo-selectivity, the possibility to perform the reaction in mild conditions, which therefore needs less energy (e.g. lower process temperature), and low by-product generation. Enzymes are proven to be biodegradable and non toxic [1]. However, enzymes are also unstable at certain process conditions. Their stability is dependent on pH, temperature and salt or organic compound concentration.

A simplified reaction mechanism of an enzyme is shown in Figure 13. Only a certain type of substrate S can bind into the active site of the enzyme (red part of the enzyme) forming an enzyme substrate complex E-S (key-lock mechanism). This is a reversible step, thus the substrate can detach from the active site without being processed to product P. The enzyme substrate complex E-S can form the product P, and the reaction products desorb from the active site. The reversibility of this step is dependent on the nature of catalyzed reactions; simple reactions might be reversible, whereas depolymerization reactions of large chain molecules, such as hydrolyzation of cellulose fibers are not. High concentrations of reactant and product might alter the reaction rate as these molecules tend to absorb on the active site and occupy it in case of reversible reactions.

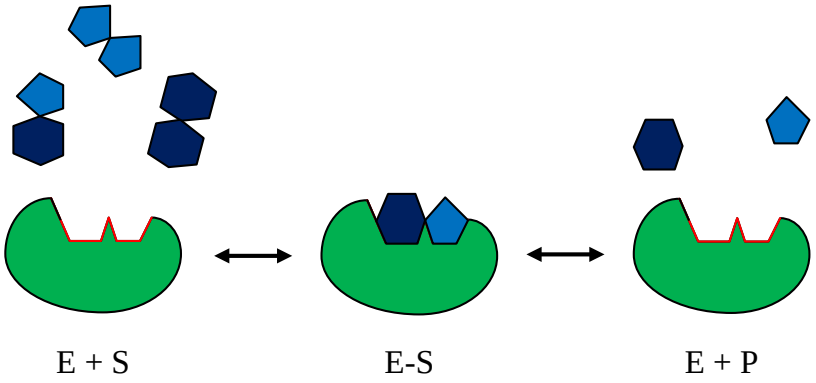

Figure 13: Reversible enzyme reaction mechanism over an enzyme substrate complex

Enzyme catalyzed reactions are underlying the same principles as chemical reactions in terms of being temperature and concentration dependent and proceeding towards the chemical equilibrium. Compared to homogeneous catalyzed reactions some differences arise from the nature of the enzymes as they are generally much bigger than the substrate. Enzyme kinetics can be regarded as a transition step between homogeneous and heterogeneous reactions, sometimes called micro-heterogeneous reactions, as they have elements of homogeneous reactions, like being dependent on the bulk concentration and not having diffusion limiting from the bulk to the catalyst, and heterogeneous reactions, like reversible substrate and product binding on the enzyme [1].

4.1.1. Reversible Michaelis Menten kinetics

The principles of enzyme reactions will be derived for the general case of a reversible reaction between substrate S and product P incorporating a reversible binding of S and P on the enzyme E forming an enzyme-substrate complex according to Figure 13. The overall reaction can be described as:

$$S + E \underset{k_{-1}}{\overset{k_1}{\rightleftarrows}} E - S \underset{k_{-2}}{\overset{k_2}{\rightleftarrows}} E + P \tag{4.1}$$

The following rate equations can be derived for the time course of the concentrations of S, E-S and P:

$$\frac{dC_P}{dt} = k_2 \cdot C_{E-S} - k_{-2} \cdot C_P \cdot C_E = r \tag{4.2}$$

$$-\frac{dC_S}{dt} = k_1 \cdot C_S \cdot C_E - k_{-1} \cdot C_{E-S} \tag{4.3}$$

$$\frac{dC_{E-S}}{dt} = k_1 \cdot C_S \cdot C_E + k_{-2} \cdot C_P \cdot C_E - \left(k_{-1} + k_2\right) \cdot C_{E-S} \tag{4.4}$$

The concentration of free enzyme C_E in solution can be calculated from the difference of the concentrations of total enzyme in solution E_{Tot} and enzyme-substrate complex E-S:

$$C_E = C_{ETot} - C_{E-S} \tag{4.5}$$

The connection between C_{E-S} and C_{ETot} can be derived under the assumption that the concentration of E-S complex is constant during reaction and therefore in quasi-steady state equilibrium $(\frac{dC_{E-S}}{dt} = 0)$. This assumption holds on the observation that the substrate concentration is in abundance compared to the enzyme in typical enzyme processes.

The enzyme mass balance from Eq. (4.5) inserted into Eq. (4.4) yields:

$$0 = k_1 \cdot C_S \cdot C_{ETot} - k_1 \cdot C_S \cdot C_{E-S} + k_{-2} \cdot C_P \cdot C_{ETot} - k_{-2} \cdot C_P \cdot C_{E-S} - \left(k_{-1} + k_2\right) \cdot C_{E-S} \tag{4.6}$$

This leads to the following correlation between C_{E-S} and C_{ETot}:

$$C_{E-S} = \frac{k_1 \cdot C_S \cdot + k_{-2} \cdot C_P}{k_1 \cdot C_S + k_{-2} \cdot C_P + \left(k_{-1} + k_2\right)} \cdot C_{ETot} \tag{4.7}$$

The correlation between C_E and C_{ETot} can be derived in a similar manner by inserting C_{E-S} from the mass balance in Eq. (4.5) into Eq. (4.4):

$$C_E = \frac{k_1 + k_{-2}}{k_1 \cdot C_S + k_{-2} \cdot C_P + \left(k_{-1} + k_2\right)} \cdot C_{ETot} \tag{4.8}$$

The expressions for C_{E-S} and C_E can then be inserted into the reaction rate described in Eq. (4.2):

$$r = \frac{dC_P}{dt} = \frac{k_1 \cdot k_2 \cdot C_S - k_{-1} \cdot k_{-2} \cdot C_P}{k_1 \cdot C_S + k_{-2} \cdot C_P + \left(k_{-1} + k_2\right)} \cdot C_{ETot} \tag{4.9}$$

In enzyme kinetics the term r_{max} is often used that describes the maximal achievable reaction rate and is the product of the reaction rate constant for the formation of the product (or educt in case of reversible reaction) and total enzyme concentration:

$$r_{max1} = k_2 \cdot C_{ETot}; r_{max2} = k_{-1} \cdot C_{ETot} \tag{4.10}$$

With r_{max1} being the maximum rate of product P production and r_{max2} being the maximum rate of substrate S production.

Multiplying Eq. (4.9) with the expression $\frac{k_{-1} + k_2}{k_1 \cdot k_{-2}}$ and inserting the following definitions for the substrate and product Michaelis Menten constants:

$$K_{MS} = \frac{k_{-1} + k_2}{k_1}; K_{MP} = \frac{k_{-1} + k_2}{k_{-2}} \tag{4.11}$$

leads to:

$$r = \frac{r_{max1} \cdot C_S \cdot K_{MP} - r_{max2} \cdot C_P \cdot K_{MS}}{K_{MP} \cdot C_S + K_{MS} \cdot C_P + K_{MP} \cdot K_{MS}} \cdot C_{ETot} \tag{4.12}$$

Similar to the chemical reaction rate described in Chapter 2 at chemical equilibrium there is no net reaction. The connection of the kinetic equilibrium and thermodynamic equilibrium can be expressed by the Haldane relationship:

$$K_{eq}^{Enz} = \frac{C_P^{eq}}{C_S^{eq}} = \frac{r_{max1} \cdot K_{MP}}{r_{max2} \cdot K_{MS}} \tag{4.13}$$

inserting in Eq. (4.12) gives:

$$r = \frac{r_{max1} \cdot K_{MP} \cdot \left(C_S - C_S^{eq}\right)}{K_{MP} \cdot C_S + K_{MS} \cdot C_P + K_{MP} \cdot K_{MS}} \tag{4.14}$$

C_S is the actual substrate concentration and C_S^{eq} is the substrate concentration that is in thermodynamic equilibrium with the actual product concentration C_P. Dividing this expression with the Michaelis Menten constant for the reverse reaction K_{MP} yields in a Michaelis Menten equation for reversible reactions of the following form [2]:

$$r = \frac{r_{max1} \cdot \left(C_S - C_S^{eq}\right)}{K_{MS} \cdot \left(1 + \frac{C_P}{K_{MP}}\right) + C_S} \tag{4.15}$$

The effect of higher product concentration on the enzyme reaction rate is often regarded as product inhibition, but it is basically a reversible reaction between substrate S and product P where both steps are considered reversible and following the Michaelis Menten kinetics. The decrease in reaction rate with higher product concentration can be explained as the substrate and product are competing for binding onto the enzymes active site and the enzyme becomes more occupied by the product when its concentration increases and therefore less substrate can bind.

4.1.2. Enzyme inhibition

Inhibitors are small molecules that bind to the enzyme and decrease the activity of the enzyme. In this study we consider just reversible enzyme inhibition which means that the inhibitor can also detach from the enzyme again. The type of inhibitor binding can influence the mechanism of the enzyme substrate reaction in different ways. If the inhibitor binds to the active site and blocks the substrate from forming the enzyme substrate complex there is a competition between substrate and inhibitor for binding into the active site. The inhibition mechanism is thus called competitive inhibition; the extent of inhibition is dependent of the substrate, inhibitor and free enzyme concentration. In case the inhibitor can just bind onto the enzyme substrate complex forming a dead end complex and preventing the product formation, the inhibition mechanism is called uncompetitive inhibition. This inhibition type

is dependent on the enzyme substrate complex concentration and the inhibitor concentration. The rate equation for the different inhibition types will not be derived in this study, but interested readers can look it up in the detailed enzyme kinetics books like the one of Segel [2] or Bisswanger [3]. A graphical illustration of the reactions considered in the different inhibitions mechanisms is given in Figure 14.

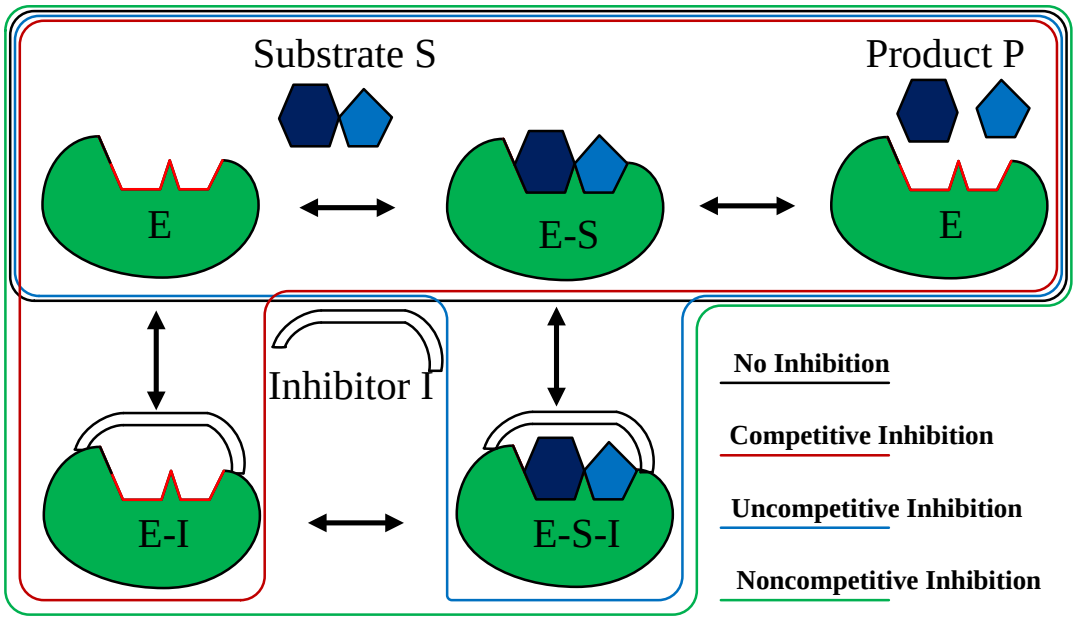

Figure 14: Different reversible enzyme inhibition mechanisms

Considering the product formation being irreversible, the rate of product formation is altered in case of the presence of a competitive inhibitor C_{CI} which competes with the substrate to bind to the active site [3]:

$$r_{enz}^{CI} = \frac{r_{max1} \cdot C_S}{K_{MS} \cdot \left(1 + \frac{C_{CI}}{K_{CI}}\right) + C_S} \tag{4.16}$$

This form describes the competitive inhibition and is denoted with CI. The similarity between Equations (4.15) and (4.16), is one reason why product inhibition is sometimes used in a wrong context.

If the inhibitor is binding on the E-S complex forming a dead end complex; the product formation rate is influenced by the inhibitor concentration C_{UI} by:

$$r_{enz}^{UI} = \frac{r_{max1} \cdot C_S}{K_{MS} + C_S \cdot \left(1 + \frac{C_{UI}}{K_{UI}}\right)} \tag{4.17}$$

This can be regarded as uncompetitive inhibition (UI). In case both inhibition mechanisms are influencing the rate it is called non-competitive inhibition:

$$r_{enz}^{NC} = \frac{r_{max1} \cdot C_S}{K_{MS} \cdot \left(1 + \frac{C_{CI}}{K_{CI}}\right) + C_S \cdot \left(1 + \frac{C_{UI}}{K_{UI}}\right)} \tag{4.18}$$

4.2. Carbonic Anhydrase

The enzyme carbonic anhydrase (E.C.4.2.1.1) was discovered, when the high mass transfer rates of CO_2 in blood were investigated by Meldrum and Roughton [4]. The interconversion of CO_2 and bicarbonate catalyzed by carbonic anhydrase that enhanced the mass transfer rates of CO_2 could explain why higher rates than by physical absorption could be obtained in blood. Researchers discovered shortly after that this enzyme can be found in several places in the body and in all animals and photosynthesizing organism [5].

The enzyme facilitates various processes like ion transport, acid–base regulation, gas exchange, photosynthesis, and CO_2 fixation [6]. The enzyme itself is capable of catalyzing several different reactions, besides the most prominent reversible hydration of CO_2 forming bicarbonate it is known to hydrate aldehydes and hydrolyze certain esters; the common feature of these reactions is the water splitting into H^+ and OH^- and reforming of the hydroxyl with an electrophilic center [7].

4.2.1. Description

Early elementary analysis of the newly discovered enzyme revealed that it contains stoichiometric quantities of zinc and belongs to the group of metallo-enzymes. The central Zn (II) ion, that was later determined to be the active site of the enzyme is the mutuality of all carbonic anhydrase families [5] that are genetically and immunologically distinct [7]. These different families show low protein sequence similarity and differ considerably in their three dimensional structure [6], [8]. The fact that several evolutionary selections resulted in enzymes with the same functionality characterizes the importance of this group of enzymes [6]. There are up to date 5 different CA families known, the α-, β-, and γ- carbonic anhydrase are the more important and more investigated families, whereas the δ and ζ family are still very unknown as they are only found in diatoms. The α-class is primarily found in vertebrates and is the only form of CA found in this species [6], due to the physiological impact on the metabolism several other important processes this family has gained the most attention in research.

4.2.2. CA Mechanism

The reaction mechanism of carbonic anhydrase was developed step by step from observations. The overall reaction observed in the experiments was:

$$CO_2 + H_2O \underset{}{\overset{CA}{\rightleftharpoons}} HCO_3^- + H^+ \tag{4.19}$$

Studies with an NMR spectroscopy with $^{13}CO_2$ and $H^{13}CO_3^-$ confirmed the carbonic anhydrase kinetics follow Michaelis-Menten behavior [7]. A reaction path with H_2CO_3 formation that would be subsequently hydrolyzed to bicarbonate could be excluded, as the calculated reaction rate would be one order of magnitude higher than diffusion limited rate constant [9].

As the product bicarbonate is released the enzyme is left with a proton that it needs to get rid of [10]. The turnover rates for CO_2 hydration were influenced by the buffer concentration, indicating the proton transfer being a rate limiting step. Experiments with O^{18} labeled water at equilibrium showed that the interconversion between CO_2 and bicarbonate is about 10 times faster than the proton release from O^{18} labeled water, confirming that the proton transfer rather than the hydration of CO_2 is the rate limiting step [11]. At high buffer concentrations the turnover rate is not influenced anymore by the buffer concentration, under these conditions another step is rate determining. Experiment with heavy water and water mixtures [9], [10] suggested that the proton transfer occurs in a two-step mechanism with one buffer dependent and one buffer independent step. The rate limiting step is buffer dependent at low buffer concentrations and non-buffer dependent at high buffer concentrations.

Two active groups with a pKa near 7 where identified to participate in the proton transfer, one of them being zinc bound water the other one an amino acid side chain, or also called proton channel (PC). The amino acid side chain was found to be the Histidin amino acid on position 64 (His 64) for the human CAII which was the only group near the active site that had an appropriate pKa near 7 to transfer the proton at that velocity [12], similar proton shuttles were found in the β-CA (His 216) and γ-CA (Glu84) [6]. These position may vary for different enzymes, but the collaboration in the proton transfer from two functional groups is similar [13]. The proton transfer needs to occur via a network of hydrogen bonded water molecules as the side chain is not close enough to the active site Zn(II) for direct transfer. The distance is about 7 Å for α-CA [6], 10 Å for β-CA and about 9 Å for γ-CA [12], which is large compared to the distance between hydrogen and oxygen in water being about 1 Å. The hypothesis of proton transfer through the intervening hydrogen bonded water molecules could be confirmed by the observed isotope effect when using mixtures of heavy water (D_2O) and water, which suggested that a proton transfer involving at least one water molecule is occurring [10][12]. Results for hCA II were consistent with proton transfer across two or three water molecules [6].

In the case of carbonic anhydrase the active side is Zn^{2+} ion with an attached hydroxyl group. The reaction mechanism of α-CAs is very well studied and a scheme is pictured in Figure 15. The

pictogramm is adapted from Pierre [14] and Salmon and House [8] to show the mechanism from a different angle and put the significance of the proton channel into focus. Even though the β- and γ-family have different structure protein sequence, the main mechanism of CO_2 hydration as well as the rate limiting steps show similarity [6], [12]. All three enzyme classes follow the two-step iso-mechanism, with a nucleophilic attach from a zinc-bound hydroxide onto CO_2, and a regeneration of the active site involving a proton removal to an amino acid side chain [13].

The enzyme is in its active state with a CO_2 molecule nearby in picture (A), the amino acid side chain PC, is releasing a proton to a buffer molecule in the solution in the intermolecular proton transfer step. The zinc bound hydroxyl reacts with an incoming carbon dioxide molecule via a nucleophilic attack onto the C-atom (B) resulting in a zinc-bound bicarbonate. The bicarbonate is swapped by a water molecule releasing bicarbonate to solution (C), leaving the enzyme in an inactive state (D). To regain its catalytic activity one proton has to be removed from the zinc-bound water molecule. The proton is transferred via a network of hydrogen bonded water molecules to the proton channel PC in the intramolecular proton transfer.

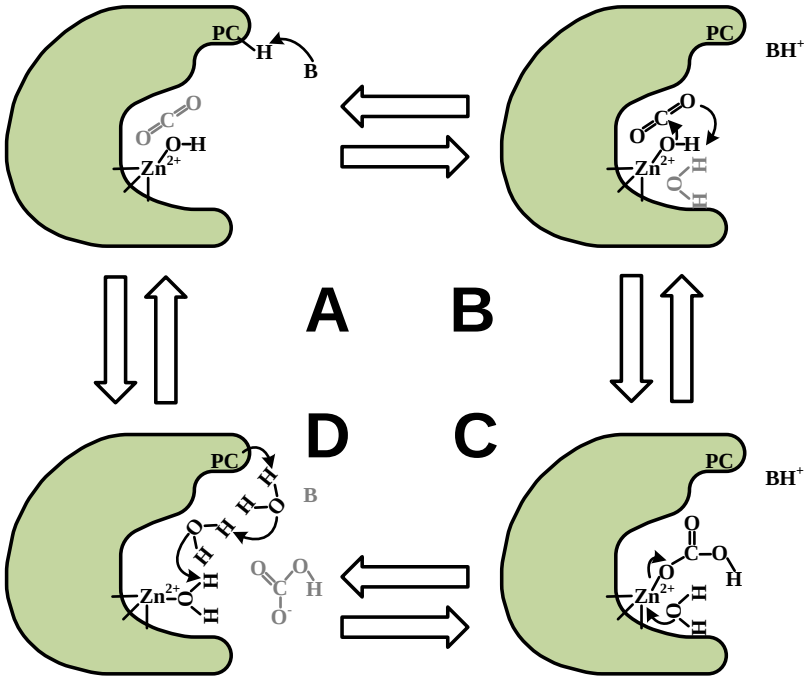

Figure 15: Reaction mechanism of α-carbonic anhydrase, adapted from Pierre [14].

As the buffer concentration must be lower than 10 mM [15], [16] to make the intermolecular proton transfer rate limiting, in carbon capture applications with solvent concentration in the order of 1 M the rate limiting step is considered to be the transfer of the proton to the side chain. The overall reaction can then be described as:

$$CO_2 + H_2O + B \overset{CA}{\rightleftharpoons} HCO_3^- + BH^+ \quad (4.20)$$

B represents any kind of proton acceptor such as hydroxyl ions or a base. The enzyme is catalyzing the reversible reactions towards the chemical equilibrium, it is therefore enhancing the rate in absorption and desorption. In desorption the reaction mechanism is following the counter clock wise path in Figure 15.

4.3. Carbonic Anhydrase as kinetic promoter in carbon capture

The experiments explained in the subsection above were merely conducted to describe the mechanism of certain CAs specifically in detail, the main idea was to rather to understand the principles inside the human or animal bodies than to capture vast amounts of CO_2 from a flue gas chimney. The focus in this section lies now on the application of CA for industrial scale CO_2 separation from flue gas mixtures.

4.3.1. Thermostability

The thermo-stability of the enzyme is the biggest question mark of applying CA in the chemical absorption process as in an conventional setup the desorption step exceeds temperatures of 100 °C [17]. Improving thermo-stability of CA can be achieved by either expression from thermophilic organism or by protein engineering [6].

Directed evolution of a β-CA lead to a robust enzyme which could sustain 24 hours at 107 ºC in 4.2 M MDEA solution (around 50 wt%) without losing activity [18]. This enzyme was tested in a pilot plant setup for 60 hours over 5 days with 25 ºC absorber temperature and 87 ºC desorber temperature and showed no decrease in capture performance during the experiments.

In CO_2 solutions demonstration runs the desorption of the 1.45 M (20 wt%) K_2CO_3 solution was carried out with hot water with a temperature inside the desorber below 80 °C [19]. The enzyme did not lose any activity in two test campaigns with around 1000 hour of continuous operation time.

Several other authors observed a decrease in enzyme activity when it was exposed to higher temperatures for a longer time [20]–[23]. The positive results from the large scale experiments encourage the application of CA in CCS and show that it is possible to develop thermostable enzymes through protein engineering.

4.3.2. CA in lab scale

Even though many studies have been carried out with carbonic anhydrase as kinetic promoter only few have presented results from absorption experiments with different solvents measured on the same equipment allowing for interpretation of interaction between enzyme and solvents.

Alper and Deckwer were one of the first to look at the effect of adding carbonic anhydrase on the absorption kinetics in a CSTR and a wetted wall column using different solvents. They compared different buffer solutions and buffers strengths under gas absorption conditions. Three different buffers, KH_2PO_4 + Na_2HPO_4 (pH 6.5-6.7), Na_2HPO_4 + Na_3PO_4 (pH 11-11.1) and $NaHCO_3$ + Na_2CO_3 (pH 9.6) were tested at temperatures ranging from 5 to 35 ºC, with most experiments conducted at 25 ºC. Crude carbonic anhydrase from bovine erythrocytes was used and the concentration was varied between 0 and 100 mg/L. They observed a linear dependency between enzymatic hydration reaction rate and enzyme concentration for experiments at high pH (9.6-11.1). A change of ions from carbonates to phosphates did not influence the catalytic activity nor did the pH change from 9.6 to 11.1. Decreasing the pH to 6.6 resulted in a considerable decrease in enzyme activity.

A similar approach to that used in this work was chosen in the study of Vinoba et al. [25]. They selected one solvent from each amine group and compared absorption rates at temperatures ranging from 10 to 60 ºC into solutions containing the same weight fraction of amine (5 wt% or 10 wt%). MEA (a primary amine), DEA (a secondary amine), MDEA (a tertiary) and AMP (a sterically hindered amine) were used in their experiments. They used a vapor liquid equilibrium cell with a stirrer in a pure CO_2 atmosphere at ambient pressure and monitored the amount of CO_2 absorbed by the pressure decrease. They compared both the solvent alone and the solvent with a 5 ppm carbonic anhydrase concentration and introduced an *Enhanced* k_{app} value according to:

$$Enhanced\ k_{app}\left(\%\right)=\frac{\left(E_{k_{app}}-C_{k_{app}}\right)\cdot 100}{C_{k_{app}}} \tag{4.21}$$

This relates the overall absorption rate of enzyme solvent $E_{k_{app}}$ to the solvent $C_{k_{app}}$ and is basically the ratio of enzyme contribution towards absorption to solvent contribution towards absorption. MDEA showed the greatest absorption enhancement with enzyme, followed by AMP, DEA and MEA. Every solvent at all the temperatures tested showed a positive effect of enzyme addition. The solvents AMP, DEA and MEA had a declining k_{app} value for rising temperatures at 5 wt% amine concentration. For MDEA the k_{app} kept rising until 40 ºC and then decreased at temperatures above.

The most extensive studies on carbonic anhydrase kinetics for CO_2 absorption with different solvents and different process conditions was performed by Penders-van Elk et al. [16], [26]–[29]. In their first study [16] they investigated the kinetics of two different carbonic anhydrase enzymes with MDEA at 298 K in a stirred cell reactor. They showed that the physical solubility of CO_2 is not altered with enzyme addition by performing N_2O solubility tests for MDEA solutions with and without enzyme. A clear increase of overall reaction rate of the solvent was visible when increasing the enzyme concentration at a fixed solvent concentration, with a linear relationship at lower enzyme concentration and a flattening out at higher enzyme concentrations. Their overall enzyme reaction rate constant (s^{-1}), the difference of overall reaction rates of the enzyme enhanced solution and the just the amine solution

without enzyme, was depended on the solvent concentration as they observed a lower first order enzyme reaction rate constant when the solvent concentration was higher indicating a negative effect of the solvent on the enzyme kinetics. They explained this difference with the lower water concentration in higher concentrated solvents. They concluded that the enzyme reaction rate is dependent on the water concentration with the power of one and calculated a k_2^* (L mol^{-1} s^{-1}) enzyme reaction rate constant which is the first order enzyme reaction rate constant divided by the water concentration.

In their second study the solvent Na_2CO_3 was tested [26]. Absorption experiments with 0.3 mol/L Na_2CO_3 solutions at different temperatures ranging from 298 to 333 K showed a decline of k_2^* with higher temperature. They also analyzed the process option of enzyme immobilization on the surface in this study. According to conservative estimates with the film theory, immobilization on the packing internal would not result in a better performance. Immobilization of carbonic anhydrase on small nylon particles resulted in a decrease of enzyme activity compared to enzymes in solution, the extent of the decrease was a function of average particle diameter. Smaller particles showed higher enzyme activity.

In their third paper [27] they used a Langmuir Hinshelwood type equation to describe the deviation from linear dependency of enzyme concentration and enzyme reaction rate which relates the k_2^* value to k_3^* (m^6 mol^{-1} kg^{-1} s^{-1}) and k_4^* (m^3 kg^{-1}) according to:

$$k_2^* = \frac{k_3^* \cdot C_{enz}}{1 + k_4^* \cdot C_{enz}} \tag{4.22}$$

They also examined several new alkanolamines: N, N-diethylethanolamine (DEMEA), N,N-dimethylethanolamine (DMMEA), monoethanolamine (MEA), triethanolamine (TEA) and tri-isopropanolamine (TIPA) at 298 K. In both TEA and DMMEA, a decrease in enzymatic activity was observed. In order to be able to measure the enzymatic reaction a very low concentration of MEA was chosen (0.1 mol L^{-1}). They compared the derived k_3^* and k_4^* values and found a relation with the pKa of the solvent. The k_3^* value was increasing and the k_4^* value was decreasing with increasing pKa, as a general trend k_2^* was increasing with increasing pKa.

In a more recent study the temperature dependency of the enzyme kinetics in 1 M MDEA was determined in a temperature range from 278-343 K [28]. When considering just experimental results at 278, 288 and 313 K they were able to derive a simplified kinetic model using the LH relation from Eq. (4.22), where the k_3^* value followed a Arrhenius type of temperature dependency whereas k_4^* was independent of temperature. The model was under predicting the results obtained at 298 K and over predicting the results at 343 K.

In the newest study they presented the temperature dependency of the enzyme reaction rate of TIPA, DMMEA, AMP and MDEA for a new enzyme [29]. They correlated the enzyme reaction rate constant to the pKA value via a Brønsted relation and were able to reproduce the experimental results within 80 % error margin with an average deviation of 20 %.

Kunze et al. [30] compared different enzyme-accelerated solvents on three different laboratory and pilot scale setups. They tested MEA (30 wt%), diethylethanolamine DEEA (30 w%), and MDEA (30 wt%) and the alkali carbonate salt K_2CO_3 (10 wt%). In a first approach these solvents where compared in a spray reactor at 296 K at 13 vol% CO_2 and a catalytic effect CE_{CA} (-) was determined which is the ratio of absorbed flux of CO_2 with CA enzyme to the absorbed flux of the solvent alone, which describes the absorption enhancement under these conditions:

$$CE_{CA} = \frac{\left(\Delta N_{CO_2}\right)_{with\ CA}}{\left(\Delta N_{CO_2}\right)_{without\ CA}} \tag{4.23}$$

MEA had a slightly lower mass transfer after enzyme addition. The two solvents that showed the highest catalytic effect, K_2CO_3 ($CE_{CA} = 4.8$) and MDEA ($CE_{CA} = 4.1$) were then tested in a pilot absorber column.

4.3.3. CA in pilot scale

Kunze et al. [30] used a packed column filled with a SULZER BX gauze packing with a height of 2.3 m and an inner diameter of 56 mm in their pilot tests. Hydrodynamic tests with these solvents showed no influence of enzyme addition on critical process parameters for technical absorbers such as pressure drop or foaming tendency. Absorption runs at 317 K and 15 vol% CO_2 in the gas phase resulted in comparable intensification of absorption compared to the results from the spray reactor, CE_{CA} values of 4.0-5.9 for K_2CO_3 and 3.3 to 4.2 for MDEA were reported.

The research on enzyme enhanced CO_2 capture at the TU Dortmund was continued within the Interact EU project [31]. They conducted several pilot scale absorption runs with MDEA solvent. The main findings from these experiments was that the absorption of CO_2 decreased when a higher MDEA concentration was used (50 wt% vs. 30 wt%) and experiments with 30 wt% MDEA at 40 °C and 20 °C showed similar CO_2 absorption rates with 2 g/L CA. They could also prove, that the process could be scaled up, as they observed similar Enhancement in mass transfer (CE_{CA}) when the diameter of the column was increased to technical scale (ID= 0.45).

Akermin Inc. performed field tests with their surface immobilized packing at the National Carbon Capture Center (NCCC) in Wilsonville Alabama. They were able to achieve 80 % capture in a absorber column with around 0.21 m diameter and a total packing height of around 8 m with 20 wt% K_2CO_3

with an L/G ratio of 7.88 (kg/kg) over a timeframe of 5 and 1 month respectively. The use of the surface immobilized enzyme lead to a 6-7 fold higher mass transfer [32].

Alvizo et al. [18] also tested their ultrastable CA on pilot plant at the NCCC in Wilsonville Alabama. The setup consisted of two inline absorbers with each 3.15 m height (6.3 m total) and 0.15 m diameter filled with 16 mm Pall rings. They tested 25 and 50 wt% aqueous MDEA solutions; the mass transfer increased 20 fold for both solutions by adding 0.2 g/L CA and 25 fold for the 25 wt% MDEA solution by adding 0.4 g/L CA compared to the counterparts without enzymes. At 0.2 g/L CA and 25 wt% MDEA concentration 60 % capture efficiency could be obtained continuously with a flue gas stream of 12 vol% CO_2 at ambient pressure over a time span of 60 hours.

The largest test runs with carbonic anhydrase were conducted by CO_2 solutions. They employed 20 wt% K_2CO_3 and could capture 10 tonnes of CO_2 per day at an average capture efficiency of 80 % over 2500 hours at an L/G ratio of 10.8 (kg/kg) and a lean and rich loading of 0.41 and 0.52 (mol CO_2 /mol K_2CO_3) [19].

BIBLIOGRAPHY

[1] P. Grunwald, *Biocatalysis*, 1st ed. Imperial College Press, 2011.

[2] I. H. Segel, *Enzyme Kinetics: Behavior and Analysis of Rapid Equilibrium and Steady-State Enzyme Systems*. Wiley-VCH, 1993.

[3] H. Bisswanger, *Practical Enzymology Enzymes in Industry Biocatalysts and Enzyme Technology*, 2nd ed. Wiley-VCH, 2008.

[4] N. U. Meldrum and F. J. Roughton, "Carbonic anhydrase: Its preparation and properties.," *J. Physiol.*, vol. 80, no. 2, pp. 113–142, 1933.

[5] S. Lindskog, "Structure and mechanism of carbonic anhydrase," *Pharmacol. Ther.*, vol. 74, no. 1, pp. 1–20, 1997.

[6] S. C. Frost and R. McKenna, *Carbonic Anhydrase: Mechanism, Regulation, Links to Disease, and Industrial Applications*, vol. 75. Springer, 2014.

[7] T. G. Spiro, *Zinc Enzymes*, 1st ed. John Wiley & Sons Ltd., 1983.

[8] S. Salmon and A. House, "Enzyme-catalyzed Solvents for CO_2 Separation", *in Novel Materials for Carbon Dioxide Mitigation Technology*,. Elsevier B.V., 2015.

[9] H. Steiner, B.-H. Jonsson, and S. Lindskog, "The Catalytic Mechanism of Carbonic Anhydrase Hydrogen-Isotope Effects on the Kinetic Parameters of the Human C Isoenzyme," *Eur. J. Biochem*, vol. 59, pp. 253–259, 1975.

[10] Y. Pocker and D. W. Bjorkquist, "Comparative studies of bovine carbonic anhydrase in H_2O and D_2O. Stopped-flow studies of the kinetics of interconversion of CO_2 and HCO_3^-," *Biochemistry*, vol. 16, no. 26, pp. 5698–5707, 1977.

[11] R. S. Rowlett, C. Tu, M. M. McKay, J. R. Preiss, R. J. Loomis, K. A. Hicks, R. J. Marchione, J. A. Strong, G. S. Donovan, and J. E. Chamberlin, "Kinetic characterization of wild-type and proton transfer-impaired variants of β-carbonic anhydrase from Arabidopsis thaliana," *Arch. Biochem. Biophys.*, vol. 404, no. 2, pp. 197–209, 2002.

[12] C. Tu, R. S. Rowlett, B. C. Tripp, J. G. Ferry, and D. N. Silverman, "Chemical rescue of proton transfer in catalysis by carbonic anhydrases in the β- and γ-class," *Biochemistry*, vol. 41, no. 51, pp. 15429–15435, 2002.

[13] B. C. Tripp, K. Smith, and J. G. Ferry, "Carbonic Anhydrase: New Insights for an Ancient Enzyme," *J. Biol. Chem.*, vol. 276, no. 52, pp. 48615–48618, 2001.

[14] A. C. Pierre, "Enzymatic Carbon Dioxide Capture," *ISRN Chem. Eng.*, vol. 2012, pp. 1–22, 2012.

[15] D. N. Silverman and S. Lindskog, "The catalytic mechanism of carbonic anhydrase: implications of a rate-limiting protolysis of water," *Acc. Chem. Res.*, vol. 21, no. 4, pp. 30–36, 1988.

[16] N. J. M. C. Penders-van Elk, P. W. J. Derks, S. Fradette, and G. F. Versteeg, "Kinetics of absorption of carbon dioxide in aqueous MDEA solutions with carbonic anhydrase at 298 K," *Int. J. Greenh. Gas Control*, vol. 9, pp. 385–392, 2012.

[17] M. E. Boot-Handford, J. C. Abanades, E. J. Anthony, M. J. Blunt, S. Brandani, N. Mac Dowell, J. R. Fernández, M.-C. Ferrari, R. Gross, J. P. Hallett, R. S. Haszeldine, P. Heptonstall, A. Lyngfelt, Z. Makuch, E. Mangano, R. T. J. Porter, M. Pourkashanian, G. T. Rochelle, N. Shah, J. G. Yao, and P. S. Fennell, "Carbon capture and storage update," *Energy Environ. Sci.*, vol. 7, p. 130, 2014.

[18] O. Alvizo, L. J. Nguyen, C. K. Savile, J. a Bresson, S. L. Lakhapatri, E. O. P. Solis, R. J. Fox, J. M. Broering, M. R. Benoit, S. a Zimmerman, S. J. Novick, J. Liang, and J. J. Lalonde, "Directed evolution of an ultrastable carbonic anhydrase for highly efficient carbon capture from flue gas.," *Proc. Natl. Acad. Sci. U. S. A.*, vol. 111, no. 46, pp. 16436–41, 2014.

[19] L. Fradette, S. Lefebvre, and J. Carley, "Demonstration Results of Enzyme-Accelerated CO_2 Capture," *Energy Procedia*, vol. 0, pp. 14–18, 2017.

[20] M. T. Gundersen, N. Von Solms, and J. M. Woodley, "Enzymatically Assisted CO_2 Removal from Flue-Gas," *Energy Procedia*, vol. 63, pp. 624–632, 2014.

[21] G. Hu, K. H. Smith, N. J. Nicholas, J. Yong, S. E. Kentish, and G. W. Stevens, "Enzymatic carbon dioxide capture using a thermally stable carbonic anhydrase as a promoter in potassium carbonate solvents," *Chem. Eng. J.*, vol. 307, pp. 49–55, 2016.

[22] M. E. Russo, G. Olivieri, C. Capasso, V. De Luca, A. Marzocchella, P. Salatino, and M. Rossi, "Kinetic study of a novel thermo-stable α-carbonic anhydrase for biomimetic CO_2 capture," *Enzyme Microb. Technol.*, vol. 53, no. 4, pp. 271–277, 2013.

[23] X. Ye and Y. Lu, "CO2 absorption into catalyzed potassium carbonate–bicarbonate solutions: Kinetics and stability of the enzyme carbonic anhydrase as a biocatalyst," *Chem. Eng. Sci.*, vol. 116, pp. 567–575, 2014.

[24] E. Alper and W.-D. Deckwer, "Kinetics of absorption of CO_2 into buffer solutions containing carbonic anhydrase," *Chem. Eng. Sci.*, vol. 35, no. 3, pp. 549–557, 1980.

[25] M. Vinoba, M. Bhagiyalakshmi, A. N. Grace, D. H. Kim, Y. Yoon, S. C. Nam, I. H. Baek, and S. K. Jeong, "Carbonic anhydrase promotes the absorption rate of CO_2 in post-combustion processes," *J. Phys. Chem. B*, vol. 117, no. 18, pp. 5683–5690, 2013.

[26] N. Penders-van Elk, E. Hamborg, P. S., J. A. Carley, S. Fradette, and G. F. Versteeg, "Kinetics of absorption of carbon dioxide in aqueous amine and carbonate solutions with carbonic anhydrase," *Int. J. Greenh. Gas Control*, vol. 12, pp. 259–268, 2013.

[27] N. J. M. C. Penders-van Elk, Fradet, S. Te, and G. F. Versteeg, "Effect of pKa on the kinetics of carbon dioxide absorption in aqueous alkanolamine solutions containing carbonic anhydrase at 298K," *Chem. Eng. J.*, vol. 259, pp. 682–691, 2015.

[28] N. J. M. C. Penders-van Elk, C. Van Aken, and G. F. Versteeg, "Influence of temperature on the kinetics of enzyme catalysed absorption of carbon dioxide in aqueous MDEA solutions," *Int. J. Greenh. Gas Control*, vol. 49, pp. 64–72, 2016.

[29] N. J. M. C. Penders-Van Elk, S. M. Oversteegen, and G. F. Versteeg, "Combined Effect of Temperature and pKa on the Kinetics of Absorption of Carbon Dioxide in Aqueous Alkanolamine and Carbonate Solutions with Carbonic Anhydrase," *Ind. Eng. Chem. Res.*, vol. 55, no. 38, pp. 10044–10054, 2016.

[30] A. Kunze, G. Dojchinov, V. S. Haritos, and P. Lutze, "Reactive absorption of CO_2 into enzyme accelerated solvents : From laboratory to pilot scale," *Appl. Energy*, vol. 156, pp. 676–685, 2015.

[31] M. Leimbrink and A. Gladis, "Enzyme accelerated solvent systems and CO_2 absorption in columns," in *Interact Industrial Workshop on Innovative Materials and Technologies for CO_2 Capture, Leverkusen*, 2017.

[32] J. Reardon, T. Bucholz, M. Hulvey, J. Tuttle, A. Shaffer, D. Pulvirenti, L. Weber, K. Killian, and A. Zaks, "Low Energy CO_2 Capture Enabled by Biocatalyst Delivery System," *Energy Procedia*, vol. 63, pp. 301–321, 2014.

Lab scale

5. Wetted wall column

This chapter explains how to derive kinetic constants from wetted wall column experiments. An experimental procedure is given and the setup is explained. Material balance, mass transfer area and contact time calculations are derived. The determination of the gas side mass transfer and liquid side mas transfer coefficients are explained in detail and compared to methods from the literature. In the end an example calculation for the determination of the solutions reaction rate constant is shown.

5.1. Experimental setup

The wetted wall column apparatus is a gas liquid contactor, with well-defined dimensions and adjustable process parameters like temperature, pressure, as well as liquid and gas concentrations, allowing for simple component balances and measurements of reaction rates of solvents with CO_2 through well-defined dimensions. The flow conditions of the liquid and partly the gas phase inside the apparatus mimic the behavior of real columns [1]. When the mass transfer coefficients for the gas and the liquid are known and solvent properties such as diffusivity and solubility are available, kinetic rate constants for the solvents can be calculated from the experimental results.

5.1.1. Apparatus

A scheme of the apparatus used for the experiments in this work is shown in Figure 1. The setup used in this study is that of Darde et al. [2] with minor modifications. In preliminary experiments the temperature probe at the liquid inlet and liquid outlet as used in the old setup gave similar results The temperature sensor for the liquid outlet was therefore moved to the NDIR (non-dispersive infra-red) CO_2 probe, because the reading showed dependency on the temperature. A smaller liquid reservoir (0.7 L vs. 2.2 L) was built and used in experiments with CA.

The setup consists of a liquid system (blue) and a gas system (red) that are in contact in the reaction chamber. The liquid system is a closed system, where the liquid (which is stored in the liquid reservoir) is pumped in a cycle. It passes a flowmeter (Sho rate Rotameter with sapphire ball) a heat exchanger that is integrated into a water bath, and then enters the reaction chamber in the inside of a small open end metal pipe with dimensions shown in Figure 1. The liquid flows down on the outside of this pipe creating a thin falling liquid film. The liquid is then pumped from the bottom of the reaction chamber via a micro pump (Cole Paler EW-07001-40) into the liquid reservoir. The gas is mixed from separate N_2 and CO_2 gas bottles using two Bronkhorst mass flow controllers. It passes through two saturators, one at ambient temperature and the other placed in the water bath where it achieves the desired temperature. The gas stream can then be led either through the reaction chamber or the bypass. In both

cases it is analyzed for pressure, temperature and CO_2 concentration by NDIR (Vaisala Carbocap GMT 221).

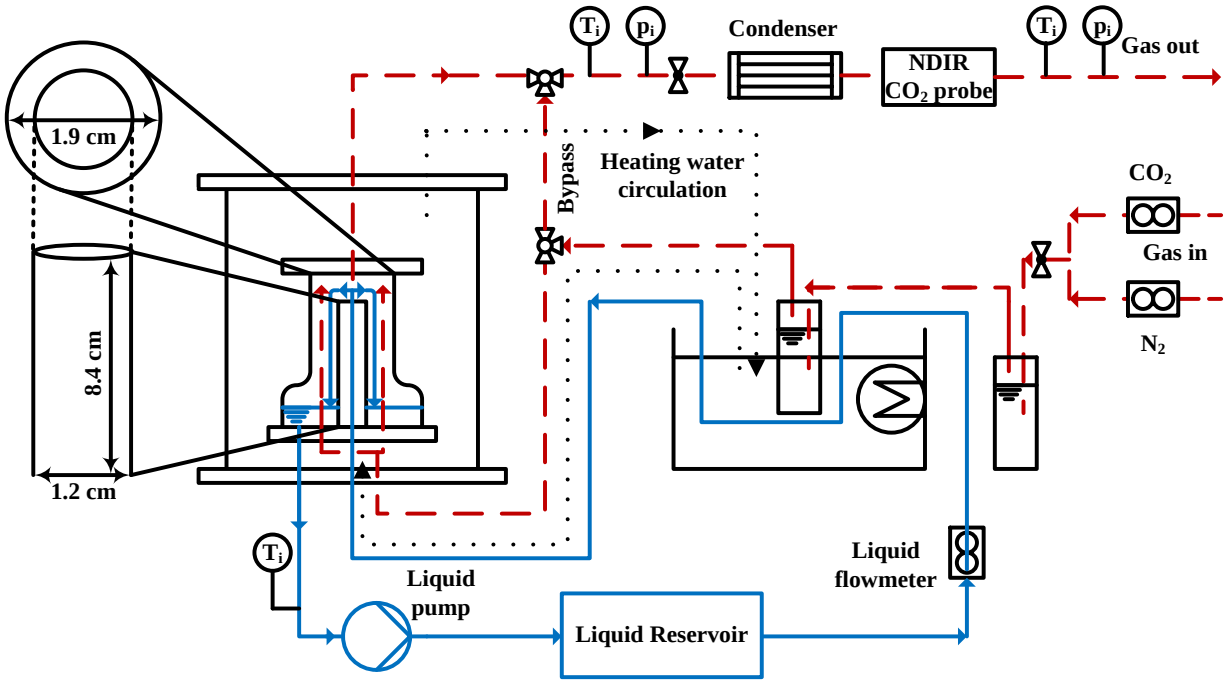

Figure 16: Scheme and dimensions of wetted wall column apparatus; blue line is the liquid and red line the gas system.

5.1.2. Procedure

The solvent was mixed with DI water and very small amounts of Teepol (0.002 wt%), a surface active agent, were added to the solution in case no CA was used in the experiments to prevent surface rippling [3]. The solutions CO_2 loading was determined with a $BaCl_2$ precipitation method described in Sønderby et al. [4]. The total solvent concentration was determined by acid titration with 0.5 M HCl solution. Density was measured with a DMA density meter (Anton Parr)) with an accuracy of ± 0.0001 g cm^{-3}. The solutions viscosity was measured in rotating ball viscosity meter (AMV 200 from Anton Parr), in case there were no literature values available.

The experimental procedure was then:

a. The pre-saturator and saturator were filled with approx. 500-600 g of DI water
b. Water bath for heating and condensator (15 °C) were started
c. Wetted wall column chamber was flushed with pure N_2 for 20 min, then gas stream was set on bypass
d. Solution was added to the liquid reservoir

e. Liquid was pumped in the cycle; it was ensured that the stream was stable and ripple-free in the column
f. CO_2 concentration was set with the mass flow controllers with gas stream still on by pass
g. After 5 min stable liquid-, gas-, sensor-temperature, pressure and CO_2 concentration, the gas stream was switched to the wetted wall column
h. Ambient pressure and liquid flow were recorded
i. After 5 min steady state inside the wetted wall column the values of pressure, temperature and CO_2 concentration were recorded and the gas stream was set on bypass again
j. The CO_2 concentration was changed and steps g-i were repeated

The liquid flow rate of the solvent was chosen to be around 4 mL s^{-1} and the total gas volume stream coming from the mass flow controller (N_2 and CO_2) were 3 norm liters per minute. The pressure inside the column was not changed in most of the experiments and was around 1.5 bara; just for experiments at high CO_2 partial pressures the pressure inside the column was increased. In total 5-7 CO_2 concentrations were tested in an experimental run and the overall mass transfer coefficient was determined.

5.2. Methods

The methods to gain the mass transfer area, the gas and liquid side mass transfer coefficient as well as the transferred flux from the experiments with the wetted wall column are explained in the next section.

5.2.1. Material balance over the wetted wall column

The experiments in the wetted wall column are carried out at very high L/G ratios. The liquid phase is in excess in these experiments therefore the changes in liquid composition can be neglected when the liquid is passing through the wetted column. The change in gas phase composition is higher and can be measured with an online system continuously. The transferred flux of CO_2 can be calculated with the following formula:

$$y_{CO_2}^{in} \cdot N_{in}^{gas} - y_{CO_2}^{out} \cdot N_{out}^{gas} = \Delta N_{CO2} \tag{5.1}$$

With N_{in}^{gas} (mole s^{-1}) and N_{out}^{gas} (mole s^{-1}) being the total incoming and outgoing gas stream. It should be noted that the incoming gas stream N_{in}^{gas} is not equal the out coming gas stream N_{out}^{gas} because some components are absorbed by the liquid solvent. In Figure 2 one can see a material balance over the gas system in the wetted wall column. The gas phase is divided into two components: inert components, which are not absorbed by the liquid solvent like N_2, O_2, noble gases, water vapor at saturation and absorbent components that get absorbed by the solvent, like CO_2. Since the inert component is not absorbed its mole flux does not change in the wetted wall column. This can also be assumed for water

vapor, if the gas stream is saturated for the process temperature before entering the wetted wall column (wwc).

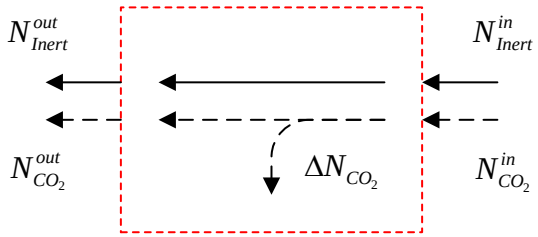

Figure 17: Material balance over the gas system in the wetted wall column

The measured mole fraction of CO_2 in these streams is equal to:

$$y_{CO_2} = \frac{N_{CO_2}}{N_{Inert} + N_{CO_2}} \tag{5.2}$$

From Equation (5.2) and (5.1) an expression of the absorbed CO_2 mole flux from the mole fraction of CO_2 before ($y_{CO_2}^{in}$) and after ($y_{CO_2}^{out}$) the wwc and the mole stream of all inert components N_{Inert} can be derived:

$$\Delta N_{CO_2} = \frac{N_{Inert} \cdot \left(y_{CO_2}^{in} - y_{CO_2}^{out} \right)}{\left(1 - y_{CO_2}^{in} \right) \cdot \left(1 - y_{CO_2}^{out} \right)} \tag{5.3}$$

If the setup is using a humidifier to saturate the gas stream with water and avoid evaporation in the wwc, the inert gas stream can be calculated from the nitrogen gas stream N_{N_2} and the CO_2 gas stream N_{CO_2} entering the wetted wall column, as well as the vapor pressure water in the humidifier P_{H_2O} (Pa) and the pressure inside the wetted wall column P_{WWC} (Pa) according to:

$$N_{Inert} = N_{N_2} + \frac{\frac{P_{H_2O}}{P_{WWC}}}{1 - \frac{P_{H_2O}}{P_{WWC}}} \left(N_{N_2} + N_{CO_2} \right) \tag{5.4}$$

Most of the NDIR probes are not measuring the mole fraction directly, but the molar concentration of CO_2 and refer the value to a standard state. The real mole fraction can be calculated using the pressure and temperature correction with the ideal gas law. The signal from the Vaisala Carbocap probe can be corrected by [5]:

$$y_{CO_2}(T;P) = y_{CO_2}(298.15K;101.35kPa)\frac{P(kPa)}{101.35kPa}\cdot\frac{298.15K}{T(K)} \tag{5.5}$$

A condenser will change the water content in the gas phase and influence the CO_2 content. The mole fraction inside the wetted wall column can be recalculated from the pressure inside the wwc and the condenser as well as the temperature dependent water vapor pressures in the wwc ($P_{H_2O}^{WWC}$) and the condenser ($P_{H_2O}^{condenser}$) by:

$$y_{CO_2}^{WWC} = y_{CO_2}^{probe}\cdot\frac{1-\frac{P_{H_2O}^{WWC}}{P_{WWC}}}{1-\frac{P_{H_2O}^{condenser}}{P_{condenser}}} \tag{5.6}$$

5.2.2. Mass transfer area

The contact area can be calculated from the dimensions in Figure 1 with a correlation for the thickness of the liquid film. The most applied correlation for the film thickness in wetted wall columns [6]–[8] is a momentum balance of a falling film on a flat plate that is described in detail by Bird et al. [9]:

$$\delta_{Film} = \left(\frac{3\cdot\mu_{liq}\cdot V_{liq}}{\rho_{liq}\cdot g\cdot L}\right)^{1/3} \tag{5.7}$$

Where μ_{liq} (Pa s) and ρ_{liq} (kg m^3) are the viscosity and density of the liquid, V_{liq} is the volume stream of the liquid (m^3 s^{-1}), g is the acceleration constant (m s^{-2}) and L (m) the width of the plate that can be taken as the perimeter of the wetted wall column. The area of the interface is then calculated from the surface of the cylindrical shaped column adding the film thickness twice to the outer diameter of the pipe and once to the height to the cylinder:

$$A_{int} = \pi\cdot(2\delta_{Film}+d_{WWC})\cdot(\delta_{Film}+h_{WWC})+\frac{\pi}{4}\cdot(2\delta_{Film}+d_{WWC})^2 \tag{5.8}$$

The height of the column has to be taken as the height above the gas inlet. Unlike packed columns wetted wall columns have surface efficiencies close to 1. That means that the whole gas-liquid interface participates in the mass transfer. Surface rippling might change interfacial area and makes interpretation of the experimental data impossible, but this can be overcome by addition of surface active agents like Teepol [3].

5.2.3. Contact time

The liquid velocity can be also calculated from the momentum balance, the velocity distribution in the liquid film perpendicular to column is according to Danckwerts [3]:

$$u_{liq}(x) = \frac{3}{2}\left(\frac{V_{liq}}{L}\right)^{2/3} \cdot \left(\frac{\rho_{liq} \cdot g}{3 \cdot \mu_{liq}}\right)^{1/3} \cdot \left(1 - x^2 \left[\frac{\rho_{liq} \cdot g \cdot L}{3 \cdot \mu_{liq} \cdot V_{liq}}\right]^{2/3}\right) \tag{5.9}$$

The velocity of the liquid at the surface (x=0) is therefore:

$$u_{int} = \frac{3}{2}\left(\frac{V_{liq}}{L}\right)^{2/3} \cdot \left(\frac{\rho_{liq} \cdot g}{3 \cdot \mu_{liq}}\right)^{1/3} \tag{5.10}$$

If the contact time τ (s) of a liquid element is defined by time a surface element needs to travel down the wetted wall column with a height h_{WWC} it can be calculated as:

$$\tau = \frac{h_{WWC}}{u_{int}} = \frac{2 \cdot h_{WWC}}{3}\left(\frac{V_{liq}}{L}\right)^{-2/3} \cdot \left(\frac{\rho_{liq} \cdot g}{3 \cdot \mu_{liq}}\right)^{-1/3} \tag{5.11}$$

5.2.4. Gas-side mass transfer coefficient

The accuracy of the kinetic measurement in a wetted wall column apparatus depends on the accuracy of the correlation for the gas side mass transfer coefficient. Absorption experiments are generally carried out in a gas mixture, thus the diffusion of the absorbing compound through the gas phase influences the overall mass transfer of that compound. The mass transfer in a flowing media can be described with a Sherwood correlation depending on flow characteristics and material properties in the following form [10]:

$$Sh = C \cdot Re^m \cdot Sc^n \tag{5.12}$$

With the following expressions for the dimensionless Sherwood (Sh), Reynolds (Re) and Schmidt (Sc) number:

$$\frac{k_{CO_2}^{gas} \cdot d_H \cdot R \cdot T}{D_{CO_2}^{gas}} = C \cdot \left(\frac{d_H \cdot v_{gas} \cdot \rho_{gas}}{\mu_{gas}}\right)^m \cdot \left(\frac{\mu_{gas}}{\rho_{gas} \cdot D_{CO_2}^{gas}}\right)^n \tag{5.13}$$

Where $k_{CO_2}^{gas}$ (mol Pa^{-1} m^{-2} s^{-1}) is the mass transfer coefficient in the gas phase, d_H (m) is the hydraulic diameter of the annulus (outer diameter of the annulus minus the diameter of the column containing the liquid film), R (J mol^{-1} K^{-1}) is the gas constant, T (K) is the gas temperature, $D_{CO_2}^{gas}$ the diffusion coefficient for CO_2 in N_2, v_{gas} (m s^{-1}) is the mean velocity in the annulus. An expression for Sherwood number incorporating R and T is used to give a mass transfer coefficient with units of (mol Pa^{-1} m^{-2} s^{-1}) rather than (m s^{-1}).

The Diffusion parameter of CO_2 in N_2 can be estimated by a binary diffusion coefficient for low pressure gases with the following correlation [9]:

$$D_{AB} = \frac{0.001858 T^{3/2} \left(\frac{1}{M_A} + \frac{1}{M_B} \right)^{1/2}}{P \sigma_{AB}{}^2 \Omega_D} \tag{5.14}$$

M_A and M_B are the molecular weights for the two compounds A and B, P is the pressure in atm, σ_{AB} is a Lennard Jones parameter and Ω_D is the collision integral that has to be taken from tables in literature. The unit of the binary Diffusion parameter D_{AB} is then cm^2/s. These binary diffusion coefficients are applicable up to 20 bar. It can be concluded that they are independent of the concentration of the diffusing component [11]. There are several other suitable correlation for binary gas Diffusion coefficients in literature [12].

Pacheco [8] proposed an expression for the gas side mass transfer coefficient in wetted wall columns where the exponents of the Schmidt number Reynolds and the factor (*d/h*) have the same exponent a. The quotient *d/h* relates the hydraulic diameter to the height of the column:

$$Sh = C_{Pa} \cdot Re^a \cdot Sc^a \left(\frac{d_H}{h_{WWC}} \right)^a \tag{5.15}$$

Luo et al. [13] suggested keeping the exponents for the Reynolds number and Schmidt number fixed at (1/2) and (1/3) respectively for a gas mass transfer coefficient correlation in wetted wall columns, as this is in accordance to the boundary layer theory:

$$Sh = C \cdot Re^{1/2} \cdot Sc^{1/3} \tag{5.16}$$

The constants and exponents in the correlations Eq. (5.15) and Eq. (5.16) have to be determined experimentally for every setup by performing absorption experiments where the main mass transfer resistance is allocated in the gas phase.

Mass transfer experiments with instantaneous liquid phase reaction, such as SO_2 absorption in NaOH [13], [14] or mass transfer experiments into solvents with well-known reaction kinetics, [2], [8] were used in literature to experimentally determine the gas side mass transfer coefficient. Some authors tried theoretical expressions [15], or even neglected the gas side mass transfer coefficient in experiments [16].

The determination of the gas side mass transfer coefficient from absorption experiment with a solvent with well-known reaction kinetics can be done with unloaded MEA in the pseudo-first order regime.

The Enhancement factor is then equal to the Hatta number and the CO_2 concentration in the liquid phase is zero, which leads to:

$$N_{CO_2} = \frac{P_{CO_2}^{gas}}{\frac{H_{CO_2}}{\sqrt{k_{2MEA} \cdot C_{MEA} \cdot D_{CO_2}^{liquid}}} + \frac{1}{k_{CO_2}^{gas}}} a_{eff} \tag{5.17}$$

which gives a k_{CO2}^{gas} of:

$$k_{CO_2}^{gas} = \frac{1}{\frac{H_{CO_2}}{\sqrt{k_{2MEA} \cdot C_{MEA} \cdot D_{CO_2}^{liquid}}} + \frac{P_{CO_2}^{gas} \cdot a_{eff}}{N_{CO_2}}} \tag{5.18}$$

With k_{2MEA} being the second order rate constant of the reaction between CO_2 and MEA that has to be taken from literature like Versteeg et al. [17]. Also literature values for the diffusion coefficient $D_{CO_2}^{liquid}$ and the Henry's coefficient H_{CO_2} are needed in this determination method for the gas side mass transfer coefficient.

The better way for determination of the gas side mass transfer coefficient is to perform absorption experiments with an instantaneous liquid phase reaction, which is independent to literature solution properties. A suitable system is the absorption of highly diluted SO_2 into NaOH solutions. Bishnoi & Rochelle [14], as well as Luo et al. [13] performed wetted wall column characterization tests with that system. In this work similar experiments were carried out for the wetted wall column described in section 5.3.

The Pacheco correlation is quite convenient as it has the same powers in the Schmidt and the Reynolds number which eliminate the density and viscosity of the gas. For the correlation by Luo et al. the density of the gas mixture was calculated according to the ideal gas equation and the viscosity was derived from a method by Wilke [18]. The diffusion coefficient of SO_2 in N_2 was correlated using Eq. (5.14).

The absorption flux of SO_2 can be obtained by a similar material balance like for CO_2. As there is no mass transfer limitation on the liquid side, the mass transfer simplifies to:

$$k_{SO_2}^{gas} = \frac{\Delta N_{SO_2}}{P_{SO_2}^{gas} \cdot a_{eff}} \tag{5.19}$$

There is also no backpressure of SO_2 from the solution, thus the driving force is equal to the partial pressure of SO_2 in the gas phase.

It is important to account for the gas side mass transfer resistance if quantitative interpretation from the wetted wall column experiments is desired. The influence of the gas side mass transfer coefficient on the overall mass transfer coefficient is increasing with increasing mass transfer. Thus especially for determining the kinetics of fast reacting solvents a good correlation for the gas side mass transfer coefficient is needed.

5.2.5. Physical liquid side mass transfer

In the wetted wall column the chemical liquid side mass transfer coefficient, the product of Enhancement factor and physical liquid side mass transfer coefficient can be experimentally determined. The Enhancement factor can just be derived when $k_{CO_2}^{liq0}$ is known. The physical liquid side mass transfer coefficient describes the mass transfer in the solvent in absence of reactions, which cannot be determined experimentally for the specific solvent. A similar Sherwood correlation can be derived for a non-reacting solvent. Luo et al. measured the absorption of pure CO_2 into water [13] and Pacheco measured the desorption of dissolved CO_2 from ethylene glycol water mixtures [8]. These determination methods are dependent on the physical properties of the test system (solubility and diffusivity).

Luo concluded from his experiments, that the penetration theory can predict the physical mass transfer coefficient accurately with the following formula including the contact time for the liquid τ [13]:

$$k_{CO_2}^{liq0} = 2\sqrt{\frac{D_{CO_2}^{sol}}{\pi \cdot \tau}} \tag{5.20}$$

Pacheco used an expression derived by Pigford [19] which uses the dimensionless numbers θ and ε, with:

$$\varepsilon = \frac{D_{CO_2}^{sol} \cdot \tau}{\delta_{Film}^2} \tag{5.21}$$

For the case that ε is greater than 0.01 the following analytical expression for calculating θ can be used [3]:

$$\theta = 0.7857 \cdot \exp\left(-5.121 \cdot \varepsilon\right) + 0.1001 \cdot \exp\left(-39.31 \cdot \varepsilon\right) + 0.0360 \cdot \exp\left(-105.6 \cdot \varepsilon\right) + 0.0181 \cdot \exp\left(-204.7 \cdot \varepsilon\right) \tag{5.22}$$

If ε is smaller than 0.01 then:

$$\theta = 1 - 3\sqrt{\frac{D_{CO_2}^{sol} \cdot \tau}{\pi \cdot \delta_{Film}^2}} = 1 - 3\sqrt{\frac{\varepsilon}{\pi}} \tag{5.23}$$

The ε parameter is dependent on the contact time. For short columns this value is below 0.01 unless the liquid film thickness is very thin or the diffusion coefficient is very large e.g. at high temperatures. Based on θ the physical liquid side mass transfer coefficient can be calculated as:

$$k_{CO_2}^{liq0} = \frac{V_{liq}}{a_{eff}}(1-\theta) \tag{5.24}$$

Although the expressions in Eq. (5.20) and Eq. (5.24) seem quite different, they result in the same values given the same contact time is used and for a_{eff} just the vertical part of the wetted wall column is considered. Inserting the contact time from Eq. (5.11) into Eq. (5.20) gives:

$$k_{CO_2}^{liq0} = \left(\frac{6 \cdot D_{CO_2}^{sol}}{\pi \cdot h_{WWC}}\right)^{1/2} \left(\frac{V_{liq}}{L}\right)^{1/3} \left(\frac{\rho_{liq} \cdot g}{3 \cdot \mu_{liq}}\right)^{1/6} \tag{5.25}$$

If Eq. (5.23) is inserted into Eq. (5.24) together with Eq. (5.21) and Eq. (5.7):

$$k_{CO_2}^{liq0} = \frac{3 \cdot V_{liq}}{h_{WWC} \cdot L}\left(\frac{2 \cdot D_{CO_2}^{sol} \cdot h_{WWC}}{3 \cdot \pi}\right)^{1/2} \left(\frac{L}{V_{liq}}\right)^{2/3} \left(\frac{\rho_{liq} \cdot g}{3 \cdot \mu_{liq}}\right)^{1/6} \tag{5.26}$$

Further simplification will give the exact same expression as in Eq. (5.31). As both literature expressions are giving the exact same results one can choose which expression that fits better.

5.3. Characterization of the wetted wall column

The gas side mass transfer coefficient was experimentally determined with SO_2 absorption experiments. Dilute Sulfur dioxide (1.5 vol% in N_2) was diluted with pure nitrogen to give a volume concentration of about 2000 ppmv (0.2 vol%). 1 M NaOH was used in the experiments at ambient temperature. The gas was sent through the wetted wall column reaction chamber at different gas velocities, lower and higher than the normal experimental conditions, and then analyzed for the SO_2 content in a Rosemount Fisher AG 200 NO/SO_2 analyzer with a measuring range between 0-2500 ppmv. No saturator was used in these experiments and the gas was conditioned in a condenser at 0 ºC prior to being sent to the analyzer. The results were then used to fit the constants for the different correlations. The results for the Sherwood correlations were:

$$Sh = 3.61 \cdot \left(Re \cdot Sc \cdot \frac{d_H}{h_{WWC}} \right)^{0.59} \tag{5.27}$$

and,

$$Sh = 1.36 \cdot Re^{1/2} \cdot Sc^{1/3}. \tag{5.28}$$

The fit to the standard formula from Eq. (5.12) resulted in:

$$Sh = 0.86 \cdot Re^{0.59} \cdot Sc^{0.21} \tag{5.29}$$

The results from the SO_2 absorption experiments and the resulting correlations are shown in Figure 18. The full analogy seems to fit best over the whole range of Reynolds number. Whereas the Pacheco correlation over predicts the Sherwood number for high Reynolds numbers and the boundary layer theory proposed by Luo [13] under-predicts the Sherwood number. The vertical line shows an average Reynolds number for the mass transfer experiments in this study. In this area all three correlations do not differ much from each other.

For model validation the Sherwood correlation was tested on predicting the CO_2 absorption for two different solvents at different gas velocities. The tested solvents were a 1 M NaOH solution at 25 ºC and 30 wt% MEA solutions at 40 ºC. Kinetic constants for the solvents were taken from Versteeg et al. [17] for MEA and from Pohorecki et al. [20] for NaOH, the diffusion coefficient for MEA was taken from Ko et al. [21] whereas that for NaOH was correlated with the Stokes Einstein equation using the viscosity from Laliberte [22]:

$$D_{CO_2}^{NaOH} = D_{CO_2}^{H_2O} \cdot \left(\frac{\mu_{H_2O}}{\mu_{NaOH}} \right)^{0.8} \tag{5.30}$$

The apparent Henry coefficient was taken from Luo et al. [23] for MEA and from Weisenberger and Schumpe for NaOH [24].

All correlations were capable of predicting the absorbed flux of CO_2 very well. The predicted fluxes differ only a little between the different correlations, which can be explained by the similar powers of the Reynolds number, as this number has the largest influence on the Sherwood number with the Schmidt number being close to 1 for all experiments. In the subsequent experiments the Pacheco correlation was used for the determination of the gas side mass transfer coefficient, as it does not require the gas density and viscosity and performed slightly better in absorption experiments when the CO_2 concentration in the gas phase was varied.

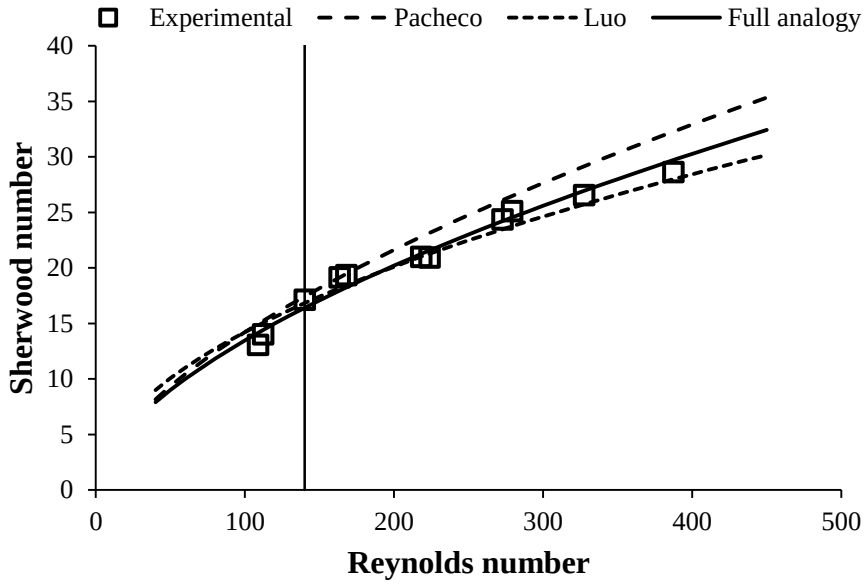

Figure 18: Results from the SO_2 absorption experiments and different Sherwood correlations

Figure 4 shows the predicted mass transfer flux using literature data for the liquid side resistance and the Pacheco correlation for the gas side resistance over the measured absorbed flux. This model is capable of predicting the trend of the gas side mass transfer resistance over a large range of Reynolds numbers (100-400) very well.

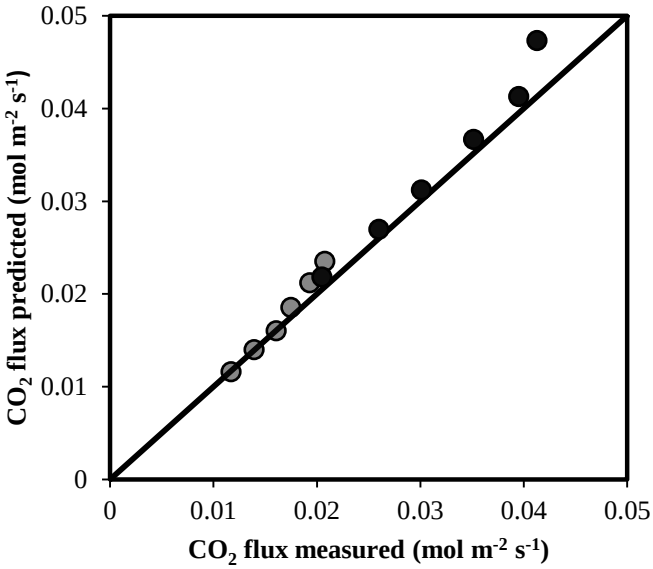

Figure 19: Experimental validation of the gas side mass transfer correlation using an Analogy proposed by Pacheco [8]

A gas side mass transfer correlation for this setup was determined with the chemical absorption method using unloaded MEA in the work of Darde et al.[2]. They reported a C_{Pa} constant of 1.53 and an exponent α of 1.02 for the Pacheco correlation. These results differ from the SO_2 absorption experiments although both Pacheco correlations are just 6-7 % apart for the typical range for gas velocities in absorption experiments carried out in the study.

5.4. Deriving kinetic constants from experimental data

Measuring the mass transfer at different partial pressures increases the accuracy of the mass transfer coefficient [25]. As CO_2 is absorbed in the wetted wall column the partial pressure is changing inside the wetted wall column. Therefore in interpretation of the experiments the mean logarithmic partial pressure of CO_2 $P_{CO_2}^{ml}$ is taken, which can be calculated as [8]:

$$P_{CO_2}^{ml} = \frac{\left(P_{CO_2}^{in} - P_{CO_2}^{out}\right)}{\ln\left(\frac{P_{CO_2}^{in}}{P_{CO_2}^{out}}\right)} \tag{5.31}$$

In Figure 20 the amount of transferred CO_2 calculated with Eq. (5.3) is plotted against the mean logarithmic CO_2 gas partial pressure. The slope regressed from the experimental data points is the overall mass transfer coefficient $K_{CO_2}^{ovG}$ (mol Pa^{-1} m^{-2} s^{-1}). The value can be derived with a linear regression. For the experiments depicted in Figure 20, the overall mass transfer coefficient is 3.92 $*10^{-7}$ mol Pa^{-1} m^{-2} s^{-1}. The intersection of the linear regression with the x-axis represents the equilibrium partial pressure of the liquid. The value in this experiment was around 11250 Pa.

The liquid side mass transfer coefficient can then be derived as the overall mass transfer resistance is the sum of gas and liquid side mass transfer resistance:

$$\frac{1}{k_{CO_2}^{liq}} = \frac{1}{K_{CO_2}^{ovG}} - \frac{1}{k_{CO_2}^{gas}} \tag{5.32}$$

It should be assured that the gas side mass transfer resistances in the different experiments used to create one slope, are equal. This can be achieved by running the experiments at the same gas velocities. Since the Pacheco correlation for the gas side mass transfer coefficient from Eq. (5.16) does not depend on the viscosity or density, the velocity is the only determining process condition. Same gas velocities can be achieved, by keeping the total gas volume stream (N_2 and CO_2) constant.

If the experiments are carried out in the pseudo first order reaction regime the determination of the kinetic constants are easy and straightforward. N_{CO_2} can be calculated with:

$$N_{CO_2} = \frac{\left(P_{CO_2}^{gas} - H_{CO_2} \cdot C_{CO_2}^{liq}\right)}{\frac{1}{k_{CO_2}^{gas}} + \frac{H_{CO_2}}{\sqrt{k_{obs}^{ps.1.} \cdot D_{CO_2}}}} \tag{5.33}$$

In that case observed pseudo-first order rate constant can be calculated:

$$k_{obs}^{ps.1.} = \frac{1}{D_{CO_2}} \left(\frac{H_{CO_2}}{\frac{P_{CO_2}^{gas} - P_{CO_2}^{liq}}{N_{CO_2}} a_{eff} - \frac{1}{k_{CO_2}^{gas}}} \right)^2 \tag{5.34}$$

This observed pseudo-first order rate constant represents the overall reaction of CO_2 with the solution.

The Enhancement factor has to be solvent for the mass transfer equation outside the pseudo-first order regime. This needs to be done iteratively by adjusting the kinetic constants until the experimentally determined flux is equal to the simulated one.

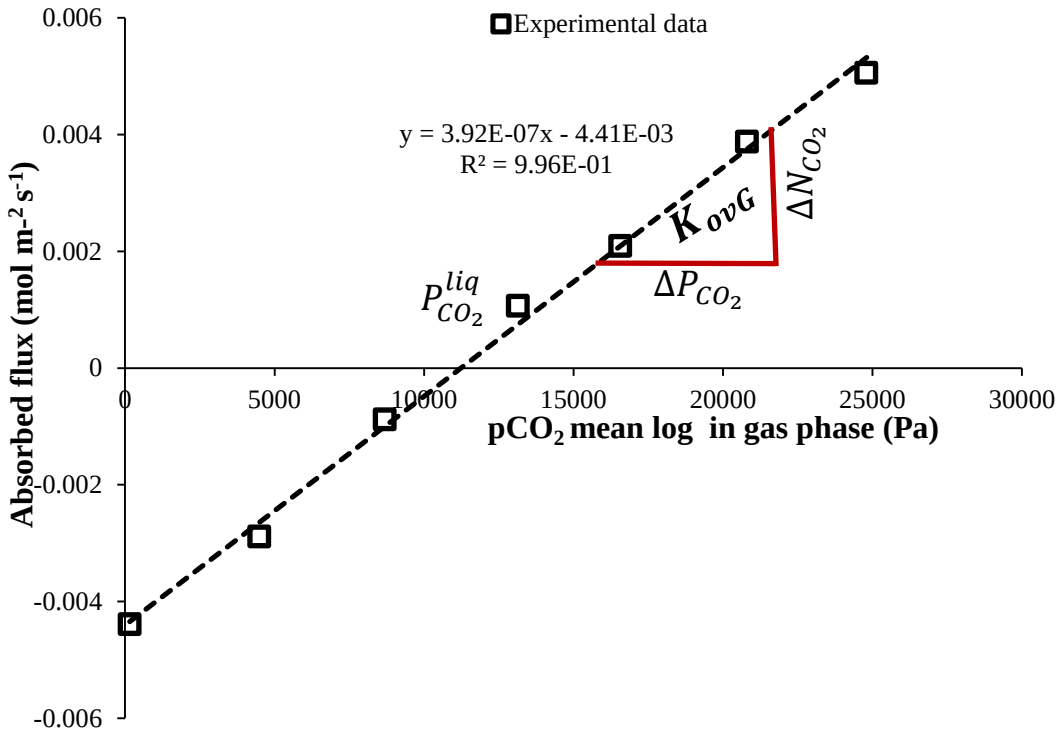

Figure 20: Determination of the overall mass transfer coefficient K_{ovG} and the CO_2 partial pressure in the liquid phase P_{liq} from experimental results in the wetted wall column

Nomenclature

Symbols:	
a	Exponent in Sherwood correlation
a_{eff}	Effective mass transfer area
C	Constant in Sherwood correlation
C_{Pa}	Constant in Sherwood correlation proposed by Pacheco
D_{AB}	Diffusion coefficient ($m^2\ s^{-1}$)
d_H	Hydraulic diameter of wetted wall column (outer- inner diameter) (m)
d_{WWC}	Diameter of wetted wall column
h_{WWC}	Height of wetted wall column
$k_{CO_2}^{gas}$	Gas side mass transfer coefficient (mol $Pa^{-1}\ m^{-2}\ s^{-1}$)
$k_{CO_2}^{liq}$	Liquid side mass transfer coefficient (mol $Pa^{-1}\ m^{-2}\ s^{-1}$)
$k_{CO_2}^{liq0}$	Physical liquid side gas mass transfer coefficient ($m\ s^{-1}$)
L	Perimeter of wetted wall column
m	Exponent in Sherwood correlation
n	Exponent in Sherwood correlation
N_i^j	Flux of i at position j (mol s^{-1})
P_i^j	Pressure of i at position j (Pa)
Re	Reynolds number
Sc	Schmidt number
Sh	Sherwood number
u	velocity ($m\ s^{-1}$)
V_{liq}	Volume stream of liquid
y_{CO_2}	Mole fraction of CO_2 in gas phase (-)
Abbreviations:	
in	Inlet
int	Interface
Inert	Inert gas compounds
ml	Mean logarithmic
NDIR	Non-dispersive infra-red
out	Outlet
Ps.1	Pseudo-first order
WWC	Wetted wall column
Greek symbols:	
δ	Film thickness (m)
ε	Parameter used in Eq. (5.21)
ρ	Density ($kg\ m^{-3}$)
μ	Viscosity

τ Contact time (s)

BIBLIOGRAPHY

[1] L. Li, H. Li, O. Namjoshi, Y. Du, and G. T. Rochelle, "Absorption rates and CO_2 solubility in new piperazine blends," *Energy Procedia*, vol. 37, pp. 370–385, 2013.

[2] V. Darde, W. J. M. van Well, P. L. Fosboel, E. H. Stenby, and K. Thomsen, "Experimental measurement and modeling of the rate of absorption of carbon dioxide by aqueous ammonia," *Int. J. Greenh. Gas Control*, vol. 5, no. 5, pp. 1149–1162, 2011.

[3] P. V. Danckwerts, *Gas-Liquid Reactions*, 1st ed. McGraw-Hill, 1970.

[4] T. L. Sønderby, K. B. Carlsen, P. L. Fosbøl, L. G. Kiørboe, and N. von Solms, "A new pilot absorber for CO_2 capture from flue gases: Measuring and modelling capture with MEA solution," *Int. J. Greenh. Gas Control*, vol. 12, pp. 181–192, 2013.

[5] Vaisala, "Application note Vaisala: how to measure carbon dioxide." [Online]. Available: http://img.en25.com/Web/Vaisala/%7B92b53609-48c2-43d8-aecb-0b68b191b748%7D_CEN-TIA-Parameter-How-to-measure-CO_2-Application-note-B211228EN-A-LOW-v7.pdf. [Accessed: 07-Dec-2015].

[6] J. T. Cullinane and G. T. Rochelle, "Kinetics of Carbon Dioxide Absorption into Aqueous Potassium Carbonate and Piperazine," *Ind. Eng. Chem. Res.*, vol. 45, no. 8, pp. 2531–2545, 2006.

[7] X. Luo, A. Hartono, and H. F. Svendsen, "Comparative kinetics of carbon dioxide absorption in unloaded aqueous monoethanolamine solutions using wetted wall and string of discs columns," *Chem. Eng. Sci.*, vol. 82, pp. 31–43, 2012.

[8] M. A. Pacheco, "Mass Transfer, Kinetics and Rate-based Modeling of Reactive Absorption," *Dr. Thesis Univ. Texas Austin*, p. 318, 1998.

[9] B. Bird, W. E. Stewart, and E. N. Lightfoot, *Transport Phenomena*, 2nd ed. Wiley & Sons, 2000.

[10] A. Mersmann, M. Kind, and J. Stichlmair, *Thermal separation Technology*, 1st ed. Springer_Verlag, 2011.

[11] T. K. Sherwood, R. L. Pigford, and C. R. Wilke, *Mass Transfer*, 1st ed. McGraw-Hill, 1975.

[12] D. Eimer, *Gas Treating: Absorption Theory and Practice*, 1st ed. John Wiley & Sons Ltd., 2014.

[13] X. Luo, "Experimental and numerical study of carbon dioxide mass transfer and kinetics in amine solutions," *Dr. Thesis from NTNU Norw.*, 2012.

[14] S. Bishnoi and G. T. Rochelle, "Absorption of carbon dioxide into aqueous piperazine: reaction kinetics, mass transfer and solubility," *Chem. Eng. Sci.*, vol. 55, no. 22, pp. 5531–5543, 2000.

[15] A. Servia, N. Laloue, J. Grandjean, S. Rode, and C. Roizard, "Modeling of the CO_2 Absorption

in a Wetted Wall Column by Piperazine Solutions," *Oil Gas Sci. Technol. – Rev. d'IFP Energies Nouv.*, vol. 69, no. 5, pp. 885–902, 2014.

[16] B. P. Mandal, A. K. Biswas, and S. S. Bandyopadhyay, "Selective absorption of H_2S from gas streams containing H2S and CO_2 into aqueous solutions of N-methyldiethanolamine and 2-amino-2-methyl-1-propanol," *Sep. Purif. Technol.*, vol. 35, no. 3, pp. 191–202, 2004.

[17] G. F. Versteeg, L. A. J. . van Dijck, and W. P. M. van Swaaij, "On the Kinetics between CO_2 and Alkanolamines both in aqueous and non-aqueous solutions. An overview," *Chem. Eng. Commun.*, vol. 144, pp. 113–158, 1996.

[18] C. R. Wilke, "A Viscosity Equation for Gas Mixtures," *J. Chem. Phys.*, vol. 18, no. 4, p. 517, 1950.

[19] R. L. Pigford, "Counter-Diffusion in a Wetted Wall Column," *Dr. thesis Univ. Illinois*, 1941.

[20] R. Pohorecki and W. Moniuk, "Kinetics of reaction between carbon dioxide and hydroxyl ions in aqueous electrolyte solutions," *Chem. Eng. Sci.*, vol. 43, no. 1959, pp. 1677–1684, 1988.

[21] J. J. Ko, T. C. Tsai, C. Y. Lin, H. M. Wang, and M. H. Li, "Diffusivity of nitrous oxide in aqueous alkanolamine solutions," *J. Chem. Eng. Data*, vol. 46, no. 1, pp. 160–165, 2001.

[22] M. Laliberte, "Model for calculating the viscosity of aqueous solutions," *J. Chem. Eng. Data*, vol. 52, no. 2, pp. 321–335, 2007.

[23] X. Luo, A. Hartono, S. Hussain, and H. F. Svendsen, "Mass transfer and kinetics of carbon dioxide absorption into loaded aqueous monoethanolamine solutions," *Chem. Eng. Sci.*, vol. 123, pp. 57–69, 2015.

[24] S. Weisenberger and a Schumpe, "Estimation of gas solubilities in salt solutions at temperatures from 273 K to 363 K," *AIChE J.*, vol. 42, no. 1, pp. 298–300, 1996.

[25] J. T. Cullinane, "Thermodynamics and Kinetics of Aqueous Piperazine with Potassium Carbonate for Carbon Dioxide Absorption," *Phd Thesis Univ. Texas Austin*, p. 318, 2005.

6. Solvent comparison

This chapter summarizes the mass transfer experiments carried out on the wetted wall column. One solvent from each different solvent type was chosen: MEA from the group of primary amines, AMP from the sterically hindered amines, the tertiary amine MDEA and the carbonate salt K_2CO_3. The solvents were first compared on their absorption performance in unloaded aqueous solutions without enzymes, and then the effect of adding 2 g/L of enzymes on the mass transfer of the solvents was compared. For the solvents showing the best effect upon enzyme addition, K_2CO_3 and MDEA, additional experiments were carried out determining the effect of enzyme concentration, temperature and solvent concentration on mass transfer. The absorption performance of the enzyme enhanced solvents was then benchmarked against literature data of solvents used in industrial gas cleaning.

6.1. Solvents without enzyme

Absorption experiments without enzyme were carried out with unloaded aqueous solutions of MEA (30 wt%), AMP (30 wt%), MDEA(30 wt%) and K_2CO_3 (15 wt%) at 298, 313 and 328 K. Additional experiments with MDEA in mixture with piperazine (PZ) was tested as a benchmark as it represents BASF's a-MDEA technology that is employed in industrial processes.

6.1.1. Pure solvents

The results for the liquid side mass transfer coefficient k_{liq} of the different unloaded solvents are shown in Figure 21 for MEA, AMP, MDEA and K_2CO_3 together with literature correlation for the liquid side mass transfer coefficient assuming pseudo-first order regime; the values for the literature correlation and the sources can be found in the Appendix A.

Good agreement between experiments and literature values could be observed for all solvents at different temperatures. Unloaded 30 wt% MEA was by far the fastest absorbing solvent in these experiments, followed by AMP and then K_2CO_3 and MDEA. The direct reaction mechanism with CO_2 for AMP and MEA makes primary/secondary amines faster than tertiary amines or carbonate salt solution that follow a base catalyzed mechanism [1]. The sterical hindrance for AMP can explain the difference in mass transfer between AMP and MEA, both primary amines, as the formation of the unstable carbamate is slower than the stable carbamate formation in MEA [2].

The liquid side mass transfer for 15 wt% K_2CO_3 and 30 wt% MDEA were almost equal, MDEA being just slightly slower. The liquid side mass transfer coefficient increases with temperature for all solvents enabling higher mass transfer fluxes at the same driving forces. Several temperature dependent properties of the solution influence the liquid side mass transfer differently: the rate of the reaction always increases with temperature as does the diffusivity, whereas the physical solubility of CO_2

decreases. A rise in liquid side mass transfer coefficient with temperature showed a greater influence of reaction kinetics and diffusivity on mass transfer than solubility.

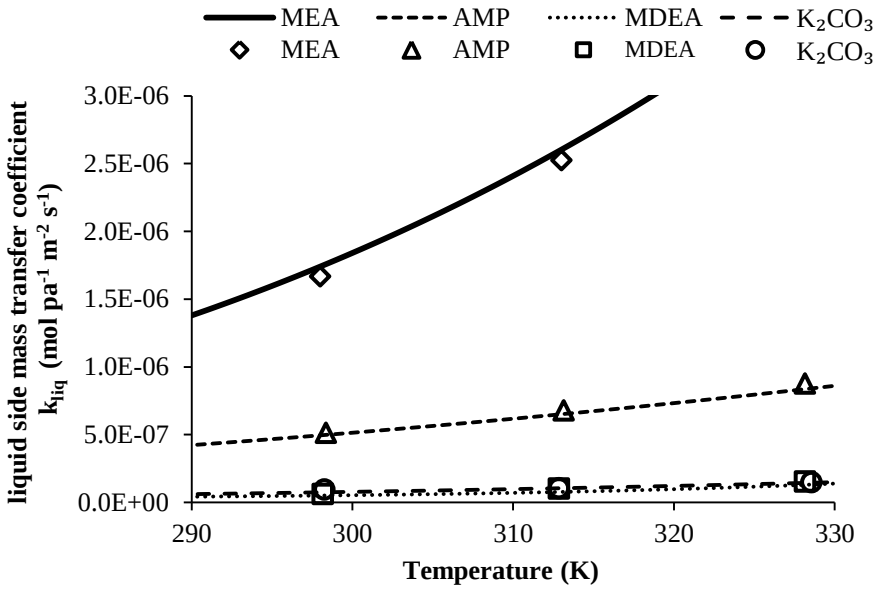

Figure 21: Liquid side mass transfer coefficient for unanalyzed solvents as a function of temperature: Comparison of experimental determined k_{liq} for 30 wt% MEA,30 wt% AMP, 30 wt% MDEA and 15 wt% K_2CO_3 at 298, 313 and 328 K

6.1.2. Piperazine promoted MDEA

Tertiary amines beneficial properties can be utilized when the slow mass transfer is enhanced with a kinetic promoter. This method is widely applied in BASF's a-MDEA solvent technology which is mixture of the tertiary amine MDEA and the secondary di-amine piperazine (PZ) (a stands for activated). In order to benchmark the enzyme enhanced solutions, especially the enzyme enhanced MDEA to solvents used in industrial gas scrubbing, experiments with MDEA-PZ mixtures were carried out at the same process conditions. There is not just one a-MDEA solution, but the processes employ mixtures with MDEA concentrations between 30 and 54 wt% with up to 7 wt% PZ [3]. 30 wt% MDEA was chosen as it represented the reference concentration for enzyme enhanced MDEA experiments, together with 5 wt% PZ, which represented a high concentration of the kinetic promoter. The results for the liquid side mass transfer resistance at different solvent loadings are shown in Figure 22.

The activation of MDEA with PZ increased the mass transfer significantly; the mass transfer at 298 K was 22 times higher than unloaded MDEA at 298 K and 20 times higher at 313 K compared to unloaded 30 wt% MDEA at 313 K. At 328 K an increase of 15 times was observed in the experiments. The measured liquid side mass transfer coefficient of PZ activated MDEA at low solvent loadings and

high temperatures was close unloaded 30 wt% MEA solution (2.3 *10^{-6} mol Pa $^{-1}$ m^{-2} s^{-1} vs. 2.5 *10^{-6} mol Pa $^{-1}$ m^{-2} s^{-1}).

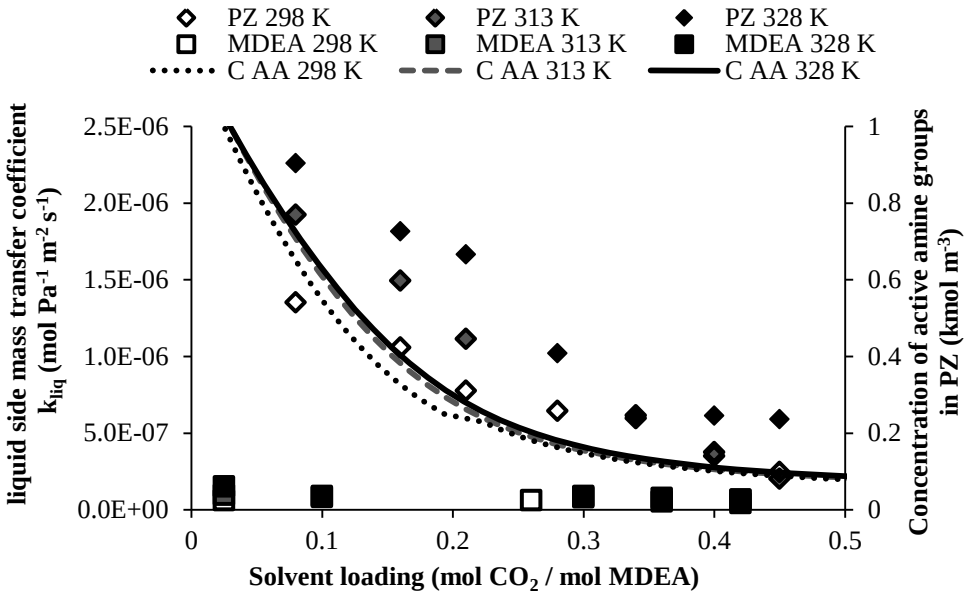

Figure 22: Liquid side mass transfer coefficient for 30 wt% MDEA and 30 wt% MDEA activated with 5 wt% piperazine as a function of solvent loading for different temperatures, concentration of active amine groups in PZ (CAA) as function of solvent loading according to the extended Uniquac model [4]

Loading of the MDEA-PZ with CO_2 decreased the liquid side mass transfer remarkably; the decrease was steeper for higher temperature. At a solvent loading of about 0.4 the catalytic effect of PZ, describing the ratio of mass transfer of activated solvent to unloaded non-activated solvent at the same temperature, dropped from 22 to 6 at 298 K, from 20 to 4 at 313 K and from 15 to 4 at 328 K. This represented a decrease in mass transfer by 72 % at 298 K, 80 % at 313 K and 73 % at 328 K.

This decreasing tendency can be explained by the concentration of the active species of promoter in the solution. When the CO_2 loading is increased in the solution, piperazine forms carbamate and gets protonated, thus the concentration of active piperazine decreases. The concentration of active amines in piperazine according to the extended UNIQUAC model is also shown in Figure 22. Piperazine can form several different reaction products in mixture with water and carbon dioxide; these species are shown in Figure 23. Of all of these species the unreacted piperazine (top left), and the monocarbamate piperazine (top right) are the main contributors to the solvent reactions [5][6]. Thus only the concentrations of these compounds are accounted for in the calculation of active amines concentration CAA in Figure 22. The concentration of unreacted PZ is counted twice in CAA, as it has two active amine groups.

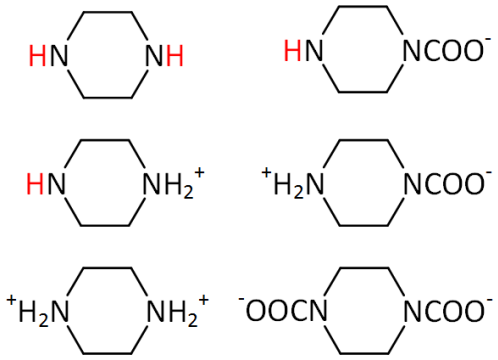

Figure 23: Speciation of piperazine in aqueous solution with CO_2

The decrease in mass transfer was coherent with the decrease in active amine groups in PZ CAA. These concentrations were not affected too much by temperature, but very much by solvent loading. Because piperazine reactions followed an Arrhenius type temperature dependency [7], the reactions are higher at high temperature, thus the mass transfer increased with temperature. This explains the temperature trend for PZ activated MDEA.

A great decrease of mass transfer with loading was also observed from Derks [8] in 4 M MDEA/0.5 M PZ and 4 M MDEA/1 M PZ solutions at 298 K, as well as from Bishnoi and Rochelle [6] in 4M MDEA/0.6 M PZ at 313 K. Bishnoi and Rochelle described the dominant reaction at low solvent loading being the monocarbamate formation from piperazine and at high solvent loading the dicarbamate formation from monocarbamate.

The mass transfer in PZ promoted MDEA is not following pseudo first order reaction kinetics [6], because of the very high reaction kinetics of PZ in combination of its dilute concentrations. The concentrations of active PZ molecules decrease a lot at higher solvent loadings. Under these conditions the mass transfer becomes influenced by the physical mass transfer of CO_2 as explained in chapter 2 [9]. Thus the measured k_{liq} values for loaded MDEA/PZ mixtures are dependent on the $k_{liq0.}$ The reported values here were measured at k_{liq0} values of $1.0*10^{-4}$, $1.2*10^{-4}$, $1.4*10^{-4}$ m s^{-1} for 298, 313 and 328 K respectively.

6.2. Effect of Carbonic Anhydrase enzyme on the liquid side mass transfer coefficient

Several enzyme charges were derived from Novozymes. The first smaller charge Batch (I) was used to compare the different solvents, AMP, MEA, K_2CO_3 and MDEA with each other, by adding 2 g/L CA to the solvent and determine the effect of temperature and solvent concentration on the mass transfer. The second bigger charge Batch (II) was used for the kinetic model development and for pilot scale absorption experiments with MDEA solutions. Small differences were observed in enzyme performance between these two charges which are addressed in Section 6.2.3.

The experimental results for the different solvents are presented in the same manner, at first the experimentally determined liquid side mass transfer coefficient k_{liq} of the unloaded solvent at the reference concentration (30 wt% for amines and 15 wt% for K_2CO_3) was compared to the enzyme enhanced solvent with 2 g/L CA added, at 298, 313 and 328 K and the temperature effect of CA is discussed. The catalytic effect CE (-) of the enzyme is reported, which is the ratio of enzyme enhanced k_{liq} to plain solvent k_{liq}, and visualizes how much faster the solvent became upon enzyme addition. Then the effect of enzyme concentration on k_{liq} is shown and afterwards the effect of solvent concentration on the mass transfer is shown and discussed. The first order enzyme reaction rate k_{ovenz} (s^{-1}) is calculated from the overall CO_2 reaction rate derived from the liquid side mass transfer coefficient applying the mass transfer theory and subtracting the first order solvent reaction rate (second order solvent reaction rate times solvent concentration). The relation between k_{ovenz} (s^{-1}) and CA concentration is discussed and the enzyme reaction rate constant k_{enz} is calculated by dividing k_{ovenz} with the enzyme concentration.

6.2.1. K_2CO_3

When adding 2 g/L CA to 15 wt% K_2CO_3 a significant increase in liquid side mass transfer coefficient could be observed, as shown in Figure 24. The liquid side mass transfer of the enzyme enhanced solvent was slightly decreasing with temperature, whereas the mass transfer for plain 15 wt% K_2CO_3 is slightly increasing.

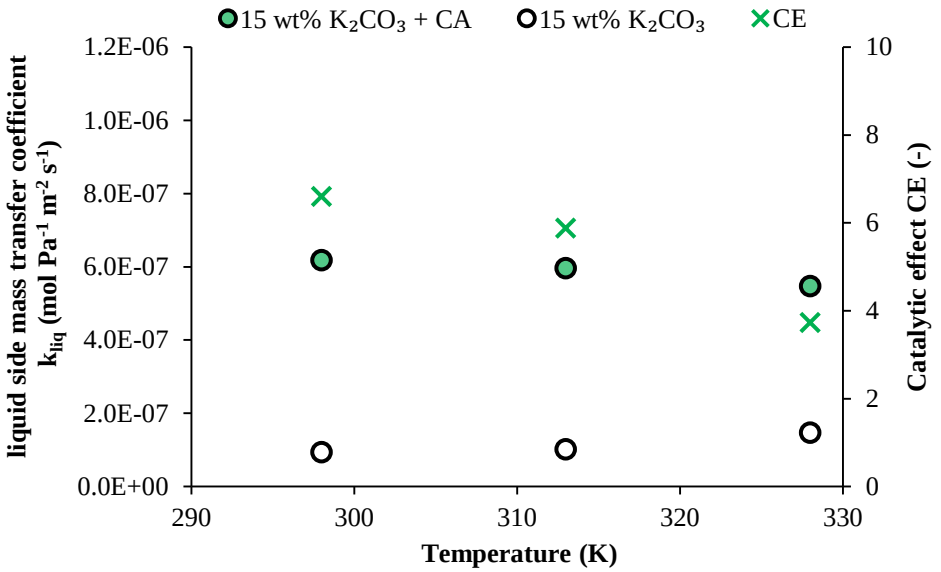

Figure 24: Effect of adding 2 g/L CA on the liquid side mass transfer coefficient k_{liq} in 15 wt% K_2CO_3 solutions for different temperatures (298–328 K)

The enzyme enhanced solvent of this solvent was about 7 times faster at 298 K and 6 times at 313 K than the solvent without enzyme. This value was decreasing to less than 4 times at 328 K. The decrease in catalytic effect with temperature resulted from the opposing trends of liquid side mass transfer between enzyme enhanced and non-enhanced solvents with higher temperatures.

For a carbonate salt solution containing 15 wt% K_2CO_3 and 2 g/L CA a low absorption temperature is clearly favorable, as liquid side mass transfer was the highest and the effect of enzyme addition was diminishing at higher temperatures. Besides that solutions have a higher cyclic capacity at lower temperatures.

The enzyme acts as a catalyst for the bicarbonate formation in carbonate salt solution, thus the conversion of CO_2 is dependent on the catalyst concentration. The influence of CA concentration on the liquid side mass transfer for 15 wt% K_2CO_3 at 313 K is shown in Figure 25.

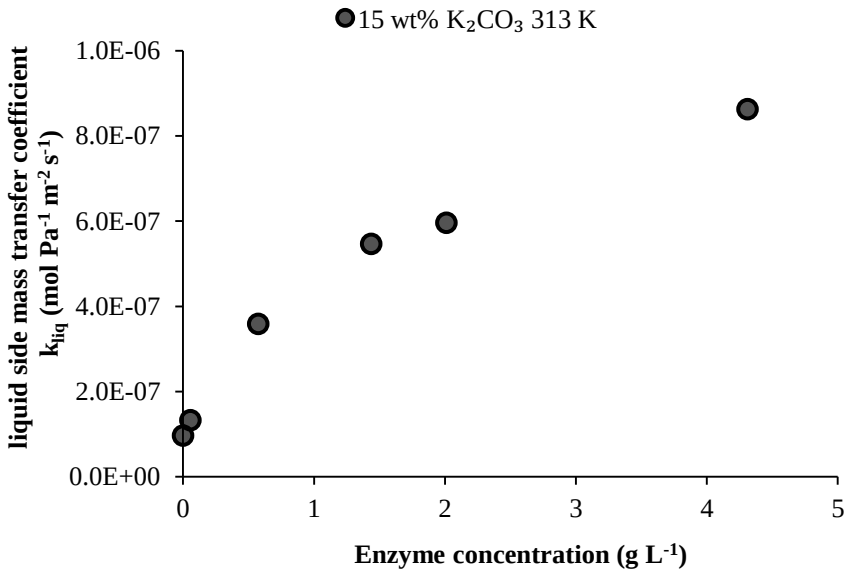

Figure 25: Influence of enzyme concentration on liquid side mass transfer coefficient k_{liq} for unloaded 15 wt% K_2CO_3 solutions at 313 K

Even small amounts of the enzyme showed a considerable effect on the mass transfer. The mass transfer could be increased furthermore by increasing the enzyme concentration up to over 4 g/L. The relation between liquid side mass transfer coefficient and enzyme concentration is non-linear as the trend was flattening out at higher enzyme concentrations. In that case a considerable higher amount of enzyme would be needed for a further increase in mass transfer. We did not observe any maximum value for the mass transfer above which a further increase in enzyme concentration did not result in higher mass transfer as reported in literature [10].

Besides temperature, solvent concentration is a crucial process parameter to influence the mass transfer. The mass transfer experiments in Figure 26 were conducted with unloaded K_2CO_3 solutions at different solvent concentrations and different temperatures.

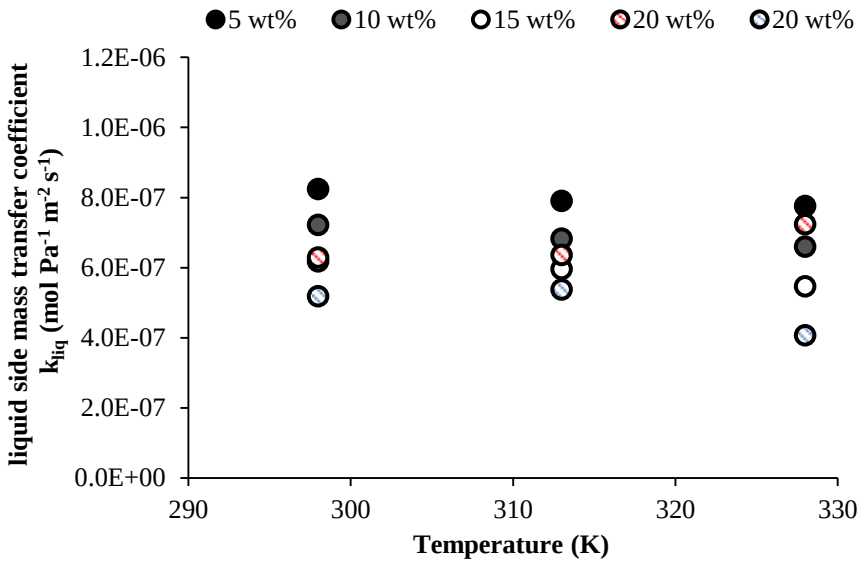

Figure 26: Influence of temperature (298-328 K) on liquid side mass transfer coefficient k_{liq} for unloaded K_2CO_3 solutions with 2 g/L CA at different solvent concentrations (5-20 wt%)

The solutions with lower K_2CO_3 concentration ranging from 5 to 15 wt% all demonstrated a decline liquid side mass transfer with higher temperature. The solvent concentration in the range of 5 to 15 w% also showed a negative effect on the mass transfer as k_{liq} was decreasing when the solvent concentration was increased. The combination of CA and K_2CO_3 solutions posed some problems in the experiments with precipitation of enzyme and foaming especially at high solvent concentrations. This might be even more induced as this solvent concentration was close to the solubility limit of K_2CO_3 in water for room temperature. Due to that reason experiments at 20 wt% K_2CO_3 were prepared in a modified procedure: by heating up of the liquid to about 40 °C and then adding of the enzyme into the warm solution. The experimental points at 20 wt% that were prepared with prior heating of the solvent are striped in red; the blue striped circles were prepared at room temperature, but also contained a lower enzyme concentration of just 1.5 g/L. The experiments conducted at 20 wt% K_2CO_3 prepared with preheated solvent did not follow the decreasing trend of k_{liq} at higher temperatures.

The solution that were prepared at room temperature showed between 18 and 15 % lower mass transfer at 298 and 313 K compared to the solutions that were preheated, which might be explained with a lower enzyme concentration of 1.5 g/L compared to 2 g/L. For 15 wt% K_2CO_3 solutions the difference in mass transfer between solutions enhanced with 1.5 g/L and 2 g/L was about 10 % as shown in Figure 25. At 328 K these values differed by almost 50 % indicating that the preparation procedure had an

influence on the enzyme performance especially for near precipitating carbonate salt solutions. The results from experiments with solutions that were prepared at room temperature show a more uniform trend for solvent concentration and temperature influence. This indicates that the preparation procedure for enzyme enhanced K_2CO_3 solutions is a crucial step and needs to be further investigated when this enzyme is applied in larger scale.

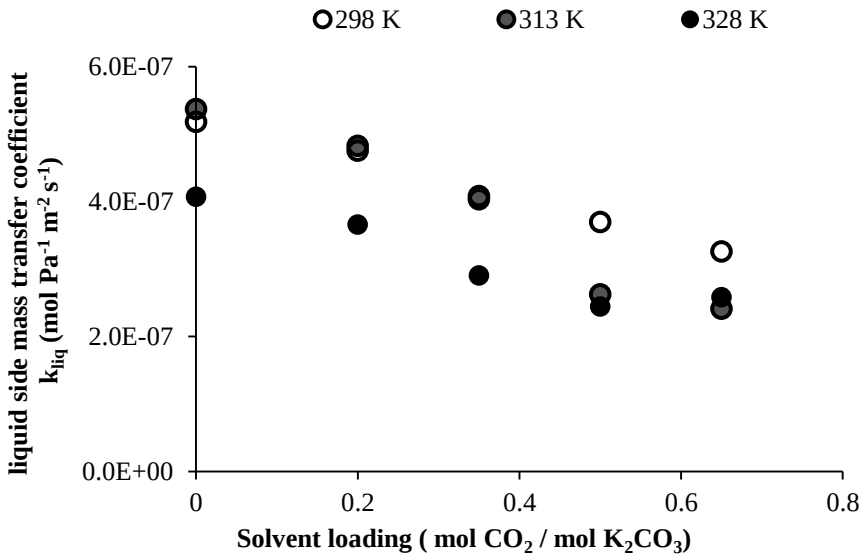

Figure 27: Effect of solvent loading on liquid side mass transfer coefficient k_{liq} for 20 wt% K_2CO_3 solution containing 1.5 g/L CA at different temperatures

The effect of solvent loading on the mass transfer was investigated for 20 wt% K_2CO_3 with 1.5 g/L (prepared at room temperature); the results are shown in Figure 27. A higher solvent loading, described in mole CO_2 bound per mole K_2CO_3 in solution, lead to a decrease in mass transfer despite the process temperature. The values for k_{liq} at high solvent loadings were 40-50 % lower than for unloaded solutions. This demonstrates the importance to account for the effect of solvent loading on mass transfer for enzyme enhanced solvents.

When the reaction rate of the solvent was calculated according to pseudo first order reaction behavior, the contribution of the enzyme to the overall reaction could be determined. The results of the enzyme contribution to the overall reaction together with the first order enzyme reaction rate constant, which is the difference of overall first order reaction rate constant in solution and the overall first order reaction rate constant of the solvent alone are shown in Figure 28.

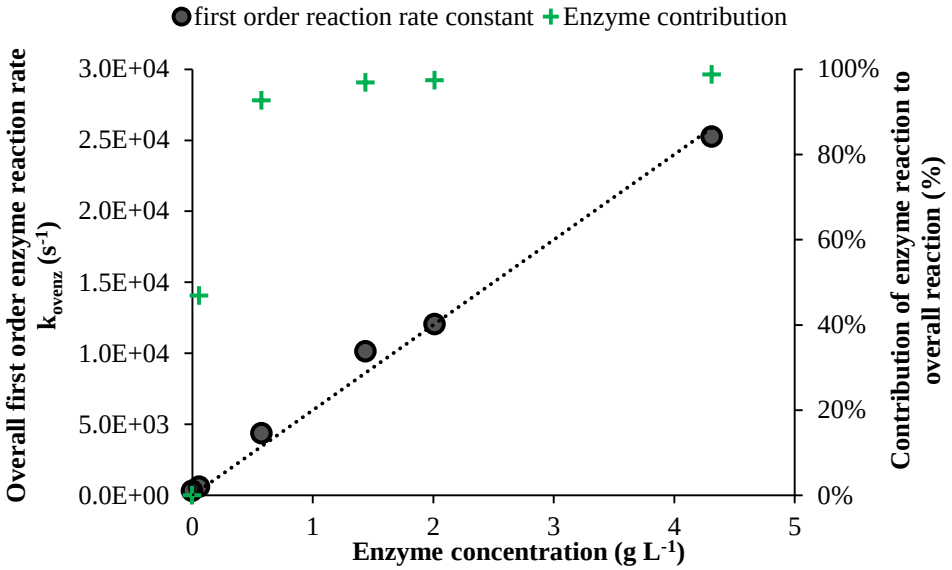

Figure 28: Overall first order enzyme reaction rate constant and contribution of enzyme reaction to overall reaction in 15 wt% K_2CO_3 at 313 K as function of enzyme concentration.

The contribution of the enzyme reaction rate to the overall reaction rate was already significant at around 0.06 g/L CA, where almost 50% could be credited to the enzyme. If the enzyme concentration was raised 10 times to 0.6 g/L already more than 90 % of the overall reaction was caused by CA. This contribution was further increased with enzyme concentration making up up to 99 % of the overall reaction at an enzyme concentration higher than 4 g/L. These findings suggest that the enzyme enhanced mass transfer in slow absorbing solvents like K_2CO_3 can be described with just an enzyme reaction rate, when high enzyme concentrations are applied. Although special care should be taken for desorber conditions at higher temperatures as it could be seen in Figure 24 that the enzyme contribution was decreasing with temperature. The relation between first order enzyme reaction rate constant and enzyme concentration is a linear trend, thus the enzyme reaction rate can be expressed with a second order enzyme reaction rate constant k_{enz} multiplied by the enzyme concentration C_{enz}.

The second order enzyme reaction rate constant k_{enz} can be derived from the first order enzyme reaction rate constant by division through the enzyme concentration. The units used for enzyme concentration was kg m^{-3}, which is equal to g L^{-1}. The results for the experiments at different temperatures and different solvent concentrations are shown Figure 29.

The trend was uniform for the lower concentration range of the solvent (5-15 wt%). In that region k_{enz} was slightly increasing with temperature, resulting in a 50 % higher value at 328 K compared to 298 K for 5 wt% K_2CO_3 and approximately 30 % higher at 10 and 15 wt% K_2CO_3. A higher solvent concentration resulted in a higher k_{enz}, 15 wt% solutions showed a 70 % increase and 10 wt% a 36 % increase compared to 5 wt% solutions at 298 K. These differences became less intense at higher

temperatures, as they were 61 and 29 % at 313 K and 42 and 20 % at 328 for 15 wt% and 10 wt% K_2CO_3 solutions compared to 5 wt%. For 20 wt% K_2CO_3 solutions k_{enz} was significantly higher than for experiments at 5-15 wt% solvent concentration.

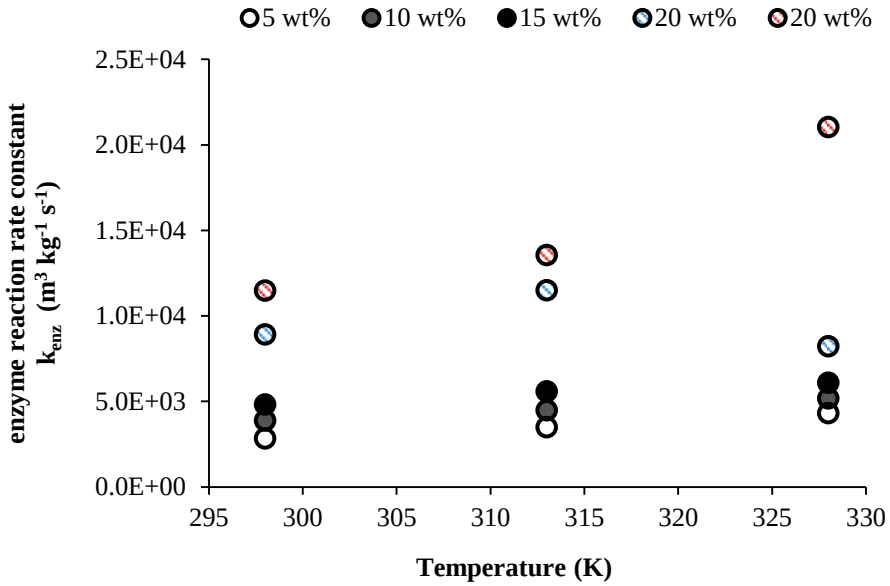

Figure 29: Second order enzyme reaction rate constant kenz (m^3 kg^{-1} s^{-1}) in K_2CO_3 solutions as a function of temperature for different solvent concentrations. Blue striped circles were prepared at room temperature; red striped circles were preheated before enzyme addition.

The solvent preparation procedure has influenced the k_{enz} value, as the experiments with warm preparation (red striped circles in Figure 29) resulted in higher k_{enz} values and showed a different temperature sensitivity as the experiments prepared at room temperature (blue striped circles). All experiments at lower solvent concentration were prepared at room temperature. These experiments were not redone with the other preparation method, thus the influence of preparation method on these results cannot be evaluated.

6.2.2. AMP

The increase of k_{liq} for 30 wt% AMP after adding 2 g/L CA was moderately as shown in Figure 30. The catalytic effect of CA addition was 1.4 for 298 K and 313 K and 1.3 for 328 K. The liquid side mass transfer coefficient of plain 30 wt% AMP was increasing with temperature; the same trend could be observed from the enzyme enhanced solution. For 15 wt% AMP and 2 g/L CA there was no increase in liquid side mass transfer coefficient with temperature, the value remained almost unchanged at 298, 313 and 328 K. At low temperatures enzyme enhanced 15 wt% AMP was faster than enzyme enhanced 30 wt% AMP. At 313 and 328 K enzyme enhanced 30 wt% AMP was faster than enzyme enhanced 15 wt% AMP at 2 g/L CA concentration.

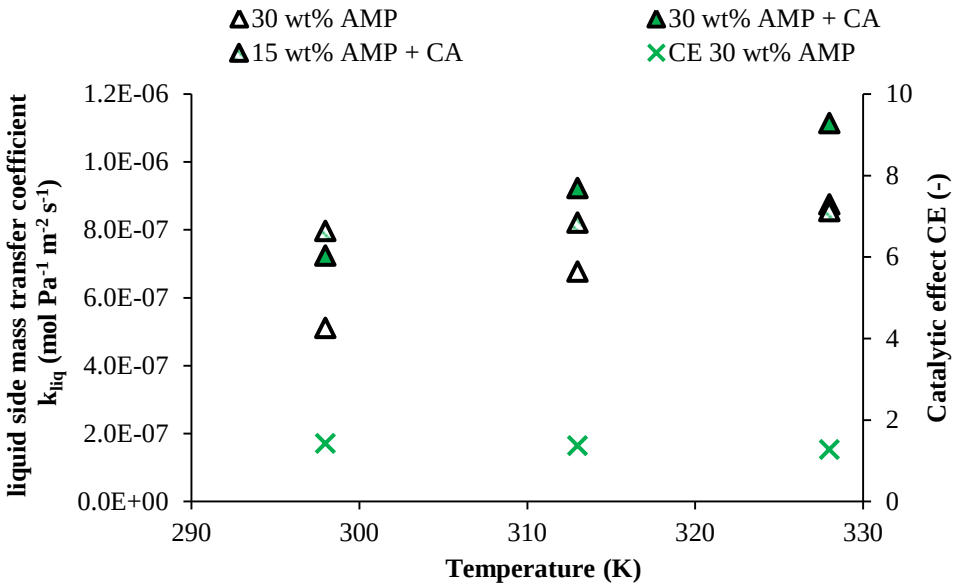

Figure 30: Effect of adding 2 g/L CA on the liquid side mass transfer coefficient k_{liq} in 15 and 30 wt% unloaded AMP solutions for different temperatures (298–328 K)

The different trends in the enzyme enhanced mass transfer for 15 and 30 wt% AMP can be explained by the different enzyme efficiency in the two solutions. The second order reaction rate constants for the enzyme in the solutions shown in Figure 31 were higher for 15 wt% AMP than for 30 wt% AMP. The enzyme reaction rate constant k_{enz} was rising with temperature for both solvent concentrations. The increase was more distinct for 30 wt% AMP even though the values were lower than the k_{enz} values of 15 wt% AMP solutions. The contribution of the 2 g/L enzyme to the overall reaction for 30 wt% AMP was about 50 % at 298 K and 46 and 38 % at 313 K and 328 K. For 15 wt% the contribution of the enzyme was higher, at 298, over 80 % of the overall reaction can be attributed to the enzyme, at 313 K it was more than 70 % and at 328 K it is 50 %.

The solvent reaction rate is mostly following an Arrhenius type temperature dependency, thus it is increasing with temperature. If the temperature dependency of the solvent reaction is rising faster with temperature than then enzyme reaction rate, then the enzyme contribution to the overall reaction is decreasing with temperature. In 30 wt% AMP solutions the amount of active solvent doubled that of 15 wt% AMP solutions, thus the solvent reaction rate was double. The overall enzyme reaction rate in 15 wt% AMP at 2 g/L CA was higher than in 30 wt% AMP, as the determined k_{enz} values are higher.

The mass transfer in enzyme enhanced AMP solutions is an interaction between solvent and enzyme reactions, unlike K_2CO_3 where the mass transfer is mainly dependent on the enzyme reaction rate. An increase in AMP concentration would likely increase the overall solvent reaction rate and decrease the enzyme reaction rate, when keeping the enzyme concentration at 2 g/L. Thus the enzyme contribution to the overall reaction would decrease even more at higher AMP concentrations.

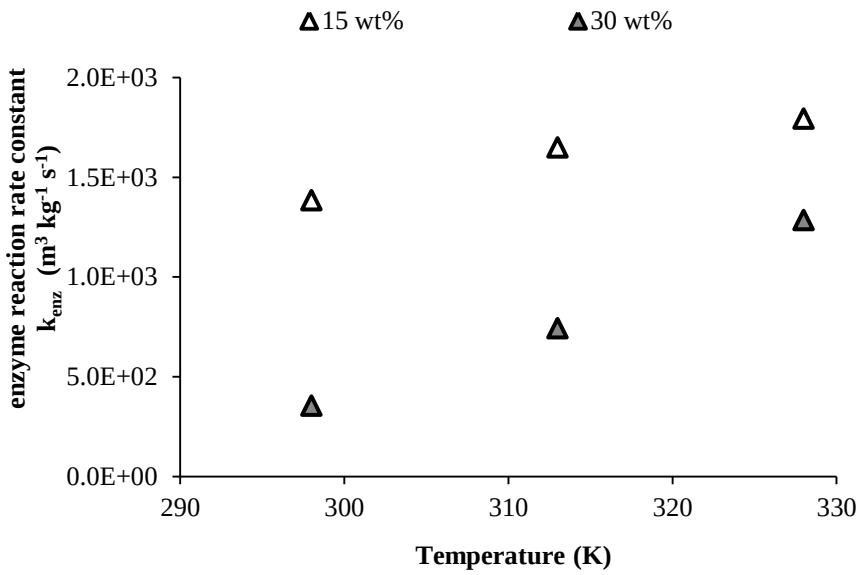

Figure 31: Influence of temperature and solvent concentration on the second order enzyme reaction rate constant kenz (m^3 kg^{-1} s^{-1}) in AMP solutions

6.2.3. MDEA

The liquid side mass transfer coefficient k_{liq} of 30 wt% MDEA solutions could be increased significantly when 2 g/L CA Batch (I) was added. The catalytic effect was close to 9 for 298 K, and dropped to 5 at 313 K and 3 at 328 K as shown in Figure 32. The liquid side mass transfer coefficient of plain 30 wt% unloaded MDEA solution showed an increase with temperature, whereas a slight decrease could be observed from the enzyme enhanced solvent. In Figure 33 the liquid side mass transfer coefficient of enzyme enhanced 30 wt% MDEA solutions at different CA concentrations from CA Batch (II) are depicted on the left side. The trend for different temperatures was similar as for CA Batch (I) as in both cases a decrease at higher temperatures could be observed, although the decrease with temperature was slightly higher for CA Batch (II) than for CA Batch (I) at similar enzyme concentration (1.8 g/L and 2 g/L). When comparing the temperature dependency of the mass transfer for the different enzyme concentrations it can be seen that the decline of k_{liq} with temperature was smaller at 0.85 g/L than for 1.8 g/L and 8.5 g/L. For lower enzyme concentrations the solvent reaction rate contributes more to the overall reaction rate, whereas for high enzyme concentrations the enzyme reaction was the dominant reaction and the solvent reaction might be neglected, similar as to K_2CO_3. The catalytic efficiency for CA Batch (II), shown in Figure 33 on the right side, was 17 for 8.5 g/L CA at 298 K and around 9 at 313 K and 5 at 328 K. The catalytic efficiency of 2 g/L CA Batch (I) and 1.8 g/L CA Batch (II) were quite close to each other, the biggest difference was at 328 K where CE was 3

and 2 respectively. Thus the difference between these two enzymes in terms of temperature dependency was small.

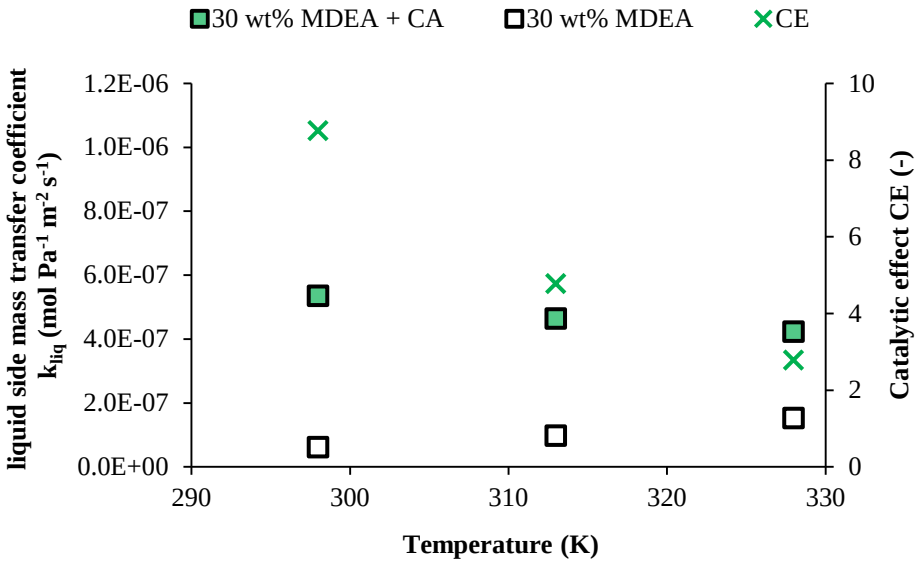

Figure 32: Effect of adding 2 g/L CA Batch (I) on the liquid side mass transfer coefficient k_{liq} in 30 wt% unloaded MDEA solutions for different temperatures (298–328 K).

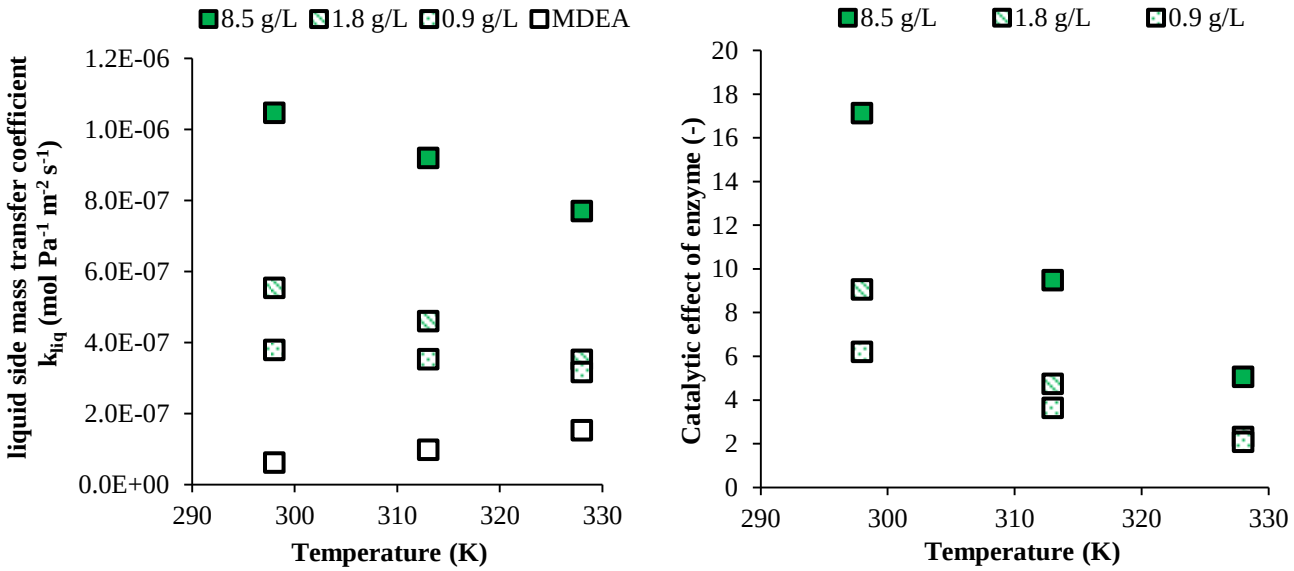

Figure 33: Effect of adding CA Batch (II) (0.85-8.5 g/L) on liquid side mass transfer coefficient k_{liq} (left) and catalytic effect CE (right) for 30 wt% unloaded MDEA solutions as a function of temperatures (298-328 K).

The influence of enzyme concentration on the liquid side mass transfer coefficient for unloaded 30 wt% MDEA solutions at different temperatures is shown in Figure 34. Solutions at 298 K had a consistently higher k_{liq} than at 313 K or 328 K when the same enzyme concentration was used. At the same time solutions at 328 K were always absorbing the slowest. The k_{liq} at the different temperatures was following the same behavior as observed in K_2CO_3 solutions (Figure 25), as sthe highest mass transfer could be observed at the lowest temperature for enzyme enhanced solvents.

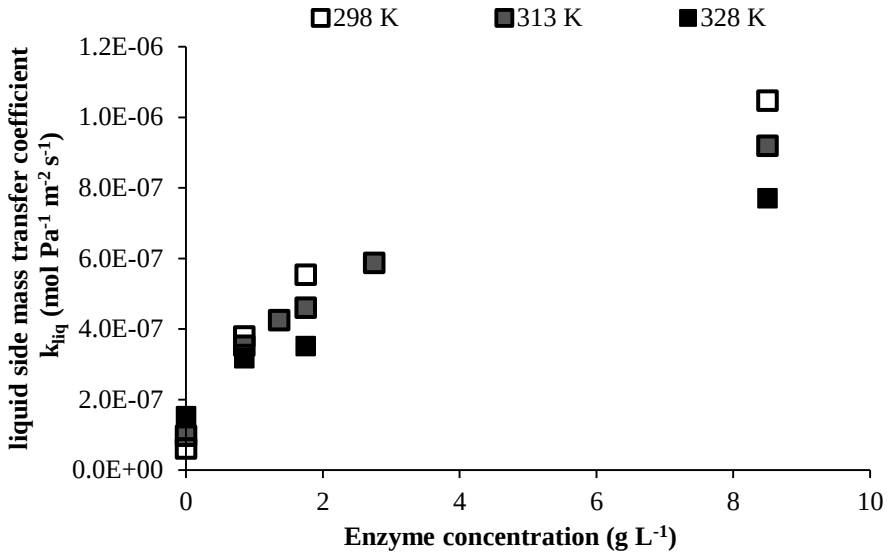

Figure 34: Influence of enzyme concentration (Batch (II)) on liquid side mass transfer coefficient k_{liq} for unloaded 30 wt% MDEA solutions at 298-328 K.

The influence of solvent concentration on the mass transfer is shown for CA Batch (I) on the left side and for CA Batch (II) on the right side of Figure 35. For both enzymes a decrease in k_{liq} was visible at higher solvent concentrations. The drop in mass transfer between 15 and 50 wt% MDEA for 0.85 g/L CA Batch (II) was 62% at 298 K, 58% at 313 K and 45% at 328 K. Whereas for 2 g/L CA Batch (I) the drop was 50, 44 and 33 % at 298, 313 and 328 K respectively. The enzymes thus showed a slightly different solvent concentration dependency. Although to draw conclusions on solvent concentration influence on the enzyme not the liquid side mass transfer coefficients should be compared but rather the enzymatic reaction rates in the solvents.

For both enzymes the temperature influence on mass transfer became less significant for higher solvent concentrations. At 50 wt% MDEA there was almost no difference in k_{liq} visible between 298 K and 328 K for enzymes from both batches.

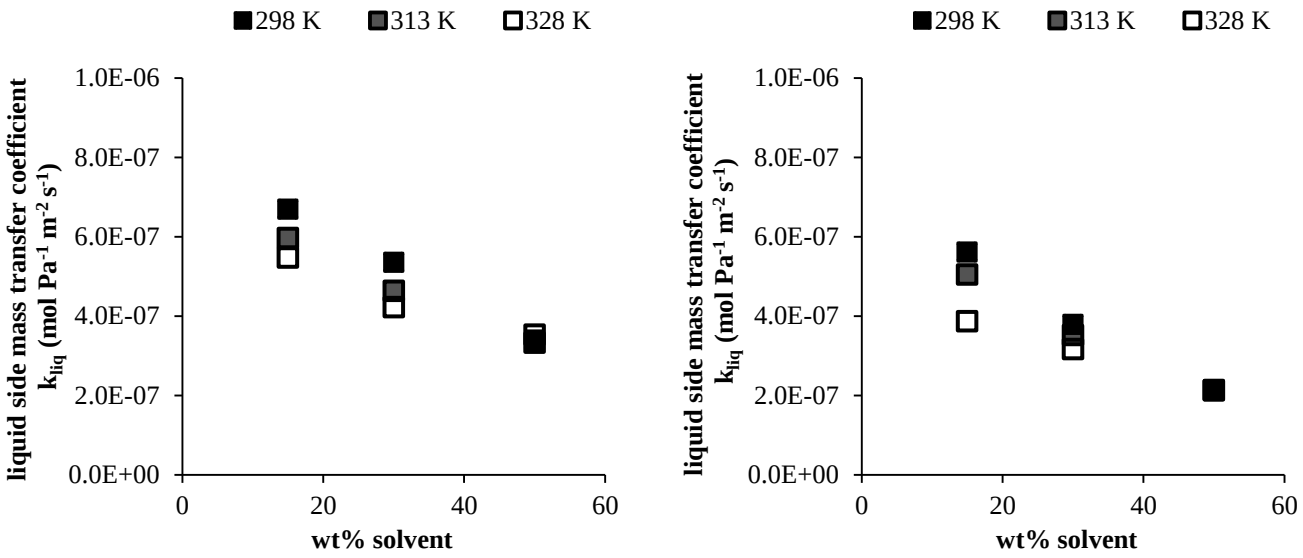

Figure 35: Influence of solvent concentrations (15-50 wt%) on liquid side mass transfer coefficient kliq for unloaded MDEA solutions with 2 g/L CA Batch (I) (left) and 0.85 g/L CA Batch (II) (right) at different solvent temperatures (298-328 K)

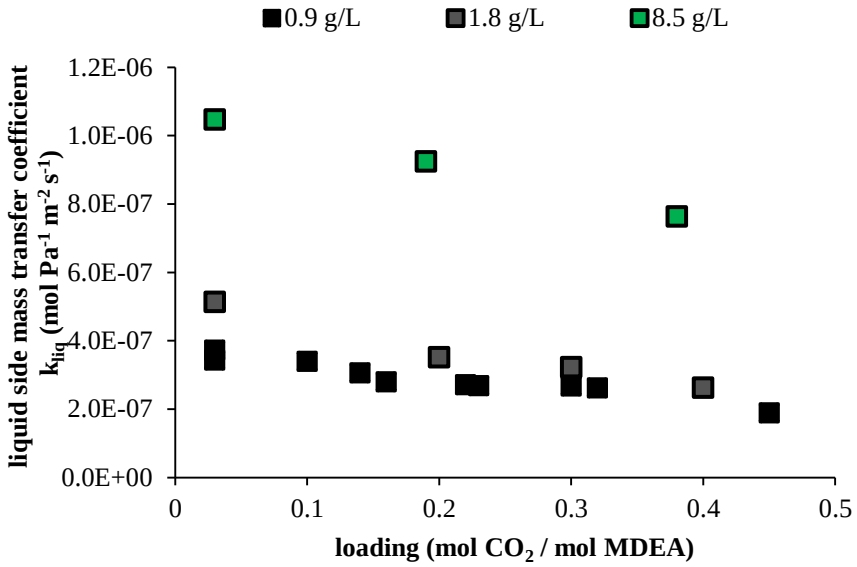

Figure 36: Influence of solvent loading liquid side mass transfer coefficient for 30 wt% MDEA solutions at 298 K

Figure 36 shows the effect of solvent loading on the liquid side mass transfer for 30 wt% MDEA at 298 K. A slight decrease in mass transfer could be observed when the loading increased. The mass transfer dropped by 28 % for 8.5 g/L CA when the loading increased from close to unloaded conditions

to almost 0.4 solvent loading. A similar increase in solvent loading resulted in a decrease of 37 % for 1.8 g/L CA and 30 % for 0.85 g/L CA. Solvent loading affected the mass transfer in enzyme enhanced MDEA solutions comparable to enzyme enhanced K_2CO_3. The observed decrease in these experiments was although far less than for PZ-promoted MDEA.

The enzyme reaction rate had a significant contribution to the overall reaction rate with CO_2 in MDEA solutions, as shown in Figure 37, where the overall first order enzyme reaction rate constant and the enzyme contribution are displayed. For 298 K and 313 K over 90 % of the overall reaction came from CA, when the concentration was higher than 0.85 g/L. At 328 K around 80 % of the overall CO_2 reaction rate resulted from CA. The enzyme contribution was steadily increasing with the enzyme concentration for all temperatures. At a CA concentration of 8.5 g/L the enzyme contribution to the overall reaction was close to 100 % at 298 K, 99 % at 313 K and 96 % at 328 K. The mass transfer at these high enzyme concentrations was completely dominated by the enzyme reactions.

A linear correlation between first order enzyme reaction rate constant and enzyme concentration for the lower end of enzyme concentrations could be observed. When applying linear regression to the first values at CA concentrations below 3 g/L, shown as a dashed, dotted and straight line in Figure 37, the deviation of the experiments with 8.5 g/L CA from the linear behavior of the other experiments became visible.

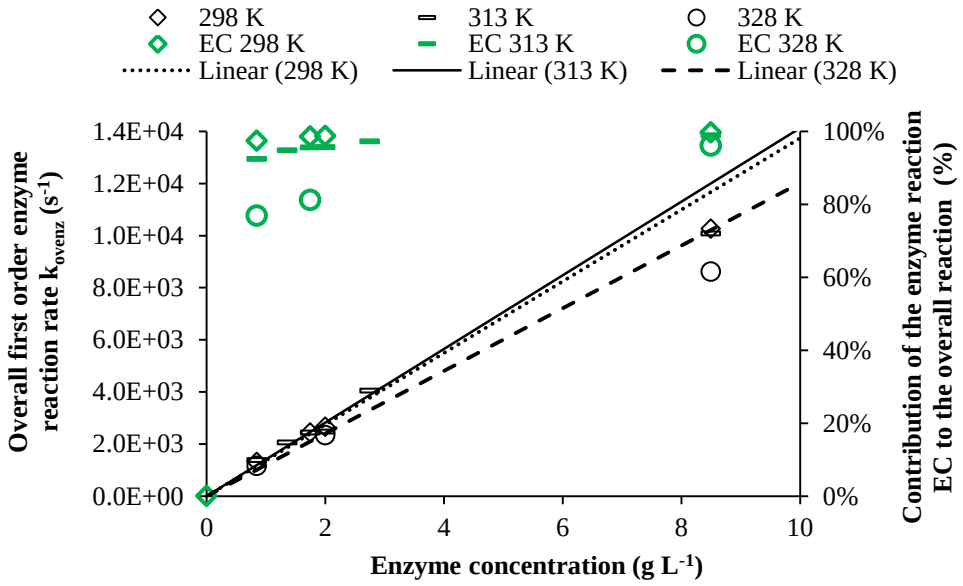

Figure 37: Overall first order enzyme reaction rate constant and contribution of enzyme reaction to overall reaction in 30 wt% MDEA at 298, 313 and 328 K as function of enzyme concentration.

The linear fit for 313 K and 298 K were almost the same, showing that the enzyme reaction rate was almost the same at the same enzyme concentration. Thus the enzyme reaction rate seems to be independent of temperature between 298 and 313 K. The decline visible for 328 K might be caused by

the few experimental data points (two) taken for the linear regression, the extrapolated line thus seems to differ, although all data points at 0.85 g/L CA are very align.

This deviation from the linear trend is about the same for all temperatures where the experimental points at 8.5 g/L CA are about 15 % beneath the linear fit through the experimental points at lower enzyme concentrations. It is difficult to conclude on what effect can describe this deviation. This might be caused by a diffusion limitation of either of CO_2 or of the buffer around the enzyme that might occur at very high reaction rates. Or it might be caused by some physical changes to the solvent properties by the enzyme. More experiments addressing this effect are needed to draw a conclusion.

A decline in first order reaction rate constant at higher enzyme concentrations has been observed in literature for MDEA solutions [11], [12]. Both studies were performed in the research group of Geert Versteeg with two different enzymes. In their first study with different MDEA concentrations and enzyme concentrations at 298 K, they observed a deviation from the linear behavior already when the overall first order enzyme reaction rate constant was higher than 400 s^{-1} and the enzyme concentration was 0.4 g/L [11], we could still observe the linear trend up to and first order enzyme rate constant of 4000 s^{-1}. In the other study with another enzyme it appears from their graphs that linear behavior was valid up to 800 s^{-1} also at 0.4 g/L CA [12]. They proposed a Langmuir Hinshelwood (LH) type relation to describe effect of enzyme concentration on the enzyme reaction rate and reported their determined values. According to their LH relation and constants the increase in enzyme reaction rate would be 2.2 fold when the enzyme concentration is increased from 0.85 to 8.5 g/L for all temperatures. Although a 7.8-7.3-fold increase in enzyme reaction rate was observed for 298-328 K in this study. Thus the constants and correlations derived for one enzyme are just valid for this enzyme and can hardly be used for another enzyme. The highest first order enzyme reaction rate constant published in their work was around 3800 s^{-1} for 1 M MDEA (around 12 wt% MDEA) at 308 K and a just slightly lower value at 298 K [13]. A first order enzyme reaction rate of 10000 s^{-1} for 298 K and 313 K and 8500 s^{-1} at 328 K could be obtained in this study showcasing the different behavior of the enzymes.

The kinetic rate constant k_{enz} (m^3 kg^{-1} s^{-1}) was calculated from the liquid side mass transfer coefficients for CA Batch (I) Batch (II) at different MDEA concentrations, the results are shown in Figure 38. The temperature seemed to have almost no effect on the enzyme reaction rate constant k_{enz} for enzymes from both batches, as besides of one outlier for each enzyme at 328 K, the values for k_{enz} at the same MDEA concentration were very close to each other at different temperatures.

The MDEA concentration had a negative influence on the enzyme reaction rate constant, as the values of k_{enz} were decreasing at higher solvent concentrations for both enzymes. The decrease is higher for enzymes from Batch (II) which can explain the steeper decline in k_{liq} for CA Batch (II) at higher MDEA concentrations observed in Figure 35. Overall enzymes from Batch (II) seemed to be more active at lower solvent concentrations.

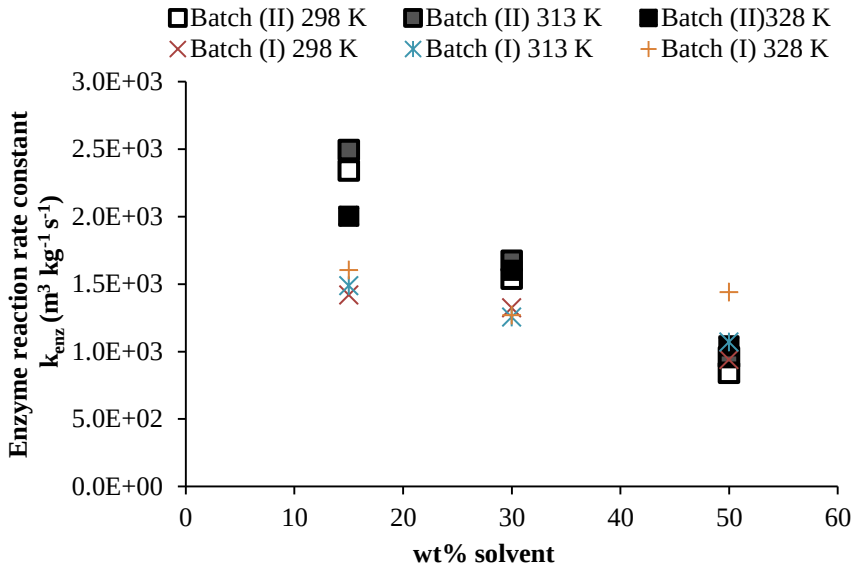

Figure 38: Influence of MDEA concentration on enzyme reaction rate constant k_{enz} (m^3 kg^{-1} s^{-1}) for CA Batch (I) and CA Batch (II) for different temperatures (298-328 K)

Penders van Elk. et al. [11] observed a similar decline in enzyme reaction rate constant at higher MDEA concentration. They concluded that the enzyme reaction rate was dependent on the water concentration in solution, thus the enzyme reaction is decreasing at higher MDEA concentrations as the molar water concentration is lower. Their values for 1, 2 and 4 M MDEA solutions could be normalized by dividing through the water concentration. The kinetic modelling of CA enhanced MDEA will be addressed in the following chapter together with the experimental results for solvent loading influence on mass transfer and CO_2 gas partial pressure influence.

6.2.4. Comparison of the different solvents

The k_{liq} of the different enzyme enhanced solvents with 2 g/L CA are compared to literature correlations of 30 wt% MEA at different solvent loadings in Figure 39. All three investigated solvents showed a positive effect on mass transfer when CA was added. Experiments with 30 wt% MEA enhanced with CA were also conducted, but we did not see any effect, which was not surprising as no bicarbonate was formed under the experimental conditions. Some authors reported an increase in absorption rate for aqueous MEA after CA addition. These experiments were either carried out at very low MEA concentrations [14] or CO_2 partial pressures above 1 bar in combination to low MEA concentrations [15], which are both conditions where MEA forms bicarbonate. These investigated process condition are although very far away from applications in CCS for power plants.

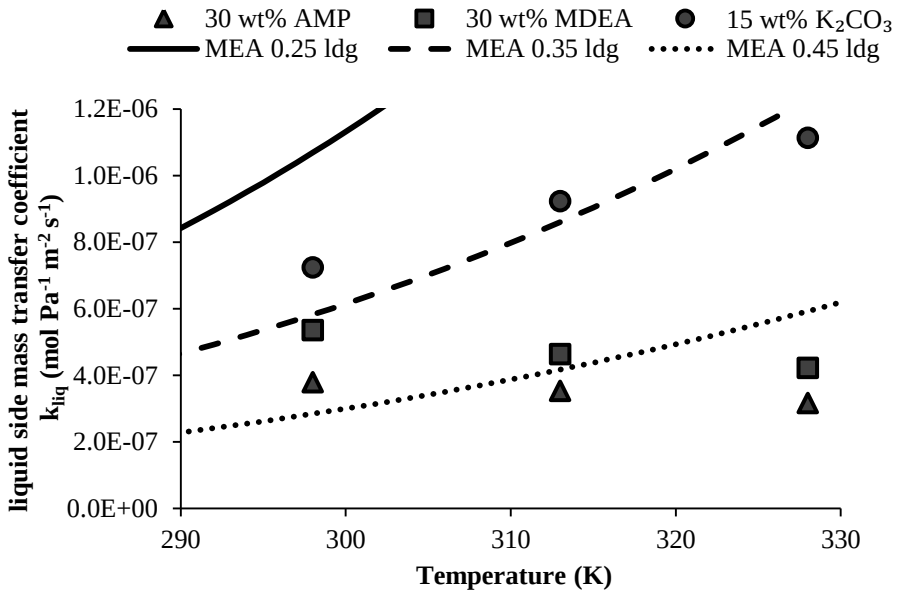

Figure 39: Liquid side mass transfer coefficient of 15 wt% K_2CO_3, 30 wt% AMP and 30 wt% MDEA with 2 g/L CA Batch (I) compared to 30 wt% MEA at different solvent loadings (mol CO_2/ mole MEA) from a literature correlations

Enzyme enhanced 30 wt% AMP was slightly faster than 15 wt% K_2CO_3 and 30 wt% MDEA at 298 K. For AMP, the solvent that was already absorbing faster without the enzyme, the liquid side mass transfer coefficient increased with temperature. Slow absorbing solvents, K_2CO_3 and MDEA, showed a decrease in k_{liq} with higher temperature, with K_2CO_3 always being slightly faster. The mass transfer of the enzyme enhanced solvents was in the range of 30 wt% MEA with 0.35 solvent loading at 298 K. At higher temperatures only enzyme enhanced AMP could compete with 30 wt% MEA at 0.35 solvent loading, whereas the decrease of k_{liq} with temperature brought the mass transfer of enzyme enhanced K_2CO_3 and MDEA closer to 30 wt% MEA at an solvent loading of 0.45 at similar temperatures. The different trends with temperature could be explained with the different levels of enzyme contribution to the overall reaction, as the enzyme reaction is the dominant reaction in K_2CO_3 and MDEA solutions, whereas is AMP the solvent reaction contributed a lot to the overall reaction .

Figure 40 compares the catalytic effect of CA on the mass transfer. For the slow absorbing solvents, MDEA and K_2CO_3, the mass transfer was increased 9- and 7-fold respectively at 298 K and the enzyme contribution to the overall CO_2 reaction was higher than 97 % in both cases. The catalytic effect was decreasing for MDEA and K_2CO_3, which is caused by the increase of k_{liq} for the solvents without enzyme with temperature. The enzyme contribution to the overall CO_2 reaction still remained over 90 % at 328 K for MDEA and K_2CO_3. This shows that mass transfer in these enzyme enhanced solvents is almost solely dependent on the enzyme reaction rate. We did not observe an increase in enzyme reaction rate with temperature for MDEA, and just a slight increase for 15 wt% K_2CO_3

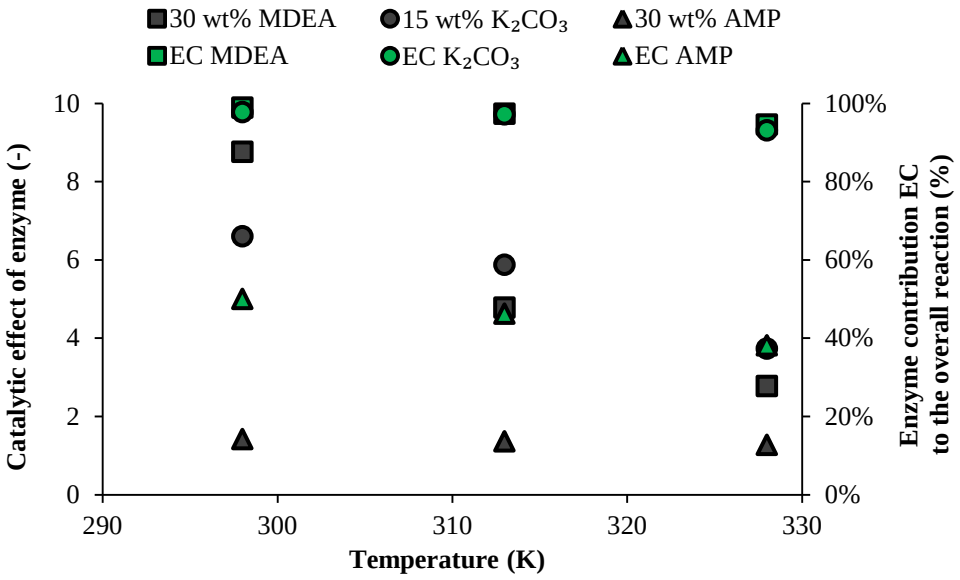

Figure 40: Catalytic effect and enzyme contribution to the overall reaction 15 wt% K_2CO_3, 30 wt% MDEA, 30 wt% AMP enhanced with 2 g/L CA Batch (I)

For pseudo-first order reactions, the Enhancement factor can be substituted with the Hatta number and the chemical liquid side mass transfer coefficient can be described as:

$$k_{liq}' = \frac{\sqrt{k_{ov}^{ps1.} \cdot D_{CO_2}}}{H_{CO_2}} = \frac{\sqrt{\left(k_{enz} \cdot C_{enz} + k_{sol} \cdot C_{sol}\right) \cdot D_{CO_2}}}{H_{CO_2}} \tag{6.1}$$

If the mass transfer coefficient k_{liq} should increase with temperature, then the numerator needs to rise faster than the denominator. The numerator is the product of overall CO_2 reaction rate and diffusivity of CO_2 in the solvent with the power of 0.5. The denominator is the partition coefficient for CO_2. The diffusivity increases with temperatures as the viscosity of the solvent is decreasing. The partition coefficient is also increasing as shown in Appendix A, where physical solvent properties are listed. If the first term of the reaction, which is the enzyme reaction rate is not increasing with temperature and the enzyme reaction is the main contributor to the overall reaction, then the diffusivity with a power of 0.5 needs to increase faster with temperature than the partition coefficient to results in a mass transfer increase with temperatures. This is not the case for MDEA and K_2CO_3, thus the mass transfer is decreasing at higher temperatures.

The enzyme reaction in 30 wt% AMP solution contributed to just 50 % of the overall CO_2 reaction rate at 298 K; this value was even decreasing at higher temperatures, as the solvent reaction rate is increasing faster with temperature than the enzyme reaction rate. For AMP we even observed an increase in enzyme reaction rate with temperature. The high contribution of the solvent reaction to the

overall reaction as well as the increase in enzyme reaction rate with temperature led to an increase in mass transfer with temperature.

Even though enzyme enhanced AMP has the highest mass transfer when 2 g/L CA was added to the solvents, a 1.4-fold increase in mass transfer will unlikely convince someone to apply enzymes in a process with all the accompanying limitations.

The solvents were compared up to now in this study solely on the basis of liquid side mass transfer coefficient, but this solvent property is just one characteristic of a good solvent. Another equally important characteristic is the solvent capacity. The solubility diagrams for the different solvents in chapter 3 showed clearly, that the solution can store more CO_2 at a lower temperature. A lower temperature increases the possible rich loading of a solution and thus the cyclic capacity.

Combining the knowledge of the solutions thermodynamics with the mass transfer behavior at different temperatures and solvent concentrations helps identifying ideal process conditions for the different solvents. K_2CO_3 and MDEA behaved quite similar as low temperature and low solvent concentrations resulted in the highest mass transfer rates. For AMP solutions the highest mass transfer was achieved at the highest solvent concentration and the highest temperature.

The conventional solvent MEA needs a high temperature for high mass transfer as shown in Figure 21. A higher solvent concentration leads to a higher amount active solvent for reaction and increases the reaction rate. The higher solvent concentration although increases the viscosity which reduces the diffusivity of CO_2 in solution. It is reported that increasing the MEA concentration in solution increased the mass transfer just up to about 18 wt% MEA, afterwards the mass transfer is starting to decline slightly due to the viscosity [3], although an increase in mass transfer between around 36 and 54 wt% MEA could be observed [16]. The mass transfer in these highly reactive solutions is then also influenced by the flowing conditions (k_{liq0}), thus it is difficult to choose the perfect solvent concentration. As a general trend it can be concluded, that the MEA concentration should be high for high mass transfer, but not as high that the viscosity hinders the mass transfer.

In piperazine enhanced MDEA we observed an increase in mass transfer at higher temperatures. We performed our experiments at just one MDEA-PZ mixture. An increase in PZ concentration will definitely increase the mass transfer of the solution [17]. Only at high PZ concentrations a change in viscosity is expected, but under these conditions PZ is not considered a promoter anymore. The beneficial solvent properties of the tertiary amine may get lost and the reboiler duty increases when the PZ concentration is increased beyond 5 wt% in mixture with 45 wt% MDEA [18]. The MDEA solvent reactions did not contribute to the mass transfer at all, as the addition of PZ increased the mass transfer more than 20 fold. The only effect that the MDEA concentration has on the mass transfer is the viscosity change of the solvent. A low MDEA concentration is thus favorable for a PZ promoted MDEA solution in terms of high mass transfer, as it offers lower viscosity and thus leads to higher diffusivity of CO_2 in solution. Bishnoi and Rochelle performed mass transfer experiments with 5 wt%

PZ and in aqueous solution [7] and 5 wt% PZ mixed with 45 wt% MDEA [6]; they observed a higher mass transfer in the aqueous solution. Our experiments at 5 wt% PZ and 30 wt% MDEA were faster than the experiments with 45wt% MDEA /5 wt% PZ and slower than aqueous piperazine at 5 wt% when comparing with experimental results at similar solvent loadings.

A low temperature enables a higher solvent capacity for all solvents. The enzyme addition does not influence the thermodynamics of the solution and solvent capacity.

MDEA solutions have shown an optimum solvent concentration around 40-45 wt% for 25 °C; this optimum is slightly shifting to lower concentration values at higher temperatures as shown in Chapter 3.4.3. For AMP solutions a higher solvent concentration led to a higher solvent capacity between 21 and 55 wt% AMP, calculated as mol CO_2 /kg solvent [19]. For MEA solutions the solutions capacity is increasing with the solvent concentration, thus a high MEA concentration is favorable for high capacity.

A higher solvent concentration enables to store more CO_2 in K_2CO_3 solutions. One issue with K_2CO_3 is the precipitation of the enzyme and solvent at higher solvent concentrations. Solvent precipitation can also be seen as an advantage, as the solvent capacity can increase further and an advanced solvent regeneration unit which can handle solids might benefit from lower energy input as less liquid phase needs to be heated up, if mainly the re-dissolved solids are fed to the desorber [20], [21]. The enzyme precipitation is a major drawback, as it remained unclear if the enzyme can regain its activity if it re-dissolved.

Table 1: Optimum conditions for high capacity and high mass transfer in different solvents

Solvent	Solvent type	Temperature	Solvent concentration
AMP + CA	Carbonate salt solution & biocatalyst	Tradeoff (high-low)	high
K_2CO_3 + CA	Sterically hindered amine & biocatalyst	low	Tradeoff (high-low)
MDEA + CA	Tertiary amine & biocatalyst	low	Tradeoff (medium-low)
MDEA + PZ	Tertiary amine & chemical promoter	Tradeoff (high-low)	Tradeoff (medium-low)
MEA	Primary amine	Tradeoff (high-low)	Tradeoff (medium-high)

Table 1 combines the optimum process conditions for high mass transfer and high capacity and defines whether there is a clear trend for the process conditions or there is need to optimize a process condition in a trade-off. The optimum enzyme enhanced AMP process is carried out at high solvent concentration with a medium absorber temperature, which represents the trade-off for high solvent capacity and high mass transfer. An enzyme enhanced K_2CO_3 process should be carried at low absorption temperature and the solvent concentration should be optimized to ensure high mass transfer and high solvent

capacity. For enzyme enhanced MDEA a low absorption temperature is needed and the solvent concentration should be optimized, between a very low concentration for high mass transfer and a medium concentration for high solubility. The temperature in the MEA process needs to be optimized for high solvent capacity and mass transfer between a high and a low value and the solvent concentration should be kept between a medium and high value. The PZ promoted MDEA process should employ a medium to low MDEA concentration and the absorption temperature needs to be optimized between a high and low value.

As CO_2 absorption is an exothermic reaction, the solvent heats up inside the column, thus decreases the solvent capacity. For fast reacting solvents with high heat of reaction "intercooling" is an applied process option to increase the solvent capacity and avoid temperature bulges inside the column [22]–[24]. Intercooling helps in the tradeoff between high temperature need for high mass transfers and low temperature requirement for high solvent capacity. This technology should definitely also be employed for the enzyme enhanced MDEA process, because it increases mass transfer as well as capacity.

When choosing solvent concentrations the effect of viscosity onto pumping energy and heat transfer ability should not be left out. Also corrosion issues might arise, especially for MEA at higher concentrations.

All over when comparing the different solvent technologies, fast reacting solvent, solvent promoted with fast reacting amine and enzyme enhanced solvent, it becomes noticeable that chemical enhanced solvents (PZ-MDEA) follow a similar temperature dependency as fast reacting solvents, where the temperature optimum for high mass transfer differs from the temperature optimum for high capacity. For enzyme enhanced slow solvents, such as MDEA and K_2CO_3, the temperature optimum is clear and just the solvent concentration needs to be optimized. For MDEA this solvent concentration optimum can even be further enclosed, as a solvent concentration of 40-45 wt% MDEA has the highest capacity, the optimal solvent concentration somewhere below that value.

6.3. Benchmarking of enzyme enhanced solvents

The comparison of different solvents for CCS applications is difficult, because the conditions are changing inside the absorber. When CO_2 is absorbed, the concentrations of the different species alter and the exothermic reactions heat up the liquid. It is possible to compare the liquid side mass transfer coefficient of two solvents, but it is difficult tell for certain which solvent will absorb faster in a process, as the changes in mass transfer due to concentration changes and temperatures changes needs to be accounted for. Also the liquid to gas ratio of the absorption process influences the rate of mass transfer as the driving forces change inside the absorber.

Li tried to derive a common basis for comparison of amine solvent performances [25]. He pointed out that the mass transfer driving force is a crucial parameter. Thus there needs to be a driving force at the liquid inlet, between the lean solution and the exiting gas stream and at the liquid outlet between the

rich solution and the incoming gas stream. Assuming that either of these points is in thermodynamic equilibrium would require very high columns, which is very capital cost intensive. He assumed that the flue gas inlet conditions were 12 kPa CO_2 and the gas outlet conditions would be 1.2 kPa with 90 % capture. In order to ensure a driving at the top of the column, the equilibrium CO_2 partial pressure of the lean solution should be 0.5 kPa; the rich conditions were defined at 5 kPa CO_2 equilibrium partial pressure of the solution. Assuming linear gas partial pressure profiles between in and outlet and linear equilibrium partial pressure profile in the liquid phase, a mean logarithmic driving force DF_{ml} can be calculated from the driving force in the top and in the bottom of the column:

$$DF_{ml} = \frac{DF_{top} - DF_{bottom}}{\ln \frac{DF_{top}}{DF_{bottom}}} = \frac{\left(1.2\,kPa - 0.5kPa\right) - \left(12kPa - 5\,kPa\right)}{\ln \frac{\left(1.2\,kPa - 0.5kPa\right)}{\left(12kPa - 5\,kPa\right)}} \approx 2.74\,kPa \tag{6.2}$$

An average liquid side mass transfer coefficient k_{liq}^{avg} (mol Pa^{-1} s^{-1} m^{-2}) can be calculated from a mean logarithmic mass transfer flux divided by the mean logarithmic driving force, when the gas side mass transfer resistance is neglected:

$$k_{liq}^{avg} = \frac{\Delta N_{CO_2}{}^{ml}}{DF_{ml}} = \frac{\frac{\left(\Delta N_{CO_2}{}^{top} - \Delta N_{CO_2}{}^{bottom}\right)}{\ln \frac{\Delta N_{CO_2}{}^{top}}{\Delta N_{CO_2}{}^{bottom}}}}{DF_{ml}} \tag{6.3}$$

The mass transfer flux at the top and the bottom of the column can be calculated from the driving forces there and the liquid side mass transfer coefficient for these conditions:

$$\Delta N_{CO_2}^{top} = k_{liq}^{top} \cdot DF_{top} = k_{liq}^{top}\left(1.2\,kPa - 0.5kPa\right) \tag{6.4}$$

$$\Delta N_{CO_2}{}^{bottom} = k_{liq}^{bottom} DF_{bottom} = k_{liq}^{bottom}\left(12kPa - 5\,kPa\right) \tag{6.5}$$

Li assumed an isothermal absorber at 40 °C and reported the average liquid side mass transfer coefficient for several solvents together with the cyclic capacities of the solvent between lean and rich conditions [26]. Rochelle extended the list to 48 solvents in his book chapter [27]. The reported values are summarized in Figure 41.

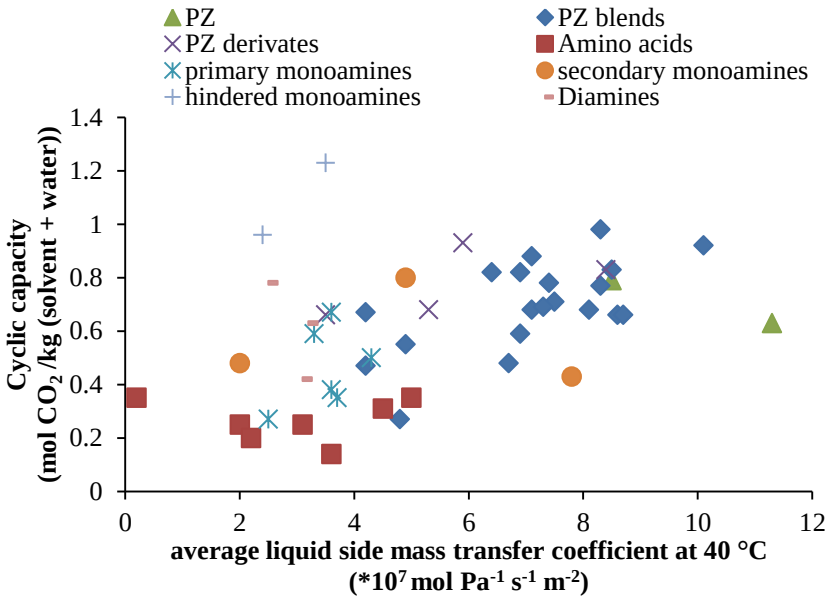

Figure 41: Average liquid side mass transfer coefficient and cyclic capacity for different solvent types at 40 °C reported by Rochelle [27]

The cyclic capacity (mol CO_2/ kg solution) is shown on the y-axis and the average liquid side mass transfer coefficient (mol Pa^{-1} m^{-2} s^{-1}) on the x-axis. A good solvent should combine high values of both properties, thus it should be on the upper right handed area. When comparing the different solvent types apart from 7 molal (34 wt%) methylmonoethanolamine, a seconday monoamine, only PZ, PZ blends and PZ derivates provide high mass transfer. The cyclic capacities of these solvents are also high in comparison with the other solvent types. Only hindered monoamines showed a higher capacity, but the average mass transfer for these solvents was much lower for them.

The results from the enzyme enhanced solvents at different loadings were compared to the conventional amines; therefore cyclic capacity had to be calculated from the equilibrium partial pressures at 0.5 and 5 kPa from the extended UNIQUAC model. The results for 298, 313 and 328 K are listed in Table 21 in the Appendix. The cyclic capacity and average liquid side mas transfer coefficient of enzyme enhanced 30 wt% MDEA at different temperatures in comparison to conventional amines are shown in Figure 42. The liquid side mass transfer coefficients for the top and bottom conditions were interpolated from experimental results when the loadings in the experiments differed more than 0.03 (mol CO_2/mol MDEA) from the loadings needed for calculation.

The addition of enzyme does not change the chemical equilibrium, thus the cyclic capacity of the solution is independent of the enzyme concentration and changes for 30 wt% MDEA solutions just with temperature.

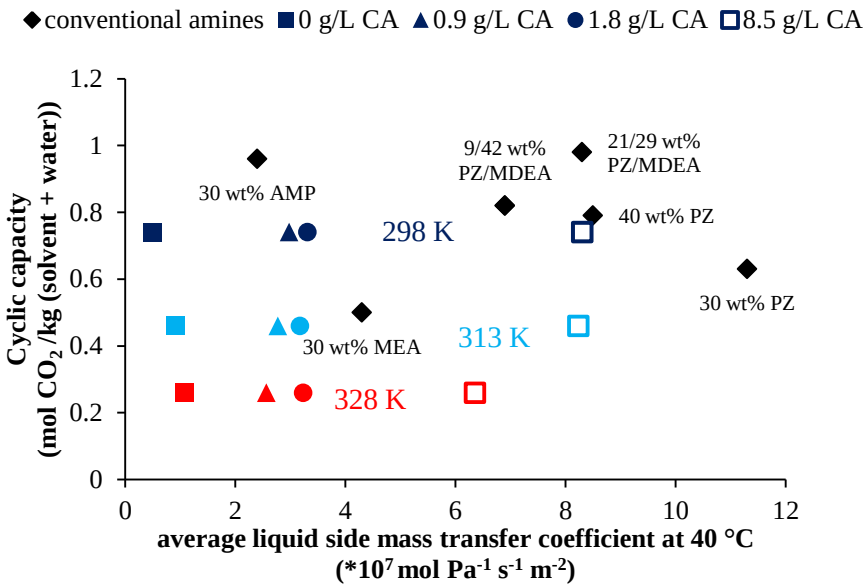

Figure 42: Comparison of cyclic capacity and average liquid side mass transfer coefficient of enzyme enhanced 30 wt% MDEA at different enzyme concentrations and temperatures with conventional amine solvents at 40 °C

A clear decrease of cyclic capacity from 298 K to 313 K and from 313 K to 328 K could be observed. 30 wt% MDEA solutions at 25 °C offered comparable cyclic capacity to 40 wt% aqueous PZ solutions and even higher cyclic capacity than 30 wt% aqueous PZ solutions. Only 30 wt% AMP solutions and MDEA/PZ mixtures with an total amine concentration of around 50 wt% exceeded the cyclic capacity of the MDEA solutions at 298 K. 30 wt% MDEA solutions at 313 K had just a slightly lower cyclic capacity than 30 wt% MEA. Thus the solutions temperature should be below 313 K to improve the cyclic capacity compared to the industrial standard. The average liquid side mass transfer coefficient of the enzyme enhanced solvents increased with the enzyme concentration. At 0.85 g/L CA the enzyme enhanced solution became faster than 30 wt% AMP, but even at 1.8 g/L CA the enzyme enhanced solvent was still slower than 30 wt% MEA. A five-fold increase in CA concentration to 8.5 g/L sparked the mass transfer to a level beyond 30 wt% MEA. The average k_{liq} of the enzyme-enhanced solvent at 298 K and 313 K became comparable to 40 wt% aqueous PZ and a 21/29wt% PZ/MDEA blend.

Only 30 wt% aqueous PZ solution offered a clear advantage over 30 wt% MDEA with 8.5 g/L CA in terms of higher average mass transfer. The almost equal cyclic capacity and average mass transfer between 40 wt% aqueous PZ and 30 enzyme enhanced wt% MDEA at 298 K is a very remarkable observation. This clearly shows that the performance of enzyme enhanced solvents cannot be judged based on comparing single mass transfer experiments in a wetted wall column. The high average liquid side mass transfer coefficient resulted from a high mass transfer flux calculated at the bottom of the absorber. The driving force at the bottom is 10 times higher than at the top of the column (7 kPa vs. 0.7 kPa). The drop of k_{liq} between top and bottom due to CO_2 absorption is much higher for conventional

solvents than for enzyme enhanced solvents. Conventional solvents have the highest liquid side mass transfer at the absorber liquid inlet, but cannot utilize it properly because the driving forces are low there. Enzyme enhanced solvents may have lower k_{liq} at the top of the column compared to conventional amine solvents, but the mass transfer decreases just slightly between top and bottom. Thus enzyme enhanced solvents (at high enzyme concentrations) have higher mass transfer coefficients than conventional solvents at the absorber bottom where the driving forces are higher, which results in higher mass transfer rates.

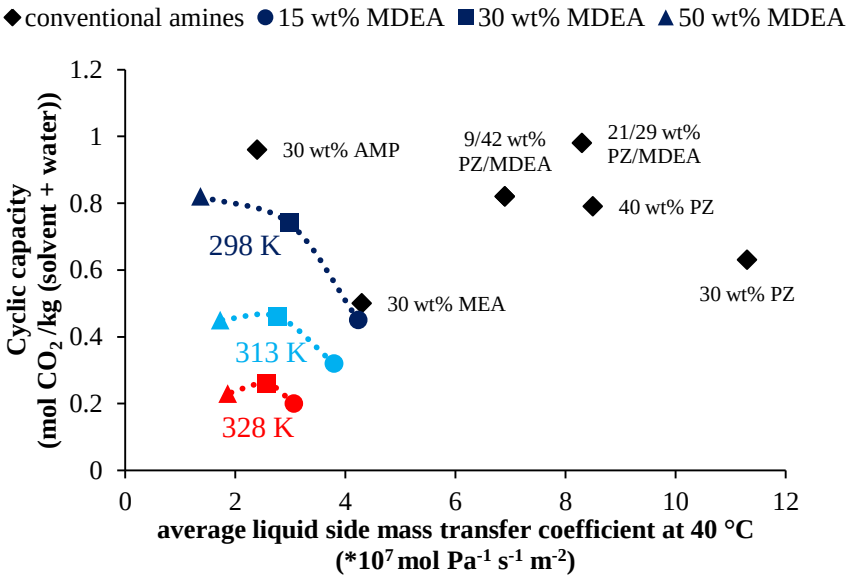

Figure 43: Comparison of cyclic capacity and average liquid side mass transfer coefficient of enzyme enhanced MDEA with 0.85 g/L CA at different solvent concentrations and temperatures with conventional amine solvents at 40 °C

In Figure 43 the cyclic capacity and average liquid side mass transfer coefficient of MDEA solutions of different solvent concentrations enhanced with 0.85 g/L CA are compared to the average liquid side mass transfer coefficient of conventional amines. The cyclic capacity of the MDEA solutions was the highest for 50 wt% MDEA solution at 298 K, and decreased when at lower solvent concentration. At 313 and 328 K 30 wt% MDEA solution presented the highest cyclic capacity. The average mass transfer coefficient decreased with increasing solvent concentration. 50 wt% and 30 wt% MDEA solutions showed a higher cyclic capacity than 30 wt% MEA at 298 K, although the mass transfer for the 30 wt% MDEA and the 50 wt% MDEA solutions were clearly lower than 30 wt% MEA. Whereas 15 wt% MDEA enhanced with 0.85 g/L CA had almost the same average mass transfer coefficient and had a cyclic capacity value that was just slightly lower than for 30 wt% MEA. On that basis 15 wt% MDEA with 0.85 g/L CA at 298 K represents a similar solvent as 30 wt% MEA at 313 K. The dotted lines are just connecting the experimental points, the tradeoff between high cyclic capacity and high mass transfer will likely follow a similar trend.

BIBLIOGRAPHY

[1] G. F. Versteeg, L. A. J. . van Dijck, and W. P. M. van Swaaij, "On the Kinetics between CO_2 and Alkanolamines both in aqueous and non-aqueous solutions. An overview," *Chem. Eng. Commun.*, vol. 144, pp. 113–158, 1996.

[2] G. Satori and D. W. Savage, "Sterically Hindered Amines for CO_2 Removal from Gases," *Ind. Eng. Chem. Fundam.*, pp. 239–249, 1983.

[3] A. Kohl and R. Nielsen, *Gas Purification*, 5th ed. Gulf Publishing Company, 1997.

[4] K. Thomsen, "Modeling electrolyte solutions with the extended universal quasichemical (UNIQUAC) model," *Pure Appl. Chem.*, vol. 77, no. 3, pp. 531–542, 2005.

[5] G. Puxty and R. Rowland, "Modeling CO_2 mass transfer in amine mixtures: PZ-AMP and PZ-MDEA," *Environ. Sci. Technol.*, vol. 45, no. 6, pp. 2398–2405, 2011.

[6] S. Bishnoi and G. T. Rochelle, "Absorption of Carbon Dioxide in Aqueous Piperazine/Methyldiethanolamine," *AIChE J.*, vol. 48, no. 12, pp. 2788–2799, 2002.

[7] S. Bishnoi and G. T. Rochelle, "Absorption of carbon dioxide into aqueous piperazine: reaction kinetics, mass transfer and solubility," *Chem. Eng. Sci.*, vol. 55, no. 22, pp. 5531–5543, 2000.

[8] P. W. J. Derks, *Carbon Dioxide Absorption in Piperazine Activated N-Methyldiethanolamine*, PhD thesis. 2006.

[9] P. T. Frailie, "Modeling of Carbon Dioxide Absorption / Stripping by Aqueous Methyldiethanolamine / Piperazine," 2014.

[10] S. Salmon, A. House, K. Liu, R. Frimpong, K. Liu, C. Freeman, G. Whyatt, J. Slater, D. Fitzgerald, and D. Babcock, "Low-energy solvents for carbon dioxide capture enabled by combination of enzymes and vacuum regeneration. Technical report," 2015.

[11] N. J. M. C. Penders-van Elk, P. W. J. Derks, S. Fradette, and G. F. Versteeg, "Kinetics of absorption of carbon dioxide in aqueous MDEA solutions with carbonic anhydrase at 298 K," *Int. J. Greenh. Gas Control*, vol. 9, pp. 385–392, 2012.

[12] N. J. M. C. Penders-van Elk, C. van Aken, and G. F. Versteeg, "Influence of temperature on the kinetics of enzyme catalysed absorption of carbon dioxide in aqueous MDEA solutions," *Int. J. Greenh. Gas Control*, vol. 49, pp. 64–72, 2016.

[13] N. J. M. C. Penders-Van Elk, S. M. Oversteegen, and G. F. Versteeg, "Combined Effect of Temperature and pKa on the Kinetics of Absorption of Carbon Dioxide in Aqueous Alkanolamine and Carbonate Solutions with Carbonic Anhydrase," *Ind. Eng. Chem. Res.*, vol. 55, no. 38, pp. 10044–10054, 2016.

[14] N. J. M. C. Penders-van Elk, S. Fradette, Ylvie, and G. F. Versteeg, "Effect of pKa on the kinetics of carbon dioxide absorption in aqueous alkanolamine solutions containing carbonic

anhydrase at 298 K," *Chem. Eng. J.*, vol. 259, pp. 682–691, 2015.

[15] M. Vinoba, M. Bhagiyalakshmi, A. N. Grace, D. H. Kim, Y. Yoon, S. C. Nam, I. H. Baek, and S. K. Jeong, "Carbonic anhydrase promotes the absorption rate of CO2 in post-combustion processes," *J. Phys. Chem. B*, vol. 117, no. 18, pp. 5683–5690, 2013.

[16] D. DeMontigny, P. Tontiwachwuthikul, and A. Chakma, "Parametric Studies of Carbon Dioxide Absorption into Highly Concentrated Monoethanolamine Solutions," *Can. J. Chem. Eng.*, pp. 137–142, 2001.

[17] S. Norouzbahari, S. Shahhosseini, and A. Ghaemi, "CO_2 chemical absorption into aqueous solutions of piperazine: modeling of kinetics and mass transfer rate," *J. Nat. Gas Sci. Eng.*, vol. 26, pp. 1059–1067, 2015.

[18] S. Mudhasakul, H. ming Ku, and P. L. Douglas, "A simulation model of a CO_2 absorption process with methyldiethanolamine solvent and piperazine as an activator," *Int. J. Greenh. Gas Control*, vol. 15, pp. 134–141, 2013.

[19] D. Silkenbäumer, B. Rumpf, and R. N. Lichtenthaler, "Solubility of Carbon Dioxide in Aqueous Solutions of 2-Amino-2-methyl-1-propanol and N -Methyldiethanolamine and Their Mixtures in the Temperature Range from 313 to 353 K and Pressures up to 2.7 MPa," *Ind. Eng. Chem. Res.*, vol. 37, no. 97, pp. 3133–3141, 1998.

[20] U. E. Aronu, A. F. Ciftja, I. Kim, and A. Hartono, "Understanding precipitation in amino acid salt systems at process conditions," *Energy Procedia*, vol. 37, pp. 233–240, 2013.

[21] E. S. Fernandez, K. He, L. V. Van Der Ham, M. J. G. Linders, E. Eggink, F. N. H. Schrama, D. W. F. Brilman, E. L. V Goetheer, and T. J. H. Vlugt, "Conceptual Design of a Novel CO_2 Capture Process Based on Precipitating Amino Acid Solvents," 2013.

[22] R. Notz, I. Tönnies, H. P. Mangalapally, S. Hoch, and H. Hasse, "A short-cut method for assessing absorbents for post-combustion carbon dioxide capture," *Int. J. Greenh. Gas Control*, vol. 5, no. 3, pp. 413–421, 2011.

[23] M. O. Schach, R. Schneider, H. Schramm, and J. U. Repke, "Techno-economic analysis of postcombustion processes for the capture of carbon dioxide from power plant flue gas," *Ind. Eng. Chem. Res.*, vol. 49, pp. 2363–2370, 2010.

[24] P. M. Mathias, S. Reddy, A. Smith, and K. Afshar, "A Guide to Evaluate Solvents and Processes for Post-Combustion CO_2 Capture," *Energy Procedia*, vol. 37, pp. 1863–1870, 2013.

[25] L. Li, "Carbon Dioxide Solubility and Mass Transfer in Aqueous Amines for Carbon Capture," *Dr. Thesis Univ. Texas Austin*, 2015.

[26] L. Li, H. Li, O. Namjoshi, Y. Du, and G. T. Rochelle, "Absorption rates and CO_2 solubility in new piperazine blends," *Energy Procedia*, vol. 37, pp. 370–385, 2013.

[27] G. T. Rochelle, Conventional amine scrubbing for CO_2 capture, In:*Absorption-Based Post-*

Combustion Capture of Carbon Dioxide 2016.

7. Kinetic model for Carbonic Anhydrase in MDEA

This chapter describes the CO_2 mass transfer model development for enzyme enhanced MDEA solutions. It compares four different mechanistic enzyme models implemented into a mass transfer model. The models performance was evaluated on how accurate they could describe the influence of solvent concentration, temperature, solvent loading and CO_2 gas partial pressure and were validated against absorption and desorption experiments.

7.1. Kinetic model for Carbonic Anhydrase as absorption accelerator in flue gas removal

The kinetics of CA has been of interest for a long time due to its physiological importance for the living organisms. The recently addressed application for carbon capture purposes has increased the interest even further. The focus of these two approaches is different, the former aims to describe the interconversion of physically bound CO_2 and bicarbonate in highly diluted aqueous buffer solutions at close to neutral pH. In contrast, the latter approach aims to describe the mass transfer of CO_2 into concentrated buffer solutions at high pH in mass transfer units such as absorber and desorber columns. The complexity and level of detail for the physiological model on the one hand may be troublesome to implement into an already very complex absorber column models, on the other hand some effects of these models, like for example the influence of water concentration might be overlooked, because the water concentration does not change significantly when small amounts of salt or buffer are added, whereas in carbon capture solvent solutions the molar water concentration might be half of the value of pure water. Also the CO_2 concentration in the liquid phase might be quite different in these two approaches.

7.1.1. CA kinetics models for CCS in literature

Several authors modelled enzyme enhanced CO_2 capture in literature. Russo et al. [1] implemented a kinetic model for CA into a bubble column to simulate the mass transfer of CO_2 into K_2CO_3 solutions; for the case of free flowing enzyme they used a reaction rate equation in the following form:

$$r = \frac{k_{cat} \cdot C_{CA}\left(C_S - \frac{C_S^{eq} \cdot C_{H+} \cdot C_{H_2O}}{C_{H+}^{eq} \cdot C_{H_2O}^{eq}}\right)}{K_{MS} + C_S - \frac{C_S^{eq} \cdot C_{H+} \cdot C_{H_2O}}{C_{H+}^{eq} \cdot C_{H_2O}^{eq}}} \tag{7.1}$$

The expression of the rate equation was slightly changed to match our notation. They described the basis for this model to be a reversible Michaelis Menten enzyme kinetics, where the product inhibition and the buffer protonation were neglected. Assuming equilibrium for the product ($C_{H+} = C_{H+}^{eq}$ and

$C_{H_2O} = C_{H_2O}^{eq}$) so the water and proton concentrations are cancelling out, will lead to different expression for the reversible enzyme reaction than Eq. (4.15) derived in Chapter 4. Russo et al. [1] took this expression from the work of Praveen et al. [2] where it is regarded as reversible Michaelis Menten kinetic. In the work of Segel [3], the kinetic expression derived for a reversible reaction has the same form as Eq. (4.15). The expression from Eq. (7.1) describes the progress curve phase of an enzyme reaction according to Michalis Menten kinetics, considering just the forward reaction and no back reaction, according to Cornish-Bowden [4].

Larachi et al. [5] simulated a packed bed scrubber and a Robinson Mahoney reactor with immobilized CA. The reversible enzyme reactions were modelled with the following reaction rate equation:

$$r = \frac{k_{cat} \cdot C_{CA} \cdot C_S}{K_{MS} \cdot \left(1 + \frac{C_P}{K_{MP}}\right) + C_S} - \frac{k_{-cat} \cdot C_{CA} \cdot C_P}{K_{MP} \cdot \left(1 + \frac{C_S}{K_{MS}}\right) + C_P} \tag{7.2}$$

Applying the Haldane relationship from Eq. (4.13) will lead to the same expression as Eq. (4.15).

Penders van Elk et al. [6] derived a kinetic model for CA in MDEA. Based on their observation the reaction rate was declining at higher MDEA concentrations; they described this trend with the lower water concentration and derived an enzyme kinetic reaction that was dependent on the water concentration.

$$r = \frac{k_3^* \cdot C_{CA}}{1 + k_4^* \cdot C_{CA}} \cdot C_{C_{H_2O}} \cdot C_S \tag{7.3}$$

The enzyme contribution term was not linear in this case; they rather used a Langmuir Hinshelwood expression. This model presented here is of special interest as it is the only model derived for MDEA solutions whereas the other models were developed for carbonate salt solutions. In their most recent study [7] the temperature dependency of the enzyme kinetics in 1 M MDEA was determined in a temperature range from 278-343 K. When considering just experimental results at 278, 288 and 313 K they were able to derive a simplified kinetic model in form of Eq., were the k_3^* value followed a Arrhenius type of temperature dependency whereas k_4^* was independent of temperature. The model was under predicting the results obtained at 298 K and over predicting the ones at 343 K. It seemed from their graph, that the enzyme reaction rate constant was almost the same for 298 K, 313 K and 343 K, describing no temperature influence in that range.

Zhang et al. [8] used a simple expression for their kinetic model for 20 wt% K_2CO_3, consisting just of an forward enzyme reaction rate constant multiplied with the enzyme concnetration.

Hu et al. [9] derived a kinetic model for water in the temperature range 298 to 328 K in a stopped flow cell and used a Michaelis Menten kinetic considering just the forward reaction.

A summary of the different kinetic models and the process conditions that they consider is given in Table 2. None of the existing models in literature incorporated the influence of more than 2 process conditions.

Table 2: Kinetic model of CA in CCS applications: Overview of the considered influencing process conditions

Reference	Solvent	Solvent conc.	Temperature	pCO_2	loading
Russo et al.[10]	K_2CO_3	-	-	✓	✓
Larachi et al. [5]	K_2CO_3	-	-	✓	✓
Penders-van Elk et al. [11], [7]	MDEA	✓	✓	-	-
Zhang et al. [8]	K_2CO_3	-	✓	-	✓
Hu et al. [9]	water	-	✓	✓	-
This work	MDEA	✓	✓	✓	✓

7.1.2. Model development

Kinetic models should be as simple as possible and as accurate as needed. Therefore several different kinetic models for the enzyme kinetics were derived, with different level of complexity and each model was tested on how good it could describe the different process parameters.

The most complex model was the reversible Michaelis Menten (MR) model:

$$r = \frac{k_{CA}^{MR} \cdot C_{CA} \left(C_S - C_S^{eq} \right)}{K_{MS} \cdot \left(1 + \frac{C_P}{K_{MP}} \right) + C_S} \tag{7.4}$$

The context of this model was the same as in the work of Larachi et al. [5]. This model could be simplified, assuming, that the reaction can be treated as following a Michaelis Menten type kinetic with regard to the substrate, but not for the reversible reaction. The following expression of the model was similar to the general Michaelis Menten equation for a forward reaction and is therefore denoted with MM:

$$r = \frac{k_{CA}^{MM} \cdot C_{CA} \cdot \left(C_S - C_S^{eq} \right)}{K_{MS} + C_S} \tag{7.5}$$

A similar expression to the MM model was used in the work of Hu et al. [9]. The simplest model was the simplified Michaelis-Menten (SM) model for forward reaction, similar to the model of Zhang et al. [8] and Penders van Elk et al. [11]:

$$r = \frac{k_{CA} \cdot C_{CA}\left(C_S - C_S^{eq}\right)}{K_{MS} + C_S} \approx k_{CA}^{SM} \cdot C_{CA}\left(C_S - C_S^{eq}\right) \tag{7.6}$$

This model could be made more complex by assuming that the product inhibited the rate, the simplified model with product inhibition (SP) was:

$$r = \frac{k_{CA}^{SP} \cdot C_{CA} \cdot \left(C_S - C_S^{eq}\right)}{1 + \frac{C_P}{K_{IP}}} \tag{7.7}$$

An overview of the different models and the number of relevant parameters is given in Table 3.

Table 3: Overview of the different kinetic enzyme models

Abb.	Description	Mathematical context	Number of	Parameters
MR	Reversible enzyme kinetics (Michaelis Menten)	Eq. (7.4)	3	k_{CA}^{MR}, K_{MS}, K_{MP}
MM	Michaelis Menten type forward reaction	Eq. (7.5)	2	k_{CA}^{MM}, K_{MS}
SP	Simple enzyme model with product inhibition	Eq. (7.7)	2	k_{CA}^{SP}, K_{IP}
SM	Simple enzyme model	Eq. (7.6)	1	k_{CA}^{SM}

7.2. Model development

Experiments were conducted at different temperatures, solvent concentrations, enzyme concentrations, solvent loadings and CO_2 gas partial pressures. It was the aim to develop a consistent model to describe the mass transfer of CO_2 into MDEA solutions by the means of a mechanistic enzyme kinetic model implemented into a mass transfer model with the process conditions as input parameters. The influence of enzyme concentration on the enzyme kinetics was determined in a previous study, where a linear dependency between first order reaction rate constant and enzyme concentration was observed [12].

The different kinetic models for the enzyme presented in Chapter 4 are not a function of process temperature or solvent concentration, even though some of the parameters might be dependent on temperature or solvent concentration. The described models differ on how the solvent loading, or more precisely the HCO_3^- concentration, and the interfacial CO_2 concentration (linked to the CO_2 gas partial pressure via the Henry coefficient) influences the enzyme kinetics. For model development a stepwise rather than a global optimization was chosen. Experiments at three different temperatures (298, 313 and 328 K) and three different solvent concentrations (15, 30 and 50 wt%) with an enzyme concentration of 0.85 g/L were used for the model development, giving a 3*3 matrix. For the development of the

mathematical description of the influence of a certain process condition (temperature, solvent concentration, HCO_3^- concentration) all the experiments were chosen around the reference experimental setpoint (313 K , 30 wt% MDEA) where just one process condition was varied, whereas all others were kept constant. The kinetic constant in the model was fitted to describe the influence of the process parameter.

For the influence of solvent concentration on mass transfer, the experiments with unloaded MDEA at 313 K were taken to derive a correlation for the simple model SM (Eq. (7.6)) via nonlinear regression. Here different powers of the reactants MDEA and water, ν_{H_2O} and ν_{MDEA} were compared to find the best correlation.

The temperature dependency of the mass transfer was derived from experiments with unloaded 30 wt% MDEA using non-linear regression at 298, 313 and 328 K. This temperature dependency was then tested for the other the other solvent concentrations, but no fitting was performed.

Afterwards the influence of gas partial pressure of CO_2 on the mass transfer was investigated and the Michaelis Menten constant K_{MS} was validated for the MM and MR model. Then the inhibition of the HCO_3^- was determined for 30 wt% MDEA at 313 K; therefore the inhibition constant K_{IP} and the reaction constant k_{CA}^{SP} were derived from the experiments at different CO_2 loadings for the SP model, as well as the k_{CA}^{MR} and K_{MP} value for the MR model. These constants were then adjusted if needed to match the mass transfer of the experiments for 30 wt% MDEA at different CO_2 loadings at the temperatures 298 K and 328 K. No fitting was conducted for the other MDEA concentrations.

7.2.1. Influence of solvent concentration on mass transfer

The liquid side mass transfer coefficient of CA enhanced MDEA at 313 K is steadily dropping if the MDEA concentration is increased from 15 over 30 to 50 wt% as shown in Figure 44. For the correlation of the liquid side mass transfer the SM (Eq. (7.6)) model was chosen with different powers of the reactants (ν_{H_2O}) water and MDEA (ν_{MDEA}) as in:

$$r_{CO_2} = k_{CA}^{SM} \cdot C_{CA} \cdot C_{H_2O}^{\nu_{H_2O}} \cdot C_{MDEA}^{\nu_{MDEA}} \tag{7.8}$$

and k_{CA}^{SM} was fitted to match the experiment at 30 wt% MDEA and 313 K. The results are shown in Figure 44. The naming of the different curves express the power of each reactant, e.g. w^1 s^1 means water (w) as well as the solvent (s) has the power 1 in Eq.(7.8). The simplest expression with no power in water and MDEA (w^0) did not result in a satisfying correlation; even though the trend was the same as the experiments, the correlation under predicted the liquid side mass transfer for low solvent concentrations and over predicted for higher solvent concentrations.

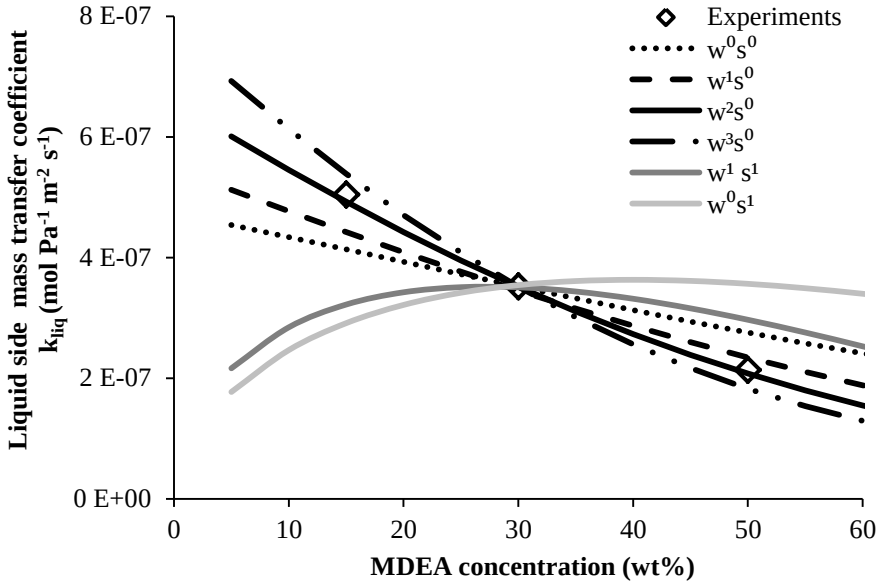

Figure 44: Influence of solvent concentration on the liquid side mass transfer coefficient k_{liq} for 30 wt% MDEA with 0.85 g/L CA at 313 K: comparison of different powers on the reactants MDEA (s) and H_2O (w) in the enzyme kinetics on the mass transfer model of CA enhanced MDEA

The solvent concentration of MDEA did not influence the reaction mechanism of carbonic anhydrase directly, as in both cases when solvent concentration was considered in the reaction rate (w^1 s^1 and w^0 s^1) the simulated liquid side mass transfer coefficient k_{liq} showed a different trend than the experimental results. Once the power of the water concentration was increased the simulated correlations for k_{liq} were closer to the experiments. From our experiments a power of the water concentration of 2 in Eq. (7.8) was most accurate to model k_{liq}. Applying the different enzyme inhibition models and taking the solvent concentration as inhibitor resulted in slightly better fits for the solvent concentration dependency. An inhibition model of the solvent was not used in this approach, as it would assume that the solvent molecule occupies the active site or blocks the enzyme substrate complex. No evidence of such a mechanism could be found in literature; therefore it lacks a mechanistic basis. Besides that an inhibition term would introduce one or two regressable parameters, which would make qualitative considerations afterwards more difficult.

The influence of MDEA concentration on the kinetics of CA has been previously investigated by Penders-van Elk et al. [11]. They came to a similar conclusion, that MDEA does not directly influence the kinetics of CA and suggested the power of the water concentration should be 1 in the reaction rate. The difference between our results might arise from the fact that we used different enzymes in our experiments. Considering that the rate limiting step in the enzyme reaction mechanism is the intramolecular proton transfer from the zinc bound water to the proton channel PC which occurs via a network of hydrogen bonded water molecules can explain why the power of the water concentration might be even higher than one as in our case.

7.2.2. Influence of temperature on mass transfer

The liquid side mass transfer coefficient decreased with temperature for 15 and 30 wt% MDEA concentration as shown in Figure 45; the decrease is more distinct for a lower solvent concentration. For 50 wt% the liquid side mass transfer coefficient k_{liq} remained almost constant over the temperature range between 298 and 328 K. Using the correlation as well as the k_{CA}^{SM} value derived in the section before without any temperature dependent adjustment, resulted in very good agreement between mass transfer model and experimental data as shown in Figure 45. This indicated that the kinetic rate constant for the CA is not temperature dependent in the range between 298 and 328 K, similar to the observation in chapter 6.

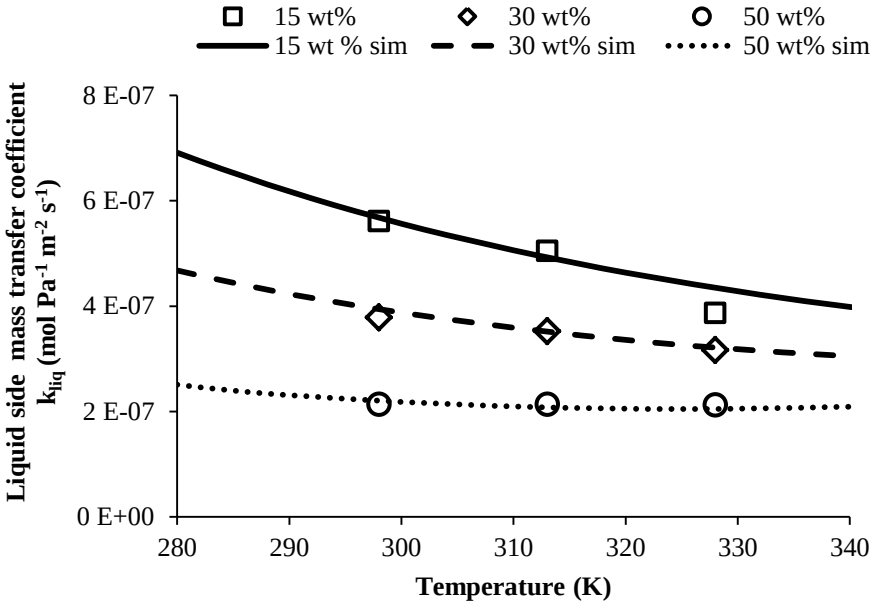

Figure 45: Influence of process temperature on the liquid side mass transfer coefficient k_{liq} for different MDEA concentrations (15, 30 and 50 wt%) with 0.85 g/L CA: Comparison between experiments and simple enzyme model (SM) with a reaction rate dependency of water with the power of two.

Some researchers found an increase in CA reaction rate constant with temperature, for MDEA [13] and K_2CO_3 [9], whereas others observed no change in K_2CO_3 [8]. In our previous study we even reported a decrease in kinetic rate constant with temperature for CA in MDEA [12]. It is important to note, that the purpose of all these experiments was to derive correlations for CA kinetics to describe the mass transfer of CO_2 into enzyme enhanced solvent solutions. As the liquid side mass transfer is dependent on the solubility of the CO_2 (H_{CO_2}), the diffusivity of CO_2 (D_{CO_2}) in the solution as well as the reaction rate with CO_2, the value and temperature dependency of the reaction rate constant for CA relies on the literature value of solubility and diffusivity as well as their temperature dependencies. When using a

kinetic reaction constant from literature it is important to use it together with the solubility and diffusivity from that same source.

7.2.3. Influence of CO_2 partial pressure on the mass transfer

When performing experiments at higher partial pressures of CO_2 a slight decrease in k_{liq} could be observed as shown in Figure 46. A higher reaction rate with CO_2 due to higher partial pressure that causes a depletion of reactant near the interface can be excluded as CA reacts with water which is abundant, and the intermolecular proton transfer to a buffer in solution is thought to be rate limiting just at low buffer concentrations [14]. A possible explanation for that behavior is a substrate saturation of CO_2 as CA is known following Michaelis Menten type reaction kinetics [15].

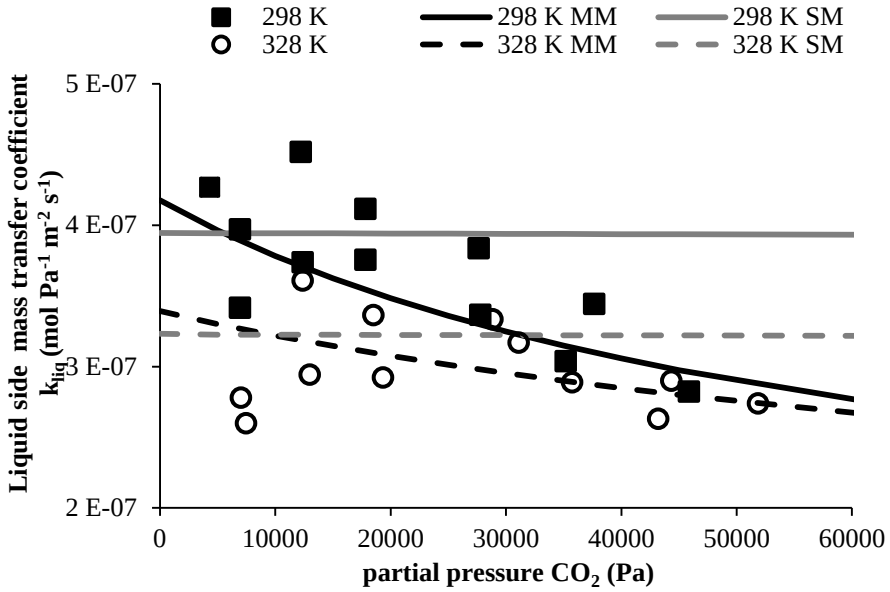

Figure 46: Influence of partial pressure of CO_2 in gas phase on liquid side mass transfer coefficient for 298 and 313 K: Comparison of SM model and MM model prediction.

The Michaelis Menten constant got neglected in most cases where the application of CA enhanced solvent for CCS on coal fired power plant was investigated, as the partial pressure in the gas was low, leading to CO_2 concentrations in the liquid one order of magnitude lower than the Michaelis Menten constant. Under these conditions the simplification described in Eq. (7.6) might be applied. Hu et al. [9] and Mirjafari et al. [16] determined the KM value for CA in K_2CO_3 and $CaCO_3$ respectively; they reported values of 12.5 and 17.8 mole m^{-3}. Taking a K_{MS} value of 15 mole m^{-3} as the approximate mean value and refitting of k_{CA}^{MM} that it matches kl_{iq} for 30 wt% MDEA at 313 K, when the CO_2 partial pressure in the gas is about 7.5 kPa (approximate arithmetic mean partial pressure of CO_2 in the column considering 15 kPa inlet CO_2 partial pressure and no CO_2 outlet partial) gives the MM model, which incorporates Michaelis Menten type behavior.

The MM model matches the trend of the experimental data quite well for 298 and 328 K. Even though the SM model is not describing the trend of the liquid side mass transfer coefficient in the range between 0 and 50 kPa, in the region of low pCO_2 (<15 kPa) typically encountered in CCS applications for coal fired power plants, the differences between the SM and MM model are quite small. This indicates that models that do not account for the influence of CO_2 partial pressure and thus CO_2 concentration in the liquid phase can be used for low CO_2 partial pressure applications. For application with a CO_2 partial pressure higher than 15 kPa it is advised to use models that incorporate the Michaelis Menten kinetics and described the effect of CO_2 partial pressure influence, otherwise the mass transfer will be overestimated.

7.2.4. Influence of solvent loading on mass transfer

Similar to the procedure for CO_2 partial pressure dependency, new models were introduced to describe the dependency of solvent loading on the liquid side mass transfer coefficient, namely the SP model (Eq. (7.7)), an extension of the SM model with an introduced product inhibition term for the bicarbonate ion, and the MR model (Eq. (7.4)**)** a Michaelis Menten mechanism for reversible reactions and thus a combination of the MM and SP model. For the SP model the k_{CA}^{SP} value was taken from the SM model (k_{CA}^{SM}), for the MR model the value for k_{CA}^{MR} was taken from k_{CA}^{MM} and the K_{MS} was the same as in the MM model. For both models just the K_{IP} and K_{MP} values were fitted to match the experimentally determined k_{liq} for 30 wt% MDEA at 313 K at different solvent loadings shown in Figure 47.

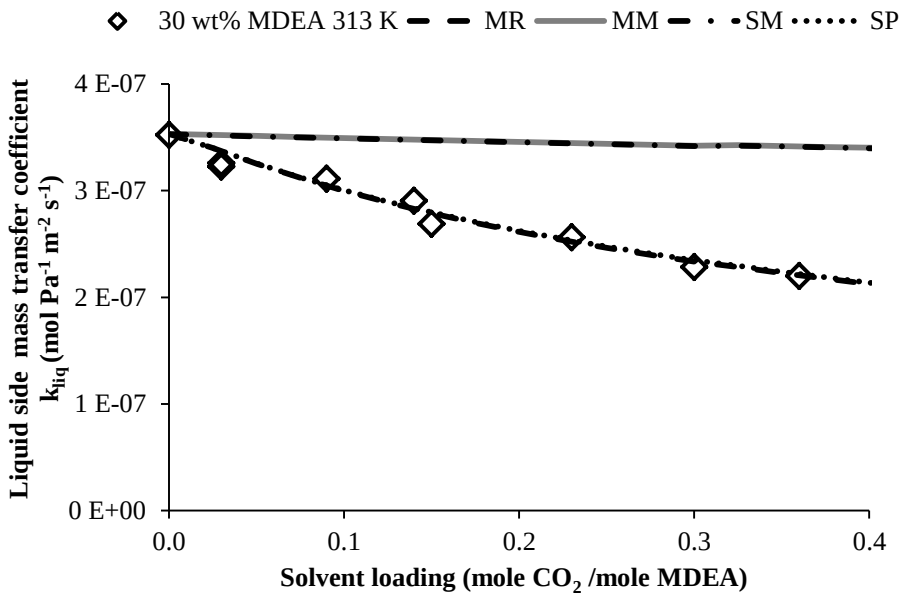

Figure 47: Influence of solvent loading on the liquid side mass transfer coefficient for 30 wt% MDEA at 313 K; Comparison of model performance of the different enzyme models

The liquid side mass transfer coefficient decreased at higher solvent loadings. A probable explanation for that behavior is a product saturation, where the bicarbonate product is occupying the active site of the enzymes at higher concentrations and influencing the reaction rates. The trend of decrease in k_{liq} with higher CO_2 solvent loading could be very well described with The SP and MR model, assuming a CO_2 partial pressure of of 7.5 kPa in the absorber for the MR model. Both models were overlapping over the whole range. The same was for the MM and SM model, but these models could not describe the trend of decreasing k_{liq} at higher solvent loadings and were over predicting the liquid side mass transfer coefficient, once the solvent was slightly loaded. A proper mass transfer model needs to account for the change in k_{liq} with loading to yield accurate predictions, as it is inevitable that the loading changes inside the absorber. The SM and MM model are therefore not suitable for use in absorber column modelling, unless it is experimentally proven that the k_{liq} is not influenced by solvent loading.

The SP and MR model could also accurately predict the decrease in k_{liq} for 30 wt% MDEA at 298 K and 328 K at different solvent loadings as shown in Figure 48. No temperature dependent adjustment to K_{MP}, K_{IP} and K_{MS} was needed. Both correlations were only slightly over predicting the experimental data, which can be explained by the fact that these models were slightly over predicting the liquid side mass transfer coefficient at 298 K and 328 K for unloaded solvent as shown in Figure 44. These deviations were quite small, and no obvious trend was noticeable.

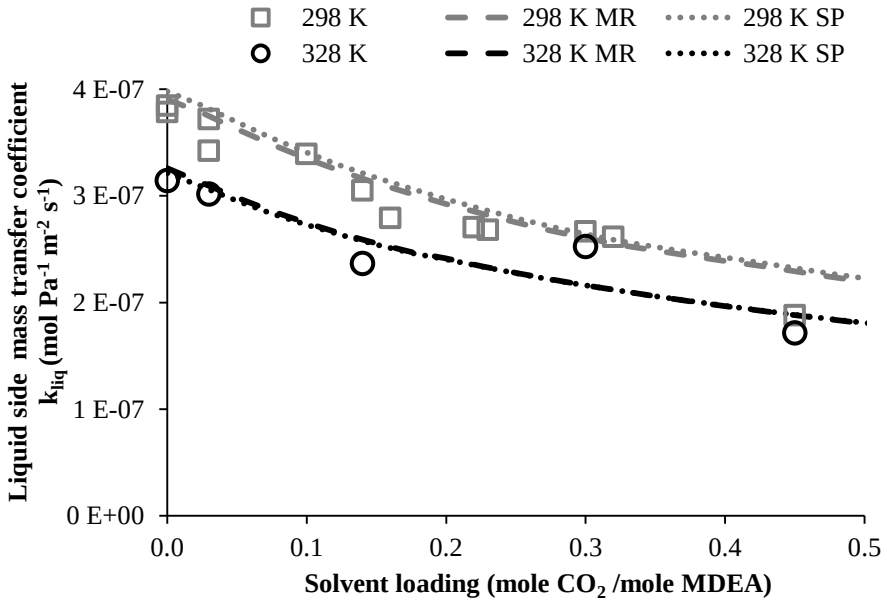

Figure 48: Influence of solvent loading on liquid side mass transfer coefficient for 30 wt% MDEA at 298 and 328 K: comparison between experiments and MR and SP model

These models could be used to describe the mass transfer at higher solvent loadings even for different solvent concentrations. The results for k_{liq} in 15 and 50 wt% MDEA at 313 K are shown in Figure 49. Both models gave almost identical results and were capable of describing the trend of the experiments. The inhibition term in the SP model and the reverse reaction term in the MR model are just indirectly linked to the solvent loading, as these terms are influenced by the bicarbonate ion concentration, which is dependent also on the solvent concentration. The bicarbonate concentration of a solvent with 50 wt% MDEA is about 3.5 times higher than for a solvent with 15 wt% at the same loading.

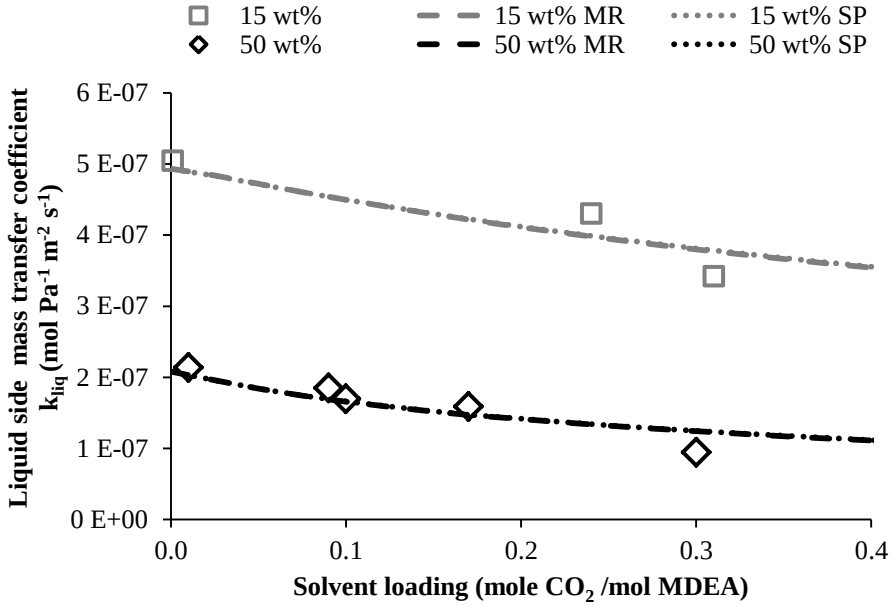

Figure 49: Influence of solvent loading on mass transfer for 15 wt% and 50 wt% MDEA at 313K: Comparison between experimental data and MR model

7.2.5. Influence of enzyme concentration on mass transfer

The enzyme concentrations is a crucial process parameter, as more enzymes will result in higher mass transfer, but at the same time increase the costs. The influence enzyme concentration on the liquid side mass transfer coefficient together with the model predictions are shown in Figure 49. The model was capable to predict the k_{liq} fairly well up to an enzyme concentration of about 3 g/L; at very high enzyme concentrations the model over predicted the mass transfer by 15 %. The model assumed a linear relationship between enzyme reaction rate and enzyme concentration, which seemed to be valid for low concentrations. Several authors reported a divergence from that linear relationship at high enzyme concentrations [11] [17][18]. Pender-van Elk used a Langmuir-Hinshelwood type of relation as in Eq. (7.3) to describe that behavior. Using that expression and keeping the k_{CA}^{SP} value in the numerator as k_3^* and adjusting just the k_4^* (0.74) value, could describe the trend very well. In that case the SP model was used, but all other gave identical results and could be used with the same derived k_4^* value. The

Langmuir Hinshelwood expression was not used for model validation, as the experiments were performed at 0-3 g/L CA and in that region both correlations did not differ too much.

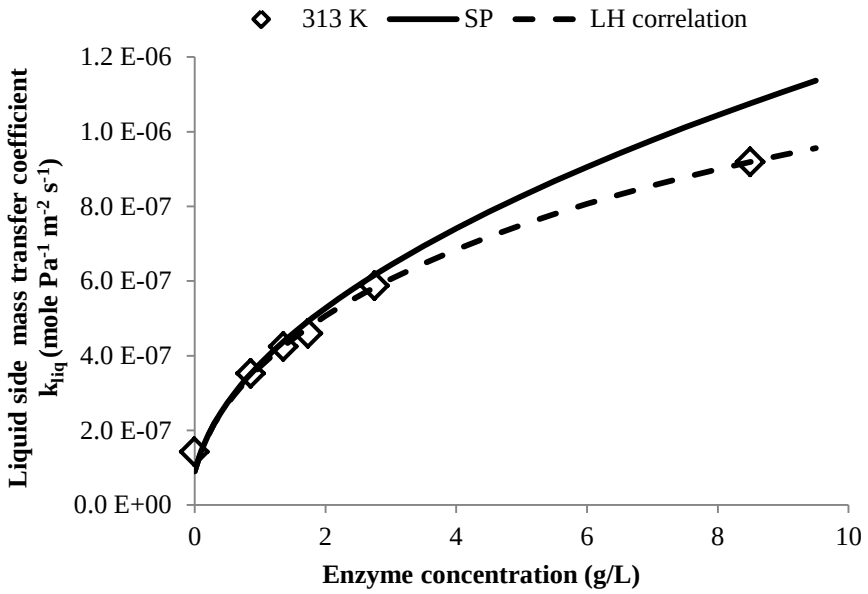

Figure 50: Influence of enzyme concentration on liquid side mass transfer coefficient for 30 wt% MDEA at 313 K: Comparison of experimental data, SP model and SP model with Langmuir Hinshelwood type of dependency on the enzyme concentration.

7.3. Model validation

The kinetic constants for the different models are summarized in Table 4. The reaction rate could be expressed as:

$$r_{CO_2}^{enz} = r_{enz} \cdot C_{H_2O}^2 \tag{7.9}$$

With $r_{CO_2}^{enz}$ being the one of the discussed enzyme model (SM, SP, MM or MR) described in Table 3. As the SP model is an extension of SM, and the MR model is the combination of the MM and SP model, some of the kinetic constants are the same.

Table 4: Kinetic constants for the different enzyme models

Abb.	1.Parameter	(m^6 kg^{-1} s^{-1})	2.Parameter	(mole m^{-3})	3.Parameter	(mole m^{-3})
SM	k_{CA}^{SM}	1.05E-06				
SP	k_{CA}^{SP}	1.05E-06	K_{IP}	5.05E+02		
MM	k_{CA}^{MM}	1.77E-05			K_{MS}	1.50E+01
MR	k_{CA}^{MR}	1.77E-05	K_{MP}	4.40E+02	K_{MS}	1.50E+01

The models were validated against 323 experiments, of which 23 % (74) were desorption experiments and 77 % absorption experiments. The performance of the different models is shown in Table 5, where the Absolute average relative deviation (AARD) of the experiments and models are listed. These values were calculated in the following manner:

$$AARD(\%) = \frac{1}{n}\sum \frac{\left|N_{CO_2}^{exp} - N_{CO_2}^{model}\right|}{N_{CO_2}^{exp}} \tag{7.10}$$

The best model prediction came from the most complex MR model, where the AARD was 14 % and the absorption experiments could be described with an accuracy of 12 %, whereas the model had 23 % accuracy for desorption. The second best model was the SP, which neglected the Michaelis Menten behavior for CO_2, but incorporated a product inhibition by the bicarbonate. It just had a slightly worse performance overall (15 vs.14 %) and for absorption (13 vs 12%); it could although predict desorption slightly better. The models which did not account for influence of solvent loading on the liquid side mass transfer coefficient, the MM and SM model, performed much worse. This shows that the product inhibition or saturation of the bicarbonate ion is a more important process parameter for the mass transfer model than the substrate saturation of CO_2. Over 90 % of the experiments were carried out at partial pressures of CO_2 below 30 kPa which explains why the accuracy of the MR model and SP model were comparable. It also justifies the use of the simplified SP model for absorber columns with low CO_2 gas partial pressure like in CCS applications for coal fired power plants.

Table 5: AARD for the different models

Number of experiments	**total** 323	**absorption** 249	**desorption** 74
SM	38%	30%	65%
SP	15%	13%	22%
MM	33%	24%	64%
MR	14%	12%	23%

The parity plots for the SP and MR model are shown in Figure 51. The upper row shows parity plots distinguishing between the different solvent concentration and lower row distinguishing between the different temperatures. Both models were predicting the mass transfer of CO_2 fairly well for absorption and desorption.

From that plots it can be seen, that the SP model tended to over predict the mass transfer at higher fluxes. It seems this is just an issue for 30 wt% MDEA, but most of the experiments with higher enzyme concentrations were carried out at 30 wt% MDEA. The temperature dependency was also described well for the SP model, no systematic deviation between experiments and simulation is visible. The MR model eliminated the trend of over predicting the absorption for higher fluxes.

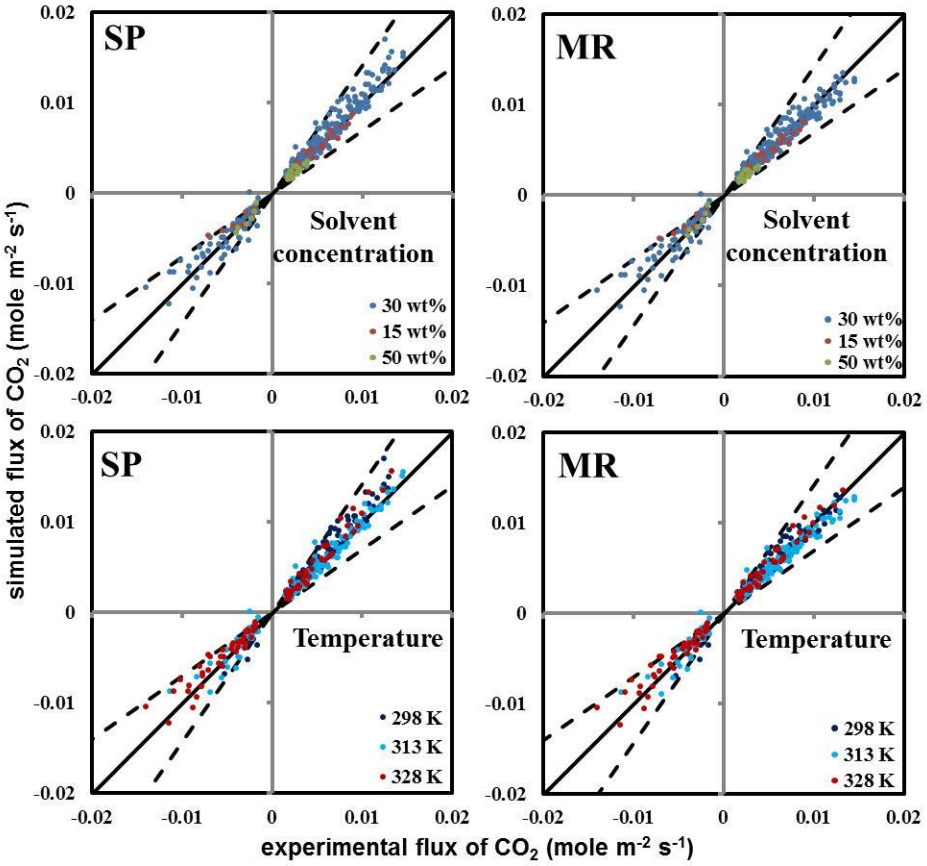

Figure 51: Parity plot for the SP and MR model validation, dashed lines indicate ± 30% deviation

BIBLIOGRAPHY

[1] M. E. Russo, P. Bareschino, G. Olivieri, R. Chirone, P. Salatino, and A. Marzocchella, "Modeling of slurry staged bubble column for biomimetic CO_2 capture," *Int. J. Greenh. Gas Control*, vol. 47, pp. 200–209, 2016.

[2] T. Praveen, P. Valencia, and L. Rajendran, "Theoretical analysis of intrinsic reaction kinetics and the behavior of immobilized enzymes system for steady-state conditions," *Biochem. Eng. J.*, vol. 91, pp. 129–139, 2014.

[3] I. H. Segel, *Enzyme Kinetics: Behavior and Analysis of Rapid Equilibrium and Steady-State Enzyme Systems*. Wiley-VCH, 1993.

[4] A. Cornish-Bowden, *Principles of ezyme kinetics*. Butterworths Inc, 1976.

[5] F. Larachi, O. Lacroix, and B. P. a Grandjean, "CO_2 hydration by immobilized carbonic anhydrase in Robinson-Mahoney and packed-bed scrubbers-Role of mass transfer and inhibitor removal," *Chem. Eng. Sci.*, vol. 73, pp. 99–115, 2012.

[6] N. Penders-van Elk, E. Hamborg, P. S., J. A. Carley, S. Fradette, and G. F. Versteeg, "Kinetics of absorption of carbon dioxide in aqueous amine and carbonate solutions with carbonic anhydrase," *Int. J. Greenh. Gas Control*, vol. 12, pp. 259–268, 2013.

[7] N. J. M. C. Penders-van Elk, C. van Aken, and G. F. Versteeg, "Influence of temperature on the kinetics of enzyme catalysed absorption of carbon dioxide in aqueous MDEA solutions," *Int. J. Greenh. Gas Control*, vol. 49, pp. 64–72, 2016.

[8] S. Zhang and Y. Lu, "Kinetic performance of CO_2 absorption into a potassium carbonate solution promoted with the enzyme carbonic anhydrase: Comparison with a monoethanolamine solution," *Chem. Eng. J.*, vol. 279, pp. 335–343, 2015.

[9] G. Hu, K. H. Smith, N. J. Nicholas, J. Yong, S. E. Kentish, and G. W. Stevens, "Enzymatic carbon dioxide capture using a thermally stable carbonic anhydrase as a promoter in potassium carbonate solvents," *Chem. Eng. J.*, vol. 307, pp. 49–55, 2016.

[10] M. E. Russo, G. Olivieri, A. Marzocchella, P. Salatino, P. Caramuscio, and C. Cavaleiro, "Post-combustion carbon capture mediated by carbonic anhydrase," *Sep. Purif. Technol.*, vol. 107, pp. 331–339, 2013.

[11] N. J. M. C. Penders-van Elk, P. W. J. Derks, S. Fradette, and G. F. Versteeg, "Kinetics of absorption of carbon dioxide in aqueous MDEA solutions with carbonic anhydrase at 298K," *Int. J. Greenh. Gas Control*, vol. 9, pp. 385–392, 2012.

[12] A. Gladis, M. T. Gundersen, P. L. Fosbøl, J. M. Woodley, and N. von Solms, "Influence of temperature and solvent concentration on the kinetics of the enzyme carbonic anhydrase in carbon capture technology," *Chem. Eng. J.*, 2017.

[13] N. J. M. C. Penders-van Elk, C. Van Aken, and G. F. Versteeg, "Influence of temperature on the

kinetics of enzyme catalysed absorption of carbon dioxide in aqueous MDEA solutions," *Int. J. Greenh. Gas Control*, vol. 49, pp. 64–72, 2016.

[14] D. N. Silverman and S. Lindskog, "The catalytic mechanism of carbonic anhydrase: implications of a rate-limiting protolysis of water," *Acc. Chem. Res.*, vol. 21, no. 4, pp. 30–36, 1988.

[15] T. G. Spiro, *Zinc Enzymes*, 1st ed. John Wiley & Sons Ltd., 1983.

[16] P. Mirjafari, K. Asghari, and N. Mahinpey, "Investigating the application of enzyme carbonic anhydrase for CO_2 sequestration purposes," *Ind. Eng. Chem. Res.*, vol. 46, no. 3, pp. 921–926, 2007.

[17] H. Thee, K. H. Smith, G. da Silva, S. E. Kentish, and G. W. Stevens, "Carbonic anhydrase promoted absorption of CO_2 into potassium carbonate solutions," *Greenh. Gases Sci. Technol.*, vol. 5, pp. 108–114, 2015.

[18] S. Salmon, A. House, K. Liu, R. Frimpong, K. Liu, C. Freeman, G. Whyatt, J. Slater, D. Fitzgerald, and D. Babcock, "Low-energy solvents for carbon dioxide capture enabled by combination of enzymes and vacuum regeneration. Technical report," 2015.

Pilot scale

8. Pilot scale absorber column setup

This chapter describes the experimental pilot plant setup, a packed column, used in this study. Characteristics of a packed column such as, hold up, pressure drop and mass transfer area are explained and experimental determination methods are described. The pilot absorber column at DTU used in this study is described in detail in the current setup together with the changes and modifications that were carried out during this study. The methods for determining the mass balances in experimental runs are described. The last part of this chapter deals with column characterization experiments and troubleshooting during the experimental campaigns.

8.1. Packed columns

Very different types of contacting equipment are in use for mass transfer operation where two phases should be brought in contact efficiently. The choice of the right equipment is very much dependent on the process conditions and the process itself. For the CCS application a gas liquid contacting device for a chemical absorption process is needed with a high surface area. The mass transfer operation is a flue gas cleaning of a diluted compound and encounters very high gas volume flows thus from an economic standpoint the equipment should offer low pressure drop.

Packed columns can provide a high specific surface area and are suitable to handle large gas volume streams as they offer high porosity. The basic principles of mass transfer phenomena have been explained in a simple manner in chapter 2. In order to describe the complex process of mass transfer in technical absorber the effects occurring in bigger scale need to be accounted for. In gas purification processes packed columns are often used because they exhibit a lower pressure drop as the gas does not need to permeate through a layer or rather several layers of liquid as in tray columns [1]. Packed columns are either packed with random packing material in all kind of different shapes and material or with a structured packing consisting of bended sheets or wire mesh. The liquid phase runs down the surface of the packing creating a thin film, whereas the gas stream flows upwards counter currently in the void spaces or flow channels. The main characteristics of packed columns compared to other gas liquid contactors are the relative high surface area compared to reactor volume and low pressure drop over the height of the absorber. They are also more favorable with liquids that tend to foam or aggressive substances that require special packing material [2].

The gas volume stream can be varied in a high range in packed column with almost no lower limit and just an upper bound that prevents the column of flooding as shown in Figure 52. In process engineering the terms gas/liquid loads are generally used describing the process conditions of an absorber, rather

than gas/liquid volume streams. The gas/liquid loads ($u_{G/L}$) are defined as ratio of gas/liquid volume flows per cross sectional area of the column a_{CS}, and thus describe the mean velocity of the phase in an empty column:

$$u_{G/L} = \frac{V_{G/L}}{a_{CS}} \tag{8.1}$$

The liquid load during operation needs to be chosen in a more narrow range, as a too high value causes flooding and a too low value a de-wetting of the packing surface [1]. While the flooding regime is represented by a hard threshold making no operation possible above this line, the minimum liquid load, which separates the regime of de-wetting is a soft threshold allowing performance in that regime with lowered mass transfer rates [3].

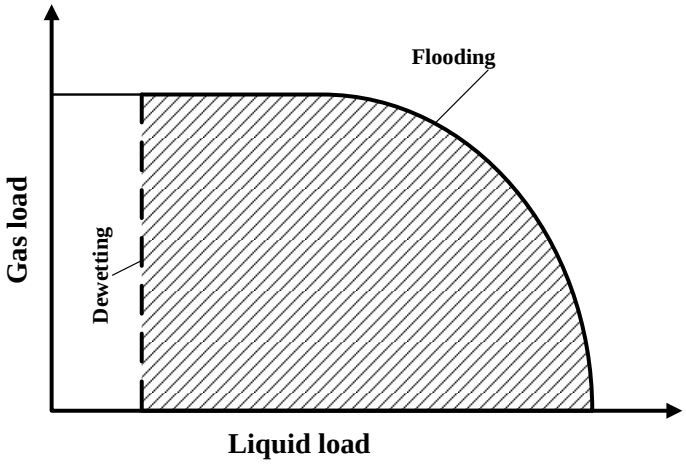

Figure 52: Operating region of a packed column modified from Mersmann et al. [1]

In this study a pilot absorber with structured packing was used in the experiments. Structured packings consist of corrugated sheets of either metal or plastic; those are fastened to each other as shown in Figure 53, where 7 sheets are stacked. The material is often perforated and structured in a way that liquid and gas are exchanged more frequently. The corrugation angle α, describes how much the corrugation is shifted from the horizontal plane. Liquid is flowing down on the surface of the packing; gas is taking up the empty space in the corrugated flow channels flowing up counter currently. The sheets are stacked in a way that the following sheet has the same corrugation angle but is pointing into the opposite direction. This ensures mixing points for liquid and gas phase where two sheets are touching each other as the phases coming from either different corrugated sheets or flow channels are mixed which intensifies the mass transfer [4]. The flow channel dimension with reference to the horizontal plane can be described with a diamond shaped cross section with a corrugation side S. Some care should be taken as some researcher define the dimensions of the flow channel perpendicular to the corrugation angle [5].

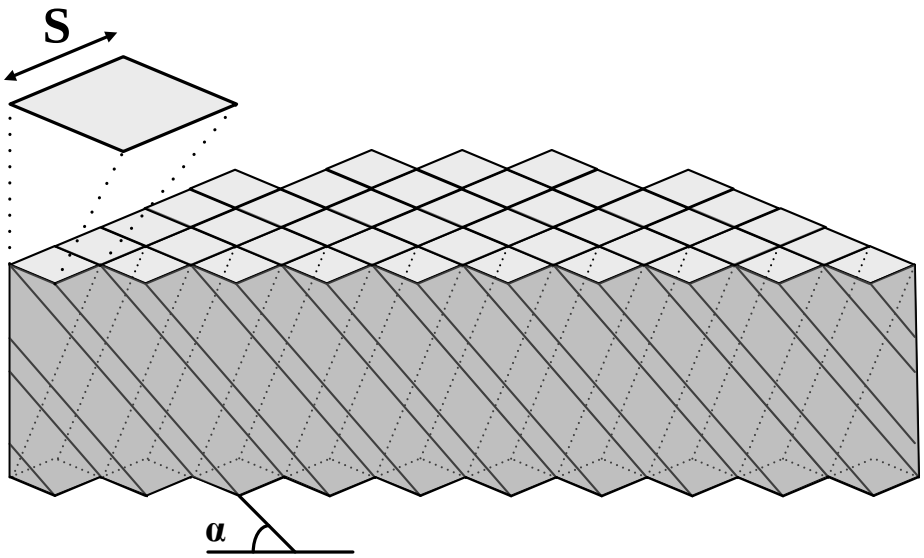

Figure 53: Scheme of a structured packing material similar to Mellapak 250 Y; darker grey resembles packing side and lighter grey top of packing, S is dimension side corrugation of packing material and α corrugation angle.

8.2. Characteristics in packed absorption columns

The most important parameters describing the hydrodynamics of packed columns are the effective mass transfer area, the pressure drop and the liquid hold up [6]. These parameters are linked to each other during operation. The liquid holdup and the effective area for a certain column packing correlate [1]. The pressure drop inside the column is dependent on the interface due to drag forces between gas and liquid phase and to the empty spaces the phases can flow through and thus also to the holdup.

8.2.1. Liquid holdup

The liquid holdup h_L (-) describes the amount of liquid inside a column during operation and is defined as the ratio of liquid volume and column volume:

$$h_L = \frac{Vol_L}{Vol_{column}} \tag{8.2}$$

The holdup of a column can be divided into two parts, a static and a dynamic holdup [7]. The static hold up represents that liquid fraction that is bound to the column internals by capillary and adhesion forces and remains there even when the liquid flow is stopped. The dynamic hold up is the liquid fraction running down the packing and participating actively in mass transfer [8]. The contribution of the dynamic holdup to the total holdup might be neglected during operation as its influence is very small [9].

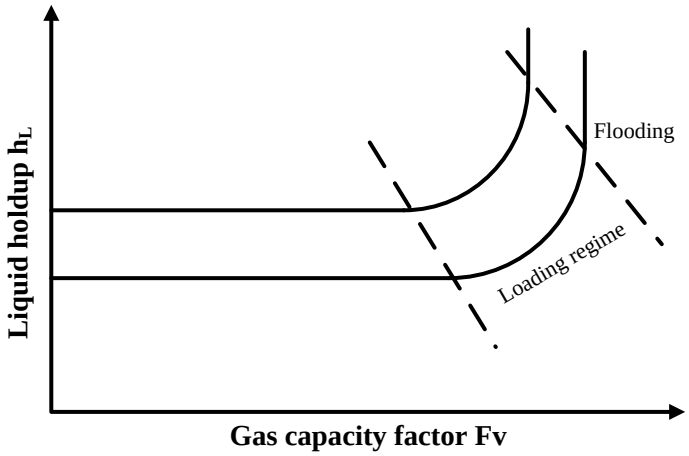

Figure 54: Holdup in a column as a function of gas capacity factor for a constant liquid load, adapted from Billet [10].

In column hydrodynamics gas capacity factors rather than gas velocities or gas loads are used to describe the gas phase because it incorporates the density and describes the gas momentum. The gas capacity factor is defined as:

$$F_V = u_G \sqrt{\rho_G} \tag{8.3}$$

The liquid hold up is constant for certain liquid load for low gas capacity factors as shown in Figure 54. Once the gas capacity is so high, that the liquid flow cannot flow down unimpeded due to drag forces between gas and liquid, liquid will accumulate inside the column and the holdup is rising. The hydrodynamic behavior where the holdup is switching from being independent of the gas flow to being a function of the gas flow is called loading of the column and the process regime is referred to as loading regime. The holdup can be increased further with a higher gas capacity until the column starts to flood. A higher liquid load results in a higher hold up.

8.2.2. Pressure drop

In an absorber column the gas and the liquid phase have to be brought in contact and the streams have to be exchanged continuously in order to maintain efficient absorption. The liquid flow is therefore pumped into the top of the column and flows down by gravitational force. For a good separation the gas flow needs to flow counter-currently in the column, meaning the gas flow needs to be pushed upwards through the column by a pre-compressor. Several obstacles hinder a simple gas flow through the column, cause friction and create a pressure drop. The main reasons for this pressure drop are gas-liquid interaction at the interface, due to the drag forces, abrupt changes of gas flow directions and interaction between gas streams at open crossings of gas flow channels [6]. From an economic standpoint this issue has to be addressed as it results in a higher energy input into the absorber blower and this energy loss may account significantly to the overall efficiency [11].

The pressure drop can be divided into being caused by column geometric and by liquid-gas interactions. The pressure drop caused by column geometry can be determined with zero liquid flow in a dry column and is called dry pressure drop. Introducing a down-flowing liquid flow into the absorber will add additional friction and increase the pressure drop; this pressure drop is referred to as irrigated pressure drop. The experimental pressure drop can be determined by taking the pressure difference between differential pressure transmitter inside the column and divide it by the vertical distance between them [6].

8.2.3. Mass transfer area

The mass transfer area is very crucial for the dimensioning of mass transfer unit operations and sometimes differs widely from the geometric surface of the packing [3]. It is not possible to simply measure the mass transfer area inside the absorber during operation. Only the mass transfer inside a column can be measured by making a material balance over the column. The mass transfer flow is dependent on the driving force as well as the mass transfer resistances in the gas and liquid phase according to the the mass transfer flux equation (Eq. (2.23) in chapter 2. In case the mass transfer resistances and driving forces are known and the total mass transfer flow inside the column is measured the effective mass transfer area can be calculated. A standard procedure for mass transfer area determination in absorber columns is the absorption of highly diluted CO_2 ($\approx$1vol% CO_2) into concentrated NaOH ($\approx$1 M NaOH) at high gas velocities [12], [13]. The low CO_2 concentration in the gas phase and the high concentration of NaOH in the liquid phase ensure that the chemical absorption follows a pseudo-first order behavior. The high gas velocity reduces the influence of gas side mass transfer resistance on the overall mass transfer resistance. The gas side mass transfer resistance be neglected at gas velocities above 0.5 m s^{-1} in experiments for interfacial mass transfer area determination [13]. Thus the liquid side mass transfer coefficient is equal to the overall mass transfer coefficient. The following correlation is reported for calculating the volumetric overall mass transfer coefficient $\left(K_{OG} \cdot a_{eff}\right)_{exp}$ (s^{-1}), which comprises of mass transfer coefficient and mass transfer area, from the experimental data [12], [13]:

$$\left(K_{OG} \cdot a_{eff}\right)_{exp} = \frac{V_G}{H \cdot a_{CS}} \ln \frac{y_{CO_2}^{in}}{y_{CO_2}^{out}} \tag{8.4}$$

H is the height of the column. This determination method assumes plug flow for the gas phase and no carbon dioxide in the liquid phase. The experimentally determined volumetric mass transfer coefficient must be equal to the calculated volumetric mass transfer coefficient, which can be calculated assuming pseudo first order reaction kinetics as:

$$k_L \cdot E \cdot a_{eff} = \frac{\sqrt{D_{CO_2} \cdot C_{OH^-} \cdot k_{OH^-}}}{m_{CO_2}} a_{eff} \tag{8.5}$$

In order to result in the right units for k_L (m s^{-1}) a dimensionless Henry coefficient m_{CO_2} (-) needs to be used which correlates the gas concentration to the liquid concentration. Special care should be obtained using a dimensionless partition function like the Henry's coefficient, as the value itself does not give any information which ratio is taken, because the reciprocal value is also dimensionless and correlates the same concentrations. The above mentioned correlation in Eq. (6.5) is valid for a dimensionless Henry coefficient defined as:

$$m_{CO_2} = \frac{C^G_{CO_2}}{C^L_{CO_2}} \tag{8.6}$$

Kunze et al. [12] used an expression like this in their description of an standardized procedure for the determination of mass transfer parameter in absorption. The effective area a_{eff} (m^2 m^{-3}) can be calculated as:

$$a_{eff} = \frac{\frac{V_G}{H \cdot a_{CS}} \ln \frac{y^{in}_{CO_2}}{y^{out}_{CO_2}}}{\frac{\sqrt{D_{CO_2} \cdot C_{OH^-} \cdot k_{OH^-}}}{m_{CO_2}}} \tag{8.7}$$

In the work of Rejl et al. [13] who also dealt with the topic of absorption mass transfer characteristics standardization they used a different dimensionless Henry coefficient defined as:

$$m^{-1}_{CO_2} = \frac{C^L_{CO_2}}{C^G_{CO_2}} \tag{8.8}$$

In that case Eq. (6.7) needs to be rewritten as:

$$a_{eff} = \frac{\frac{V_G}{H \cdot a_{CS}} \ln \frac{y^{in}_{CO_2}}{y^{out}_{CO_2}}}{m^{-1}_{CO_2} \sqrt{D_{CO_2} \cdot C_{OH^-} \cdot k_{OH^-}}} \tag{8.9}$$

A Henry's coefficient that correlates the partial pressure in the gas with the equilibrium concentration in the liquid in the units Pa m^3 $mol^{-1}$is often used as partition coefficient. This value can be transformed to the dimensionless partition coefficient m_{CO_2} applying the ideal gas law:

$$m_{CO_2} = \frac{C^G_{CO_2}}{C^L_{CO_2}} = \frac{\frac{n^G_{CO_2}}{V}}{C^L_{CO_2}} = \frac{\frac{P_{CO_2}}{R \cdot T}}{C^L_{CO_2}} = \frac{H_{CO_2}}{R \cdot T} \tag{8.10}$$

Rejl et al. pointed out that if a kinetic constant, e.g. k_{OH^-} (m^3 mol^{-1} s^{-1}), is taken from a literature source its value should be just used together with the solubility and the diffusion coefficient from the same source. The effective area determined with the procedure here is the area that participates in mass transfer. Some authors distinguish between effective mass transfer area and hydraulic area, which is related to the pressure drop [10].

8.3. Experimental setup at DTU

Pilot scale mass transfer experiments in this study were carried out on DTU's pilot absorber column in the pilot hall tower. The column was built in the time 2008-2009 for research purpose. In the meantime several student projects were conducted on that unit operation. The results from an MEA campaign got published by Sønderby et al. [14]. The column was taken over in the spring of 2014 and modified for pilot campaigns with enzyme-enhanced solvents.

8.3.1. Previous setup

The PI diagram of the setup at the start of this study is shown in Figure 66 at the end of the chapter. The setup can be divided into three different parts that will be discussed separately: the actual column, the liquid system and the gas system. The column consists just of the column body with the packing and the sample points, measurement sensors inside the column as well as the gas and liquid in- and outlets. The liquid system comprises storage tanks, pumping, heating/cooling devices as well as measurements along the liquid flow line. The gas system describes the gas flow outside the column.

The gas was introduced into the column 0.25 m below the packing with an open end pipe. The liquid was distributed into the column with a round spray nozzle with 18 dripping points, which would refer to about 1400 drip points per square meter. The drip points were positioned that they equally distribute the liquid over the cross section. The absorber column itself consisted of 10 glass bodies with an inner diameter of 0.1 m. They were connected with flanges, which incorporate a patented liquid sampling system [15] and were equipped with a temperature sensor. On every second flange was a liquid inlet, every other flange had a liquid re-collector build in, which transferred the liquid from the wall towards the center of the column. The height of each glass body including the flange was approximately 1 m; thus the glass body was about 10 m high. The liquid inlets were in 2, 4, 6, 8 and 10 m height, the liquid re-collectors on 1, 3, 5, 7 and 9 m. Each glass body was equipped with 4 structured packing elements of the type Mellapak 250 Y with a diameter of 0.084 m and a height of 0.205 m each. The total packing height was 8.2 m and the packing volume is 0.0454 m^3. The total column volume, counting the part between the gas and liquid inlets (10.25 m in height) was 0.0805 m^3. The packing material was taking up approximately 56 % of the column volume. The Sulzer Mellapak structured packing has a specific surface area of the packing of 250 m^2 per m^{-3} packing volume, thus DTU's pilot absorber had a specific surface area of packing of 141.12 m^2 m^{-3}, when taking the whole column volume (10.25 height and 0.1 m diameter) as a reference. The differential pressure to outside atmosphere was measured in the

bottom, the middle (5 m) and the column head. At the bottom of the column was no sump, the liquid was pumped directly into a storage tank. The outside of the glass column was not insulated.

The solvent from the liquid could be stored in in two stainless steel tank with each 1 m^3 volume. A system of 2 and 3 way valves made it possible to switch between the tanks and use both of them as supplying and buffer tanks independently. The liquid was pumped by a centrifugal pump from Danfoss and transferred in DN15 pipes. The volume stream was regulated with a globe valve and value was measured visually from a variable area flowmeter. Liquid temperature was measured shortly after the pump.

The gas inside the system was circulated by a gas fan in a closed loop. Pure CO_2 and nitrogen was added from gas bottles to the gas loop right before the gas inlet into the column, although after the measurement point for the gas volume stream. CO_2 concentration was measured before and after the column. The gas volume stream was regulated by the fan speed; the value was recorded by taking the visual reading from a variable area flowmeter. A double pipe heat exchanger with a length of 2 m that worked with cooling water was setup after the fan. The amount of CO_2 added to the system was tracked by measuring the weight of the CO_2 gas bottle over time. Freezing of the gas bottles were prevented during operation, by dripping water around the head of the gas bottles.

8.3.2. Modifications/Current setup

The main intention of the modifications was improvement of accuracy as well as access to online data. The column itself was not modified apart from heat insulation of the glass body with 13 mm Thermaflex.

The gas system was changed that it was possible to run the setup either in a closed loop with the fan or in an open loop using pressurized air as feed gas and venting the gas off. The gas feed point (inlet for CO_2 from the bottles) was moved to the top of the setup right after the fan and before the double pipe heat exchanger. The gas could now be mixed in the 8 m pipe before entering the column, thus ensuring that the gas is very well mixed and saturated at the gas inlet into the column. The variable area flowmeter for gas volume stream measurement was exchanged with a Coriolis flowmeter which now could provide accurate and online mass flow measurement for the gas stream. The CO_2 measurement points were moved closer to column inlet and column outlet. Additional temperature and absolute pressure measurement probes were introduced at the CO_2 measurement points, as the reading of nondispersive infrared probes (NDIR) are influenced by temperature and pressure [16]. An electrical gas heater was used to prevent the gas bottles from freezing. An additional Coriolis flow meter was attached to the CO_2 bottle to monitor the CO_2 flux into the system.

For better liquid handling two stationary 300 l plastic tanks and one mobile 400 l stainless steel tank equipped with a heating jacket were added to the setup. Two laser distance sensor were added to the 1 m^3 tanks to estimate the liquid level inside the tanks. The setup was modified, that a mobile heating

unit, consisting of a pump which recirculated hot water between a house hold water boiler and a countercurrent plate heat exchanger for the solvent, could be used. The hot water circuit was also connected to the heating jacket of the mobile tank during operation. The variable area flowmeter for measuring the liquid flowrate into the column was exchanged with Coriolis flowmeter and a temperature sensor was implemented at the flow measurement point. The PI diagram of the upgraded setup is shown in Figure 67 at the end of the chapter.

8.4. Experimental procedure and methods

The solvent was mixed in one of the storage tanks to the desired concentration and then pumped around bypassing the column for a proper mixing and heated when required; the solvent concentration was tested in the lab with an acid titration with 0.5 M HCl.

The column was flushed with pure N_2 for half an hour in an open loop before the experiments were started. The loop was then closed and pure nitrogen was circulated and CO_2 introduced to reach a mole fraction of 0.12. When the solvent was introduced into the column, CO_2 was added to reach a steady inlet mole fraction of around 0.12. After having 10 min of constant CO_2 outlet mole fraction, liquid samples were drawn from a sample valve at each meter of the column starting from the bottom to the top to not disturb the liquid flow inside the column and influence the absorption. The liquid sampling procedure was performed fast, never exceeding 5 minutes. Afterwards one process condition was changed, either column height or liquid flowrate until a new steady state was achieved. The liquid samples were analyzed afterwards in the lab.

8.4.1. Material balance

The amount of CO_2 transfer was calculated from the reading and measurements on the column. The material balance was done for the gas phase and for the liquid phase. For the gas phase the following formula was applied:

$$\Delta N_{CO_2}^{G} = y_{CO_2}^{in} N_{Gas}^{in} - y_{CO_2}^{out} N_{Gas}^{out} \tag{8.11}$$

The mole fractions of CO_2 were measured with the NDIR probes and corrected for pressure and temperature. The molar flux of CO_2 going into the column was calculated from the mass flow of the Coriolis flowmeter knowing the composition comprising water vapor, carbon dioxide and nitrogen. The molar fraction of water was calculated from the water vapor pressure with an Antoine equation and the total pressure. It was assumed that the gas stream was saturated with water vapor as the gas was recycled in a closed loop. Only the molar flow of nitrogen was assumed to be constant inside the column, as CO_2 was absorbed and water was evaporated inside the column. The total molar gas flow was calculated from the material balance of nitrogen over the column:

$$\Delta N_{N_2}^{G} = 0 = y_{N_2}^{in} N_{Gas}^{in} - y_{N_2}^{out} N_{Gas}^{out} \tag{8.12}$$

This leads to the following expression for total gas flow exiting the column:

$$N_{Gas}^{out} = \frac{y_{N_2}^{in} N_{Gas}^{in}}{y_{N_2}^{out}} \tag{8.13}$$

The mole fraction of nitrogen was calculated from the mole-fractions of the other two compounds, as they add up to 1.

The material balance over the liquid phase was calculated from the molar flow of solvent and the solvent loading:

$$\Delta N_{CO_2}^{L} = \alpha_{CO_2}^{in} N_{sol}^{in} - \alpha_{CO_2}^{out} N_{sol}^{out} \tag{8.14}$$

It was assumed that the amount of solvent evaporating inside the column was negligible, thus the incoming and outgoing molar flow of solvent is the same and can be calculated from the mass fraction of solvent, the molecular weight and the mass flow reading from the Coriolis flow meter.

Setting up the material balance like that was based on some assumptions:

- the gas stream was saturated with water at the inlet and outlet
- the vapor phase consisted just of water, CO_2 and N_2, no solvent was evaporated
- the molar flow of solvent in the liquid phase did not change throughout the column.

8.4.2. Liquid phase analysis

The amount of liquid samples derived from pilot plant experiments was so high that the solvent loading determination with a titration method such as the BaCl method by Sønderby et al. [14] would require too much time. The solvent loading in the column profiles was therefore correlated by the solution's density. This method had worked great for MEA solutions on this pilot plant [17] using the density model from Weiland et al. [18].

The Weiland model correlated the density as ratio of average molecular weight and total volume. In order to work for enzyme containing solutions, their expression was extended by a CA term for the molecular weight and the volume, leading to the following form:

$$\rho = \frac{x_{Am} \cdot M_{Am} + x_{H_2O} \cdot M_{H_2O} + x_{CO_2} \cdot M_{CO_2} + x_{CA} \cdot Mw_{CA}}{x_{Am} \cdot V_{Am} + x_{H_2O} \cdot V_{H_2O} + x_{CO_2} \cdot V_{CO_2} + x_{CA} \cdot V_{CA} + x_{Am} \cdot x_{H_2O} \cdot V^{*} + x_{Am} \cdot x_{CO_2} \cdot V^{**}} \tag{8.15}$$

With x_i being the molefraction, and V_i the molar volume of the different solvent compounds. The non-ideality of the density is accounted for with an interaction parameter for water amine interaction V^* and for CO_2 amine interaction V^{**}. The molar volume and amine-CO_2 interaction parameter can be calculated from constants given in their paper. It was assumed that CA interaction did not create

another excess molar volume. The molecular volume for CA was calculated from the results of a X-ray diffraction data for hCA-II [19]:

$$V_{CA} = \frac{A \cdot a \cdot b \cdot c \cdot \sin\beta}{z} = 0,0722 \frac{m^3}{mole} \tag{8.16}$$

Where A, is the Avogadro's constant, a,b and c are the cell axis dimensions of a unit cell, β is the inclination of the a-axes in the unit cell and z is the number of molecules in a unit cell all values are listed in the work of Robbins et al. [19]. It was assumed that the molar volume of CA did not change with temperature; an average molecular weight of 30 000 g mol^{-1} was assumed for CA.

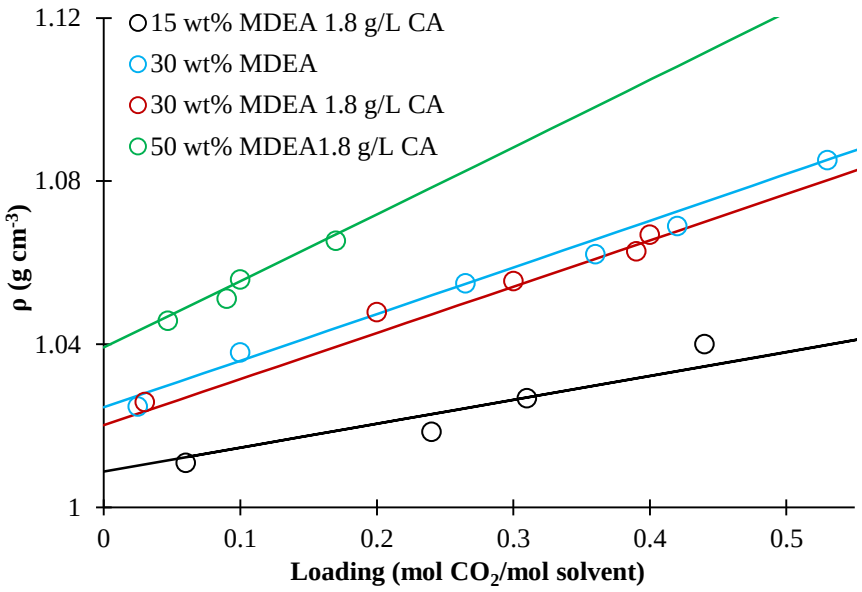

Figure 55: Density of solution as a function of solvent loading, for 15, 30 and 50 wt% MDEA with 1.8 g/L CA at 298 K. Comparison between experimental results and extended Weiland et al. model [18]

The results of the extended Weiland model in comparison to experimental data at 298 K are shown in Figure 55. A clear increase in solvent density could be observed with higher solvent loading. The density of the blue circles indicating 30 wt% MDEA without enzyme could be predicted very accurately with the Weiland model (blue line). The density of the solution slightly decreased when 1.8 g/L CA were added (red circles); this effect could be captured by the extension of the Weiland model (red line). This extended model was also capable to describe the density of a 15 wt% and 50 wt% MDEA solution as function of solvent loading with 1.8 g/L CA added.

The extended Weiland model was validated against density data from 15, 30 and 50 wt% MDEA at 298, 313 and 328 K with 0.9 and 1.8 g/L CA concentration at different solvent loadings. The results are shown in Figure 56. The extended model was capable to describe the solutions density very accurately

for process temperatures between 298-328 K and 15-50 wt% MDEA with up to 1.8 g/L CA concentration.

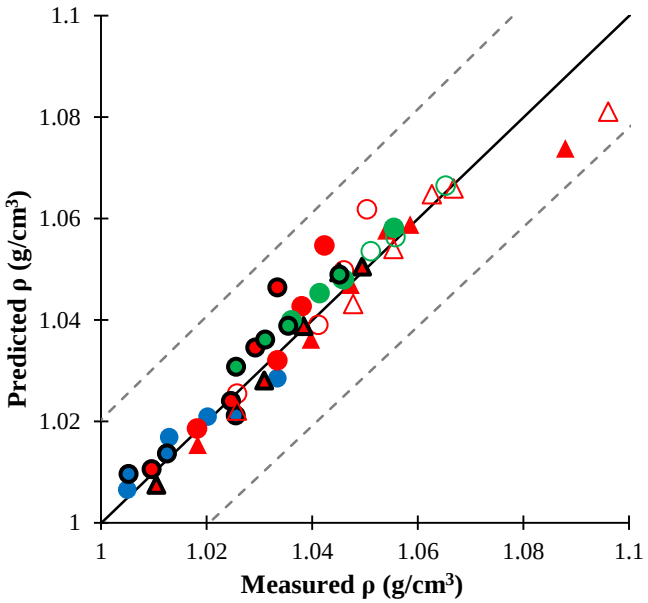

Figure 56: Parity plot of the extended Weiland model at 298 to 328 K and 0.9 and 1.8 g/L CA; blue symbols correspond to 15 wt% MDEA, red symbols to 30 wt% MDEA and green symbols 50 wt% MDEA, dashed lines indicated ±2 % deviation.

8.5. Column characterization

Several experiments were carried out to characterize this specific column. The points of interest were liquid hold up, effective mass transfer area and dry/irrigated pressure drop of the column.

8.5.1. Hold up

Liquid hold up describes the amount of liquid inside the absorber. This value is dependent on the liquid flow and column packing. Aim was to determine the hold up in the column below the loading point and find the process region where the column is loading. The experiments were carried out with air and water. A certain liquid and gas flow was set to the column. At the exact same time the liquid and gas inlets were closed and the liquid exiting the column was collected for 5 minutes after the turn down. In order to eliminate end effects at the liquid outlet two runs were performed at the same gas and liquid setpoints, one with 10 m column and one with 2 m column height. The amount of water collected at 2 m column height was subtracted from the amount of water collected at 10 m column under the same conditions. The holdup (difference) was then correlated to the 8 m packing between the two measurement points. All experiments were carried out in triplicates. The holdup measured in these

experiments was the dynamic holdup. There was no intention in measuring the static holdup for this column. There are different ways to calculate the holdup, mainly due to the definition of the reference volume. The whole empty column can be considered the reference volume or just the volume of packing material. In a test setup these volumes might be very close to each other, but depending on all auxiliary items and measurement equipment these volumes might differ quite a bit in bigger columns.

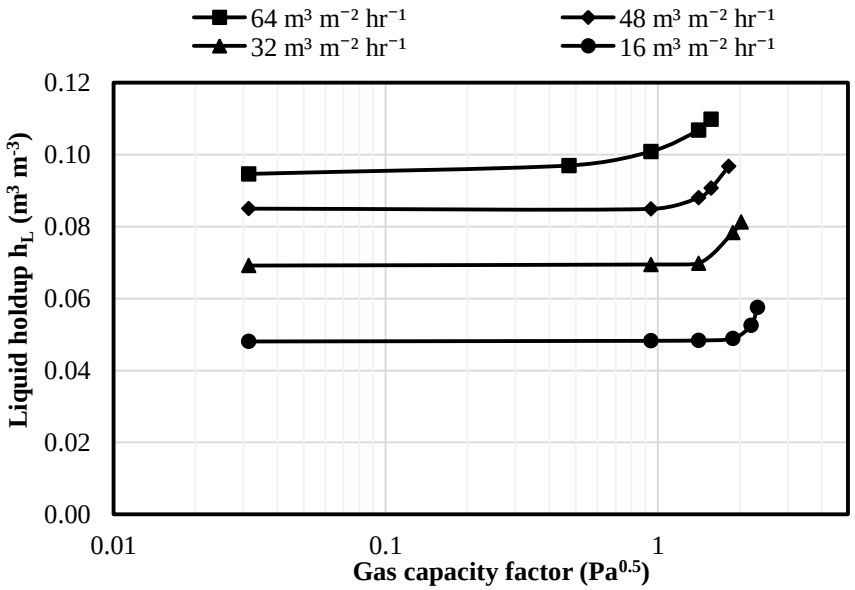

Figure 57: Liquid hold up as a function of gas capacity factor for different liquid loads. Packing volume taken as a reference value for holdup

The column holdup as a function of the gas capacity factor for different liquid loads is shown in Figure 57. The liquid holdup was increasing with liquid load. The superficial gas velocity was not influencing the hold up for low gas capacity factors. At a certain gas capacity the holdup increased and the column starts loading. This loading regime occurred at lower gas capacities when the liquid load was increased, as the experiments with 64 m^3 m^{-2} hr^{-1} was already in the loading regime at a gas capacities of around 1 $Pa^{0.5}$, whereas all other experiments were still outside the loading regime. The lowest liquid load entered the loading regime when the gas capacity was increased to over 2 $Pa^{0.5}$. The holdup of the column as function of the hydrodynamics (liquid load, gas capacity) followed the same trend as the trend the example picture from literature in Figure 54.

Suess and Spiegel determined experimentally the holdup for different Mellapak structured packing [20]. They could derive an empirical correlation for the holdup below the loading point. The comparison of their literature correlation with our experiments is shown in Figure 54. There is a clear deviation for the liquid holdup when the holdup was calculated with reference to the total column volume, as the literature correlation was over predicting the holdup by up to 40 %. If the Volume of the packing material was chosen as a reference to calculate the holdup a much better fit could be achieved.

Here the literature correlation was about 10 % lower than the experiments. In this case it seems more suitable to compare the experimental holdup per packing volume with literature correlations. The slight bend in the literature correlation can be explained, as the factors and exponents are changing in the correlation of Suess and Spiegel at a liquid load of 40 m^3 m^{-2} hr^{-1}.

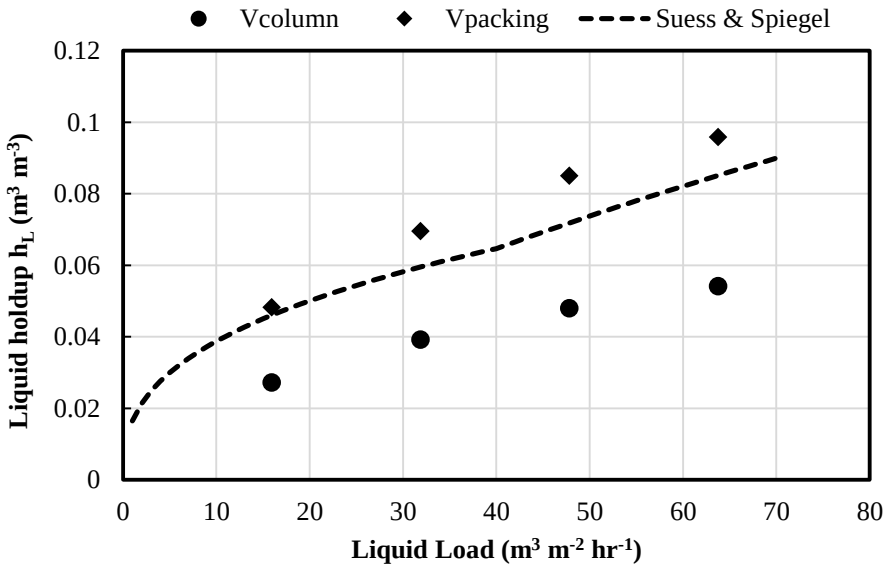

Figure 58: Liquid holdup in the column below the loading regime; holdup either calculated with reference to the column volume or the packing volume.

8.5.2. Pressure drop

The pressure drop of the column was measured for different gas capacity factors in dry state and with a liquid flowing counter-currently. Three differential pressure probes, situated in the bottom, middle and top of the column measured the pressure drop over the column. The pressure drops as a function of gas capacity factor for the dry column, a high and a low liquid load are shown in Figure 59. An increase in liquid load resulted in a higher specific pressure drop. Differences between pressure drops in the lower part of the column and upper part of the column for high gas capacity factors were observed in the experiments. The pressure drop in the bottom part was always higher and in some cases partial flooding in bottom could already be observed whereas the top part remained unchanged.

The flooding started in the connection between two column sections, where the cross section was slightly smaller and grew steadily from there. Full flooding of the column could not be achieved, because the water lock blew out the gas once the total pressure drop over the column was higher than 100 mbar. A correlation for dry pressure drop proposed by Stichlmair et al. [21] for Mellapak 250 Y resulted in very good agreement with the experimental dry pressure drop as shown in Figure 60. The slightly higher experimental values could be caused by the changes in cross sectional area between the column sections. It looked like there was a constant offset which could be caused by an additional

friction. The irrigated pressure drop was not correlated as the literature correlations that could be applied assume a homogeneous process regime, so either loading or non-loading conditions over the column which is in contrast with our observation where just the bottom part of the column started to flood whereas the other part remained unaffected. A proper modeling approach would require discretization of the column into different parts and treating them separately.

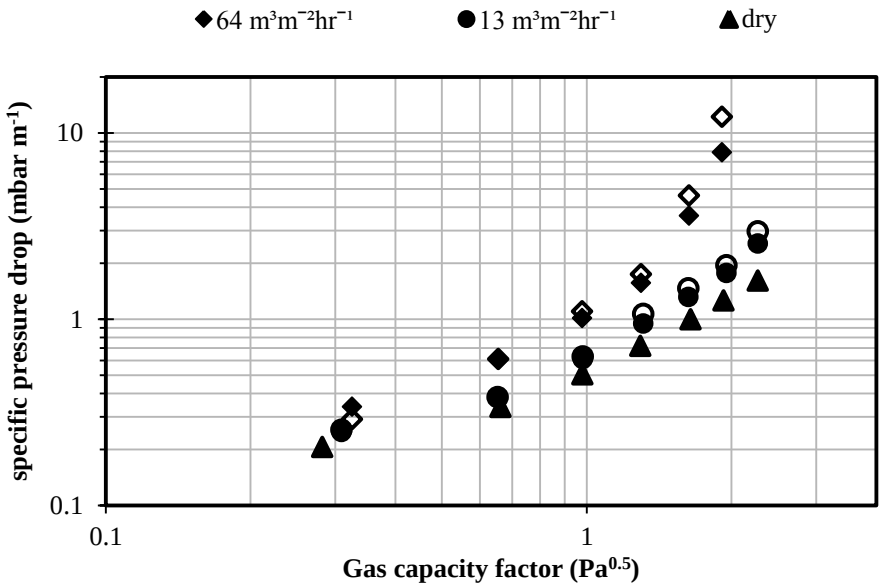

Figure 59: Pressure drop at different gas capacity factors; filled symbols describe pressure drop over the whole column, empty symbols describe pressure drop over the bottom part of the column

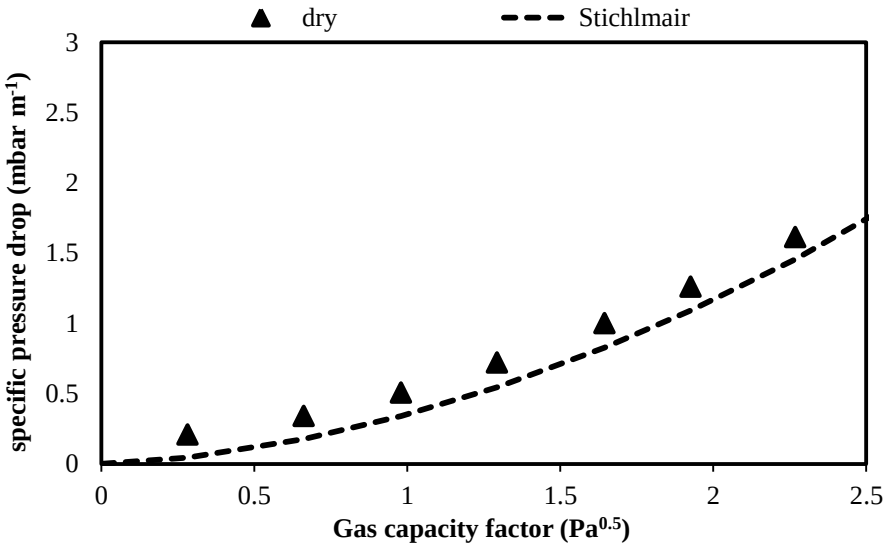

Figure 60: Dry pressure drop, comparison of experimental results with literature correlation proposed by Stichlmair et al. [21]

8.5.3. Effective area

Characterization experiments were carried out with 1 M NaOH and column heights of 2, 4 and 6 m. The column was fully wetted by introducing a very high liquid volume stream into the column before the experiments. The volume stream was then reduced to the desired lowest setpoint and gas stream with different superficial velocities with about 1 vol% CO_2 was started. The liquid flow was increased once, 10 minutes steady state was achieved. The results from the mass transfer experiments with 1 M NaOH and a column height of 2 m at 0.5, 0.7 and 0.9 m s^{-1} superficial gas velocity are shown in Figure 61. The properties of the solvent needed to calculated the interfacial mass transfer area were all taken from Pohorecki and Moniuk [22].

The interfacial area was slightly increasing with the liquid load. There seemed to be almost no effect of the gas velocity on the mass transfer area. All experiments were performed in a process region where no column loading was expected which might alter the interfacial area, because the holdup was constant under these set points (compared with Figure 57). This was in agreement with the findings of Rejl et al. [13] who claimed, that the effect of gas side mass transfer resistance which might influence the mass transfer and thus change the measured mass transfer area can be neglected at velocities above 0.5 m s^{-1}.

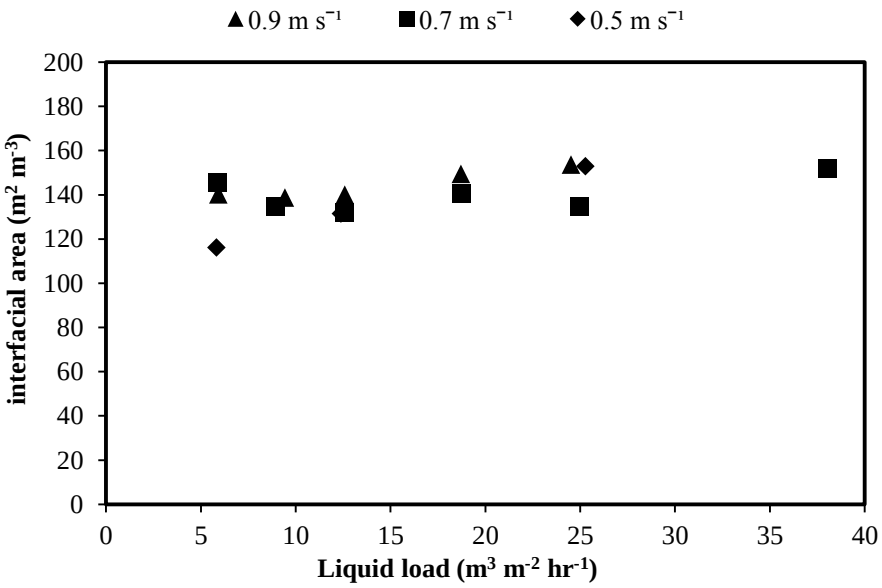

Figure 61: Mass transfer area in the absorber column at 2 m height as function of liquid load determined with 1 M NaOH: comparing the effect of gas velocities.

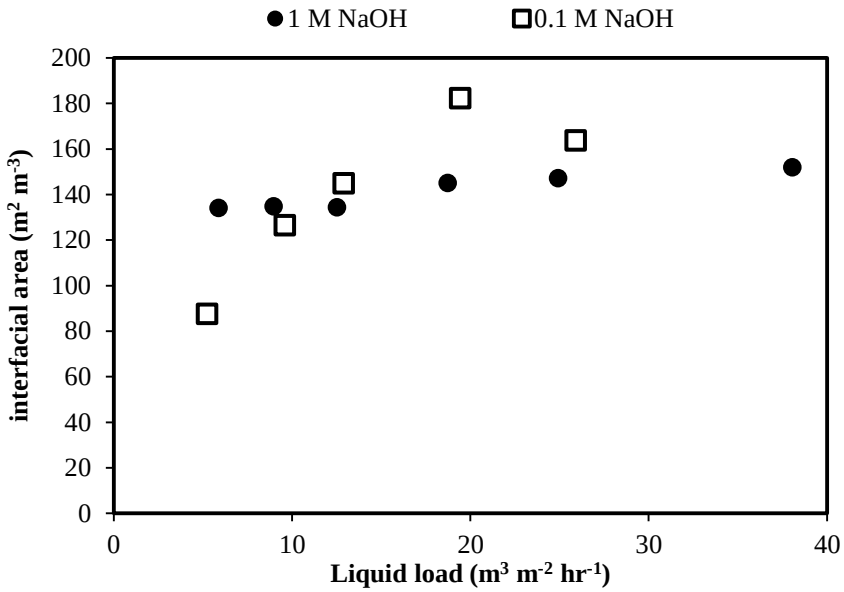

Figure 62: Mass transfer area in the absorber column with 2 m column height as function of liquid load: comparing experimental results with 0.1 M and 1 M NaOH

Mass transfer experiments were also conducted with lower concentrated NaOH solution (0.1 M) with a gas velocity of 0.7 m s^{-1} the results are shown in Figure 62. For the run with 1 M NaOH in that graph the average mass transfer area from the experiments at 0.5, 0.7 and 0.9 m s^{-1} was taken. It can be seen that the results differed especially at low liquid loads. A possible explanation might be a depletion of OH^- ions in the liquid phase; this effect is more distinct at lower liquid load as the liquid hold up is lower and the same absorption will results in higher concentration changes in the liquid phase. The experimental results at 13 and 25 m^3 m^{-2} hr^{-1} were in agreement between 0.1 and 1 M NaOH, the reason for the high interfacial area at 19 m^3 m^{-2} hr^{-1} for 0.1 M NaOH is unknown; though it is thought to be a measurement error and not a column effect. The results suggest that the interfacial area can be determined with 0.1 M NaOH, but just for higher liquid loads. The depletion of OH^-ions for 0.1 M NaOH might be counteracted, by either reducing the inlet CO_2 concentration or the column height.

When the column height was increased in the experiments the measured mass transfer area decreased as shown in Figure 63. Reasons for that behavior can be two-fold; maldistribution of the liquid inside the column can lead to a change in interfacial area, as some areas of the column remained un-wetted whereas more liquid is flowing on other parts. Otherwise the assumptions for the determination method, like pseudo-first order reaction might not hold anymore for higher columns. A clear distinction on how much each of the reasons effects the mass transfer is not possible on basis of these experiments, further experiments are needed. According to Hoek et al. [23] liquid tends to partially accumulate at the wall of the column. As a general trend the effect of maldistribution becomes larger for a higher number of transfer units.

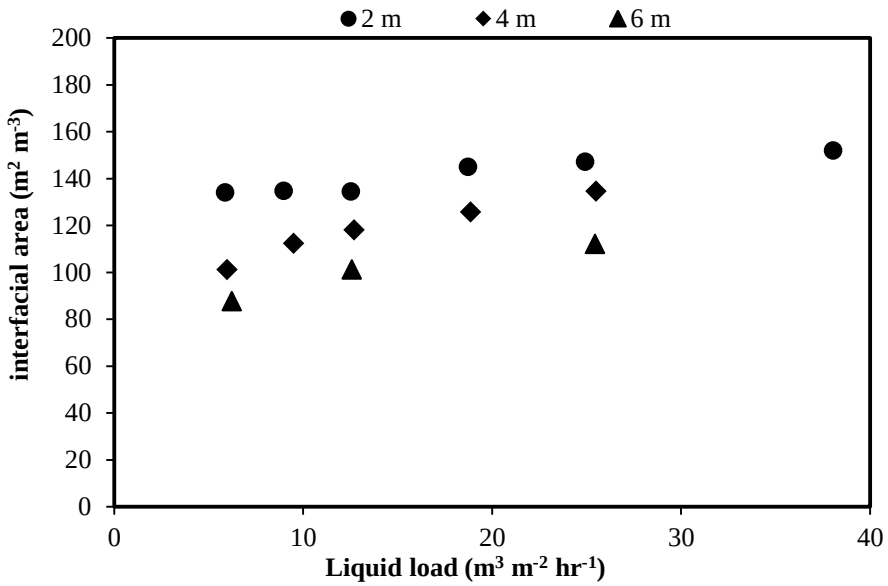

Figure 63: Mass transfer area in absorber column as function of liquid load determined with 1 M NaOH comparing results from different column heights

8.6.Troubleshooting in pilot scale experiments

Even with the best preparation experiments in pilot scale will seldom give the expected results. Pilot scale operation is a continuous learning process. The following problems encountered during the execution of the experiments

8.6.1. Finding the right experimental conditions

In the first 30 wt% MEA campaign experiments in full column height were conducted and gas and liquid loads just were varied. A lower range of liquid loads, between 6 and 38 m^3 m^{-2} hr^{-1} were chosen compared to Sønderby et al., who conducted experiments at liquid loads ranging from 16 to 83 m^3 m^{-2} hr^{-1}, this range was closer to operating conditions of an industrial absorber, the same CO_2 gas concentration of 10 vol% was chosen. Full absorption of CO_2 was observed in all the experiments except the experiment at the lowest liquid load tested. It was difficult to compare the mass transfer rates of this campaign with other experiments, as the absorbed CO_2 flux was just dependent on the total gas flow and the CO_2 concentration at the gas inlet. It could not be concluded by how much the mass transfer could potentially be increased or if the absorption performance of the solvent was at the limit. A higher CO_2 inlet concentration of 12 vol % was chosen and experiments at liquid loads higher than 26 m^3 m^{-2} hr^{-1} excluded for future experiments. The aim for the next experiments was to always have a detectable outlet CO_2 concentration, which was particularly important for process model validation. A high gas velocity was therefore also chosen together with the higher CO_2 concentration, the focus was changing the L/G ratio by varying the liquid load rather than the gas load.

A very high temperature increase inside the column could be observed at low L/G ratios with a maximum temperature of 66 °C measured inside the column. The outside of the glass body became very warm and heat loss occurred due to free convection of the surrounding air which influenced the temperature inside the column and therefore also the mass transfer of the solvent. The column glass body was therefore insulated in the next campaigns.

8.6.2. Fixing errors with liquid outlet loading

In the next two campaigns one with plain 30 wt% MDEA and one with enzyme enhanced 30 wt% MDEA with 0.85 g/L CA more experiments were carried out at different liquid loads and column heights. Full column profiles were not taken for every run, thus only measuring inlet and outlet loading in some experiments. When closing the mass balance at first errors up to more than 100 % occurred between absorbed CO_2 transfer measured in the gas phase and in the liquid phase. One potential reason was identified very soon: the liquid outlet sample valve was situated at a water lock, where the solution collected in a pipe in pipe prevented the gas from running out of the bottom in the absorber. The dead volume of liquid volume inside that water lock was about 5 liter; it needed some time until the liquid phase inside replenished. A back mixture of the solution had influenced the outlet loading of the sample and thus disturbed that mass balance. This effect came up mainly at very low liquid loads, and high changes in process conditions which altered the outlet loading between two setpoints a lot. This effect did seldom occur when full column profiles were taken, as by the end enough time went by that the liquid at the sample valve was renewed. At a liquid load of 10 $m^3\ m^{-2}\ hr^{-1}$ at least 20 min had to pass in order to replenish the liquid 5 times at the sample valve. In experiments taking just inlet and outlet loadings, the setpoints was changed once 10 min steady CO_2 gas inlet and gas outlet concentrations were measured and no drift in temperature, or gas/ liquid volume stream was observed. The liquid outlet sampling point was moved away from the water look and closer to the column outlet for the next campaigns.

8.6.3. Closing the mass balance

The new sampling point gave better consistency between liquid outlet loading and bottom of the column loading. The mass balance could then be closed within +/- 25 % deviation. A consistently higher mass transfer was observed in the gas phase than in the liquid phase, calculated with a material balance over the gas and liquid phase. The constant difference led to the conclusion that either the liquid mass flow controller or the gas mass flow controller gave incorrect readings.

Both Coriolis flowmeter were calibrated with water and gave close to perfect results. A test with a gas bottle on a scale revealed, that the reading of the gas Coriolis flow meter was incorrect for the gas reading. The Coriolis flowmeter for this measurement point was over-specified for that measurement range. It was chosen to be oversized in the start to not produce a too high pressure drop on the gas system and thus limiting the fan. An additional Coriolis flowmeter at the CO_2 gas bottle was measuring the CO_2 injected into the closed gas loop during experiments.

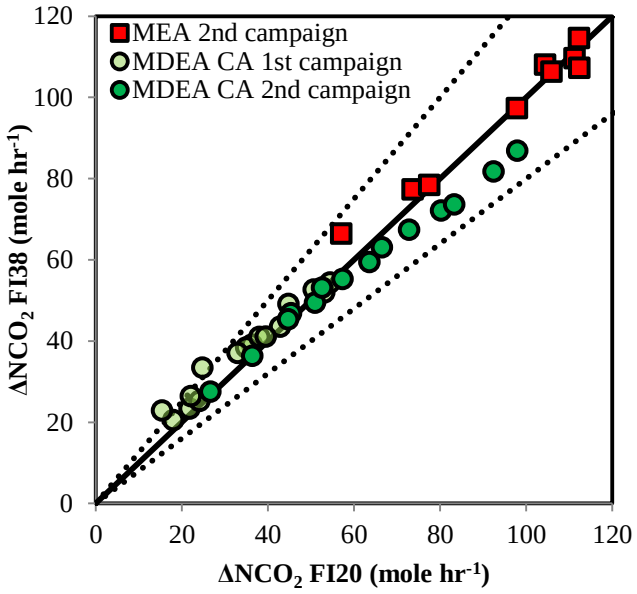

Figure 64: Parity plot between flow of CO_2 from the gas bottle into the system (FI20) and measured absorbed flow inside the column after correction; dotted lines indicate +/- 20% deviation.

A calibration experiment with a CO_2 bottle on a scale showed, that the Coriolis flowmeter attached to the CO_2 bottle gave correct readings of the gas flow whereas the reading from the total gas flow reading were about 10 % too high. The CO_2 flow from the gas bottles into the gas loop was equal to absorbed flow of CO_2 from the gas phase at steady state conditions. When comparing these values, a correction of the total flow measured by multiplying with a constant (0.9) resulted in a good agreement between CO_2 flow into the system from the bottle and CO_2 flow absorbed from the gas as shown in Figure 64.

The Coriolis flowmeter at the gas bottle (FI20) although could not measure low gas flows, but applying the same correction factor to the reading of FI38, the total gas mass flow going into the column provided very satisfying results for the mass balances of all campaigns as shown in the parity plot of Figure 65. The absolute average relative deviation, calculated as the average of all relative deviations between gas and liquid phase material balance was quite low for these campaigns as listed in Table 6. The higher values for the first CA campaign are likely due to the problem with the liquid outlet sampling valve.

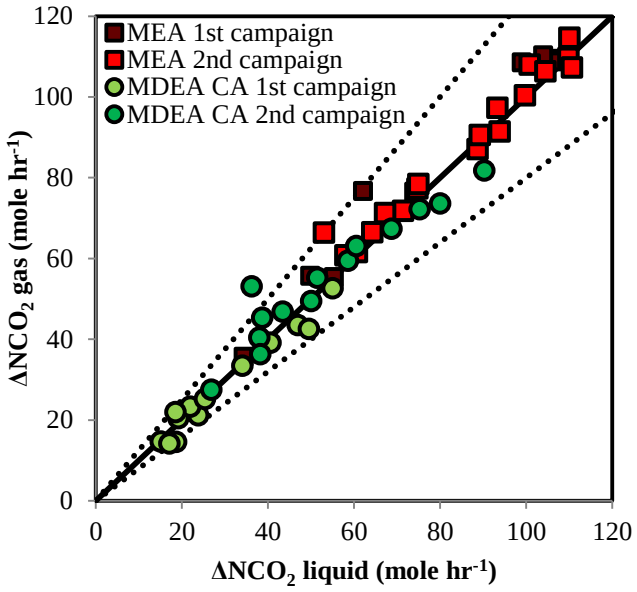

Figure 65: Parity for the material balance measure for the gas and for the liquid phase; dotted lines represent +/- 20 % deviation

Table 6: Average absolute relative deviation (AARD) for the different campaigns

Campaign	AARD
MEA 1st campaign	6,1 %
MEA 2nd campaign	3,9 %
MDEA CA 1st campaign	12,6 %
MDEA CA 2nd campaign	5,6 %

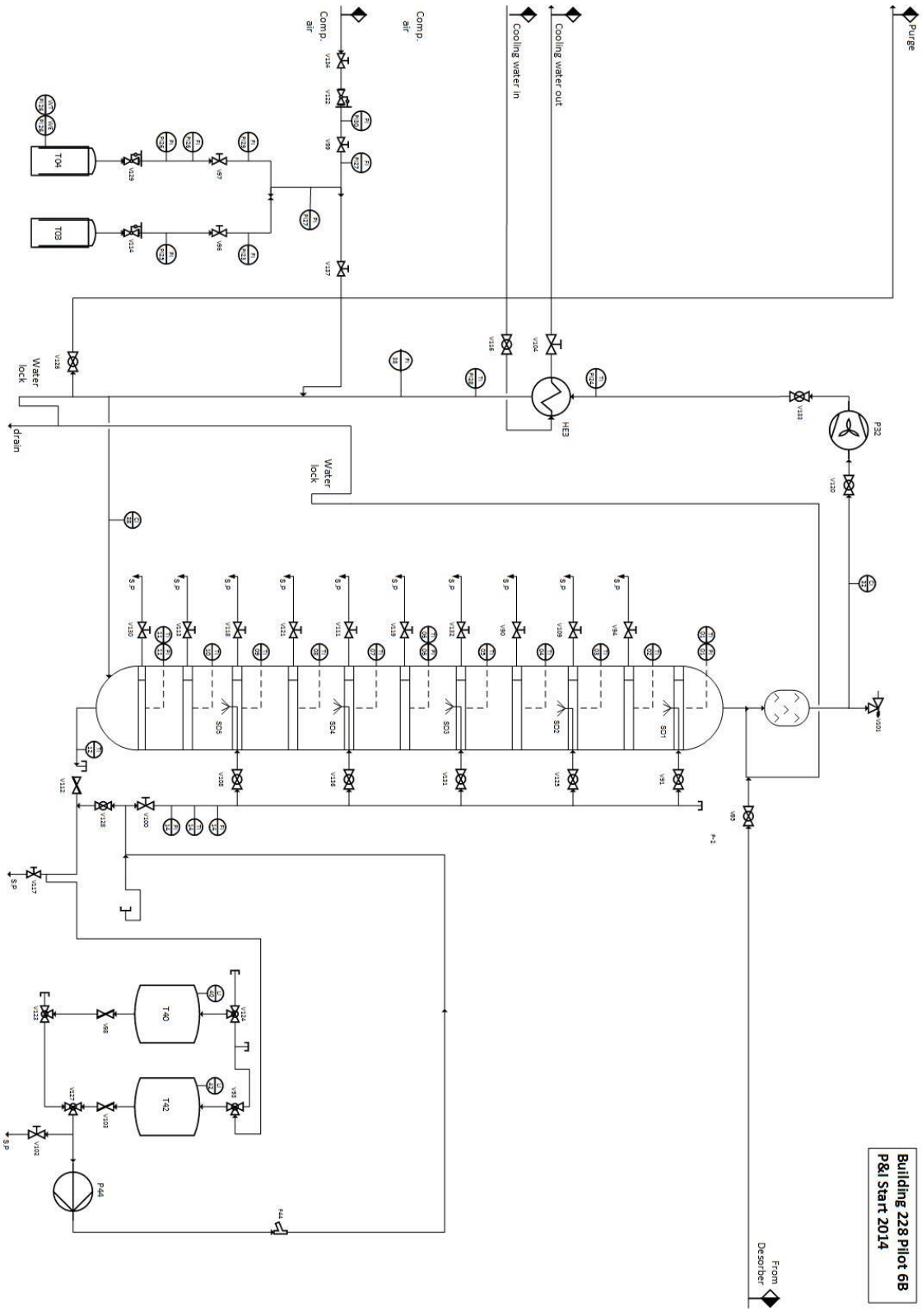

Figure 66: Pilot plant setup February 2014

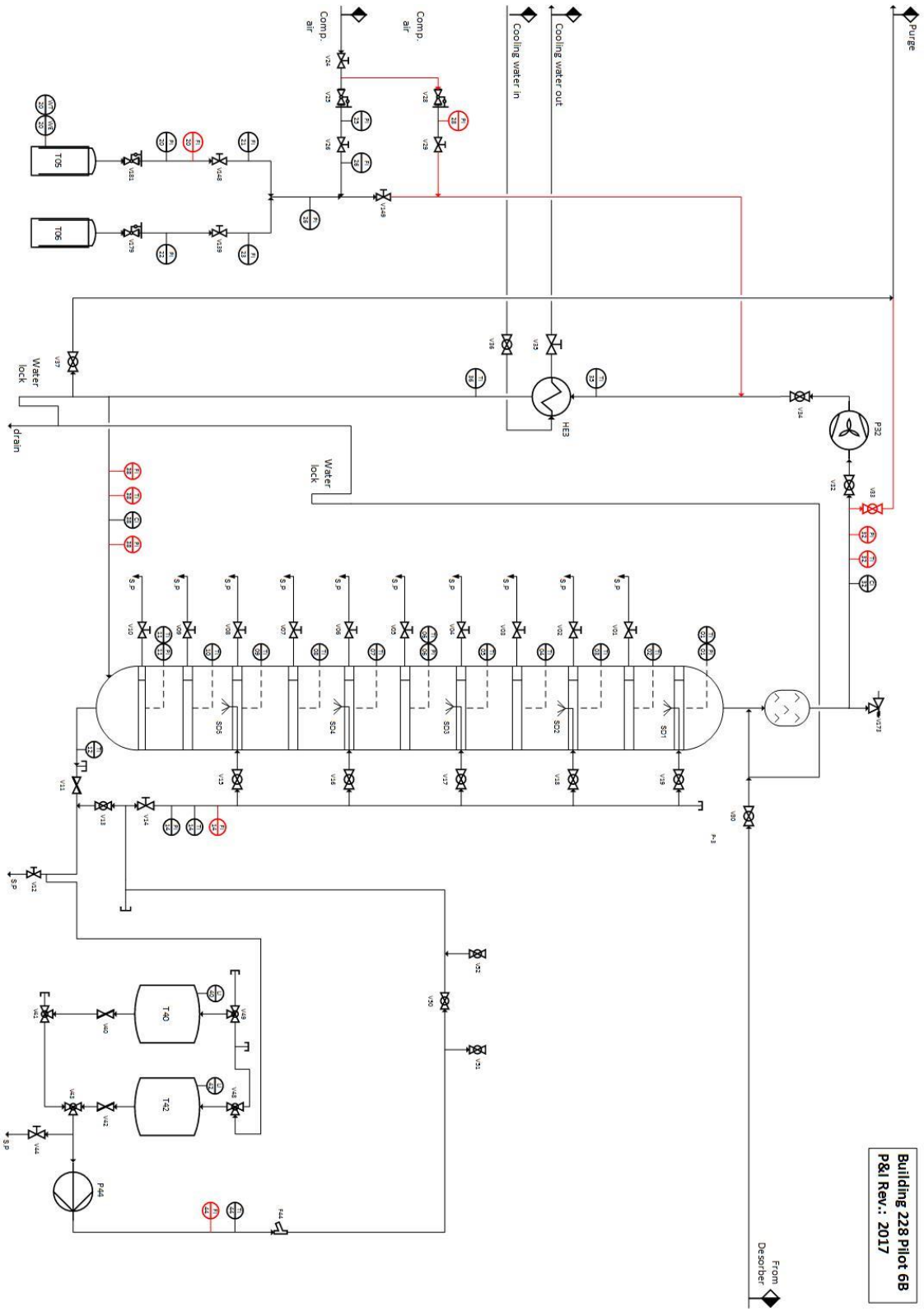

Figure 67: Pilot plant setup in Spring 2017; changes are marked red.

BIBLIOGRAPHY

[1] R. Billet, *Packed Towers*. VCH, 1995.

[2] A. Kohl and R. Nielsen, *Gas Purification*, 5th ed. Gulf Publishing Company, 1997.

[3] A. Mersmann, M. Kind, and J. Stichlmair, *Thermal separation Technology*, 1st ed. Springer_Verlag, 2011.

[4] C. Wang, M. Perry, F. Seibert, and G. Rochelle, "Packing characterization for post combustion CO_2 capture: Mass transfer model development," *Energy Procedia*, vol. 63, pp. 1727–1744, 2014.

[5] C. Wang, D. Song, F. A. Seibert, and G. T. Rochelle, "Dimensionless Models for Predicting the Effective Area, Liquid-Film, and Gas-Film Mass-Transfer Coefficients of Packing," *Ind. Eng. Chem. Res.*, vol. 55, no. 18, pp. 5373–5384, 2016.

[6] A. Zakeri, A. Einbu, and H. F. Svendsen, "Experimental investigation of pressure drop in structured packings," *Chem. Eng. Sci.*, vol. 73, pp. 285–298, 2012.

[7] A. Zakeri, A. Einbu, and H. F. Svendsen, "Experimental investigation of liquid holdup in structured packings," *Chem. Eng. Res. Des.*, vol. 90, no. 5, pp. 585–590, 2012.

[8] A. Zakeri, A. Einbu, P. O. Wiig, L. E. Øi, and H. F. Svendsen, "Experimental investigation of pressure drop, liquid hold-up and mass transfer parameters in a 0.5 m diameter absorber column," *Energy Procedia*, vol. 4, pp. 606–613, 2011.

[9] J. A. Rocha, J. L. Bravo, and J. R. Fair, "Distillation Columns Containing Structured Packings: A Comprehensive Model for Their Performance. 2. Mass-Transfer Model," *Ind. Eng. Chem. Res.*, vol. 35, pp. 1660–1667, 1996.

[10] R. Billet, "of Packed Columns up to the Flood Point," vol. 18, pp. 371–379, 1995.

[11] H. F. Svendsen, E. T. Hessen, and T. Mejdell, "Carbon dioxide capture by absorption, challenges and possibilities," *Chem. Eng. J.*, vol. 171, no. 3, pp. 718–724, 2011.

[12] A.-K. Kunze, P. Lutze, M. Kopatschek, J. F. Maćkowiak, J. Maćkowiak, M. Grünewald, and A. Górak, "Mass transfer measurements in absorption and desorption: Determination of mass transfer parameters," *Chem. Eng. Res. Des.*, vol. 104, no. 0, pp. 440–452, 2015.

[13] J. F. Rejl, V. Linek, T. Moucha, and L. Valenz, "Methods standardization in the measurement of mass-transfer characteristics in packed absorption columns," *Chem. Eng. Res. Des.*, vol. 87, no. 5, pp. 695–704, 2009.

[14] T. L. Sønderby, K. B. Carlsen, P. L. Fosbøl, L. G. Kiørboe, and N. von Solms, "A new pilot absorber for CO_2 capture from flue gases: Measuring and modelling capture with MEA solution," *Int. J. Greenh. Gas Control*, vol. 12, pp. 181–192, 2013.

[15] K. B. Carlsen, T. L. Sønderby, and N. von Solms, "Flange and method for liquid sampling," WO

2012175604 A1, 2013.

[16] Vaisala, “Application note Vaisala: how to measure carbon dioxide.” [Online]. Available: http://img.en25.com/Web/Vaisala/%7B92b53609-48c2-43d8-aecb-0b68b191b748%7D_CEN-TIA-Parameter-How-to-measure-CO2-Application-note-B211228EN-A-LOW-v7.pdf. [Accessed: 07-Dec-2015].

[17] J. Gaspar, A. Gladis, J. B. Jørgensen, K. Thomsen, N. Von Solms, and P. L. Fosbøl, “Dynamic operation and simulation of post-combustion CO_2 capture,” in *Energy Procedia*, 2016, vol. 86.

[18] R. H. Weiland, J. C. Dingman, D. B. Cronin, and G. J. Browning, “Density and viscosity of some partially carbonated aqueous alkanolamine solutions and their blends,” *J. Chem. Eng. Data*, vol. 43, no. 3, pp. 378–382, 1998.

[19] A. H. Robbins, J. F. Domsic, M. Agbandje-Mckenna, and R. McKenna, “Structure of a monoclinic polymorph of human carbonic anhydrase II with a doubled a axis,” *Acta Crystallogr. Sect. D Biol. Crystallogr.*, vol. 66, no. 5, pp. 628–634, 2010.

[20] P. Suess and L. Spiegel, “Holdup of Mellapak structured packings,” *Chem. Eng. Process.*, vol. 31, no. 2, p. 119, 1992.

[21] J. Stichlmair, J. L. Bravo, and J. R. Fair, “General model for prediction of pressure drop anc capacity of countercurrent gas/liquid packed column,” *JGas Sep. Purif.*, vol. 61, no. 12, pp. 19–28, 1989.

[22] R. Pohorecki and W. Moniuk, “Kinetics of reaction between carbon dioxide and hydroxyl ions in aqueous electrolyte solutions,” *Chem. Eng. Sci.*, vol. 43, no. 1959, pp. 1677–1684, 1988.

[23] P. J. Hoek, J. A. Wesselingh, and F. J. Zuiderweg, “Small scale and large scale liquid maldistribution in packed columns,” *Chem. Eng. Res. Des.*, vol. 64, pp. 431–449, 1986.

9. Absorption experiments in pilot scale

This chapter summarizes all absorption experiments in pilot scale with MEA and MDEA solutions at different process conditions carried out on the pilot absorber at DTU. The first part describes the general methodology of the experiments runs; the second part describes the findings of the 5 different campaigns carried out. The campaigns are not listed in chronological order, but sorted by solvent, beginning with campaigns with 30 wt% MEA, followed by a campaign with 30 wt% MDEA without enzyme and 30 wt% MDEA with CA.

9.1. Methodology

In total five different absorption campaigns were carried on pilot scale with almost 100 runs: two campaigns for 30 wt% MEA solutions, one with plain 30 wt% MDEA and two with 30 wt% MDEA enhanced with either 0.85 or 3.5 g/L CA. Before starting with experiments, the setup was analyzed and several changes were conducted as described in the previous chapter. All measuring equipment was calibrated and the hold up and pressure drop was characterized with an air water system. Then the first 30 wt% MEA campaign was conducted during spring/summer 2015 to follow up the experiments by Sønderby et al. [1] and determine the limits of the setup. An absorption campaign with 30 wt% MDEA followed in winter 2015/2016, and in spring 2016 the first campaign with enzyme enhanced 30 wt% MDEA was conducted with 0.85 g/L CA concentration. In fall 2016 another 30 wt% MEA campaign was performed to provide more comparable experimental results between enzyme-enhanced 30 wt% MDEA and 30 wt% MEA. A second 30 wt% enzyme-enhanced MDEA campaign with 3.5 g/L CA followed in winter 2016 - spring 2017 for a proper benchmark of the enzyme enhanced solvent technology with the industrial standard 30 wt% MEA.

It was difficult to perform experiments at the exact same conditions in pilot scale on that setup. Some of the process parameter were linked to each other and influence the column performance. For example a different gas volume stream influenced the CO_2 concentration of the gas phase at the column gas outlet in the top, because of the gas recycle it also affected inlet CO_2 concentration of the gas unless the CO_2 feed was adjusted constantly. In order to normalize the results of the experimental runs, capture efficiency (%), describing the fraction of CO_2 being captured inside the column rather than total mole stream of CO_2 absorbed is reported. Also L/G ratios on mass basis are reported, rather than different gas and liquid loads.

The actual process setpoints, mass transfer rates, column solvent loading and column temperature profiles are listed in Appendix B. All experiments are labeled with an identification number, e.g. R25. All MEA experiments start with R, followed by a number, the MDEA experiments without enzyme and with 0.85 g/L CA start with M and the experiments with 3.5 g/L CA start with C. All results and plots linked to that number are from the same experiment.

9.2. MEA campaigns

The MEA was mixed in a one m^3 tank; the solvent was not heated up before entering the column. It was tried to keep the coloring for each campaign the same, thus a red curve in two different graphs represents the same experiment.

9.2.1. 1st 30 wt% MEA campaign (Spring/Summer 2015)

The first MEA campaign was the first test run for the absorption column. It was used to find out the limits of all the equipment and identify interesting process regions. Full column height was chosen, which represents 10.25 m between gas and liquid inlet and 8.2 m packing. The influence of changing the gas and the liquid load was investigated and it was determined whether experiments at similar liquid to gas ratios (L/G) gave similar results. The solvent in these experiments was 30 wt% MEA with a lean loading of 0.23 mol CO_2 per mol MEA. The inlet temperature of the solvent was around 25 °C. The gas stream was fed into the column water saturated at room temperature with a CO_2 concentration of around 10 vol%.

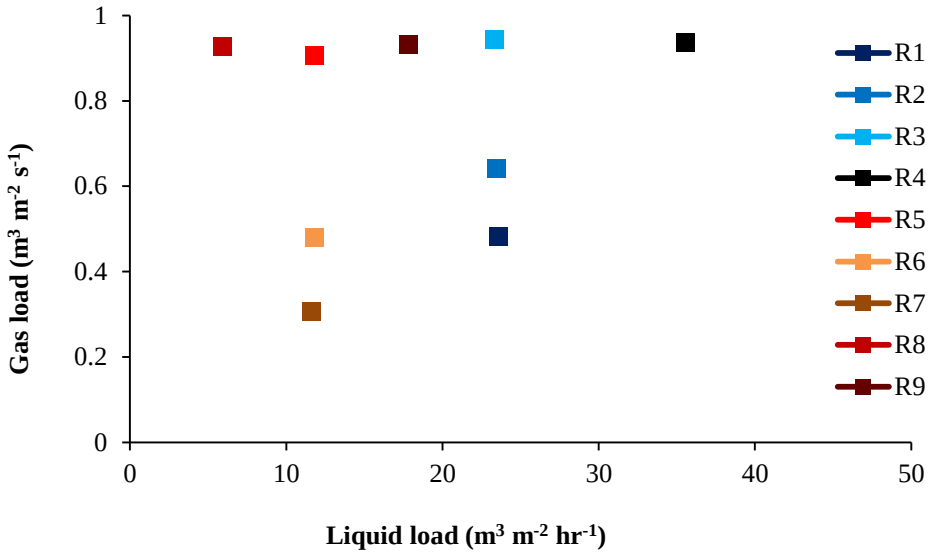

Figure 68: Overview of gas loads and liquid loads in the different experimental runs in the first 30 wt% MEA campaign at 10 m column height and 10 vol% CO_2 gas inlet concentrations.

An overview of all the experiments conducted in the first pilot campaign with 30 wt% MEA solution is given in Figure 68. The values of the different set points for each run are listed in Table 7. In total 9 experiments were carried out in the first campaign with liquid loads ranging from 6 to 36 $m^3\ m^{-2}\ hr^{-1}$ and gas loads ranging from 0.3 to 0.9 $m^3\ m^{-2}\ s^{-1}$. The L/G ratio was in the range of 12.3 and 1.6 on mass/mass basis and 15.1 and 1.9 on mol/mol basis. In all experiments except R8, with the lowest L/G ratio, a capture efficiency of 100 % was achieved.

Table 7: Process parameters for experiments in the first 30 wt% MEA campaign at 10.25 m column height and 10 vol% CO_2 inlet concentration

Parameter	unit	R1	R2	R3	R4	R5	R6	R7	R8	R9
Liquid load	(m^3 m^{-2} hr^{-1})	23.6	23.4	23.3	35.5	11.8	11.8	11.6	5.9	17.8
Gas load	(m^3 m^{-2} s^{-1})	0.48	0.64	0.94	0.94	0.91	0.48	0.31	0.93	0.93
L/G	(kg/kg)	12.3	9.1	6.2	9.5	3.2	6.2	9.5	1.6	4.7
L/G	(mol/mol)	15.1	11.2	7.6	11.7	3.9	7.6	11.7	1.9	5.8
Capture efficiency	(%)	100	100	100	100	100	100	100	65	100

The effect of changing the gas load in the range of 0.48 to 0.94 m^3 m^{-2} s^{-1} while keeping the liquid load constant at around 23.5 m^3 m^{-2} hr^{-1} on the temperature and solvent loading profile inside the column is shown in Figure 69. The L/G ratios in these experiments were between 12.3 and 6.2 on mass basis.

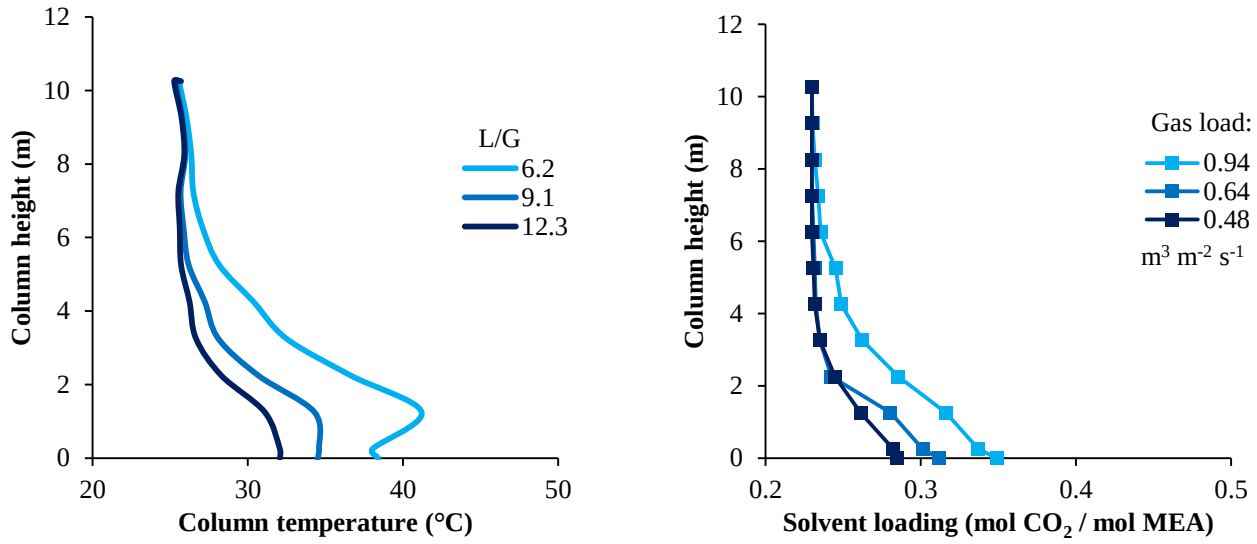

Figure 69: Influence of gas load on temperature and solvent loading profiles for absorption runs at 10 m column height with 30 wt% MEA, 0.23 mole CO_2/mol MEA lean loading, 25 °C inlet temperature and 23.5 m^3 m^{-2} hr^{-1} liquid load at different gas loads

A higher gas load resulted in a higher temperature increase inside the column. The highest temperature measured was at the liquid outlet for the experiments at the highest L/G ratio (12.3); at the medium L/G ratio 9.1 the outlet temperature was equal to the column temperature at 1 m column height. For the lowest L/G ratio, a temperature peak was measured at 1 m column height with a maximum temperature of 41 °C. At a capture efficiency of 100 % a lower L/G ratio will result in higher increase in solvent loading and due to exothermic reaction in a higher temperature increase. A temperature increase in the column indicated that a reaction occurs. The reaction zone inside the column was in the lower part, as changes in solvent loading could be seen just in that region. The reaction zone was until 4 m column height for 9.1 and 12.3 L/G ratio and until 6-8 m for 6.2 L/G ratio. The loading profiles were almost linear between the outlet and the end of the reaction zone for high L/G ratios. At the lowest L/G ratio,

there was also a linear trend in the bottom of the column up to 4 m, above that point the loading just changes slightly. The temperature and solvent loading profile showed the same trend. The temperature profile indicated a reaction up to 6-8 m column height for 6.2 L/G ratio and a reaction zone up to 4-6 m for 12.3 and 9.1 L/G ratio. The decrease in temperature between 1 m column height and liquid outlet for experiments at a gas load of 0.94 m^3 m^{-2} s^{-1} was a gas inlet effect. The saturated gas stream entered the column at room temperature and got in contact with the already heated up liquid phase. The gas phase heated up and water evaporated to maintain saturation; this cooled down the liquid phase. This gas inlet effect is no disadvantage; it actually can enable higher rich loadings and is a natural cooling effect of the liquid.

Another experimental run was carried out at different gas loads varying between 0.31 and 0.91 m^3 m^{-2} s^{-1} at a lower liquid load of around 11.8 m^3 m^{-2} hr^{-1}. The L/G ratio on mass basis was 9.2, 6.2 and 3.2 for 0.31, 0.40 and 0.91 m^3 m^{-2} s^{-1} gas loads respectively. The temperature profile and the solvent loading profile of the column are shown in Figure 70. The capture efficiency was still 100% for these experiments.

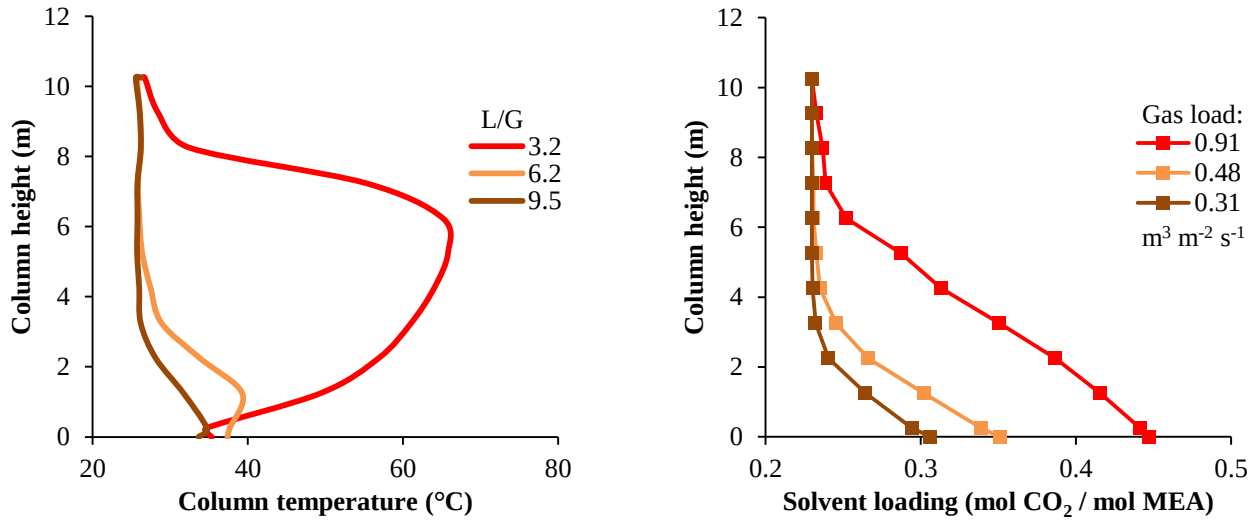

Figure 70: Influence of gas load on temperature and solvent loading profiles for absorption runs at 10 m column height with 30 wt% MEA, 0.23 mole CO_2/mol MEA lean loading, 25 °C inlet temperature and 11.8 m^3 m^{-2} hr^{-1} liquid load at different gas loads

A higher L/G ratio resulted in lower temperature increase inside the column and a lower outlet loading of the solvent. This trend agrees with the findings from the experiments of the previous run. Running experiments at a low L/G ratio of 3.2 resulted in a huge increase in temperature inside the column, where a maximum temperature of 66 °C was measured. The highest temperature was measured in the middle of the column between 5 m and 6 m column height. The linear solvent loading increase for this experiment now reached 6 m height, and the total reaction zone, defined as region where a solvent loading increase could be observed, was up to 9 m, although most of the reaction took place below 6 m.

The column temperature was also the highest in the zone where most of the reactions happened. A higher column temperature increased the solvent reaction kinetics and intensified the mass transfer in that area further.

In the last series of this campaign experiments at the same gas load of around 0.93 m^3 m^{-2} s^{-1} with different liquid loads ranging from 5.9 to 35.5 m^3 m^{-2} hr^{-1} were compared. The temperature and solvent loading profiles are depicted in Figure 71. The L/G ratio in this series ranged from 9.5 at the highest liquid load to 1.6 at the lowest liquid load.

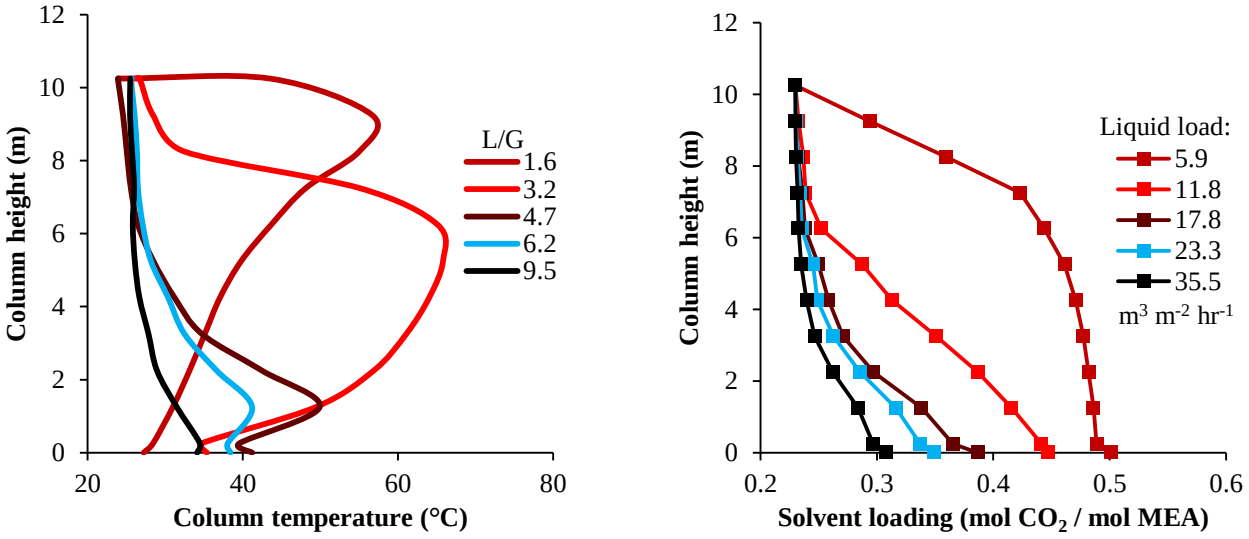

Figure 71: Influence of liquid load on temperature and solvent loading profiles for absorption runs at 10 m column height with 30 wt% MEA, 0.23 mole CO_2/mol MEA lean loading, 25 °C inlet temperature and around 0.93 m^3 m^{-2} s^{-1} gas load

The temperature profile at the highest L/G was showing just a slight increase in the bottom of the column. When the L/G ratio was decreased to 6.2, a small temperature maximum (41 °C) evolved at 1 m column height, which became larger (49 °C) when the L/G was decreased to 4.7. When the L/G was decreased further to 3.2 the temperature maximum migrated inside the column to 5-6 m and the column temperature increased to 66 °C in that area. At even lower L/G ratios of 1.9 a higher positioned temperature peak could be measured at 9 m column height, although the maximum temperature was lower with 57 °C. In these experiments the highest mass transfer occurred in areas with the highest temperature similar to the experiments before.

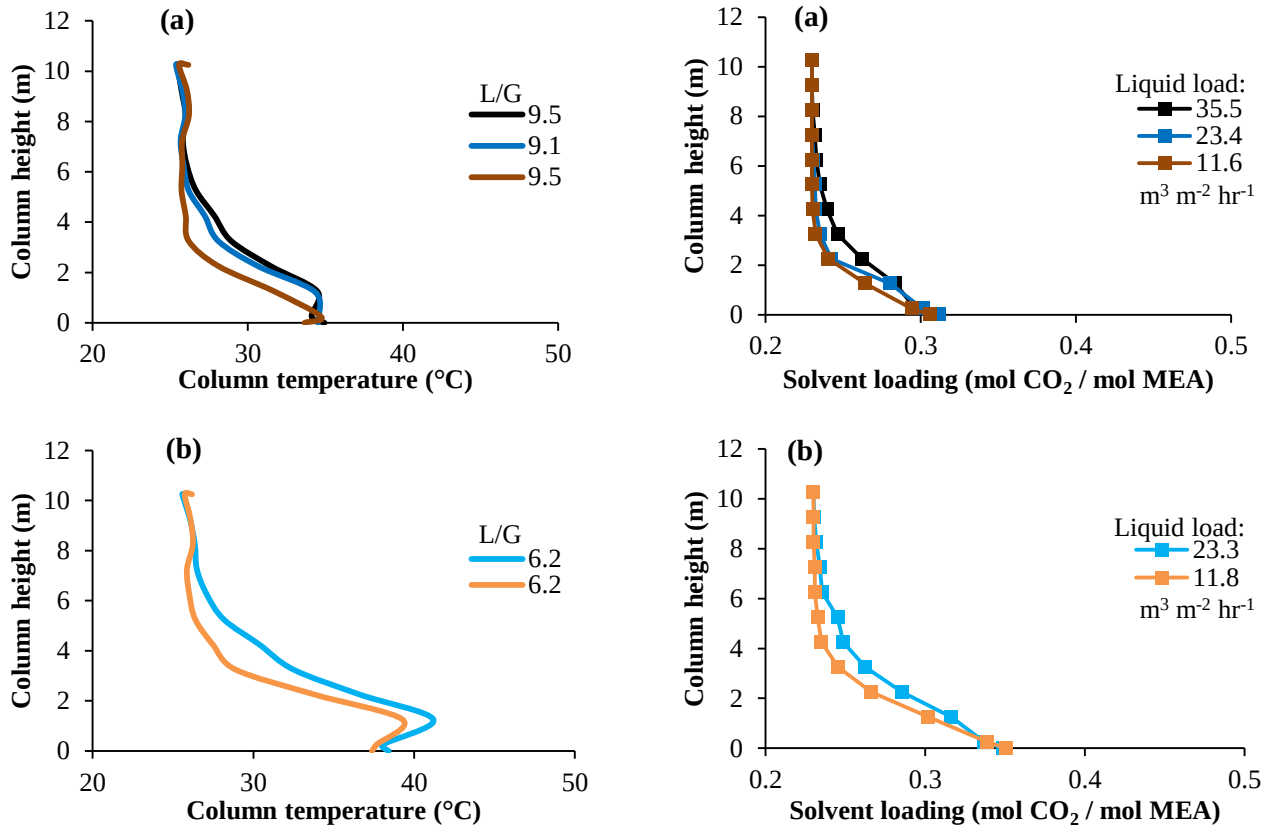

Figure 72: Influence of L/G ratio on temperature and solvent loading profiles inside the column at 10 m column height 0.23 mole CO_2/mol MEA lean loading, 25 °C inlet temperature; pictures (a) are experiments at 9.3 (kg/kg) L/G ratio, pictures (b) were performed at 6.2 (kg/kg) L/G ratio.

Experiments at different liquid loads, but similar L/G ratios resulted in very similar temperature and solvent loading profiles and almost identical rich solvent loadings as shown in Figure 72. The column temperature and solvent loading inside the column was slightly lower for the lowest liquid loads. At lower liquid load, the gas load also had to be lower to result in the same L/G ratio. At low gas loads the gas side mass transfer resistance is higher resulting in lower mass transfer rates, which might explain the trend. Apart from that effect there seemed to be no obvious reason to conduct experiments at similar L/G ratios, if not another process conditions, such as column height, inlet solvent loading, or temperature was changed.

9.2.2. 2nd 30 wt% MEA campaign (Fall 2016)

With the experience gained from the first MEA campaign, a second MEA was planned and performed. In this run the gas load was kept constant at a high value of around 0.8 $m^3\ m^{-2}\ s^{-1}$ and the L/G was changed by altering the liquid load in the range 5.9 to 20.9 $m^3\ m^{-2}\ hr^{-1}$,which resulted in L/G ratios of 1.9 to 7.6 (kg/kg). Three different L/G ratios, of around 2.7, 4.7 and 6.7 were tested at different column heights of 2, 4, 6, 8 and 10 m. The inlet loading in the experiments for 2 and 4 m column height was

0.24 mol CO_2 per mole MEA and 0.29 mol CO_2 per mole MEA at 6, 8 and 10 m. For the experiments in 2 and 4 m, just inlet and outlet samples were taken, whereas for the other experiments full column liquid loading profiles were determined. At 10 m column height additional L/G ratios were tested, so in total 6 solvent loading profiles were taken. The set points for the experimental run R10–R27 are listed in Table 8 and graphically illustrated in Figure 73.

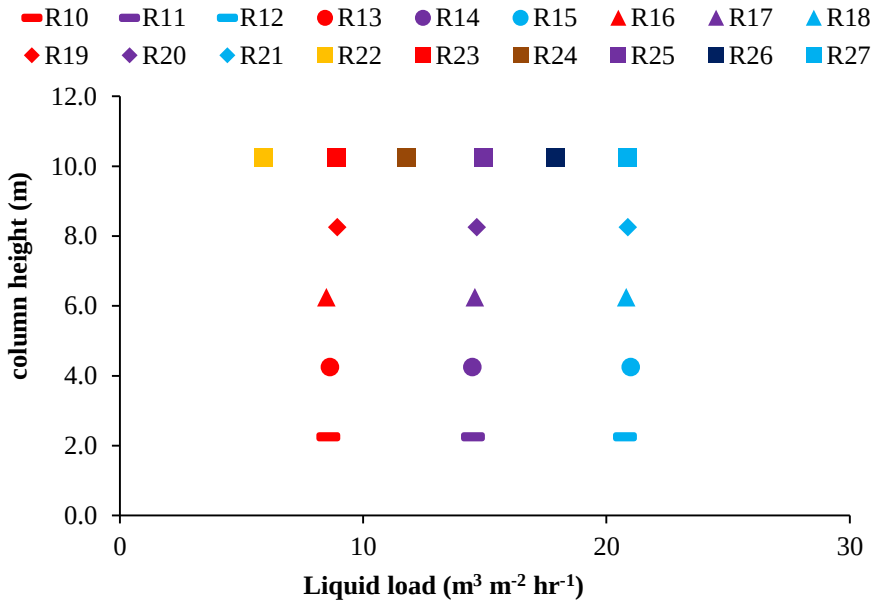

Figure 73: Overview of column height and liquid load in the experimental runs in the second 30 wt% MEA campaign at a constant gas load of about 0.8 m^3 m^{-2} s^{-1} with around 12 vol% CO_2 gas inlet concentration.

Table 8: Overview of the process parameter for the 2nd 30 wt% MEA campaign

Parameter	**unit**	**R10**	**R11**	**R12**	**R13**	**R14**	**R15**	**R16**	**R17**	**R18**
Liquid load	(m^3 m^{-2} hr^{-1})	8.6	14.5	20.8	8.6	14.5	21.0	8.5	14.6	20.8
Gas load	(m^3 m^{-2} s^{-1})	0.75	0.76	0.75	0.75	0.76	0.76	0.83	0.81	0.82
L/G	(kg/kg)	2.7	4.7	6.7	2.8	4.6	6.7	2.4	4.3	6.1
L/G	(mol/mol)	3.4	5.7	8.1	3.4	5.6	8.1	3.0	5.2	7.4
Column height	(m)	2.25	2.25	2.25	4.25	4.25	4.25	6.25	6.25	6.25
Capture efficiency	(%)	45	53	58	60	74	79	52	77	84
Parameter	**unit**	**R19**	**R20**	**R21**	**R22**	**R23**	**R24**	**R25**	**R26**	**R27**
Liquid load	(m^3 m^{-2} hr^{-1})	8.9	14.7	20.9	5.9	8.9	11.8	15.0	17.9	20.9
Gas load	(m^3 m^{-2} s^{-1})	0.78	0.79	0.80	0.78	0.78	0.78	0.79	0.79	0.80
L/G	(kg/kg)	2.7	4.4	6.2	1.8	2.8	3.6	4.5	5.4	6.3
L/G	(mol/mol)	3.3	5.3	7.5	2.1	3.3	4.4	5.5	6.5	7.6
Column height	(m)	8.25	8.25	8.25	10.25	10.25	10.25	10.25	10.25	10.25
Capture efficiency	(%)	65	85	95	46	68	77	89	97	98

All experiments performed in this campaign had capture efficiencies below 100 %. The liquid inlet loading was changed after the experiments at 2 m and 4 m column height by mixing higher loaded MEA solution with the solvent in the tank to ensure that the capture efficiency was below 100 % in all experiments as just these results can be used for proper absorber column model validation.

The temperature profile and the liquid in- and outlet loading of experiments with 2 m and 4 m column height at different L/G ratios are compared in Figure 74. At these column heights experiments with the lowest L/G ratio resulted in the highest temperature increase. For 2.7 and 4.7 L/G ratio (kg/kg) a temperature bulge could be observed inside the column. At 4.7 L/G this temperature bulge was in the lower part of the column, and a total temperature increase of 10 °C and 22 °C was observed at 2 and 4 m height.

For 2.7 L/G ratio the temperature increase was 22 °C at 2 m and 30 °C at 4 m and the temperature bulge was located in the middle of the column. The highest liquid loading increase could be observed for the lowest L/G ratio. Increasing the L/G ratio reduced the liquid loading at the column outlet. The increase over the column, described as the slope of solvent loading increase over the column height, became less when the height was increased from 2 to 4 m.

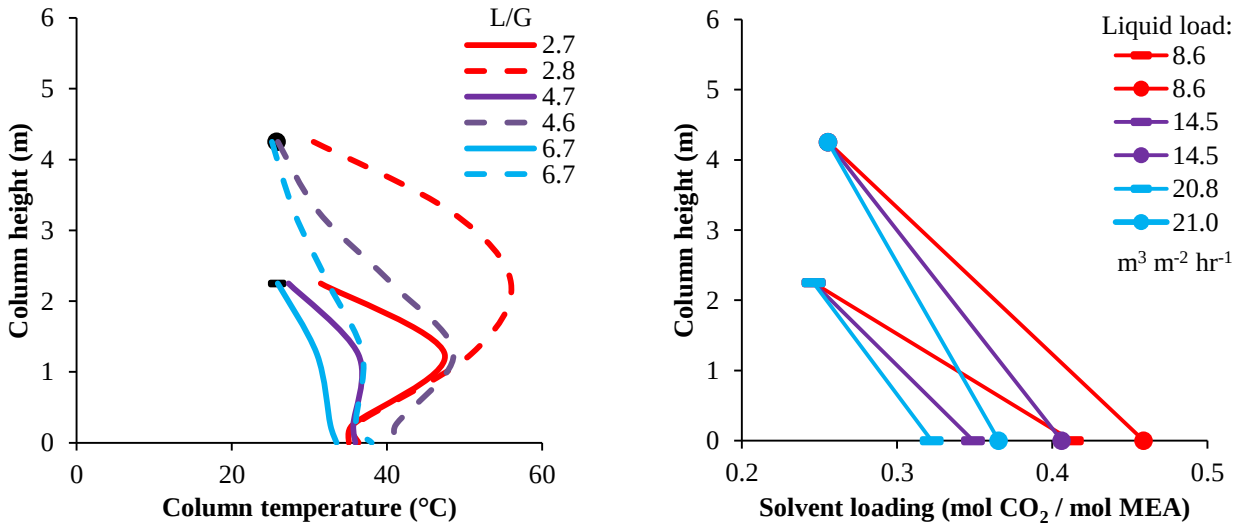

Figure 74: Influence of column height (2 and 4 m) and liquid load on temperature and solvent loading profiles for experiments with 30 wt% MEA, 0.24 (mol CO_2 /mol MEA) inlet loading, 25 °C inlet temperature at a gas load of 0.8 m^3 m^{-2} s^{-1} and around 12 vol% CO_2 inlet concentration.

The solvent loading and temperature profiles of the experiments at 6 and 8 m column height are shown in Figure 75. The total temperature increase in the column was almost equal for experiments at 2.7 and 4.4 L/G ratio and significantly higher than for the experiments at 6.2 L/G ratio. At a column height of 6 m a temperature increase of 22 °C (48 °C total) was measured for 4.3 L/G ratio at around 1 m column height. This temperature bulge wandered to 4 m column height and increased to 53 °C when the L/G

ratio was decreased to 2.4. For 8 m column height the highest temperature was measured near the top of the column at 7 m for 2.7 L/G and in the middle of the column at 3 m for 4.4 L/G ratio with an total increase of about 37 °C (63 °C total) measured in both runs. The somewhat lower temperature at similar L/G ratios measured at 4 and 6 m column height can be explained by the higher inlet solvent loading used in the experiments at 6 m column height. The solvent loading profiles show that the most reactive part of the absorber column was in the top of the column for experiments at 2.4-2.7 L/G ratios and liquid loads between 8.5 and 8.9 m^3 m^{-2} hr^{-1}. At a higher L/G the reactive part wandered down inside the column.

For 4.3 L/G ratio and 8 m column the solvent loading inside the column was almost increasing linearly representing that the mass transfer was equally distributed over the column height. When the L/G ratio was increased to 6.1 the top of the column became less reactive and the reaction zone wandered down. The solvent outlet loading was increasing with column height and decreasing with higher L/G a similar trend as observed in the experiments at 2 and 4 m column height. The capture efficiency and mass transfer rates increased with higher L/G ratio and higher column height. At 6 m a maximum capture efficiency of 84 % could be reached at 6.1 L/G ratio; this value dropped to 77 % and 54 % at 4.3 and 2.4 L/G ratio. The capture efficiency surpassed 90 % at 8 m column height for 6.2 L/G ratio, where 95 % of the CO_2 could be captured. At an L/G ratio of 4.4 85 % of the CO_2 was captured, whereas 65 % capture efficiency was reached at 2.7 L/G ratio.

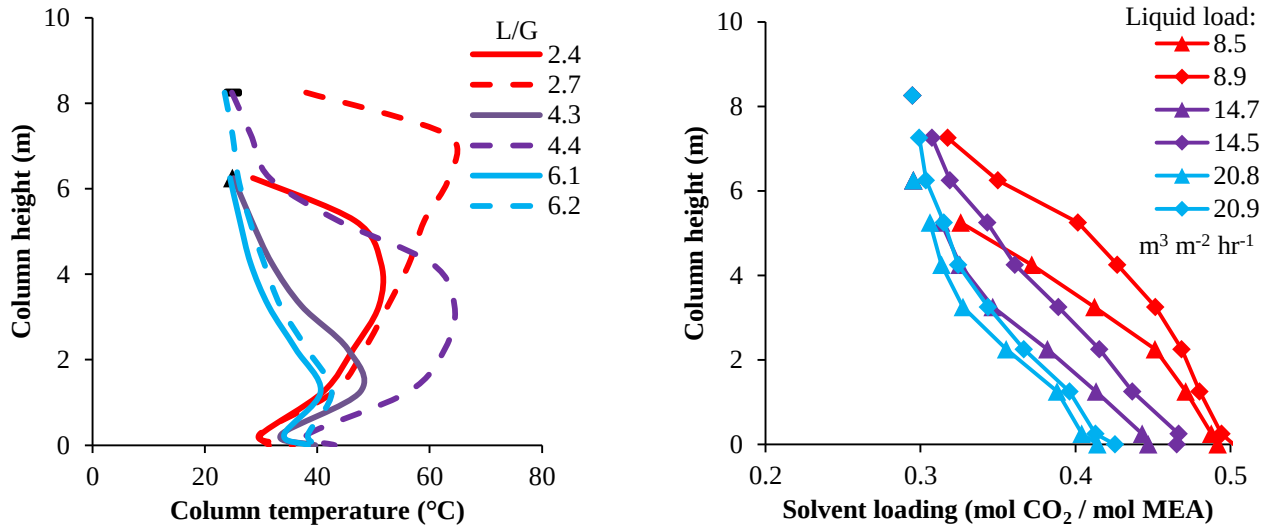

Figure 75: Influence of column height (6 and 8 m) and liquid load on temperature and solvent loading profiles for experiments with 30 wt% MEA, 0.24 (mol CO_2 /mol MEA) inlet loading, 25 °C inlet temperature at a gas load of 0.8 m^3 m^{-2} s^{-1} and around 12 vol% CO_2 inlet concentration.

At 10 m column height the L/G ratio was varied in a broader range between 1.8 and 6.3. The solvent loading and temperature profiles of these experiments are compared in Figure 76. The temperature bulge inside the column was increasing and wandering from the top of the column towards the middle

of the column when the L/G ratio was increased from 1.8 to 2.8, 3.6 and 4.5. The maximum temperature inside the column increased from 54 °C to 68 °C, which represented a total increase of more than 42 °C. When the L/G ratio was increased further to 5.4 and 6.3, the temperature bulge moved further down and the maximum temperature decreased to 56 °C and 43 °C respectively.

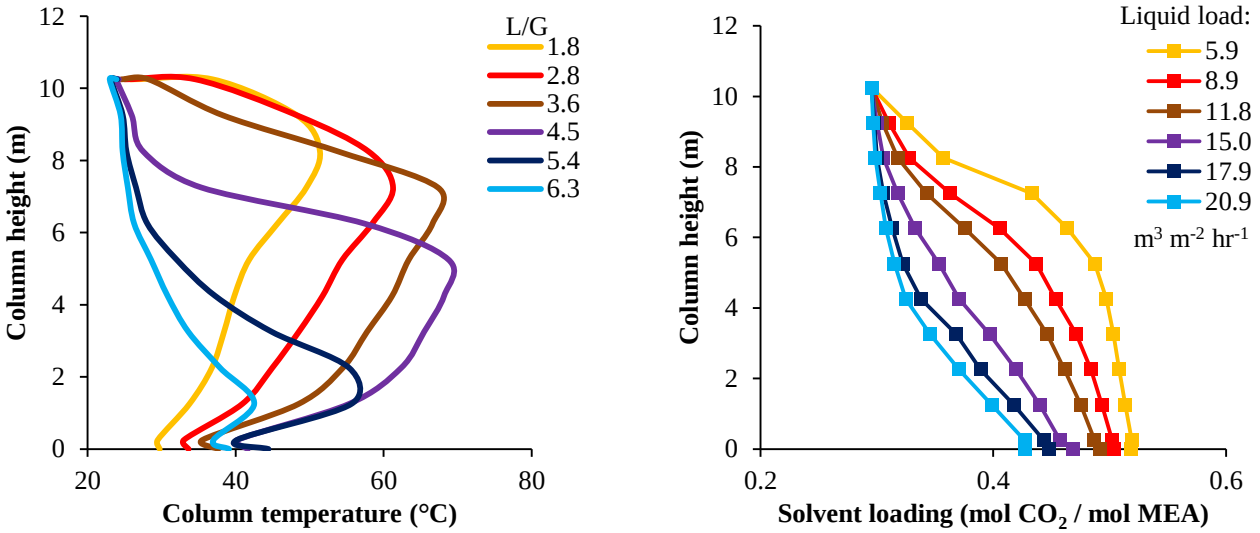

Figure 76: Influence of liquid load on temperature and solvent loading profiles for experiments at 10 m column height with 30 wt% MEA, 0.24 (mol CO_2 /mol MEA) inlet loading, 25 °C inlet temperature at a gas load of 0.8 m^3 m^{-2} s^{-1} around 12 vol% CO_2 inlet concentration.

The solvent loading profiles also showed that the reaction zone was moving downwards when the liquid load and L/G ratio was increased similar to the experiments at lower column heights. For 5.9 m^3 m^{-2} hr^{-1} liquid load the top part of the column was the most reactive area as the loading increase was highest there; below 5 m column there was not much reaction happening and the solvent loading was close to the equilibrium loading of 0.5 mol CO_2 per mole MEA. This reaction zone became bigger, but was still connected to the top of the column when the liquid load is increased. The reaction zone seemed to take up the whole column somewhere between 11.8 and 15 m^3 m^{-2} hr^{-1} liquid load (3.6-4.5 L/G ratio). If the L/G ratio was increased further the reaction zone decoupled from the top and moved downwards.

The experiments at different column heights and L/G ratio showed the same effects. The L/G ratio in the experiments determined the position of the reaction zone. The reaction zones with the highest mass transfer were also the areas with the highest temperatures for 30 wt% MEA. For low L/G ratios the reaction zone could be found close to the top in the column, for medium values in the middle and for high values in the bottom part of the column. At low column heights low L/G lead to the highest temperature increase inside the column, whereas at high column heights medium L/G values resulted in the highest temperature increase. The rich loading was always the highest for the experiments at the lowest L/G ratio.

The transferred flux of CO_2 as a function of the column height as well as the L/G ratio as a function of the capture efficiencies is depicted in Figure 77.

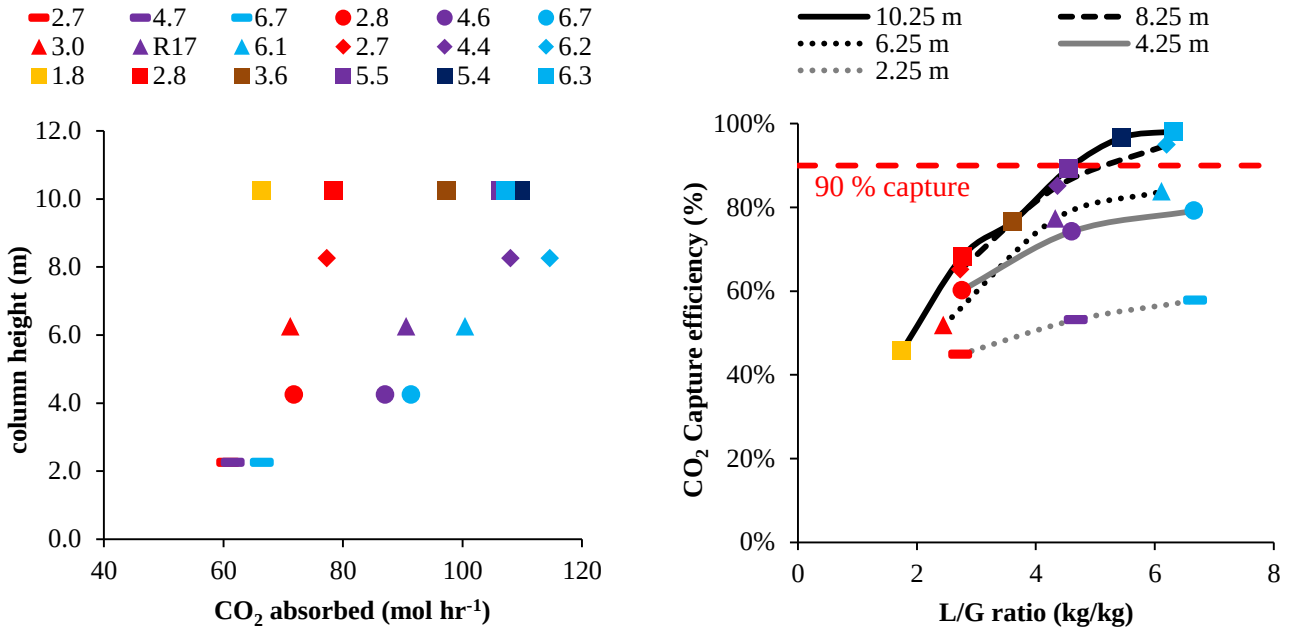

Figure 77: Mass transfer flux of CO_2 measured in the gas phase as function of the column height for all experiments carried out in the second 30 wt% MEA campaign on the left, Capture efficiency as a function of L/G (kg/kg) ratio for different column heights on the right.

Increasing the column height led to a higher mass transfer flux, as well as higher CO_2 capture efficiency. An increase in L/G ratio resulted likewise in higher mass transfer rates and capture efficiencies, this trend was nonlinear. Thus changing the L/G from 2.7 to 4.7 resulted in a higher increase in transfer rate and capture efficiency than increasing from 4.7 to 6.6. It was not possible to reach 90 % capture efficiency at 4 m column height; the closest value measured was 79 % at 4 m column height and an L/G ratio of 6.7.

Even though the highest mass transfer of CO_2 was measured at 8 m column height for 6.3 L/G ratio, the highest capture efficiency (98 %) was achieved at the highest column height and the highest L/G ratio. Only 3 setpoints resulted in capture efficiencies of more than 90 %, with 10 m and 4.5 L/G being just short 1% as shown in Figure 77. When comparing the results at higher column heights (6-10 m), that were performed with the same lean loading it showed up, that the increase in column height from 6 to 8 m increased the capture efficiency much more than the increase between 8 m and 10 m column height.

To achieve 90 % capture at 10 m column height an L/G ratio of more than 4.5 was required. If a slightly higher L/G ratio was chosen, the column could be also operated with 8 m column height. Lower column heights than 8 m were not feasible for this separation task. The absorber column should

be generally operated at the lowest L/G ratio possible, in order to limit liquid circulation rates and thus save energy. The decision of either operating an 8 m column with a higher L/G ratio or a 10 m column with lower L/G ratio should just be taken based on a techno economic analysis taking the capital and operational costs into account.

Comparing the results of 2-4 m column height with the results from 6-10 m that were performed at different lean loadings it appeared that the trend between capture efficiency and L/G ratio is influenced by the lean loading. A lower lean loading seems to make the capture efficiency less dependent on the L/G ratio as the trends less steep. At high column heights the capture efficiency became very dependent on the L/G ratio.

9.3. MDEA campaigns

First an experimental campaign with 30 wt% MDEA without CA was carried out, followed by a campaign with 30 wt% MDEA with 0.85 g/L CA and another campaign with 30 wt% MDEA with 3.5 g/L CA.

9.3.1. Plain 30 wt% MDEA campaign (Winter 2015-2016)

The campaign with plain 30 wt% MDEA was carried out at 10 m column height, as it was expected that the solvent without activator would absorb very slow, thus the influence of column height on the mass transfer would be difficult to determine. In total 12 experiments were conducted, 6 at 28 ºC and 6 at 40 ºC inlet temperature. Three experiments at each temperature were carried out at around 4-5 vol% CO_2 inlet concentration, representing conditions of a gas fired power plant, and the other three with 12-14 vol% CO_2, representing flue gas compositions of a coal fired power plant. The gas load was kept constant at around 0.6-0.7 $m^3\ m^{-2}\ s^{-1}$, whereas the liquid load was varied between 8.9 and 21.3 $m^3\ m^{-2}\ hr^{-1}$. The different setpoints of the runs M1-M12 are collected in Table 9.

Table 9: Setpoints of the 30 wt% plain MDEA campaign all at 10.25 m column height

Parameter (unit)	**M1**	**M2**	**M3**	**M4**	**M5**	**M6**	**M7**	**M8**	**M9**	**M10**	**M11**	**M12**
Liquid load($m^3\ m^{-2}\ hr^{-1}$)	8.5	15.0	21.3	21.3	15.0	8.9	21.2	15.1	8.6	9.0	15.3	21.3
gas load ($m^3\ m^{-2}\ s^{-1}$)	0.6	0.6	0.6	0.6	0.6	0.6	0.6	0.6	0.6	0.6	0.6	0.6
L/G (kg/kg)	3.4	6.0	8.8	8.3	5.9	3.5	9.2	6.8	3.7	3.7	6.3	8.9
L/G (mol/mol)	4.0	7.2	10.5	10.4	7.3	4.4	10.9	8.1	4.4	4.6	7.7	11.0
yCO_2 (-)	0.05	0.05	0.05	0.14	0.13	0.12	0.04	0.04	0.05	0.14	0.12	0.13
Capture efficiency (%)	19%	20%	21%	23%	20%	18%	24%	21%	19%	19%	20%	22%

The temperature and solvent loading profiles of the experiments carried out at 12-14 vol% CO_2 are compared in Figure 78.

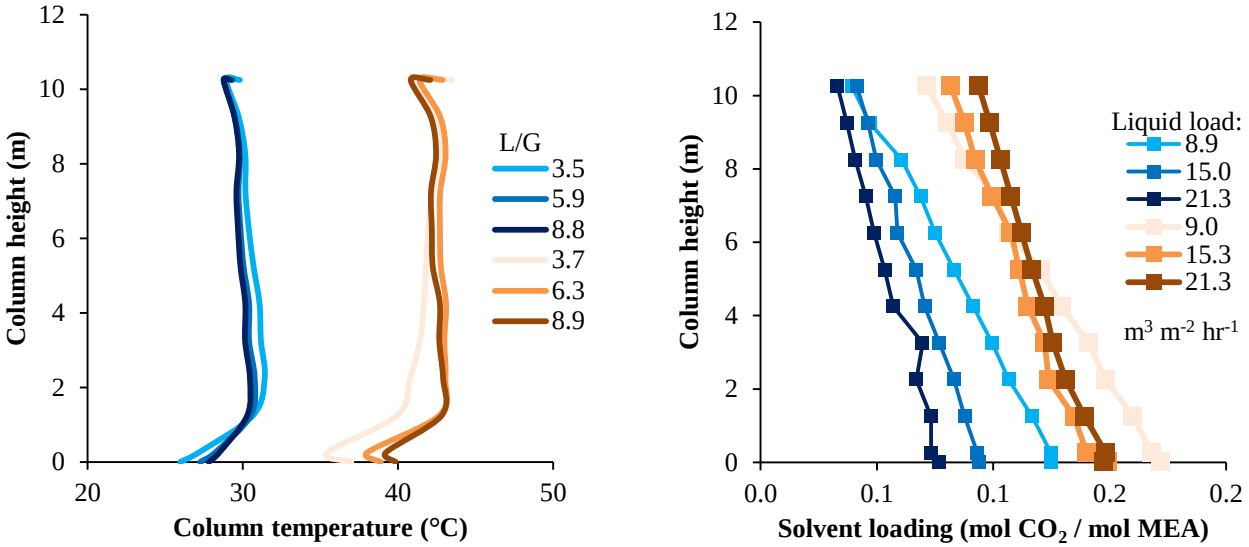

Figure 78: Column temperature and solvent loading profiles for plain 30 wt% MDEA at 25 and 40 C full column height at different L/G ratios and CO_2 inlet concentrations between 12-14 vol%.

There were no big differences in the temperature profiles between the different experiments visible at 28 ºC inlet temperature. In all experiments a slight increase of around 2-3 ºC without a temperature bulge could be observed. In the bottom of the column at the gas inlet a decrease in temperature most likely due to the gas inlet effect could be observed. For experiments at 40 ºC inlet temperature the temperature increase with 2-3 ºC was similar to 28 ºC for higher L/G ratios. For the lowest L/G the temperature even decreased in the bottom of the column, which might be linked to insufficient thermal insulation for the experiments at that point. The solvent loading profiles were almost straight lines over the whole column. The increase in solvent loading is the highest at the lowest L/G ratio. The capture efficiencies could be increased with the L/G ratio, although the differences were rather small. Compared to MEA, MDEA was much slower absorbing, because of slower reaction kinetics. The slower reaction kinetics resulted also in a much lower temperature increase of the column temperature as well. With capture efficiencies of around 18 to 24 % at 10 m column height plain 30 wt% MDEA is not a suitable solution for the separation task of CCS at coal fired power plants.

9.3.2. 1st 30wt% MDEA campaign with 0.85 g/L CA (Spring 2016)

In the experimental campaign with 30 wt% MDEA and 0.85 g/L CA, the effect of solvent temperature, solvent loading, column height as well as L/G ratio was investigated. The experiments were conducted with a recycle of the solvent in a closed loop. The total amount of solvent was 300 kg and the highest liquid flow rate tested was around 175 kg/hr. During 20 min steady state the change in solvent composition was quite small, but over the total course of the experiments the solvent loading changed.

At first the effect of column height changes on the mass transfer were investigated at two different L/G ratios for 28 °C inlet temperature. Afterwards full solvent loading profiles were taken at 10 m column height. The solvent was then heated up to 40 °C and another run was started with different column heights, the solvent loading by then was already 0.27 (mol CO_2/mol MDEA). After taking full column loading profiles at 10 m height, the liquid was cooled down again over night and additional experiments were carried out with the highly loaded solvent at 28 °C with full column height. An additional solvent batch with 30 wt% MDEA and 0.85 g/L CA was prepared and full column loading profiles were taken at 40 °C at low lean solvent loadings.

The results of the capture efficiencies of enzyme enhanced MDEA with 0.85 g/L CA at different column heights are shown in Figure 79. The lean loading in the experiments at 28 °C was around 0.1 (mol CO_2/mol MDEA) and 0.27 (mol CO_2/mol MDEA) at 40 °C. The results at 28 °C showed an increase in capture efficiency when increasing the column height; this increase was more profound between low column heights and seemed to have a limiting trend at higher column heights for low L/G ratios. The capture efficiency increased at higher L/G ratios for both temperatures, although 90 % capture could not be realized under these conditions with 56 % capture efficiency being the highest value measured for 10 m column height and 7.7 L/G ratio.

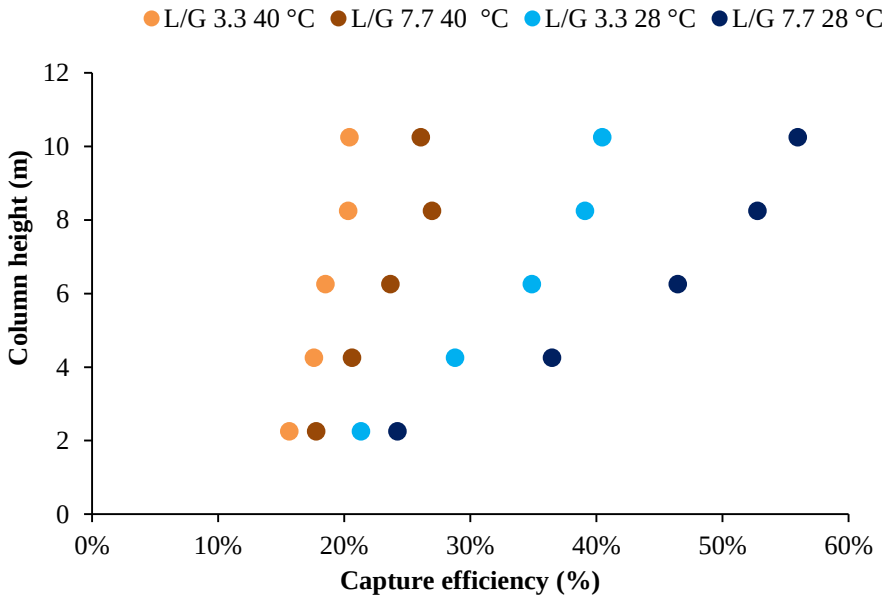

Figure 79: Influence of column height of capture efficiency for 30 wt% MDEA with 0.85 g/L CA; inlet loading for 28 °C experiments around 0.1 and 40 °C experiments 0.27 mol CO_2 per mol MDEA.

The capture efficiency decreased for experiments at 40 °C and an inlet loading of around 0.27 (mol CO_2/mol MDEA). The capture efficiency for both L/G ratios could be increased with higher column height in the range of 2 to 8 m; between 8 and 10 m column no increase capture efficiency could be observed for experiments at 40 °C. The capture efficiency was higher for higher L/G ratios. A

total 27 % of CO_2 could be captured at 7.7 L/G ratio and 20 % at 3.3 L/G ratio. The lower capture efficiency measured for the experiments at 40 °C compared to 28 °C are caused by the higher solvent loading and the higher temperature, as they both resulted in a higher CO_2 equilibrium partial pressure of the solutions, which decreased the driving force for the mass transfer. Also the inhibition of the enzyme by the bicarbonate ion affected the mass transfer.

The temperature and solvent loading profile of the experimental runs at 28 °C and 0.2 (mol CO_2/ mol MDEA) lean loading at full column height for different L/G ratios are compared in Figure 80.

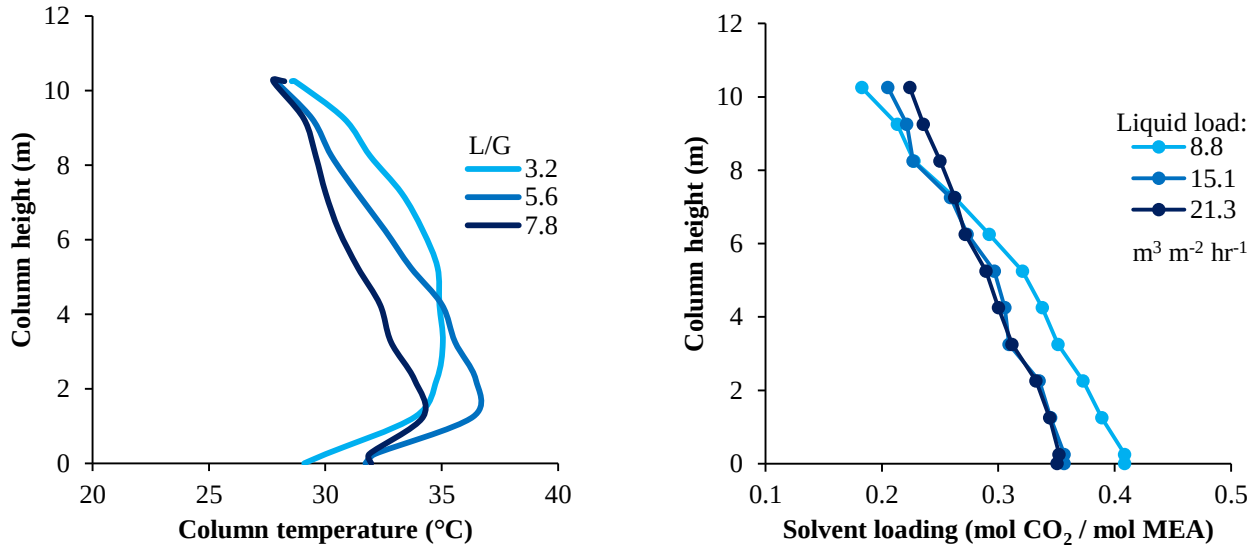

Figure 80: Influence of L/G ratio on temperature and solvent loading profile for 30 wt% MDEA with 0.85 g/L CA, 0.2 mol CO_2 per mol MDEA inlet loading and 28 °C inlet temperature

For a low L/G ratio the temperature in the bottom half of the column increased, although no clear temperature peak was visible in these experiments, as the temperatures measured at 1 to 5 m column height differed by only 1 °C. The total temperature increase inside the column was about 6-7 °C for 3.2 L/G ratio; the liquid cooled down to approximately the inlet temperature at the liquid outlet due to the gas inlet effect. When the L/G ratio was increased to 5.6, the total temperature increase inside the column rose to 8 °C (36 °C total) and a temperature bulge evolved in the bottom of the column at around 1 m column height. A further increase in L/G to 7.8 decreased the maximum temperature inside to 34 °C, but did not change the position of the temperature bulge nor the outlet temperature. All solvent loading profiles for enzyme enhanced MDEA showed a close to linear trend with just a very slight bend for low L/G ratios. The increase in solvent loading over the column is the highest for the lowest L/G ratio. A linear loading increase over the column height describes equally distributed mass transfer inside the column is i.e. there were no zones where higher mass transfer occurs or less-reactive zones. The temperature and the loading profiles showed that the addition of enzymes intensified the reaction and mass transfer significantly compared to plain 30 wt% MDEA.

At 40 °C inlet temperature and 0.05 (mol CO_2/ mol MDEA) lean loading a temperature increase of 12-13 °C could be observed at 3.5 and 6.1 L/G ratio as shown in Figure 81.

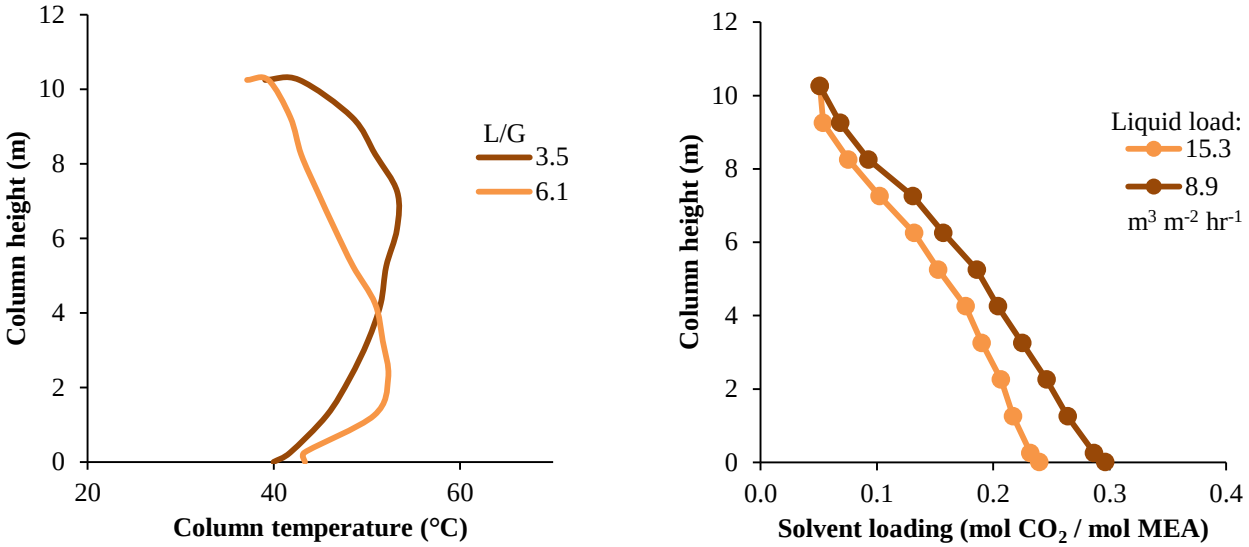

Figure 81: Influence of L/G ratio on temperature and solvent loading profile for 30 wt% MDEA with 0.85 g/L CA, 0.05 mol CO_2 per mol MDEA inlet loading and 40 °C inlet temperature

The highest temperature of 52 °C was measured at around 2 m column height for 6.1 L/G ratio and 53 °C was obtained for an L/G ratio of 3.5 at 7 m column height. The total temperature increase inside the column was slightly higher and at a higher position for the experiments at 40 °C compared to the experiments 28 °C. It should though not be left out that the lean loading was around 0.05 for the experiments at 40 °C and 0.2 for experiments at 28 °C. The solvent loading profile trends were similar at 28 and 40 °C as both trends were linear with a very slight bend.

The effects of solvent inlet temperature, solvent loading as well as the L/G ratio for all experiments at 10 m column height are summarized in Figure 82. Three effects could be observed from these experiments:

a) At the same temperature and similar lean loading, an increase in L/G ratio led to an increase in capture efficiency.
b) An increase in lean loading decreased the capture efficiency of the solvent, which was expected as the driving force for the process decreases with the solvent loading. Although the capture efficiency was not dropping strongly when the solvent was loaded. At 3.3 L/G ratio the capture efficiency with 19% of a highly loaded solvent at 0.37 (mol CO_2/ mol MDEA) was about just the half of the capture efficiency the same solvent showed at 0.13 (mol CO_2/ mol MDEA) inlet loading.
c) At comparable solvent loadings and L/G ratios, experiments at 28 °C resulted in a higher capture efficiency as experiments at 40 °C inlet temperature. A similar behavior could be

observed at the wetted wall column, where the mass transfer coefficient at 25 °C was higher than at 40 °C for 30 wt% MDEA solutions with CA.

In general enzyme enhanced solutions have shown a remarkable mass transfer enhancement at different process conditions compared to 30 wt% MDEA without enzyme. Nonetheless none of the different process conditions with 30 wt% MDEA with 0.85 g/L CA could provide capture efficiencies comparable to industrial standard 30 wt% MEA.

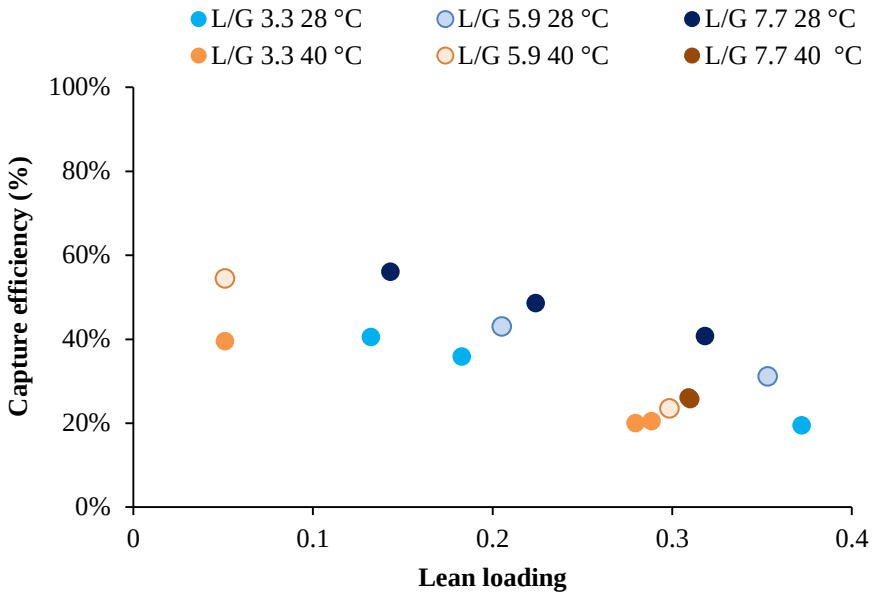

Figure 82: Influence of solvent loading, solvent temperature and L/G ratio on capture efficiency for 30 wt% MDEA with 0.9 g/L CA at 10 m column height

9.3.3. 2nd 30 wt% MDEA campaign with 3.5 g/L CA (Winter 2016-Spring 2017)

A second campaign with enzyme enhanced 30 wt% MDEA was conducted with a higher CA concentration of 3.5 g/L. Full column profiles were taken at 10 m column height and different L/G ratios and the influence of column height on the capture efficiency was determined. No solvent recycle was conducted in this campaign, thus the lean loading of the solvent did not change during the experiments.

The temperature and solvent loading profile of the experiments at full column height are shown in Figure 83. The highest temperature increase inside the column was observed at the lowest L/G ratio where 40 °C could be measured at 2 m column height, which was 14 °C above the inlet temperature. When L/G ratio was increased to 4.7 and then to 6.5 the temperature bulge decreased to 38 and 33 °C and moved down to 1 m column height. The outlet temperature was similar to the inlet temperature in all experiments. The highest increase in solvent loading could be observed at the lowest L/G ratio; the top part of the column seemed to be less active than the bottom part, as the loading did just slightly

change in the range between 8 m and 10 m column height. This might be due to the fact, that the volume concentration of CO_2 in the gas phase near the outlet was much lower than in the previous campaign due to higher mass transfer inside the column. The column part below 8 m showed a similar linear profile as the experiments with 0.85 g/L CA with a slight bend for lower L/G ratios.

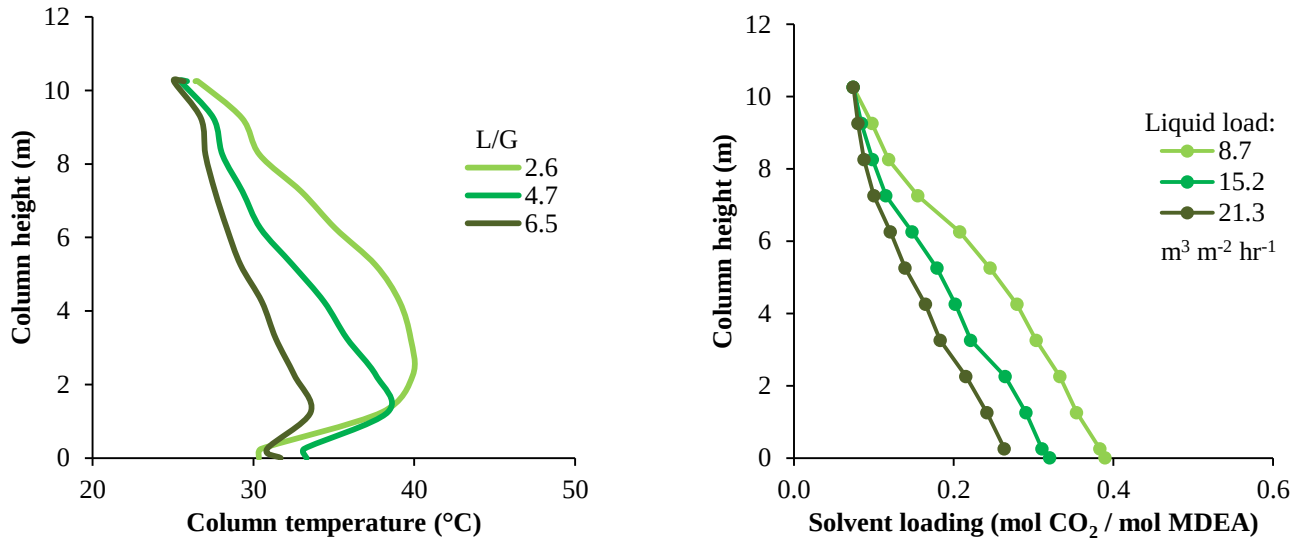

Figure 83: Influence of L/G ratio on temperature and solvent loading profile for 30 wt% MDEA with 3.5 g/L CA at 28 C inlet temperature, 10 m column height and 0.07 (mol CO_2/mol MDEA) inlet loading.

The CO_2 capture efficiency for a L/G ratio of 4.5 at different column heights for experiments with a lean loading of 0.07 and 0.22 mol CO_2 /mol MDEA as well as the influence of L/G ratio on the CO_2 capture efficiency at 10 m column height are shown in Figure 84. The solutions with the lower lean loading had a higher CO_2 capture efficiency, the difference between the capture efficiencies for the two solutions with different loadings even increased with height. An increase in column height above 10 m will likely not provide a beneficial effect for the solution with higher solvent lean loading, as the capture efficiency increased by just one percentage point from 43 to 44 % between 8 and 10 m column height. At experiments with 0.07 inlet loading the CO_2 capture efficiency increased from 60 to 65 % when the column height was increased from 8 to 10 m. An increase in column height would likely result in a higher capture efficiency in that case. The capture efficiency at 10 m column height could be just changed by altering the L/G ratio. When the L/G ratio was decreased from 4.5 to 2.6 the capture efficiency dropped from 65 to 48 % for the lower loaded solvent (0.07 ldg) and from 44 to 32 % for the higher loaded solvent (0.22 ldg). When the L/G ratio was increased from 4.5 to 6.5 the capture efficiency increased to 75 and 54 % for the experiments at 0.07 and 0.22 solvent lean loading respectively. A further increase in L/G ratio to 9.3 led to a capture efficiency of 83 % for the lower loaded solvent.

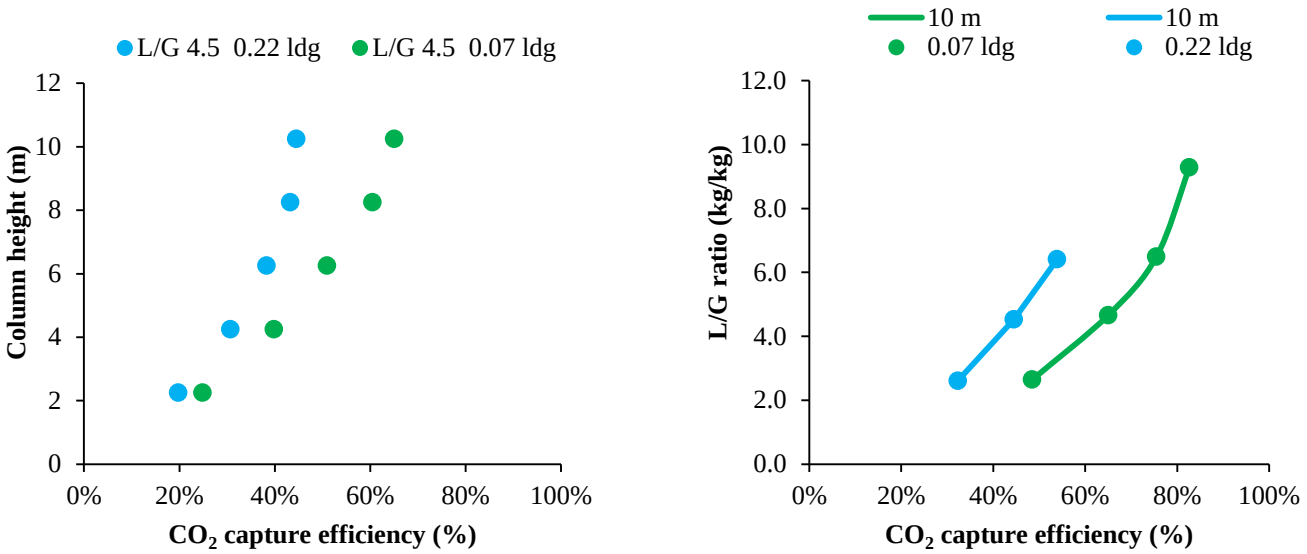

Figure 84: Influence of column height at 4.5 L/G ratio and L/G ratio at 10 m column height on capture efficiency for 30 wt% MDEA with 3.5 g/L CA, 28 C and 0.07 and 0.22 (mol CO_2/mol MDEA) solvent loading.

Even the higher enzyme concentration did not result in a capture efficiency of more than 90 %, although the trends suggest, that the capture efficiency can be increased with either a higher column height or a higher L/G ratio. As the trend between capture efficiency and L/G is very steep, the L/G ratio has to be brought to a very high level to result in capture efficiencies of 90 %. The effect of solvent lean loading on the trend between L/G ratio and capture efficiency seemed to be less distinct. Based on the experimental results a decrease in lean loading will likely shift the capture efficiency to a higher level. As the two trends at different lean loading are almost parallel on the right side in Figure 84, a lower lean loading than 0.07 might represent a parallel line shifted further to the right. It might be thus more helpful to reduce the lean loading of the solvent below 0.07 mol CO_2 / mol MDEA to reach a capture efficiency of 90 %.

Alvizo et al. performed pilot scale experiments with 25 wt% MDEA with 0.2 g/L CA at the National Carbon Capture Center in Wilsonville Alabama USA [2]. Their setup consisted of two in line columns with 0.15 m diameter and 3.15 m height each packed with 16 mm Pall rings (6.3 m total height). In their long term experiments they measured a capture efficiency of 60 % from a flue gas with 12 vol% inlet CO_2 concentrations at an L/G ratio on mass basis of around 9[2]. This value was higher than the experimental results at 6 m column height in this study; for 30 wt% MDEA with 0.85 g/L CA 46 % capture efficiency was measured at 7.7 L/G ratio and 51 % for 30 wt MDEA with 3.5 g/L CA at 4.4 L/G ratio.

[2] calculated assuming a liquid density of 1000 kg m^{-3} and a gas density of 1.2 kg m^{-3}

The effective surface area of the packing in Alvizio et al.'s experiments was 316 m^2 m^{-3} according to the supplier [3] thus higher than that of Mellapak 250 Y with 250 m^2 m^{-3} used in our setup; the effective surface area of DTU's column should be closer to 141 m^2 m^{-3} as the packing material is not filling the total cross-section and height. Their setup had more than double the mass transfer area. When comparing with experiments at 10 m column height, where the total mass transfer areas inside the columns are comparable, the results obtained with 0.85 g/L CA with 56 % capture efficiency at 7.7 L/G ratio are closer to Alvizo et al.'s results. The experiments with 3.5 g/L CA and 9.3 L/G ratio resulted with 83 % in higher capture efficiency than in the experiments from Alvizio et al. The enzyme concentrations applied in this study were also higher than in Alvizio et al.'s study (0.9-3.5 g/L vs. 0.2 g/L) although the enzyme was coming from different sources making a head to head comparison difficult. The capture efficiencies reported by Alvizio et al. could be achieved and even surpassed in this work, when the experiments at similar mass transfer areas and L/G were compared.

Kunze et al. determined the catalytic effects CE of enzyme addition from their experiments in pilot scale in their work [4]. For 30 wt% MDEA with 0.2 wt% CA (around 2 g/L) they reported catalytic effects of 3.3 to 4.2 depending on the liquid load.

The CE value is useful to compare smaller scale experiments where the process conditions, such as CO_2 concentration in gas phase, solvent loading and temperature do not change much. It is though difficult to compare CE values derived from different equipment [5]. In case of high columns all of these process conditions change. Especially with fast absorbing enzyme enhanced solvents the changes over the height of the column might be significant and influence the mass transfer. That implies that mass transfer for the fast reacting solvent is changed to a larger extent over the column, than for a slow reacting solvent which represents the reference value in the CE calculation. Calculating the CE values[3] from the different experiments at different column heights showed a decrease of CE with column height. These changes were not caused by a less active enzyme, but by the change in process conditions over the height of the column, which influenced the mass transfer of the enzyme enhanced solvent more than the slow absorbing MDEA solvent without enzyme. Therefore the CE value should just be used on comparable equipment and in experiments where the changes in the process conditions do not influence the mass transfer a lot.

The mass transfer performance of enzyme enhanced solutions in pilot scale was referenced to the industrial benchmark 30 wt% MEA in this study as described in the next section.

[3] The reference values for plain 30 wt% MDEA at different column heights, was calculated from the solvent loading profiles, as no experiments at different heights were conducted with this solvent.

9.4. Comparison of MEA and enzyme enhanced MDEA

Temperature maxima could be observed for 30 wt% MEA and for enzyme enhanced MDEA, although the total temperature increase inside the column was much higher for MEA where a temperature increase of more than 40 °C could be observed compared to a maximum of 14 °C for enzyme enhanced MDEA. The temperature profiles inside the columns in the experiments were influenced by several effects. First the heat of reaction heated up the liquid phase and the liquid phase transported this enthalpy downwards by gravitational forces. When the gas phase had a lower temperature than the liquid phase or the gas phase was not saturated, water and small quantities of solvent evaporate and heats up the gas phase while cooling the liquid phase. The heat was then transported upwards in the column by the gas phase. Condensation of a warm gas stream at a cooler liquid phase could heat up the liquid even above the reaction zone. The importance of the two convective heat fluxes in the gas and the liquid phase on the column profile changed with the L/G ratio. At high L/G ratios the convective flux of heat in the liquid phase was dominant. When decreasing the L/G ratio, the convective heat flux of the gas phase became more important.

These differences in temperature profiles between MEA and MDEA are caused on the one hand by the higher heat of reaction of MEA compared to MDEA. The reaction of 1 mol CO_2 with MEA will release 83 kJ of energy, whereas just around 57 kJ are released for the reaction of 1 mol CO_2 with MDEA [6]. This will lead to a higher heat generation in MEA solvents during absorption.

On the other hand the mass transfer of CO_2 into MEA solutions was higher than into enzyme enhanced solutions, thus more CO_2 was converted which also led to an even higher generation of heat. The mass transfer into enzyme enhanced MDEA was although not much slower absorbing than 30 wt% MEA. Enzyme enhanced 30 wt% MDEA with 3.5 g/L CA could provide more than 80% of the mass transfer performance of 30 wt% MEA over the full column height. The mass transfer of CO_2 into MEA solutions was although more concentrated to a certain area of the column. Figure 85 compares the mass transfer of CO_2 per meter of column over the total height, calculated as the increment in solvent loading starting from the top of the column.

The mass transfer is much more equally distributed for the enzyme enhanced 30 wt% MDEA solutions shown on the left side than for 30 wt% MEA shown on the right side. For 30 wt% MEA there are clearly more active parts in the column visible. At a low L/G ratio most of the absorptions took place in the top part, this active part of the column wandered down inside the column if the L/G ratio was increased until almost all the absorption took place in the bottom. For enzyme enhanced MDEA also a slight trend was visible, as the bottom part of the column became a little more active when the L/G ratio was increased. The L/G had although a much lower influence on the mass transfer inside the column.

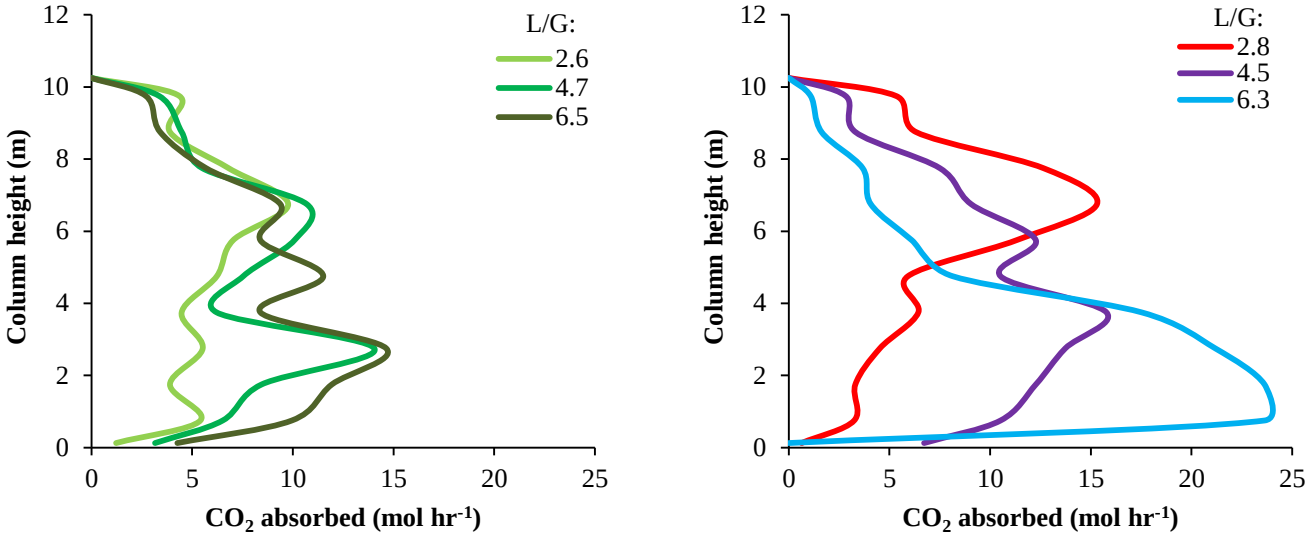

Figure 85: Mass transfer of CO_2 over the column height for 30 wt% MDEA with 3.5 g/L CA and 30 wt% MEA at different L/G ratios

This behavior can be explained with the different temperature influence on the mass transfer between enzyme enhanced MDEA and MEA. An increase in temperature will increase the mass transfer coefficient for 30 wt% MEA solutions, whereas the mass transfer coefficient for enzyme enhanced MDEA will decrease. The absorption of CO_2 into MEA solutions increases the temperature, which will spike the mass transfer even further. This will result in hot spots inside the column and influence the loading and temperature profiles. For enzyme enhanced MDEA solutions, the mass transfer will decrease once the temperature raises which regulates the mass transfer and prevents hot spots. The control of a process with 30 wt% MEA will be more difficult than for an enzyme enhanced MDEA process, as small changes in L/G ratio will result in bigger changes in capture efficiency as well as column temperature and solvent loading profiles; the enzyme enhanced processes are much less sensitive on changes in L/G ratio.

Table 10: Comparison of capture efficiencies of 30 wt% MEA and 30 wt% MDEA with varying enzyme concentrations for different L/G ratios at a column height of 10 m

Solvent	Loading (mol/mol)	T (^{0} C)	L/G 2.1	L/G 2.6	L/G 3.3	L/G 4	L/G 4.5	L/G 5.5	L/G 6.5	L/G 7.6	L/G 9.5
30 wt% MEA	0.29	28	46%		68%		77%	89%	97%	98%	
0 g/L CA	0.05	28			18%			20%		23%	
0.85 g/L CA	0.1	28				40%					56%
0.85 g/L CA	0.27	40				20%					26%
3.5 g/L CA	0.07	28		48%			65%		75%		83%
3.5 g/L CA	0.22	28		32%			44%				54%

The enzyme enhanced MDEA solutions could not provide the same CO_2 capture efficiencies as 30 wt% MEA under comparable process conditions; the capture efficiencies for experiments column heights of 2-8 m are summarized in Table 22 in the Appendix and for experiments with a column height of 10 m in Table 10. 30 wt% MEA exhibits a higher CO_2 capture efficiency than 3.5 g/L CA enhanced MDEA despite the column height as shown in the left part of Figure 86. The column height showed a similar influence of the CO_2 capture efficiency for 30 wt% MDEA with 3.5 g/L CA and 30 wt% MEA for an L/G ratio of 4.5. In both cases the capture efficiencies could be increased with a higher column and the incremental increase diminished slightly at higher column heights. The addition of CA to 30 wt% MDEA significantly increased the capture efficiency of MDEA solutions at full column heights as shown in right part of Figure 86 where the capture efficiencies of the different solvents tested in pilot scale at 10 m column height are compared. The enzyme addition did however not result in higher CO_2 capture efficiencies than 30 wt% MEA at similar L/G ratios.

The addition of enzyme resulted in a higher increase in capture efficiencies at higher L/G ratio, as the trend in the right side of Figure 86 became steeper the higher the enzyme concentration was. 30 wt% MEA had a steeper trend than 30 wt% MDEA with 3.5 g/L CA. An increase in CA concentration will most likely increase the inclination of the trend and make close the gap between MEA and enzyme enhanced MDEA.

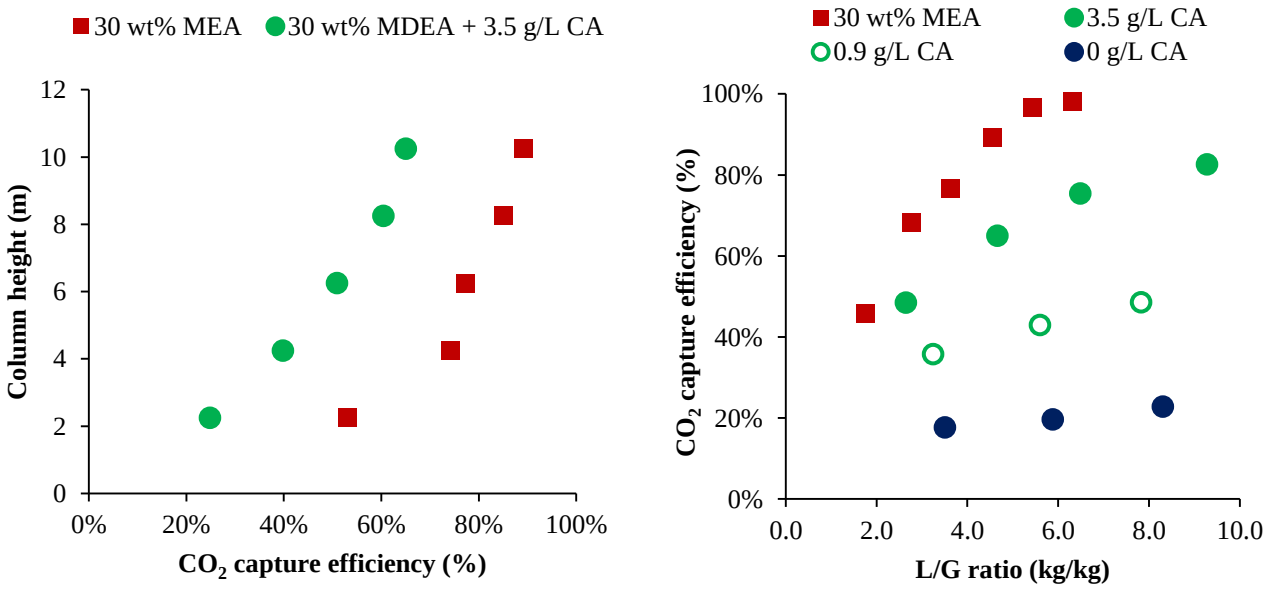

Figure 86: Comparison of CO_2 capture efficiencies of enzyme enhanced 30 wt% MDEA and 30 wt% MEA at different column heights for 4.5 L/G ratio (left) and different L/G ratios at 10 m column height (right).

The mass transfer performance of enzyme enhanced MDEA solutions are compared to the industrial standard 30 wt% MEA in Figure 87. The value was calculated as ratio of CO_2 capture efficiency at similar L/G ratios and column heights. The ratio of the capture efficiencies was chosen rather than the

total absorbed CO_2 flow in order to normalize the results. An enzyme concentration of 0.85 g/L had around 50 % of the mass transfer performance of the industrial standard, whereas 3.5 g/L CA could result in over 80 % of 30 wt% MEA's mass transfer performance[4]. 30 wt% MDEA without a kinetic promoter had just around 20 % of the industrial standards mass transfer performance. The performance compared to MEA can be slightly increased at higher column heights and higher L/G ratios for 3.5 g/L CA. The effect of L/G ratio on the performance compared to MEA should although not be overemphasized, as the capture efficiency of 30 wt% MEA cannot be higher than 100 % and at an L/G ratio of 6.5 already 98 % of the CO_2 was captured.

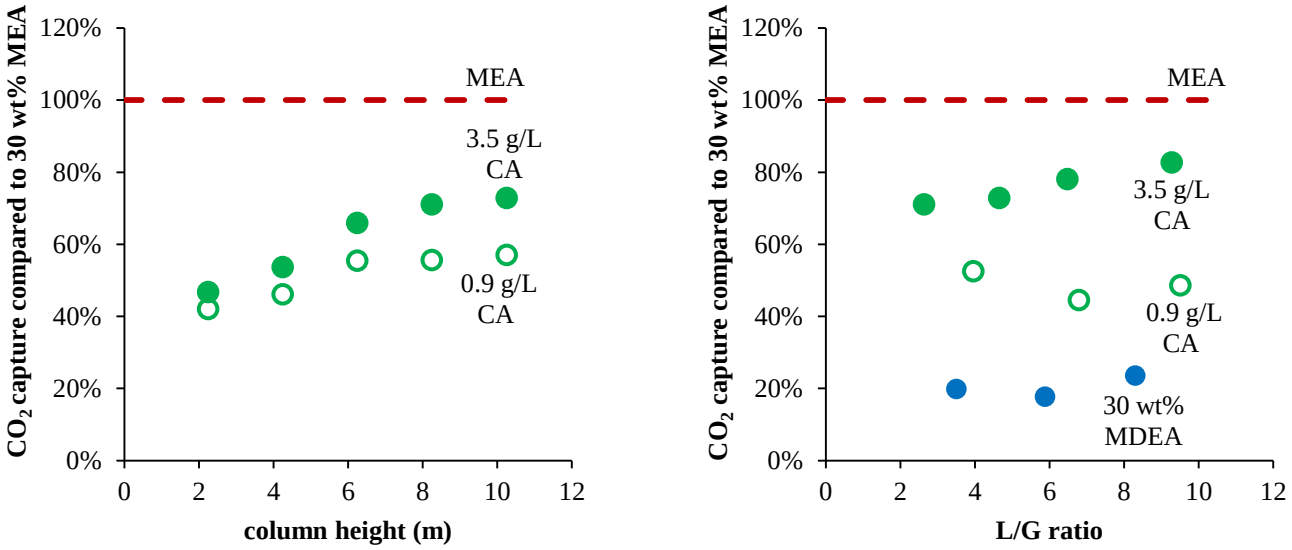

Figure 87: Mass transfer performance of 30 wt% MDEA and enzyme enhanced 30 wt% MDEA compared to the industrial standard 30 wt% MEA as a function of column height (left) and L/G ratio at full column height (right).

[4] The capture efficiency of the MEA reference was taken at 100 %, because no comparable experiment was carried out at that L/G ratio with 30 wt% MEA

BIBLIOGRAPHY

[1] T. L. Sønderby, K. B. Carlsen, P. L. Fosbøl, L. G. Kiørboe, and N. von Solms, "A new pilot absorber for CO_2 capture from flue gases: Measuring and modelling capture with MEA solution," *Int. J. Greenh. Gas Control*, vol. 12, pp. 181–192, 2013.

[2] O. Alvizo, L. J. Nguyen, C. K. Savile, J. a Bresson, S. L. Lakhapatri, E. O. P. Solis, R. J. Fox, J. M. Broering, M. R. Benoit, S. a Zimmerman, S. J. Novick, J. Liang, and J. J. Lalonde, "Directed evolution of an ultrastable carbonic anhydrase for highly efficient carbon capture from flue gas.," *Proc. Natl. Acad. Sci. U. S. A.*, vol. 111, no. 46, pp. 16436–41, 2014.

[3] "Technical information for Pall rings from supplier." [Online]. Available: http://www.pallrings.co.uk/products/pall-rings-stainless-steel/. [Accessed: 07-Apr-2017].

[4] A. Kunze, G. Dojchinov, V. S. Haritos, and P. Lutze, "Reactive absorption of CO_2 into enzyme accelerated solvents : From laboratory to pilot scale," *Appl. Energy*, vol. 156, pp. 676–685, 2015.

[5] A. Gladis, M. T. Gundersen, P. L. Fosbøl, J. M. Woodley, and N. von Solms, "Influence of temperature and solvent concentration on the kinetics of the enzyme carbonic anhydrase in carbon capture technology," *Chem. Eng. J.*, vol. 309, 2017.

[6] I. Kim and H. F. Svendsen, "Comparative study of the heats of absorption of post-combustion CO_2 absorbents," *Int. J. Greenh. Gas Control*, vol. 5, no. 3, pp. 390–395, 2011.

10. Absorber column modelling

This chapter describes the CAPCO2 model validation to simulate the pilot plant results for enzyme enhanced CO_2 capture. At first a short overview of literature mass transfer models for packed column is given. Then the CAPCO2 model with the incorporated enzyme kinetic model from chapter 7 is validated against the experimental results, followed by a short sensitivity analysis of the influence of relevant process parameter predicted by the model.

10.1. Mass transfer models

In rate based absorber column models the mass transfer unit is discretized into different cells where the liquid phase is running from top to bottom and the gas phase counter currently. The transferred amount per cell is calculated from the driving force as well as the overall mass transfer coefficient. Good correlations for the gas and liquid side mass transfer coefficient as well as for the mass transfer area are needed for accurate description of mass transfer in technical absorber columns. These correlations should be simple but still be able to consistently describe the phenomena in absorbers. The first packed column model was developed by Onda et al. (1968) [1] for random packings. The models were improved throughout the time; today's most popular mass transfer models for packed columns were derived by Billet & Schultes (1993) [2] and Rocha et al. (1996) [3]. In the last year Wang et al. [4] proposed a new mass transfer model to describe hybrid or random as well as structured packings. In the following subchapters assumptions and main differences of these models are explained and the models are compared.

10.1.1. Billet and Schultes model

Billet and Schultes proposed a theoretical mass transfer model for packed columns based on the penetration theory from Higbie 1935. The mass transfer parameter for the liquid and gas side used had the following basis:

$$k_{transfer} = 2\sqrt{\frac{D_{CO_2}}{\pi \cdot \tau}} \tag{10.1}$$

With $k_{transfer}$ (m s^{-1}) being the physical mass transfer coefficient, and τ (s^{-1}) being the contact time of the fluid element, i.e the time required for the interfacial area to be renewed after each flow path of the length l_τ (m) has been traversed. In order to describe the complexity in a packed column apparatus they choose a vertical two phase channel model and simulated the absorber as a number of flow channels in parallel whose number is dependent on the void fraction ε (-) and specific surface area a_p (m^2 m^{-3}) of the packing. This channel model must agree with real column in terms of same specific surface and same porosity. The same specific surface was achieved when the following was true:

$$N \cdot \pi \cdot d_{channel} \cdot h = a_p \cdot V_{column} \tag{10.2}$$

with N (-) being the number of channels and $d_{channel}$ and h (m) being the diameter and height of the channel. Same free volume or porosity ε (-) inside the column was described by:

$$N \cdot \frac{\pi}{4} \cdot d_{channel}^2 \cdot h = \varepsilon \cdot V_{column} \tag{10.3}$$

Eliminating the number of channel *N* from Eq. (10.2) and (10.3) leads to the following relation between specific surface area of the packing a_p, porosity ε and channel diameter $d_{channel}$:

$$d_{channel} = \frac{4 \cdot \varepsilon}{a_p} = d_h \tag{10.4}$$

The channel diameter is often referred to as hydraulic diameter d_h (m). The flow channel consists of three regions, the packing, the liquid holdup and the gas holdup. The liquid phase is in between the packing and the gas phase. The volume fraction of each region is (1-ε) for the packing, h_L for the liquid phase and (ε-h_L) for the gas phase. The effective gas and liquid velocities $\bar{u}_L / \bar{u}_G$ can therefore be calculated from the volume streams V_L / V_G (m^3 h^{-1}) or gas and liquid load u_L / u_G (m^3 m^{-2} h^{-1}) according to:

$$\bar{u}_L = \frac{u_L}{h_L} = \frac{V_L}{a_{cs} \cdot h_L} \tag{10.5}$$

and,

$$\bar{u}_G = \frac{u_G}{\varepsilon - h_L} = \frac{V_G}{a_{cs} \cdot \left(\varepsilon - h_L\right)}. \tag{10.6}$$

The contact time τ is the ratio of characteristic flow path length l_τ (m) and fluid velocity u (m s^{-1}):

$$\tau = \frac{l_\tau}{u} \tag{10.7}$$

This led to the following expression for liquid and gaseous phase:

$$\tau_L = \frac{h_L \cdot l_\tau}{u_L} \tag{10.8}$$

and

$$\tau_G = \frac{(\varepsilon - h_L) l_\tau}{u_G} \tag{10.9}$$

Dimensional analysis showed that the mass transfer coefficients could be determined most accurately if the characteristic length was described with the hydraulic diameter [5] from Eq. (10.4).

The liquid holdup has been calculated by the force equilibrium between gravity and shear forces inside the liquid film and drag forces from the gas stream at the interface. Up to the loading point the following theoretical expression was used for uniform and complete wetting:

$$h_L = \left(12 \frac{\eta_L}{g \cdot \rho_L} u_L \cdot a_p^2 \right)^{\frac{1}{3}} \tag{10.10}$$

When packing surface was not completely wetted the holdup expression changed to:

$$h_L = \left(12 \frac{\eta_L}{g \cdot \rho_L} u_L \cdot a_p^2 \right)^{\frac{1}{3}} \left(\frac{a_h}{a_p} \right)^{\frac{2}{3}} \tag{10.11}$$

The second factor accounted for the lower liquid surface due to de-wetting and was derived from experimental studies for two different liquid flow ranges:

$$\frac{a_h}{a_p} = C_h \cdot Re_L^{0.15} \cdot Fr_L^{0.1} \; ; \; for \; Re_L < 5 \tag{10.12}$$

and,

$$\frac{a_h}{a_p} = 0.85 \cdot C_h \cdot Re_L^{0.25} \cdot Fr_L^{0.1} \; ; \; for \; Re_L > 5 \tag{10.13}$$

The hydraulic area per volume packing a_h ($m^2\ m^{-3}$) should not be mistaken as the effective area per volume packing a_{eff} ($m^2\ m^{-3}$) which relates to the mass transfer area. They might differ due to a_h also accounting for the liquid volume in dead spaces that does not contribute to mass transfer [6]. The effective mass transfer area a_{eff} was calculated by:

$$\frac{a_{eff}}{a_p} = 3 \cdot \varepsilon^{0.5} \cdot \left(Re_L \right)^{-0.2} \cdot \left(Fr_L \right)^{-0.45} \cdot \left(We_L \right)^{0.75} \tag{10.14}$$

The mass transfer coefficients for the liquid phase were derived from inserting Eqs. (10.10) and (10.8) into (10.1)

$$k_L = 2 \cdot 12^{-\frac{1}{6}} \cdot \pi^{-\frac{1}{2}} \cdot \left(\frac{g \cdot \rho_L}{\mu_L} \right)^{\frac{1}{6}} \cdot \left(\frac{D_{CO_2}}{d_h} \right)^{\frac{1}{2}} \cdot u_L^{\frac{1}{3}} \cdot a_p^{-\frac{1}{3}} \tag{10.15}$$

Comparing this expression with experimental data for different material systems and different packings showed that this expression can be used with a packing constant C_L (-) which is characteristic for a certain shape and structure of packing:

$$k_L = C_L \left(\frac{g \cdot \rho_L}{\mu_L} \right)^{\frac{1}{6}} \left(\frac{D_{CO_2}}{d_h} \right)^{\frac{1}{2}} \cdot u_L^{\frac{1}{3}} \cdot a_p^{-\frac{1}{3}} \tag{10.16}$$

The gas side mass transfer coefficient was derived in a similar manner by inserting Eq. (10.9) into Eq. (10.1)

$$k_G = 2 \cdot \left(\frac{D_{CO_2}}{\pi \cdot d_h \cdot (\varepsilon - h_L)} \right)^{\frac{1}{2}} \cdot u_G^{\frac{1}{2}} \tag{10.17}$$

In order to account for the influence of gas load on the mass transfer Eq. (10.17) was expanded with the dimensionless Reynolds and Schmidt number [2].

$$k_G = C_V \cdot \left(\frac{a_p}{d_h \cdot (\varepsilon - h_L)} \right)^{\frac{1}{2}} \cdot D_{CO_2} \left(\frac{u_G \cdot \rho_G}{a_p \cdot \eta_G} \right)^{\frac{3}{4}} \left(\frac{\eta_G}{\rho_G D_G} \right)^{\frac{1}{3}} \tag{10.18}$$

The exponent ¾ for the Reynolds number and $^1/_3$ for the Schmidt number gave the best results. In order to keep the units right the expression was multiplied with $(D_{CO_2} \cdot a_p)^{(1/2)}$ and a characteristic packing constant C_V (-) was introduced. The constant C_V was experimentally determined for different shaped and structured packing

The mass transfer models often apply dimensionless numbers to correlate mass transfer parameters. It is very important to check how these numbers are defined, especially when a characteristic length is involved which might be defined differently in different models. The dimensionless numbers in the Billet & Schultes model were defined as [2]:

$$Re_G = \frac{u_G \rho_G}{\eta_G a_p}$$
$$Re_L = \frac{u_L \rho_L d_h}{\eta_L}$$
$$Sc_{L/G} = \frac{\eta_{L/G}}{\rho_{L/G} D_{L/G}} \qquad (10.19)$$
$$We_L = \frac{u_L{}^2 \rho_L d_h}{\sigma_L}$$
$$Fr_L = \frac{u_L{}^2}{g d_h}$$

10.1.2. SRP models

The coworkers Rocha, Bravo and Fair from the Separations Research Program (SRP) at the University of Texas at Austin conducted pioneering work on mass transfer models for structured packings. The first model was developed for gauzed metal packing [7]. They implemented characteristics from the packing geometry into their model by using an equivalent diameter d_{eq} (m). This diameter was calculated from the ratio of perimeter to cross section of the flow channel. In their later work they considered the diamond shaped flow channel and set the equivalent diameter d_{eq} equal to S like in Figure 88 [3], [8].

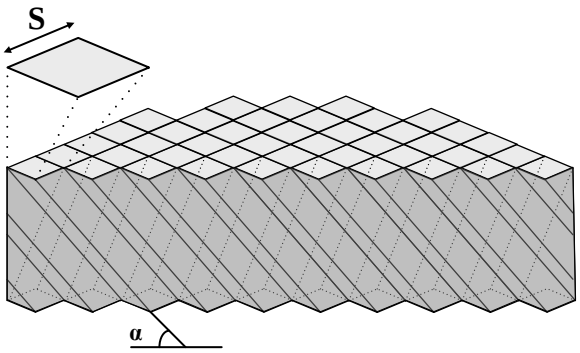

Figure 88: Structured packing geometry

The gas side mass transfer coefficient was modeled according to a wetted wall column proposed by Johnstone and Pigford [3]. The liquid side mass transfer coefficient was calculated according to the Penetration theory in Eq. (10.1). For gauze packing complete wetting ($a_{eff} = a_p$) was assumed, an assumption which did not hold for packing materials other than gauze. In 1993 [8] and 1996 [3], their expression has been reworked for the gas and liquid side coefficients slightly and a correlation for the mass transfer area was introduced. Effective gas and liquid velocities used in their models took the

volume fraction for of each phase as well as the inclination of the flow channels in the structured packing into account. For the liquid phase the effective gas velocity was calculated as:

$$u_{Le} = \frac{u_L}{\varepsilon \cdot h_L \cdot \sin\alpha} \tag{10.20}$$

With α being the inclination of the packing flow channel compared to a horizontal plane as in Figure 88. The effective gas velocity was defined as:

$$u_{Ge} = \frac{u_G}{\varepsilon \cdot (1 - h_L) \cdot \sin\alpha} \tag{10.21}$$

The incorporation of inclination of the flow channels resulted in a more realistic description of the flow conditions. Given that the velocity of fluid element inside the column is described by ratio of distance, i.e. difference in column height between two measuring points, and traveling time the elements needs between the points will give a reference velocity assuming that fluid element travelled in a straight line between the two measuring points. It does not describe the effective velocity that this fluid element exposed towards the mass transfer interface. Dividing by the sinus of the inclination angle gave the relation between reference and effective velocity.

The gas side mass transfer was calculated from a Sherwood correlation derived from wetted wall column experiments:

$$Sh_G = 0.054 \cdot \left(Re_G\right)^{0.8} \cdot \left(Sc_G\right)^{0.33} \tag{10.22}$$

With the following definitions of the dimensionless numbers:

$$Re_G = \frac{\rho_G \cdot S \cdot \left(u_{Ge} + u_{Le}\right)}{\eta_G}; Sh_G = \frac{k_G \cdot S}{D_G} \tag{10.23}$$

The gas Reynolds number was also taking the effective liquid velocity into account, as the corresponding velocity was the sum of effective gas and liquid velocity[5] . The side of the corrugation S was taken as equivalent diameter. The correlation in their earlier work from 1985 [7] used the same Sherwood correlation with the same powers, only the constant was slightly different; 0.0338 was used instead of 0.054.

[5] or rather difference between the two phases, accounting that sign is negative for the liquid velocity as it flowing into the opposite direction

The liquid side mass transfer coefficient was calculated based on the penetration theory similar to Eq. (10.1) with an exposure time τ_e:

$$\tau_e = \frac{S}{C_E \cdot u_{Le}} \tag{10.24}$$

Where C_E (-) is a correction factor with the value 0.9, accounting for parts "that do not encourage rapid surface renewal" (Rocha et al. 1996 [3]). The liquid side mass transfer coefficient became thus:

$$k_L = 2 \cdot \left(\frac{D_L \cdot C_E \cdot u_{Le}}{\pi \cdot S} \right)^{1/2} \tag{10.25}$$

For the interfacial mass transfer area correlation the surface flow model by Shi and Mersmann [9] was expanded to different inclination angles:

$$\frac{a_{eff}}{a_p} = F_{SE} \frac{29.12 \left(We_L \cdot Fr_L \right)^{0.15} S^{0.359}}{Re_L^{0.2} \cdot \varepsilon^{0.6} \left(1 - 0.93 \cos\theta \right) \left(\sin\alpha \right)^{0.3}} \tag{10.26}$$

Where θ is the contact angle between liquid and surface; the $\cos\theta$ value can be calculated as a function of the surface tension σ (N m^{-1}):

$$\cos\theta = 0.9 \; for \; \sigma < 0.055 \frac{\mathrm{N}}{\mathrm{m}}; \; \cos\theta = 5.211 \cdot 10^{-16.835\sigma} \; for \; \sigma > 0.055 \frac{\mathrm{N}}{\mathrm{m}} \tag{10.27}$$

The factor for surface enhancement F_{SE} was dependent on the packing material and needed to be determined experimentally for each packing. The dimensionless numbers used in Eq. (10.26) were defined as:

$$\begin{aligned} Re_L &= \frac{u_L \rho_L S}{\eta_L} \\ We_L &= \frac{{u_L}^2 \rho_L S}{\sigma_L} \\ Fr_L &= \frac{{u_L}^2}{gS} \end{aligned} \tag{10.28}$$

The effective gas and liquid velocities and thus the gas and liquid side mass transfer coefficients were dependent of the liquid hold up. They assumed in their holdup correlation that the static holdup can be neglected due to its very small contribution. For calculating the holdup from the diamond shaped flow channel as in Figure 88 with complete wetting they proposed:

$$h_L = \frac{Vol_L}{Vol_{column}} = \frac{4 \cdot \delta_{film}}{S} \tag{10.29}$$

This expression is correct if the inclination in the diamond shaped flow channel is 90 degree and the film thickness is quite small. The fractional area that was actually wetted was calculated from the expanded Shi-Mersmann correlation (Eq. (10.26) without F_{SE}). The film thickness was calculated from a modified correlation for a falling film from Bird et al. [10] incorporating effective velocity and effective gravity which accounts for liquid buoyancy, vapor pressure drop and drag force by vapor. The liquid hold up for a column could be calculated as:

$$h_L = \left(\frac{4 \cdot F_t}{S} \right)^{2/3} \left(\frac{3 \cdot \eta_L \cdot u_L}{\rho_L \cdot \varepsilon \cdot g_{eff} \cdot \sin\theta} \right)^{1/3} \tag{10.30}$$

with:

$$g_{eff} = g \left(\left(\frac{\rho_L - \rho_G}{\rho_L} \right) \left(1 - \frac{\frac{\Delta P}{\Delta Z}}{1025} \right) \right) \tag{10.31}$$

The pressure drop $\frac{\Delta P}{\Delta Z}$ needed to be inserted in Pa m^{-1}. The fractional wetted area F_t was calculated from Eq. (5.29), as it is the expression on the right side without the surface Enhancement factor F_{SE} . In a rebuttal Rocha et al. [11] acknowledged that the expression in Eq. (10.29) is just correct for a wetted wall columns, whereas for a real packed column the denominator needs to be multiplied by the packing porosity.

Overall the Rocha, Bravo, Fair correlations described the mass transfer in columns with structured packing as flow channels in parallel. Each flow channel was described similar to a wetted wall column with the dimensions of the actual flow channel inside the structured packing. The equivalent diameter for the calculations was taken as side of the corrugation S. The wetted area was calculated from a correlation derived from surface flow studies with various different solvents. Together with an expression for the film thickness of a falling film the holdup was calculated. This holdup influenced the effective gas and liquid velocities and thus the gas and liquid side mass transfer coefficients. They distinguished between wetted surfaces, a parameter related to hold up, and mass transfer area, by introducing the surface enhancement factor F_{SE} which was the fraction of wetted area that participated in mass transfer. This factor was determined experimentally for each packing, or packing series; it was generally in the range between 0.3 and 0.4 [3].

10.1.3. Rochelle group

The well-known research group around Dr. Rochelle developed a mass transfer model from their extensive research on carbon capture. At first they started developing a dimensionless mass transfer area model for structured packing [12]. Therefore they measured the mass transfer area for CO_2 absorption into 0.1 M NaOH with different surfactants that altered the surface tension. They proposed the following model [13]:

$$\frac{a_{eff}}{a_p} = 1.34\left[\left(We_L\right)\left(Fr_L\right)^{-1/3}\right]^{0.116} = 1.34\left(\left(\frac{\rho_L}{\sigma_L}\right) g^{1/3}\left(\frac{V_L}{L_p}\right)^{4/3}\right)^{0.116} \tag{10.32}$$

They used the film thickness according to falling film as characteristic length in the dimensionless numbers. The wetted perimeter was calculated from the packing geometry according to:

$$L_P = \frac{4 \cdot S}{B \cdot h} \cdot a_{CS} \tag{10.33}$$

Wang et al. [4] extended the model for application with random packings. As there were no easy accessible packing geometries available for random packing they exchanged the term (V_L / L_p) by (u_L / a_p) and modified the coefficient slightly for a better fit with the now larger database to:

$$\frac{a_{eff}}{a_p} = 1.41\left(\left(\frac{\rho_L}{\sigma_L}\right) g^{1/3}\left(\frac{u_L}{a_p}\right)^{4/3}\right)^{0.116} \tag{10.34}$$

For the gas and liquid side mass transfer coefficients a Sherwood analogy was chosen in the form of:

$$Sh_{L/G} = C \cdot {Re_{L/G}}^{m} \cdot {Sc_{L/G}}^{n} \cdot Mi^{p} \tag{10.35}$$

Mi was a newly introduced dimensionless mixing point density. The observation, that the gas and the liquid side mass transfer coefficients were both increasing with specific packing surface a_p and decreasing with the corrugation angle α [6], which was coherent with the mixing points density [14] led the implementation of a mixing point density into the Sherwood Analogy. Mixing points were defined as the contact points of metal sheets in the packing; its density was the amount of mixing points per unit volume. In dimensionless form Mi was defined as:

[6] In their original paper they referred to the corrugation angle as θ; the notation was changed in this work to circumvent confusion between the Rocha et al. and Wang et al. model.

$$Mi = \frac{3\sin\alpha\cos\alpha}{32\sqrt{2}} = \frac{M}{a_p{}^3} \tag{10.36}$$

They regressed the following exponents for the gas and liquid phase Sherwood number from their experimental data [4]:

$$Sh_L = 21 \cdot Re_L{}^{0.78} \cdot Sc_L{}^{0.5} \cdot Mi^{1.11} \tag{10.37}$$

and:

$$Sh_G = 14 \cdot Re_G{}^{0.59} \cdot Sc_G{}^{0.5} \cdot Mi^{1.1} \tag{10.38}$$

The characteristic length in the Reynolds and Sherwood number was taken as the reciprocal value of characteristic surface area of the packing a_p:

$$Sh_{L/G} = \frac{k_{L/G}}{D_{L/G} \cdot a_p}; Re_{L/G} = \frac{\rho_{L/G} \cdot u_{L/G}}{\eta_{L/G} \cdot a_p} \tag{10.39}$$

The exponent for the Schmidt number was not regressed, but selected from literature conclusions. The liquid hold up was calculated by multiplying the mass transfer area with the thickness of a falling liquid film.

10.2. Model Comparison

Even though with all that literature correlations for mass transfer coefficients and interfacial mass transfer area one might be tempted to pick the correlations from different sources and mix them to represent their own experimental data. Special care needs to be taken as the models are based on several assumptions, for instance the mass transfer coefficients are derived with an expression for the mass transfer area [15]. Errors in the parameter estimation are frequently canceling out when model by the same author are used together [4]. The mass transfer application itself should also be considered when choosing the right model. The different physical properties in distillation applications, which are in general mixtures of organic compounds, and absorption applications, where often aqueous solutions are used lead to difficulties to derive a mass transfer model capable to describe absorption as well as distillation [16].

The Rocha et al. model [3], as well as the Billet and Schultes model [17] were developed with a broad range of experiments of different material systems mainly in distillation processes. The Wang model was specifically developed for absorption processes from absorption experiments [4].

In order to estimate which model was suitable for the process simulation the models were compared to each other on how the effective mass transfer area a_{eff} in columns was calculated. As a reference case a

liquid load of 10 m^3 m^{-2} hr^{-1} was assumed for water, 1 M NaOH, 30 wt% MDEA and 30 wt% MEA at 40 °C. A porosity of 0.95 was taken which represents the porosity of Mellapak 250 Y [3] and the specific surface area of the packing a_p (m^2 m^{-3}) was changed accordingly.

The results of these calculations shown in Figure 89 revealed several interesting insights into the different models. The different models did account for the differences between the different solvents, 30 wt% MDEA had always the highest mass transfer area, followed by 30 wt% MEA; water and 1 M NaOH gave almost identical results. The effective surface area calculated by the Billet and Schultes model [17] were just indirectly linked to the specific surface area of the packing a_p. The model did not describe a change in effective mass transfer area once the specific area of the packing was changed. This behavior can be explained by inserting the definition of the hydraulic diameter from Eq. (10.4) into the equation for the effective mass transfer area (Eq.(10.14)). The exponents of the specific surface area of the packing a_p are then -1 on the left side and -1 (0.2-0.75-0.45=-1) on the right side thus a_{eff} is independent of a_p. The effective mass transfer area in the Billet and Schultes model just changes when the porosity is altered. According to that the mass transfer area in two different columns is the same if they have the same porosity.

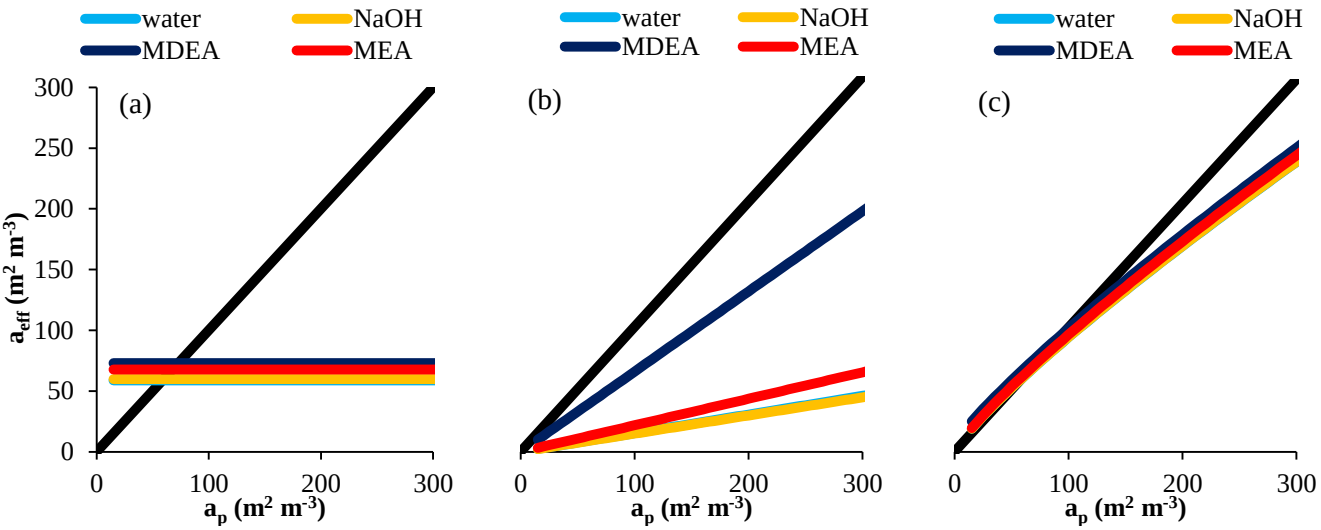

Figure 89: Effective mass transfer area a_{eff} (m^2 m^{-3}) as a function of specific area of packing a_p according to the Billet and Schultes model [17] (a), Rocha et al. model [3] (b) and Wang et al. model [4] (c) for water, 1 M NaOH, 30 wt% MDEA and 30 wt% MEA at 40 °C at 10 m^3 m^{-2} hr^{-1} liquid load; black lines indicate where a_p and a_{eff} are equal

The effective mass transfer area a_{eff} changed when the specific surface area of the packing was changed in the Rocha et al. model [3] (b). The dependency between a_{eff} and a_p was linear because the dimensionless numbers Re, We and Fr in the effective area calculation were just dependent on the liquid load (Eq. (10.28)), this value remained the same even when the surface area of the packing was changed. The mass transfer area for 30 wt% MDEA was close the surface area of the packing and much higher than for 30 wt% MEA, water and 1 M NaOH and. The great difference between

30 wt% MDEA and the other solvents was caused by the surface tension of MDEA which is slightly lower than the critical value of 0.055 N m^{-1} at 40 °C [18]. The $\cos\theta$ value jumps then to 0.9 according to Eq. (10.27) this will decrease the denominator in Eq. (10.26) and thus increase the effective area; the function for $\cos\theta$ is not consecutive around the critical surface tension as 0.055001 N m^{-1} surface tension gives a $\cos\theta$ value of around 0.618 thus a different effective area. This represents a crucial problem for the simulation of an absorber with MDEA solutions, as the surface tension of a 30 wt% MDEA solution at 20 C is above the critical surface tension, whereas at 40 °C the value is below and the temperature during absorption inside the column is likely to change.

The Wang model predicted an a_{eff} value close to the surface area of the packing; for low a_p values the a_{eff} value was even higher than the surface area of the packing. The difference between the different solvent was quite small for the Wang et al. model.

Figure 90 compares how the holdup was influenced by changes in surface area of the packing according to the different models at a constant liquid load of 10 m^3 m^{-2} hr^{-1}. For the Billet and Schultes model, the holdup increased with increasing surface area of the packing; there was almost no difference between the liquids. In the Rocha model, the holdup was not changing for difference surface areas in the packing. The holdup was higher for MDEA than for the other three liquid, a similar behavior is for the mass transfer area; the higher value of MDEA can be explained also with the critical surface tension. The effect that the holdup did not change at different surface areas of the packing can be explained as the holdup correlation from Eq. (10.30) is just sensitive to the hydraulic diameter S and not the surface area of the packing. The Wang model predicted a slight increase in hold up at higher surface areas of the packing; here almost no differences between the liquid could be observed.

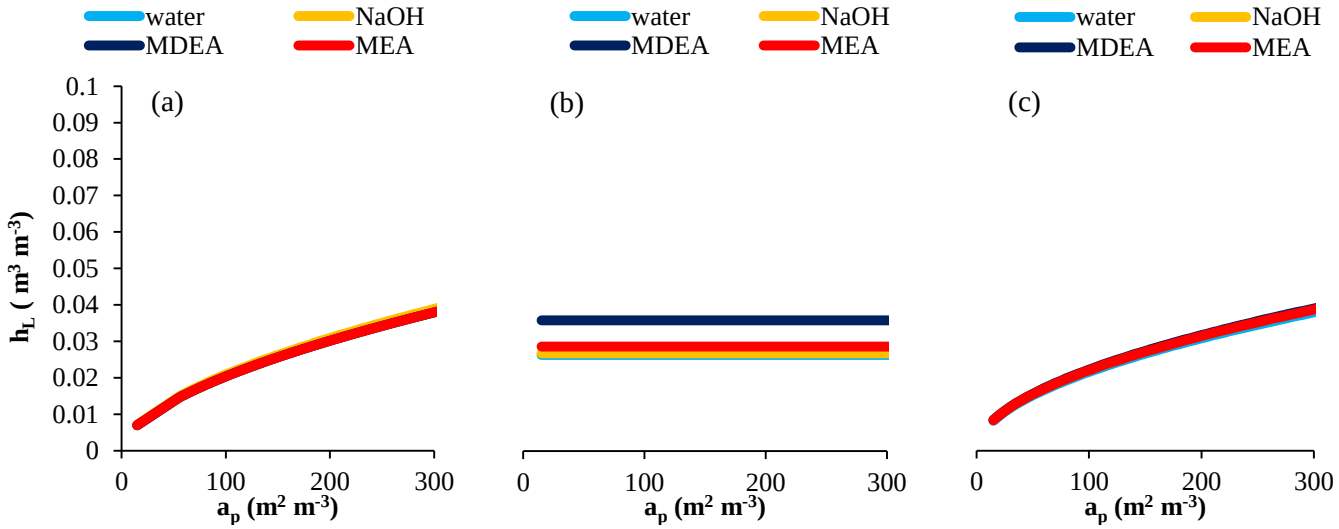

Figure 90: Liquid holdup (m^3 m^{-3}) as a function of specific area of packing a_p according to the Billet and Schultes model [17] (a), Rocha et al. model [3] (b) and Wang et al. model [4] (c) for water, 1 M NaOH, 30 wt% MDEA and 30 wt% MEA at 40 °C at 10 m^3 m^{-2} hr^{-1} liquid load

Combining the results of Figure 89 and Figure 90 gives an overview how the different models describe different columns that are just differing in surface area of the packing whereas all other properties are the same:

- The Billet and Schultes model predicted a change in liquid holdup, but not in effective mass transfer areas at different surface areas of packing.
- The Rocha et al. model predicted a change in effective surface but not in the liquid holdup at different surface areas of the packing.
- The Wang et al. model predicted an increase in liquid hold up as well as effective mass transfer area when the surface area of the packing a_p was increased.

10.2.1. Holdup

The holdup was experimentally determined for DTU's pilot absorber with water. The different model predictions for these experiments taking the surface area of the packing into account (a_p=141.12 m^2 m^{-3}) are shown in Figure 91. The Rocha model was over predicting the hold up and described a steeper trend with higher liquid loads than the experimental results. The Billet and Schultes model was also over predicting the holdup, but deviation was smaller. The Wang et al. model matched the experimental data almost perfectly for all liquid loads with and AARD of 4.4 %.

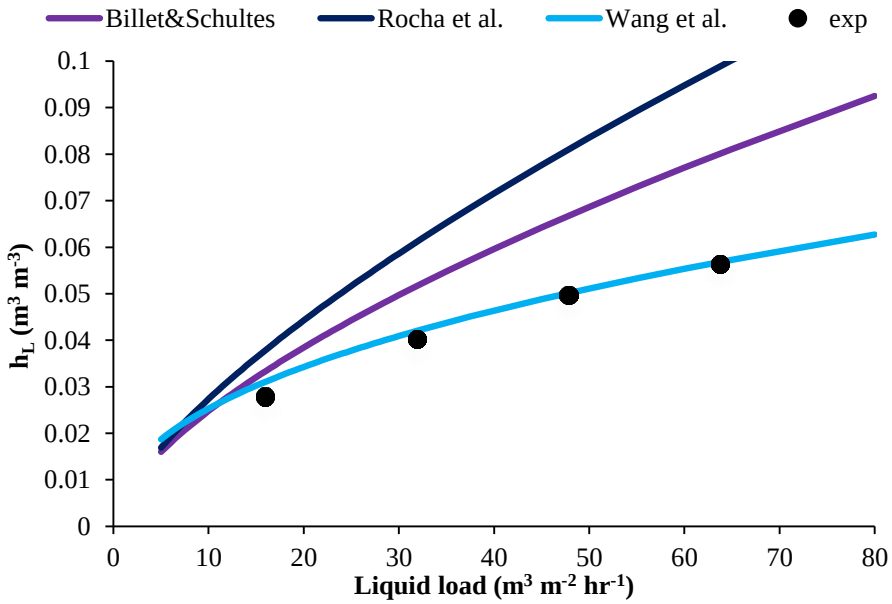

Figure 91: Comparison of Billet & Schultes, Rocha et al. and Wang et al. model predictions for holdup h_L (-) with experiments

10.2.2. Interfacial area

The mass transfer area of the column was determined by CO_2 absorption experiments into 1 M NaOH solutions as described in the chapter 8. The results from these experiments together with the results from Wang et al., Billet and Schultes and Rocha et al. model for a surface area of the packing of a_p=141.12 m^2 $m^{-3}$are shown Figure 92. The Rocha et al. as well as the Billet and Schultes model were both under predicting the effective mass transfer area. The Wang et al. model was matching the effective mass transfer area for the experiments at 2 m column very good and over predicted the results from 4 and 6 m. The Billet and Schultes model was closest to the experiments at 6 m column height.

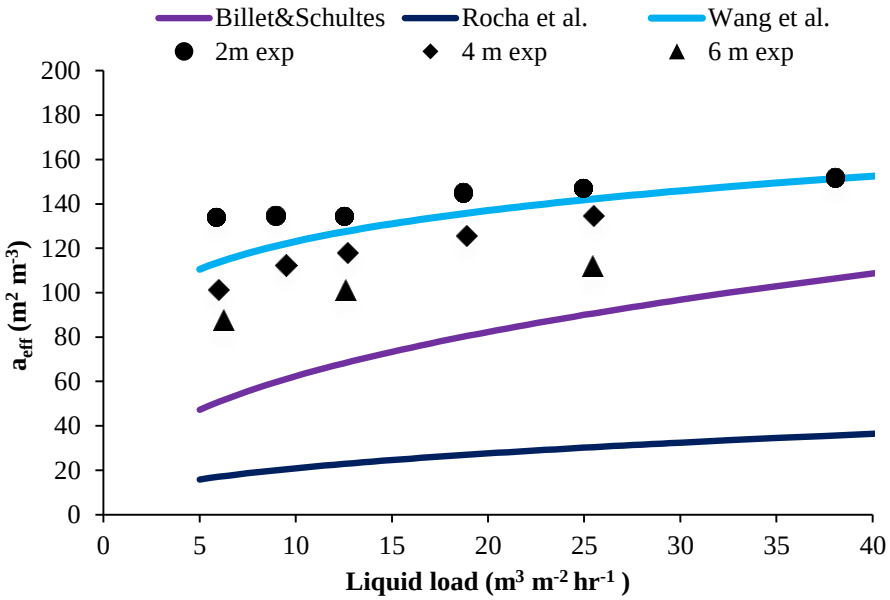

Figure 92: Comparison of Billet and Schultes, Rocha et al. and Wang et al. model predictions for effective mass transfer area a_{eff} (m^2 m^{-3}) with experiments.

10.2.3. Mass transfer model selection

The experimental pilot scale absorber in DTU is a unique setup, which offers a lot of interesting features, like variable column heights and the possibility of taking liquid samples on each meter of column height. On the same time difficulties arise in column modelling due to peculiarities connected to these features, like the packing volume not filling the whole column volume. There are two possibilities to model DTU's setup, either the column is modelled just with the volume of the packing, this would represent a 8.2 m high column with 0.084 mm diameter; or the whole volume of the glass body is taken into account, this would refer to 10.25 m height with 0.1 m diameter. The column packing Mellapak 250 Y is well studied and all the necessary parameters for the mass transfer models in literature are determined and available. These characterization experiments have been conducted in very well-defined setups, where the packing filled the whole cross section and height of the column. In case the column is just modelled with packing volume, the parameters derived from the literature can be used. The transferability of these parameters to a model, which takes the whole column as reference,

is questionable. On the other side modelling DTU's column with just the packing volume results in wrong residence times for the liquid and the gas phase.

For column modelling it was decided refer to the whole column volume of the empty glass body and modify the other parameters, like the surface area of the packing accordingly. This choice impinged the selection of the Wang et al. model for the column modelling. The Wang et al. model performed the best in simulating the holdup and mass transfer area for 2 m. It also offered the ability to modify the mass transfer area by changing the surface area of the packing.

10.3. CAPCO2 modelling

CAPCO2 is a rate-based DTU CERE inhouse absorber/desorber column model for carbon capture. The foundation for that model was developed by Jostein Gabrielsen in 2007 [19]. The model was later extended in several steps. It is based on several equations for heat and mass balance and considers changes in composition and temperature of the gas and liquid flow rates. The model describes the phases as two counter currently flowing plugflow reactors with a certain contact area. The model is solved with a formulated boundary value problem with fixed inlet conditions for the phases. The mass transfer areas as well as the mass transfer coefficients come from the implemented mass transfer models. The CAPCO2 model was previously used to simulate CO_2 capture with AMP solutions [20], MEA solutions [21] as well as aqueous PZ [22] and enzyme enhanced MDEA [23].

Within this study the enzyme enhanced MDEA model by Gaspar et al. [23] was upgraded by implementation of an new enzyme kinetic model for the CA reaction and the Wang et al. model [4] for mass transfer was implemented. The implementation of these features into the framework of CAPCO2 was performed by Jozsef Gaspar. The CAPCO2 model was then validated against the pilot plant data derived within this work. For the model validation, just the surface area of the packing was changed and no fitting of kinetic constants or other properties was conducted.

10.3.1. MEA results

A surface area of the packing a_p of 250 m^2 m^{-3} gave the best results for the MEA campaign. A value higher than the surface area of the packing in the column might seem unreasonable, although this value might most likely come from MEA model implemented into CAPCO2, as it uses a Henry's coefficient from the extended UNIQUAC model. The model's values for the Henry's coefficient were on average 2-3 times higher than values from the N_2O analogy of Luo et al. for the same concentrations and temperatures.

The comparison of solvent loading profile in experiments and simulation is shown in Figure 93. The model was capable of describing the rich loading of every experiment with very high accuracy. The trend of the solvent loading inside the column was also predicted with very high accuracy, indicating a reaction zone in the top of the column at low L/G ratios and in the bottom of the column at high L/G

ratios. There was a slight deviation in solvent loading in the top part of the column for very low L/G ratios, which might be linked to overestimation of the column temperature in the top of the column. The temperature trends were described very well in the bottom part of the column with the CAPCO2 model, only at higher temperature a deviation of less than 5 °C, most likely due to heat loss, were observed. For very high and very low L/G ratios the temperature profiles are very much align. In the top part of the column the model over predicted the actual column temperature as it described the hottest part in the column head for L/G ratios of 4.5 or below.

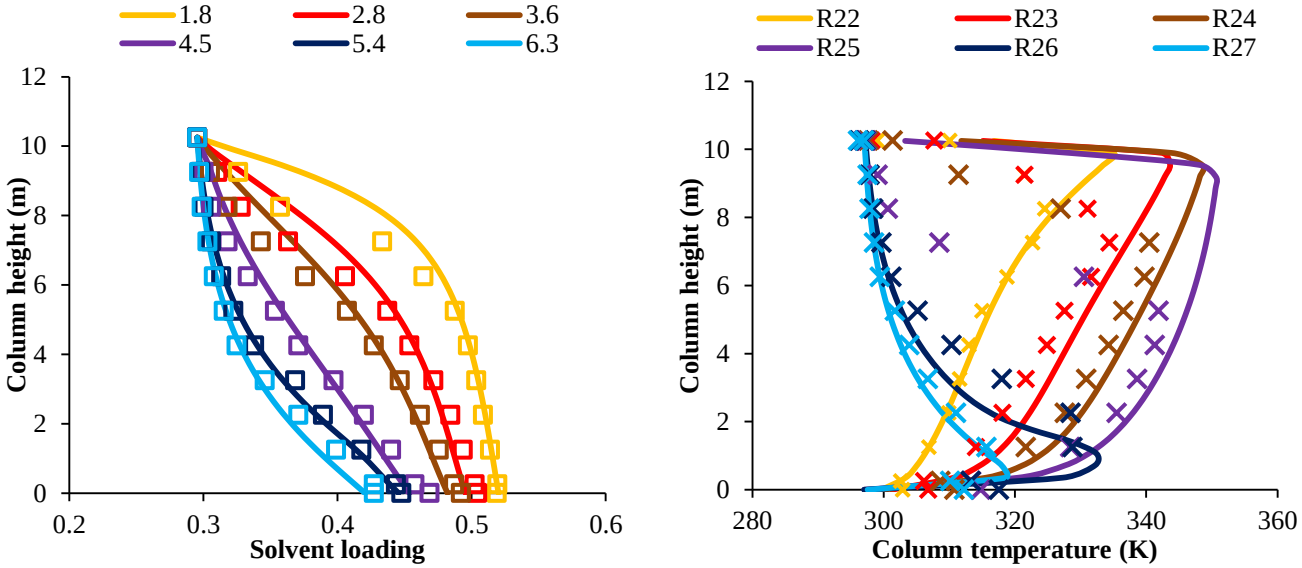

Figure 93: Comparison of solvent loading and temperature profiles between CAPCO2 model simulation and experiments for 30 wt% MEA at 10 m column height; numbers indicate L/G ratio of the experiments

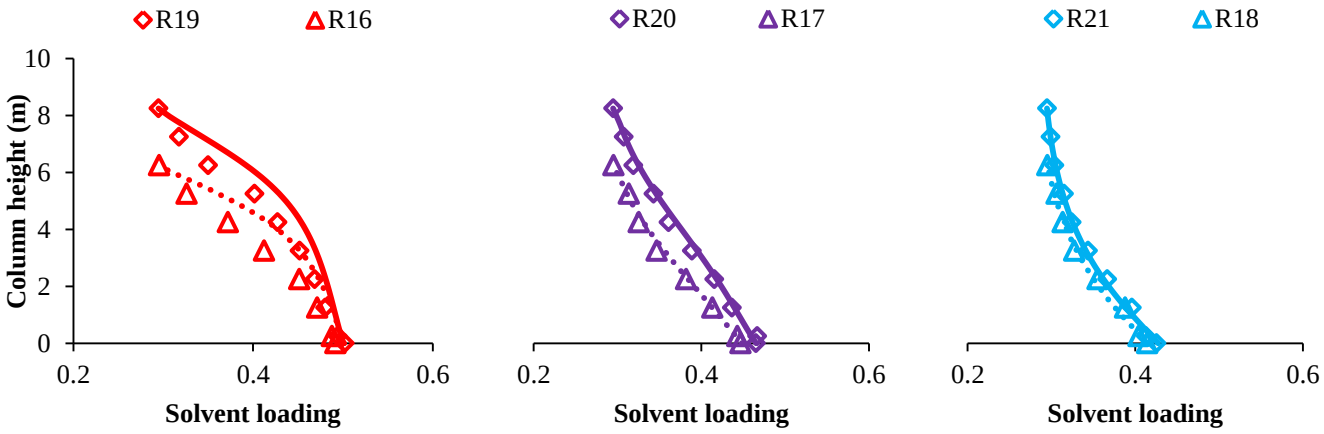

Figure 94: Comparison of solvent loading profile between CAPCO2 model simulation and experiments for MEA experiments at 6-8 m column height for 2.7 (a), 4.4 (b) and 6.2 (c) L/G ratio

The CAPCO2 also described the solvent loading profile very good at 6 and 8 m column height as shown in Figure 94. Only 2.7 L/G ratio the model over predicted the solvent loading profile inside the column a bit, although the outlet loading was described correctly. The experimentally determined solvent loading profiles for 4.4 and 6.2 L/G were perfectly aligned with the model predictions.

10.4. MDEA campaigns

In this model the Henry's coefficient was the same as the one used in to derive kinetic enzyme model in chapter 7. A surface area of the packing a_p of 100 m^2 m^{-3} was found to suit best, which is much closer to the theoretical total packing inside the column (141.12 m^2 m^{-3}). The mass transfer area determination experiments with NaOH in Figure 89 had shown results slightly over 100 m^2 m^{-3} for 6 m column height, making 100 m^2 m^{-3} reasonable for 10 m column height. This surface area of the packing resulted in good agreement of solvent loading profile for 30 wt% MDEA without CA at 10 m column height for 28 and 40 °C as shown in Figure 95.

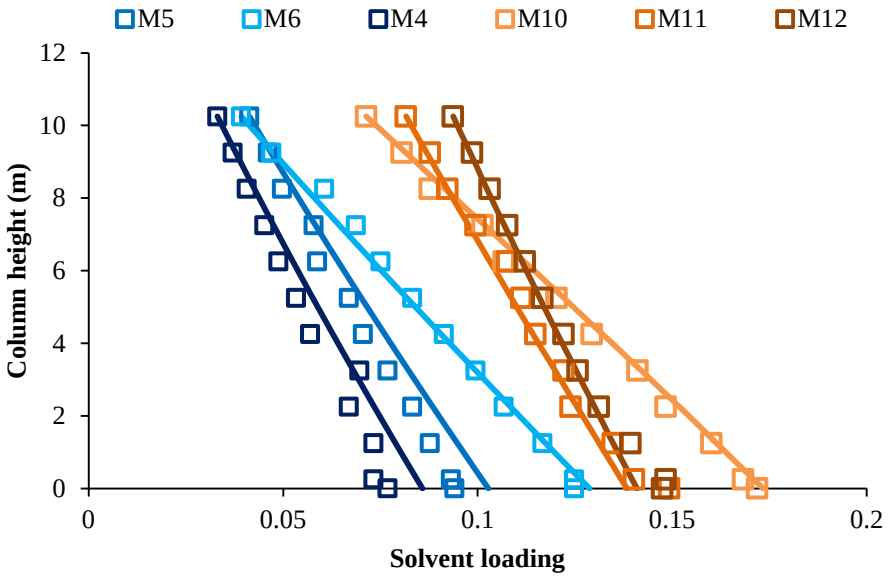

Figure 95: Comparison of solvent loading profile between CAPCO2 model simulation and experiments for MDEA without enzyme at 10 m column height; blue symbols were carried at 28 °C, brown-orange symbols at 40 °C

The implementation of the enzyme kinetic model with reversible enzyme reactions (MR) and the kinetic constants derived in chapter 7 without adjusting the surface area of the packing resulted in very good prediction of the solvent loading profile for enzyme enhanced MDEA solutions with 0.85 g/L CA at 28 and 40 °C as shown in Figure 96. Only experiments at 40 °C and a low L/G ratio (3.5) show a slight deviation between experiments and simulation. This deviation was caused by an over estimation

of column temperature in the model. As the equilibrium partial pressure of CO_2 is very temperature dependent for MDEA solutions, this will lead to an underestimation of the driving force.

The CAPCO2 model gave very good results even at a CA concentration of 3.5 g/L as shown in Figure 97. The solvent loading profiles and temperature profiles for absorption experiments were very much aligned with the model over the total height of 10 m for L/G ratios of 4.7 and 6.5. For the low L/G ratio a similar behavior as before could be observed as the solvent loading profile was under predicted in the bottom of the column. The temperature profile to this experiment could confirm that this behavior was responsible for the deviation between model and experiments.

The graphs in Figure 96 and Figure 97 exemplify that the incorporated kinetic enzyme model is capable of describing the mass transfer inside the column during absorption.

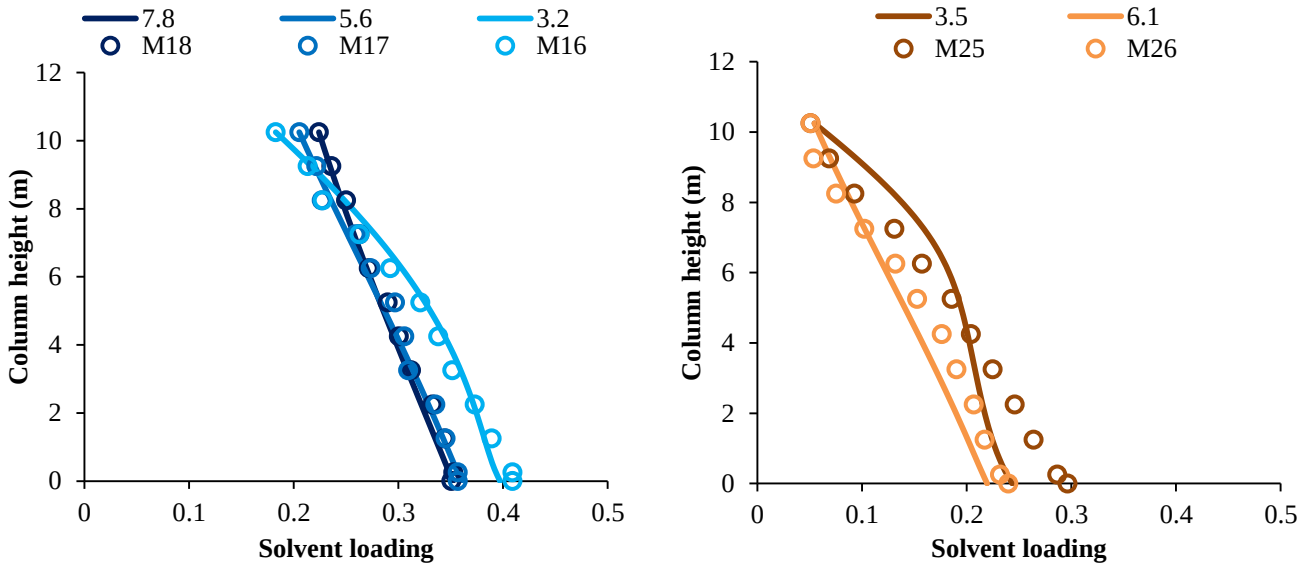

Figure 96: Comparison of solvent loading profile between CAPCO2 model simulation and experiments for MDEA with 0.85 g/L CA at 28 °C (left) and 40 °C (right); numbers indicate L/G ratio label the identification number.

The simulation results from the experiments at different column heights for MDEA solutions at 28 °C and 40 °C enhanced with 0.85g/L CA as well as for 30 wt% MDEA solutions with 3.5 g/L at two different lean loadings are shown in Figure 98. The CAPCO2 model with implemented enzyme kinetics was very accurately describing every trend depicted in these graphs. The influence of solvent temperature as well as the L/G was predicted very well for every column height for experiments with 0.85 g/L CA. The model was also capable to describe the influence of lean loading for every column height tested with very high precision for experiments with 3.5 g/L CA shown on the right side of Figure 98.

The influence of L/G ratio on capture efficiency could be simulated with good agreement to the experiments for 10 column height shown in Figure 99. Only for low L/G ratios there was a deviation between model and experiments, where the model under predicted the capture efficiency. This could be attributed to overestimation of process temperature inside the absorber for low L/G ratios.

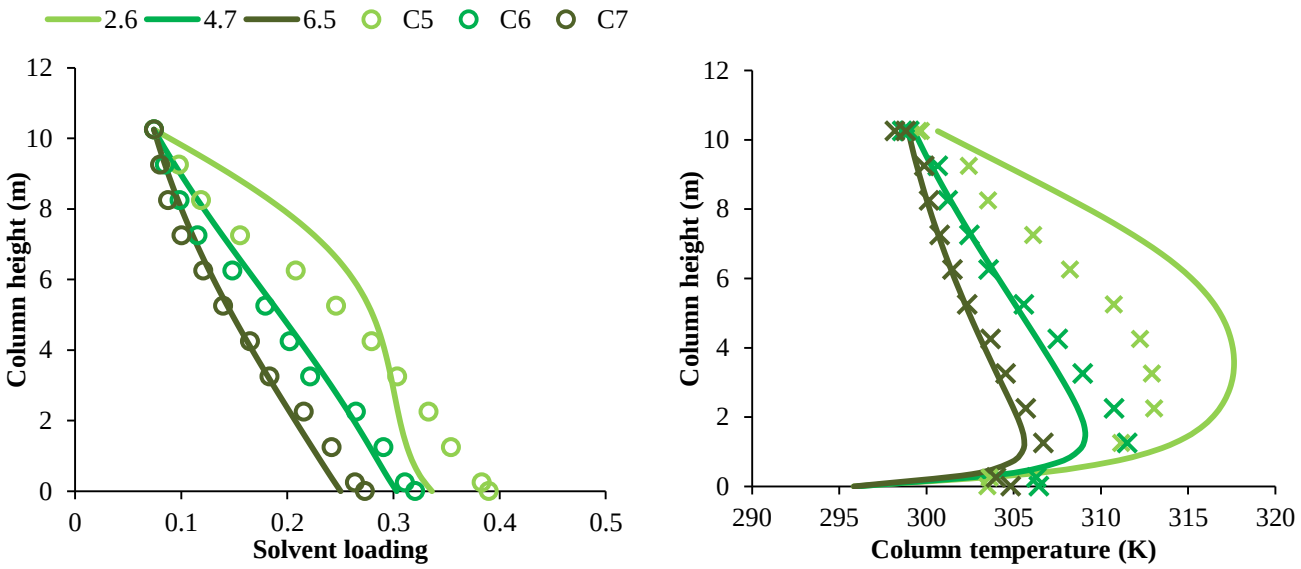

Figure 97: Comparison of solvent loading and temperature profile between CAPCO2 model simulation and experiments for MDEA with 3.5 g/L CA at 28 °C

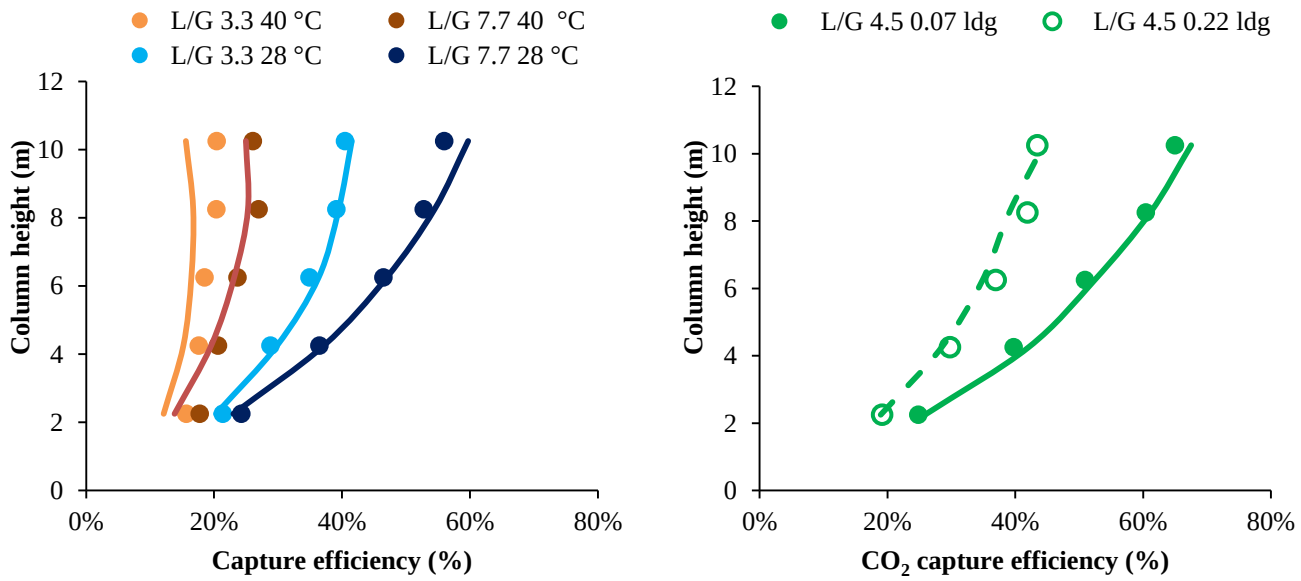

Figure 98: Comparison of capture efficiency between CAPCO2 model simulation and experiments for MDEA with 0.85 g/L CA on the left and 3.5 g/l CA on the right, at different column heights

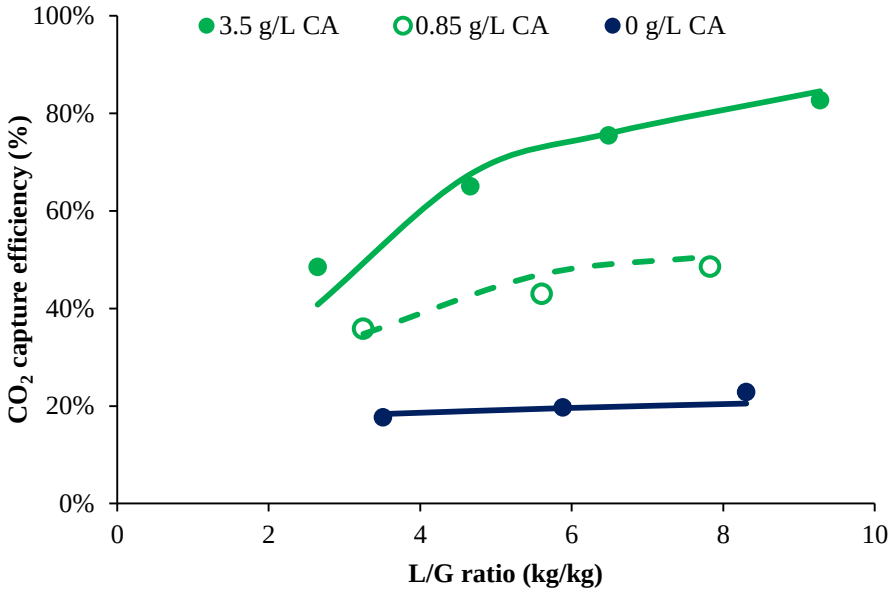

Figure 99: Comparison of capture efficiency between CAPCO2 model simulation and experiments for 30 wt% MDEA, 30 wt% MDEA with 0.85 g/L CA and 30 wt% with 3.5 g/l CA at 10 m column height for different L/G ratios

The simulation results presented here were calculated with the MR model, incorporating the mechanism of reversible enzyme reactions. The differences in the simulation results for the different models are shown in Figure 100.

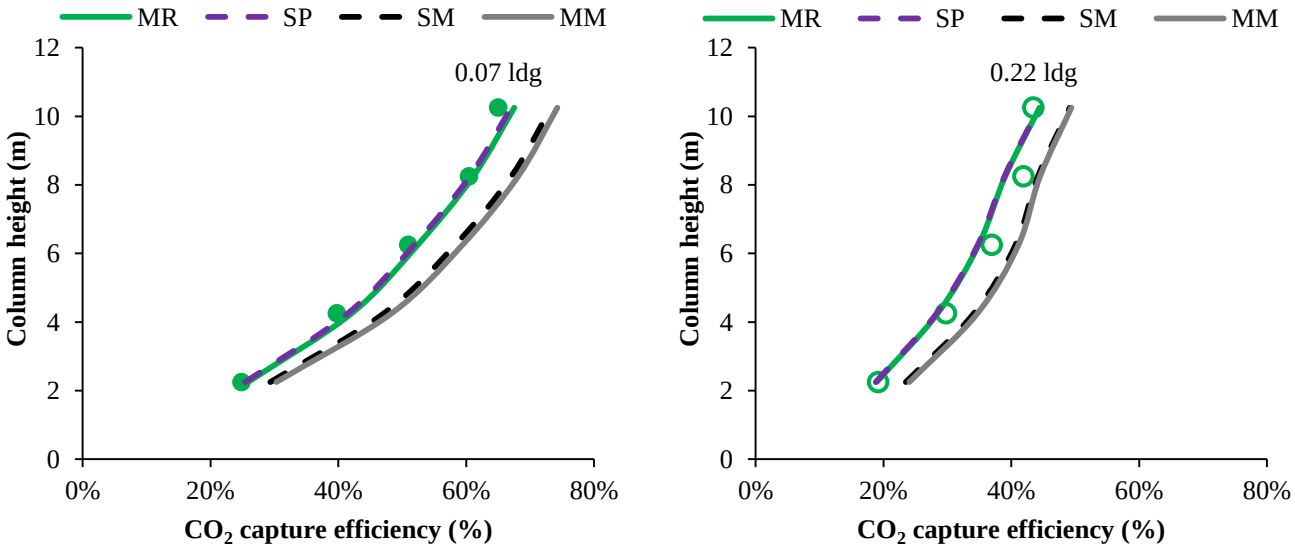

Figure 100: Comparison of the different enzyme kinetic models (MR, SP, SM and MM) implemented into CAPCO2 with experimental results for experiments with 30 wt% MDEA with 3.5 g/L CA at different column heights for 0.07 lean loading (left) and 0.22 lean loading (right)

Here no adjustment to the surface area of the packing was conducted. The MR and SP model were overlapping and were predicting the trends of capture efficiency for the different column heights and different solvent loadings accurately. The SM and MM model were also overlapping and were over predicting the mass transfer. The gap between the experimental results and the simulation was increasing for the higher loaded solvent, which resulted from the missing solvent loading influence in the enzyme kinetics.

The parity plots for all experiments with 30 wt% MDEA, and 30 wt% MDEA with 0.85 g/L CA at 28 °C and 40 °C as well as MDEA at 28 °C with 3.5 g/L are shown in Figure 101. The CAPCO2 model was accurately describing the absorption into 30 wt% MDEA at different temperatures. For 30 wt% MDEA solutions with 0.85 g/L CA at 28 °C experiments were carried out at different column heights ranging between 2 and 10 meters for different liquid loads (or L/G ratios) as well as different lean solvent loadings. Here the CAPCO2 could describe the mass transfer with an average absolute relative deviation (AARD) of 3.3 % with a maximum deviation of 6.9 % for a total of 19 pilot scale runs at all different process conditions. The model prediction for 30 wt% MDEA solutions with 0.85 g/L CA at 40 °C was worse. Excluding three runs with an average deviation of around 45 % under the assumption of a systematic error in the three following runs brings the AARD of model prediction to 14.6 % for the remaining 14 pilot scale experiments with a maximum deviation of 24.6 %. If the three runs are included the AARD value is 17.9 % for 17 pilot scale experiments in total.

For a 30 wt% MDEA solution with a CA concentration of 3.5 g/L the CAPCO2 was capable of describing the mass transfer with an AARD of 6.9 % for 22 pilot experiments with the highest deviation being 20.1 %.

The highest deviations were observed at high loaded solvents and solutions at higher temperature. This does not prove that the inhibition model is not capable to describe solutions with high solvent loading or failed at higher temperature, it is more an indicator that the model is very sensitive to temperature changes in that range as that the equilibrium CO_2 partial pressure of the solutions are changing.

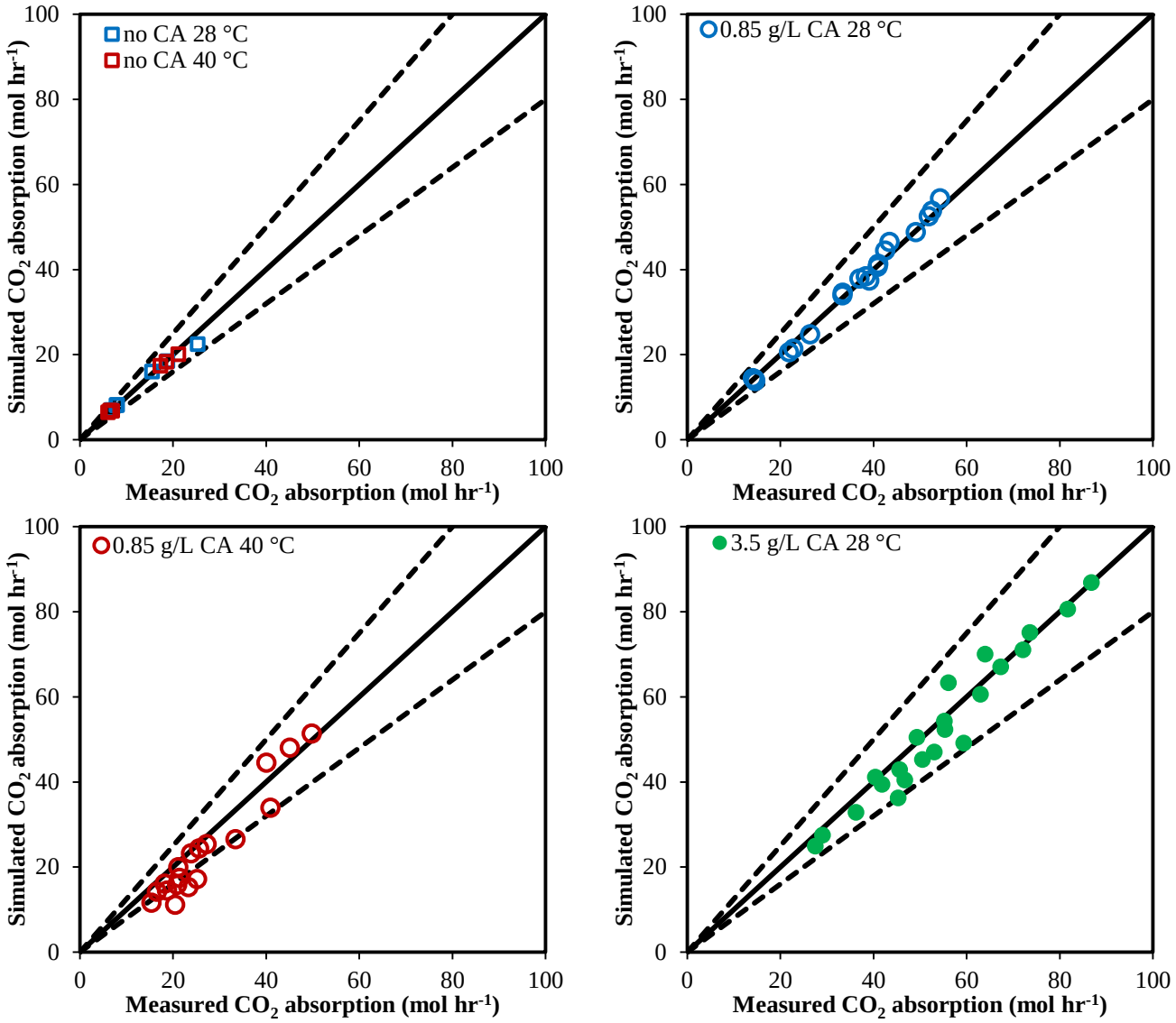

Figure 101: Parity plots for the pilot plant experiments conducted with MDEA and enzyme enhanced MDEA; dashed lines indicate ±20% deviation

10.5. Sensitivity analysis

A small sensitivity analysis was conducted with the CAPCO2 model to visualize the effect of the different process parameter on the capture efficiencies for an absorber column. The process parameters for the reference case are summarized in Table 11. The column characteristics are thought to be the same as the pilot plant at DTU (100 m^2 m^{-3} surface area of the packing) although the dimensions were chosen larger. The solvent was 30 wt% MDEA with a lean loading of 0.12 at 25 °C according to the average liquid side mass transfer coefficient case calculated in chapter 6, this represents an equilibrium CO_2 partial pressure of the solution of 0.5 kPa at the liquid inlet; the enzyme concentration was 1 g/L.

Table 11: Process parameter for the reference case in the sensitivity analysis

height	m	20
diameter	m	5
LL	$m^3\ m^{-2}\ hr^{-1}$	16
L/G	$kg\ kg^{-1}$	7
MDEA	wt%	30
Loading	$mol\ mol^{-1}$	0.12
T Liquid	°C	25
T gas	°C	50
yCO_2	-	0.12
yH_2O	-	0.12
P	kPa	101.35
Cenz	g/L	1

The Liquid load of 16 $m^3\ m^{-2}\ hr^{-1}$ was chosen as this was in the range of the pilot plant experiments conducted in this study. The gas stream in the sensitivity analysis had a temperature of 50 °C with a CO_2 mol fraction of 0.12 and was assumed to be saturated with water vapor. The volume flow of the gas was based on the L/G ratio, which was chosen as 7 in the reference case.

The reference case resulted in a capture efficiency of 88 % and was thus close the 90 % capture that is aimed for in most processes. The sensitivity analysis was simulated by changing just one parameter and keeping all others constant to the reference case. For the variation of the L/G ratio, it was assumed that the liquid load is changing and not the gas load. The results for the sensitivity analysis are shown in Figure 102, with the red dashed line representing 90 % capture, the values are summarized in Table 56 and Table 57 in Appendix C.

The enzyme concentration had a strong influence on the capture efficiency for low enzyme concentrations. At an enzyme concentration between 1 and 1.5 g/L 90 % of the CO_2 could be capture in the column. A further increase in enzyme concentration did just increase the capture efficiency slightly; 100 % capture efficiency could not be achieved with MDEA. The L/G ratio of the process was influencing the capture efficiency for values below 6 a lot. The solvent was loaded up to the thermodynamic equilibrium in that which can explain the almost linear increase in capture efficiency in that region. 90 % capture could be obtained at an L/G ratio of about 8; a further increase in L/G ratio hardly affected the capture efficiency.

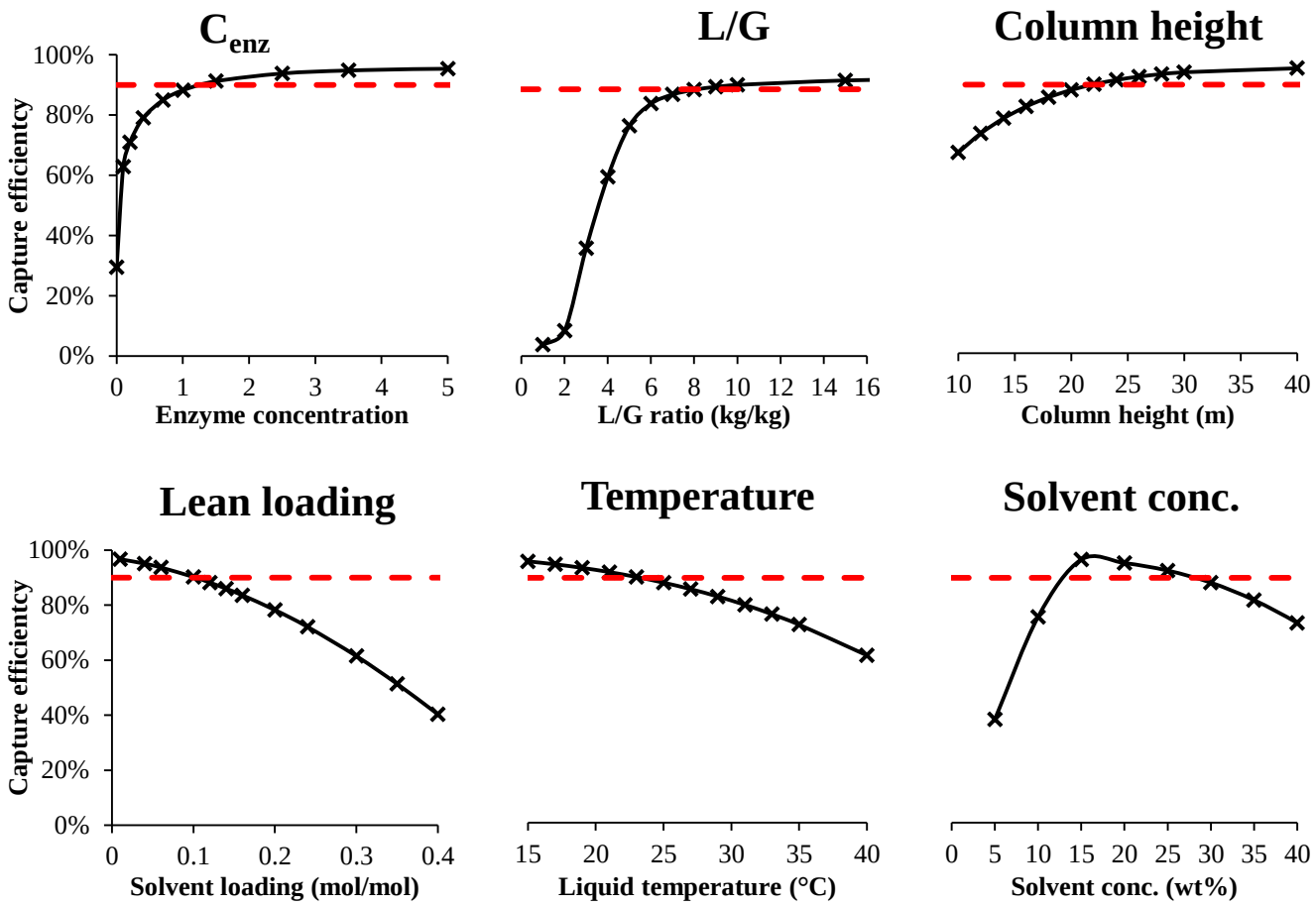

Figure 102: Sensitivity analysis for the enzyme enhanced CO_2 capture process

The capture efficiency was decreasing at values below reference height of 20 m. A column half the height would have a capture efficiency of around 67 %. The capture efficiency could be increased with a lower lean loading and a lower liquid temperature. An increase in lean loading to 0.3 (mol/mol) and inlet temperature to 40 °C had similar effects, as both decreased the capture efficiency to 61 %. The effect of solvent concentration on the capture efficiency showed an interesting effect, as solvent concentrations of 15-25 wt% MDEA provided higher capture efficiencies than the reference case. A higher solvent concentration led to a decrease in capture efficiencies. The effects shown in this sensitivity analysis are dependent on the reference case. A change in one parameter will likewise bring different trends. In this sensitivity analysis it looked like, a change in enzyme concentration to a value higher than the reference case hardly affected the capture efficiency which holds for a column height of 20 m and an L/G ratio of 7.

The effect of enzyme concentration at different L/G ratios and different column heights is shown in Figure 103, with the values summarized in the Appendix. On the left side the capture efficiencies of 30 wt% MDEA with no enzyme or 0.5, 1 and 3.5 g/L CA at different L/G ratios are shown. The effect

of the enzyme is clearly visible as the plain 30 wt% MDEA can just capture 35 % of the CO_2 in the column at an L/G ratio of 20, whereas all enzyme enhanced solvents can capture 90 %. At high enzyme concentrations the capture efficiency can be explained with two linear trends, at low L/G ratios the capture efficiency was rising linearly up to 5 L/G ratio, at L/G ratios over 7 the capture efficiency becomes almost constant., all enzyme enhanced solvents are all following the same linear trend despite their enzyme concentration for low L/G ratios. This indicates that in this region the capture efficiency is limited by the solvent capacity. The solvent cannot take up more CO_2 because it is loaded until the thermodynamic equilibrium and the capture efficiency is thermodynamically limited; this thermodynamic limitation is linked to the gas inlet and liquid outlet.

When the L/G ratio is increased more solvent participates in the mass transfer, which will decreases the solvent loading and shift the mass transfer away from the thermodynamic limitation towards a kinetic limitation. In that region the mass transfer of CO_2 becomes dependent on the reaction rates of solvent and CO_2. The second asymptotic line where the capture efficiencies are not increasing anymore at higher L/G ratios is another thermodynamic limitation linked to the gas outlet and liquid inlet. The solvent can just decrease the CO_2 partial in the gas phase to a level, where the CO_2 partial pressure in the gas outlet is equal to the equilibrium CO_2 partial of the lean solvent.

The L/G ratio needed to achieve 90 % capture decreased with higher enzyme concentration. With 0.5 g/L CA a L/G ratio of 20, at 1 g/L 8 L/G ratio and at 3.5 g/L around 5.5 L/G ratio would be needed for a 90 % capture. An increase in enzyme concentration will not enable lower L/G ratios because of the thermodynamic limitation at the gas inlet (liquid outlet) as the solvent will be loaded to equilibrium and cannot take up more CO_2.

On the right side in Figure 103 the effect of column heights on the capture efficiencies for different enzyme concentrations are compared. Increasing the column height to 40 m still did not result in capture efficiencies of over 90 % for MDEA without enzyme. The effect of enzyme concentration becomes more apparent at different column heights, as for a 90 % capture just a 14 m high column is needed with a CA concentration of 3.5 g/L. At 1 g/L CA concentration the column should be 22 m and for 0.5 g/L the column should be double the height than for 3.5 g/L CA (28 m).

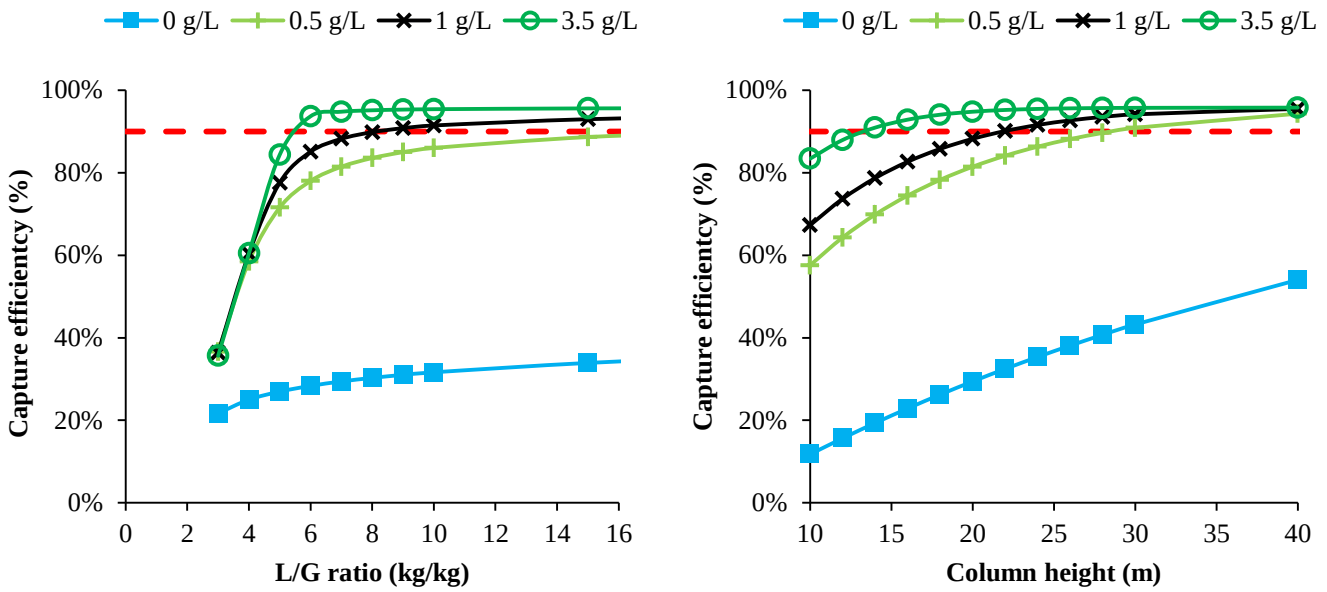

Figure 103: Sensitivity analysis for influence of L/G ratio (left) and column height (right) on capture efficiency for different enzyme concentrations

Two simulation efforts with enzyme enhanced MDEA solutions in packed columns can be found in literature. The approach to simulate the absorbers was different in these studies. Penders van Elk and Versteeg [24] used enzyme kinetics derived from lab experiments and implemented it into an absorber column model without validation to experimental pilot plant data. Leimbrink et al. derived the mass transfer model by fitting the kinetic constants against pilot plant data at two temperatures [25]. The model validation was shown by predicting experiments at different liquid loads, although no sensitivity analysis was carried out.

The findings of the simulation study of Penders van Elk and Versteeg [24] were in agreement with the sensitivity analysis as well as the experiments in this study. They concluded that the enzymes enhancement is the highest at low to moderate temperatures. The highest mass transfer was obtained with 10 wt% MDEA solutions, in this study the highest capture efficiency was obtained at around 15 wt% MDEA. They concluded that a too low MDEA concentration is not favorable for a process, as it results in higher liquid flows. Adding 1 g/L or more CA to MDEA solutions with 20-30 wt% solvent concentrations resulted in absorber heights required for 90 % CO_2 capture comparable to 30 wt% MEA (30 m or less). They also showed that the energy demand for the total capture process for enzyme enhanced 30 wt% MDEA was equal to 30 wt% MEA at the same column heights. An increase in column height led to higher reduction in energy requirement for enzyme enhanced solvents compared to 30 wt% MEA. In this study no energy requirements for the whole process have been calculated due to the uncertainty regarding the desorption conditions.

BIBLIOGRAPHY

[1] K. Onda, H. Takeuchi, and Y. Okumoto, "Mass Transfer Coefficients Between Gas and Liquid Phases in Packed Columns," *J. Chem. Eng. Japan*, vol. 1, no. 1, pp. 56–62, 1968.

[2] R. Billet and M. Schultes, "Predicting mass transfer in packed columns," *Chem. Eng. Technol.*, vol. 16, no. 1, pp. 1–9, 1993.

[3] J. A. Rocha, J. L. Bravo, and J. R. Fair, "Distillation Columns Containing Structured Packings: A Comprehensive Model for Their Performance. 2. Mass-Transfer Model," *Ind. Eng. Chem. Res.*, vol. 35, pp. 1660–1667, 1996.

[4] C. Wang, D. Song, F. A. Seibert, and G. T. Rochelle, "Dimensionless Models for Predicting the Effective Area, Liquid-Film, and Gas-Film Mass-Transfer Coefficients of Packing," *Ind. Eng. Chem. Res.*, vol. 55, no. 18, pp. 5373–5384, 2016.

[5] R. Billet, *Packed Towers*. VCH, 1995.

[6] R. Billet, "of Packed Columns up to the Flood Point," vol. 18, pp. 371–379, 1995.

[7] J. L. Bravo, J. A. Rocha, and J. R. Fair, "Mass transfer in gauze packings," *Hydrocarb. Process.*, pp. 91–95, 1985.

[8] J. A. Rocha, J. L. Bravo, and J. R. Fair, "Distillation Columns Containing Structured Packings: A Comprehensive Model for Their Performance. 1. Hydraulic Models," *Ind. Eng. Chem. Res.*, vol. 32, pp. 641–651, 1993.

[9] M. G. Shi and A. Mersmann, "Effective interfacial area in packed columns," *Ger. Chem. Eng.*, vol. 8, pp. 87–96, 1985.

[10] B. Bird, W. E. Stewart, and E. N. Lightfoot, *Transport Phenomena*, 2nd ed. Wiley & Sons, 2000.

[11] J. A. Rocha, J. L. Bravo, and J. R. Fair, "Rebuttal to the Comments of Dr . Jun-Hong Qiu on ' Distillation Columns Containing Structured Packings : A Comprehensive Model for Their Performance. 1. Hydraulic Models,'" *Ind. Eng. Chem. Res.*, vol. 38, pp. 3188–3189, 1999.

[12] R. E. Tsai, P. Schultheiss, A. Kettner, J. C. Lewis, a. F. Seibert, R. B. Eldridge, and G. T. Rochelle, "Influence of surface tension on effective packing area," *Ind. Eng. Chem. Res.*, vol. 47, no. 4, pp. 1253–1260, 2008.

[13] R. E. Tsai, F. A. Seibert, R. B. Eldridge, and G. T. Rochelle, "A Dimensionless Model for Predicting the Mass-Transfer Area of Structured Packing," *AIChE J.*, vol. 7, no. 5, pp. 1173–1184, 2011.

[14] C. Wang, M. Perry, F. Seibert, and G. Rochelle, "Packing characterization for post combustion CO2 capture: Mass transfer model development," *Energy Procedia*, vol. 63, pp. 1727–1744, 2014.

[15] C. R. Murrieta, A. F. Seibert, J. R. Fair, and J. A. Rocha-u, "Liquid-Side Mass-Transfer Resistance of Structured Packings," *Ind. Eng. Chem. Res.*, vol. 43, pp. 7113–7120, 2004.

[16] J. F. Rejl, J. Haidl, and L. Valenz, "Development of the novel rate-based mass-transfer model for the packed absorption and distillation columns," in *22nd International Congress of Chemical and Process Engineering CHISA*, 2016.

[17] R. Billet and M. Schultes, "Prediction of Mass Transfer Columns with Dumped and Arranged Packings: Updated Summary of the Calculation Method of Billet and Schultes," *Chem. Eng. Res. Des.*, vol. 77, no. September, pp. 498–504, 1999.

[18] E. B. Rinker, D. W. Oelschlager, a. T. Colussi, K. R. Henry, and O. C. Sandall, "Viscosity, Density, and Surface Tension of Binary Mixtures of Water and N-Methyldiethanolamine and Water and Diethanolamine and Tertiary Mixtures of These Amines with Water over the Temperature Range 20-100.degree.C," *J. Chem. Eng. Data*, vol. 39, no. 2, pp. 392–395, 1994.

[19] J. Gabrielsen, "CO 2 capture from coal fired power plants," *Phd thesis Tech. Univ. Denmark*, 2007.

[20] J. Gabrielsen, M. L. Michelsen, E. H. Stenby, and G. M. Kontogeorgis, "Modeling of CO2 Absorber Using an AMP Solution," *AIChE J.*, vol. 52, no. 10, pp. 3443–3451, 2006.

[21] L. Faramarzi, G. M. Kontogeorgis, M. L. Michelsen, K. Thomsen, and E. H. Stenby, "Absorber model for CO2 capture by monoethanolamine," *Ind. Eng. Chem. Res.*, vol. 49, no. 8, pp. 3751–3759, 2010.

[22] J. Gaspar and P. L. Fosbøl, "Simulation and multivariable optimization of post-combustion capture using piperazine," *Int. J. Greenh. Gas Control*, vol. 49, pp. 227–238, 2016.

[23] J. Gaspar, A. Gladis, J. M. Woodley, K. Thomsen, N. von Solms, and P. L. Fosbøl, "Rate-based Modelling and Validation of a Pilot Absorber Using MDEA Enhanced with Carbonic Anhydrase (CA)," *Energy Procedia*, 2016.

[24] N. J. M. C. P. Elk and G. F. Versteeg, "Enzyme-enhanced CO2 absorption," in *Absorption-Based Postcombustion Capture of Carbon Dioxide*, no. 2014, Elsevier Ltd, 2016, pp. 225–258.

[25] M. Leimbrink, S. Tlatlik, S. Salmon, A. Kunze, and T. Limberg, "CO 2 Capture by Enzymatic Reactive Absorption in Packed Columns - Experimental Investigation and Modelling," *Int. J. Greenh. Gas Control*, 2017.

11. Desorption

This chapter summarizes the efforts conducted concerning desorption of enzyme containing solutions. It analyzes the process options for enzyme catalyzed CO_2 desorption and presents a process outline for low temperature desorption without a reboiler utilizing a stripping gas carrier. The influences of liquid flow rate, stripping gas flow rate as well as column height on the desorption process are compared on the pilot scale setup.

11.1. Process outline of enzyme handling CCS processes

In a simplified process outline for the CCS process the setup consists of an absorber and desorber column. The enzyme in the process can be either flowing free in the solution or can be immobilized on the packing material. The immobilization as well as separation of the enzyme with a filtration unit like a membrane can hinder the enzyme to be present in the other column. Considering the process options enzyme in solution, immobilized enzymes and no enzyme present, the following process combinations for a CCS process applying enzyme are possible as shown in Figure 104.

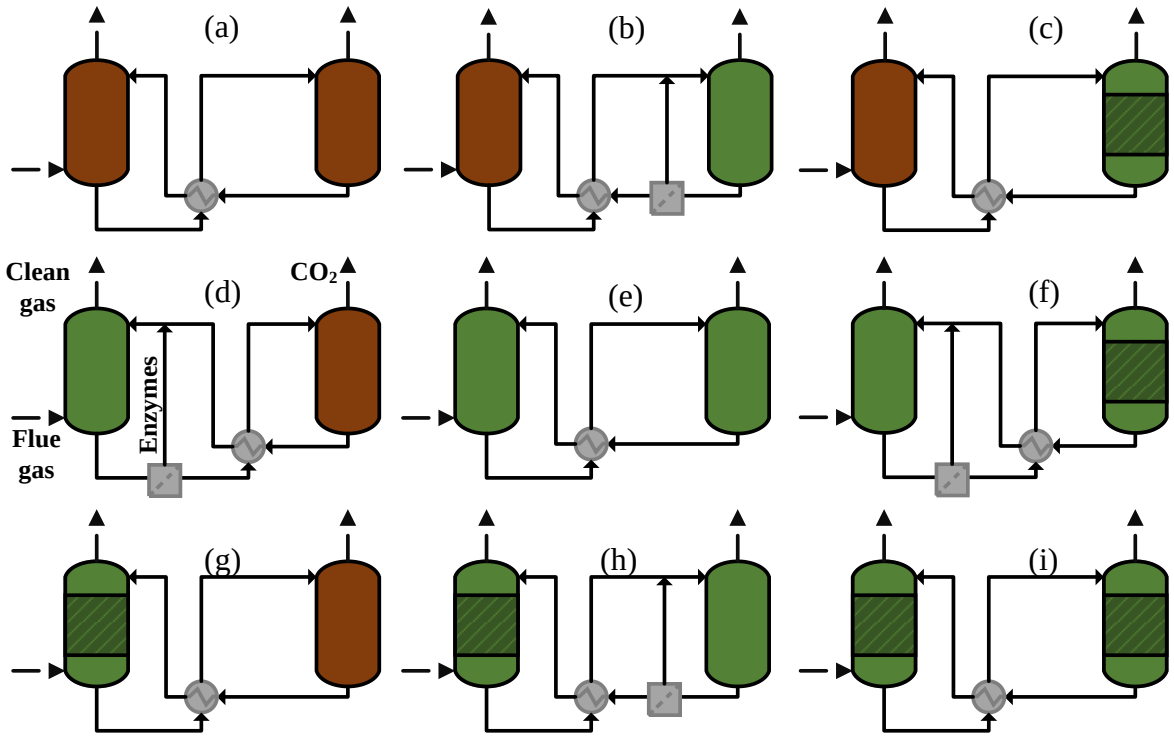

Figure 104: Process options for handling CA in CCS; brown color indicates no enzyme present, streaked green indicates immobilized enzyme on the packing and regular green represents free flowing enzyme in solution.

The first row considers no enzyme in the absorber, the second row free flowing enzyme in absorber and the third row immobilized enzyme in the absorber. The first column represents no enzyme in the desorber, the second column represents enzyme in solution in the desorber and the third column the desorber employs surface immobilized enzymes. In case of free flowing enzyme, a separation unit for the enzyme is considered between the two columns if there is no enzyme in solution or immobilized enzyme in the other unit. Some of these combinations are not feasible at all. The process options where enzyme is present in the desorber but not in the absorber is not fesasible (a-c), because if the enzymes are exposed the harsh environment in the desorber, there is no need to apply another separation to prevent the enzyme entering the less harsh environment of the absorber. Combining free flowing enzyme together with immobilized enzymes and applying an enzyme separation unit is just useful if the immobilized enzyme is in the desorber, because it would prevent the enzyme from going into the reboiler which represents the hottest spot in the desorber; thus process (h) is also not feasible.

The enzyme enhancement of the mass transfer in surface immobilization on the packing is unlikely the same as the one of free flowing enzyme. The mass transfer enhancement due to reaction is caused by the reaction rate at the interface between gas and liquid and enzyme immobilized on the packing cannot contribute to the reaction rate on the gas liquid interface. Therefore the process option of free flowing enzyme is superior in mass transfer enhancement.

Leimbrink et al. [1] compared the mass transfer enhancement of CA in 30 wt% MDEA solutions and measured the catalytic effect CE compared to 30 wt% MDEA without. The surface immobilized enzyme did just result in a slight intensification of the mass transfer (CE =1.3) whereas the enzyme in solution resulted in 4 times higher absorption flow. This would suggest that enzyme in solution should be employed, at least in absorption, as there is otherwise a drawback in mass transfer and no benefit is generated. This would eliminate process option (g) and (i), leaving (d), (e) and (f) as only feasible process options.

Gundersen et al. [2] has investigated the possibility of enzyme separation with a membrane unit. They considered process option (d) and calculated the activity of the enzyme in the process with different membrane selectivities and different desorber temperatures. Theses membranes were thought to retain 90 %, 99 % or 99.9 % of the enzymes which would result in 10%, 1% or 0.1 % respectively of the enzymes passing the separation unit and entering the desorber. The enzyme deactivation was calculated according to an average residence time in the desorber and an first order deactivation constant derived from own experiments [3]. Above 100 °C it was assumed, that the enzyme loses all activity when entering the desorber. The calculations showed that at desorber temperatures above 100 °C even the best membrane with enzyme retention of 99.9 %, a theoretical value so high that it might be questionable to that it can be achieved on a real unit, gave bad results, as the enzyme lost 50 % of its activity after one month of operation. These results show that even the application of membranes for the separation of enzymes after the desorber will not release from the process restrictions of high temperature avoidance in the desorber. The technical performance, the additional capital and

operational costs of the membrane separation of the enzymes still remain unknown. Thus a lot of further research is needed to evaluate the feasibility of the membrane separation.

11.2. Low temperature desorption for enzyme enhanced solutions

The temperature sensitivity of the enzyme can be also targeted by changing the process conditions itself. Desorption happens when the partial pressure in the gas phase is below the equilibrium partial for CO_2 in the solution. The equilibrium partial pressure for CO_2 in the solution is dependent on the composition of the solution and also the temperature as described in Chapter 3.4. If there is a temperature limitation for the desorption process due to the enzyme stability the equilibrium CO_2 partial pressure can just be increased to a certain value; it thus has a certain maximum temperature. To enable a desorption process under these conditions the gas CO_2 partial pressure has to be lowered, so that the value is below the one of the equilibrium partial pressure of the solution.

According to Raoult's law the total pressure of a system is the sum of the partial pressures of all components. The gas phase consists of water vapor and gaseous CO_2 in the conventional desorption with a solvent with low volatility. The CO_2 gas partial pressure can be lowered by two means: either by lowering the total pressure in the desorber or adding another component into the gas phase and keeping the total pressure constant. Changing the total pressure would require applying vacuum to the desorber top. This technology is currently applied in *CO_2 solutions* enzyme accelerated CO_2 capture process with K_2CO_3 as solvent [4].

The introduction of an additional compound into the gas phase to lower the temperature of the separation task is done in steam distillation in the crude oil distillation in the refinery process [5]. Water is added to the organic non polar phase, thus the liquid phase separates into a water phase and the organic phase. The vaporization of water decreases the partial pressure of the oil compounds in the gas phase enabling vaporization below boiling temperature of the compounds. This technique is also widely applied in the fractionation of compounds from temperature sensitive essential oils [6].

Two studies modelled the effect of adding a volatile immiscible non polar compound into the desorber in a carbon capture process. Tobiesen and Svendesen [7] calculated the reboiler heat duty for a 30 wt% MEA process with hexane added to the desorber in different amounts. They investigated to two different effects, first changing the desorber pressure and keeping the temperature constant or keeping the pressure constant and reducing the reboiler temperature. The heat duty of the reboiler increased when hexane was added in both cases. The desorber temperature could be reduced by 8 °C from 120 to 112 °C.

Kossman et al. [8] modelled also a 30 wt% MEA process with either hexane or octane being added to the desorber. They observed a similar trend of higher energy requirement by adding the volatile compound; the results for hexane were worse than for octane. At a total pressure of 2.1 bars, the

reboiler temperature could be reduced from 124 to 111 °C by adding octane and to 82 °C by adding hexane.

The addition of a volatile compound could not reduce the energy requirement, but could reduce significantly the temperature in the desorber. These findings from that study are just valid for processes employing MEA and might be different for other solvents [9]. This technology could be used for enzyme enhanced solvents to reduce the regeneration temperature and limit the harm due to temperature deactivation.

The deactivation of the enzyme is dependent on the temperature and the residence time it is exposed to the temperature [3]. The hottest spot in the desorber is the reboiler. The reboiler is generally a heat exchanger that is heated with high temperature steam. The enzymes that are close to the reboiler are more likely to be deactivated, especially if the liquid element stays longer in the reboiler. Some processes feed the slightly super saturated steam directly into the desorber and get rid of a reboiler, this process is called live steam stripping [10]. The idea behind is to utilize larger quantities of the latent heat could be used in this process [11].

The following process outline for a low temperature regeneration unit for enzyme enhanced solutions in Figure 105 represents a combination of live steam stripping and volatile stripping agent.

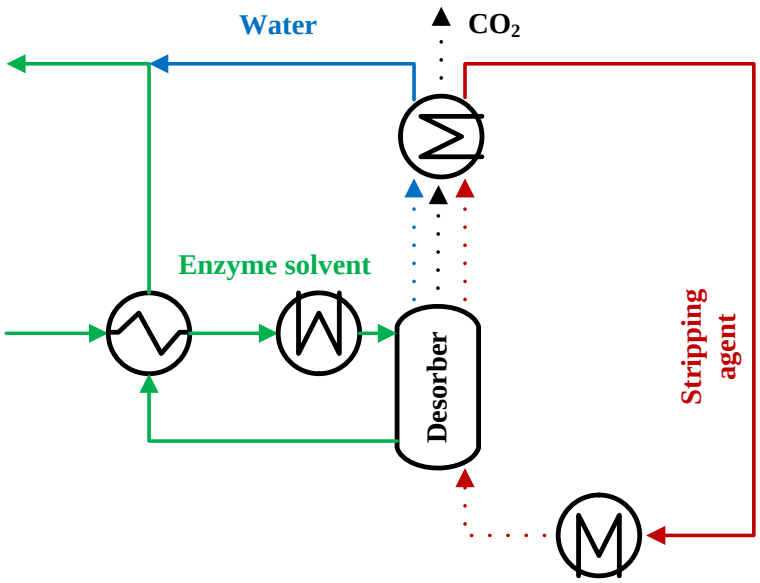

Figure 105: Process outline of low temperature regeneration of enzyme enhanced solvents

The rich solvent from absorption is first heated up in a cross heat exchanger by the liquid phase exiting the desorber and then brought to desorption temperature in a second heat exchanger before it is introduced into the column. The evaporated stripping agent is introduced into the bottom and strips the

liquid on the way up. The gas phase is condensed at the top and the water will be mixed with solvent again before the absorber. Key elements of this process are:

- Short residence time in the second heat exchanger which will decrease enzyme denaturation compared to a conventional reboiler.
- Liquid cooling down inside the desorber due to evaporation of water and CO_2, and thus no hot spot inside the desorber.
- Use of a stripping agent in desorption results in a lower temperature compared to a conventional process, this allows using heating sources that are of low value for the energy generating process, such as low pressure steam.
- Condensed water helps to cool the lean solvent which is beneficial for the thermodynamics and mass transfer of CA enhanced solvents [12].

A more sophisticated process outline could envision using the latent heat for condensing the stripping agent to heat up the enzyme solvent before entering the desorber column.

11.3. Pilot scale experiments

The technical feasibility of this process was tested in the pilot scale absorber with 30 wt% MDEA as well as 30 wt% MDEA with 3.5 g/L CA by mimicking the volatile stripping agent with pressurized air. The solvent was heated up to approximately 50 °C and then introduced into the column at different column heights and different liquid and gas load.

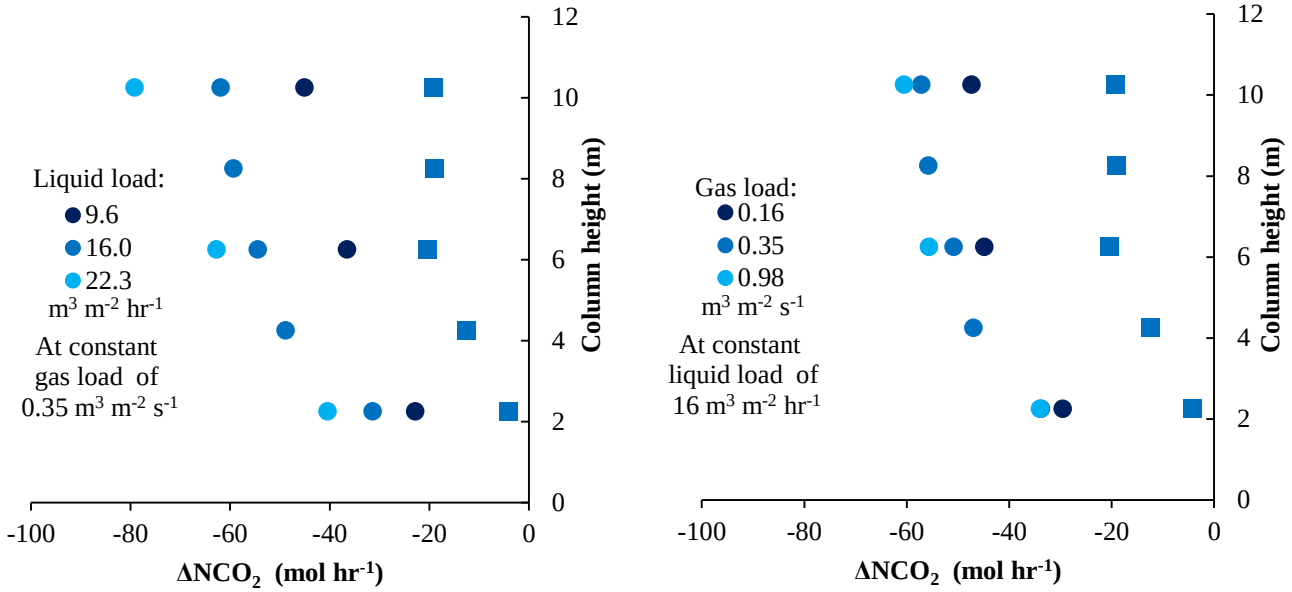

Figure 106: Mass transfer flux measured in stripgas desorption experiments at around 50 °C, circles describe experiments with enzyme enhanced solvents squares experiments without enzyme.

The inlet temperature ranged from 50 to 52 °C and the solvent had a loading of over 0.5 prior to heating. During the heating some of the CO_2 bubbled off, so that the inlet loading was 0.42

mol CO_2 /mol MDEA in both runs. Two different desorption runs were performed. In the first run the liquid load was varied between 9.6 and 22.3 m^3 m^{-2} hr^{-1} at a constant gas load of 0.35 m^3 m^{-2} s^{-1} for column heights between 2 and 10 m. In the second the gas load was varied between 0.16 and 0.98 m^3 m^{-2} s^{-1} at a constant liquid load of 16 m^3 m^{-2} hr^{-1}. The results of these experiments are shown in Figure 106.

The mass transfer flux of CO_2 in the stripgas desorption could be increased with higher liquid loads at a constant gas load of 0.35 m^3 m^{-2} s^{-1}. Higher column heights also increased the mass transfer of CO_2; this effect was more distinct for high liquid loads where the mass transfer seemed to be almost linearly dependent on the column height. When the liquid load was kept constant the mass transfer could be just slightly increased by increasing the gas load. The increase from 0.16 to 0.35 m^3 m^{-2} s^{-1} was more effective than the increase from 0.35 to 0.98 m^3 m^{-2} s^{-1}.

The effect of enzyme addition on desorption is clearly visible from Figure 106, where the squares represent desorption experiments at with 30 wt% MDEA at 50 °C without enzymes at 16 m^3 m^{-2} hr^{-1} liquid load and 0.35 m^3 m^{-2} s^{-1}. In these experiments the liquid was recirculated unlike in the experiments with CA, which lead to a decrease in solvent loading during the experiments. The solvent loading at the beginning of the experiments was around 0.5 mol/mol; this value dropped to 0.34 at the end of the experiments. The experiments with low column heights were conducted first, this can explain to some extend the bend in the trend for desorption of non-enzyme solvent. Nonetheless strip gas desorption with enzyme enhanced solvents resulted in much higher CO_2 mass transfer.

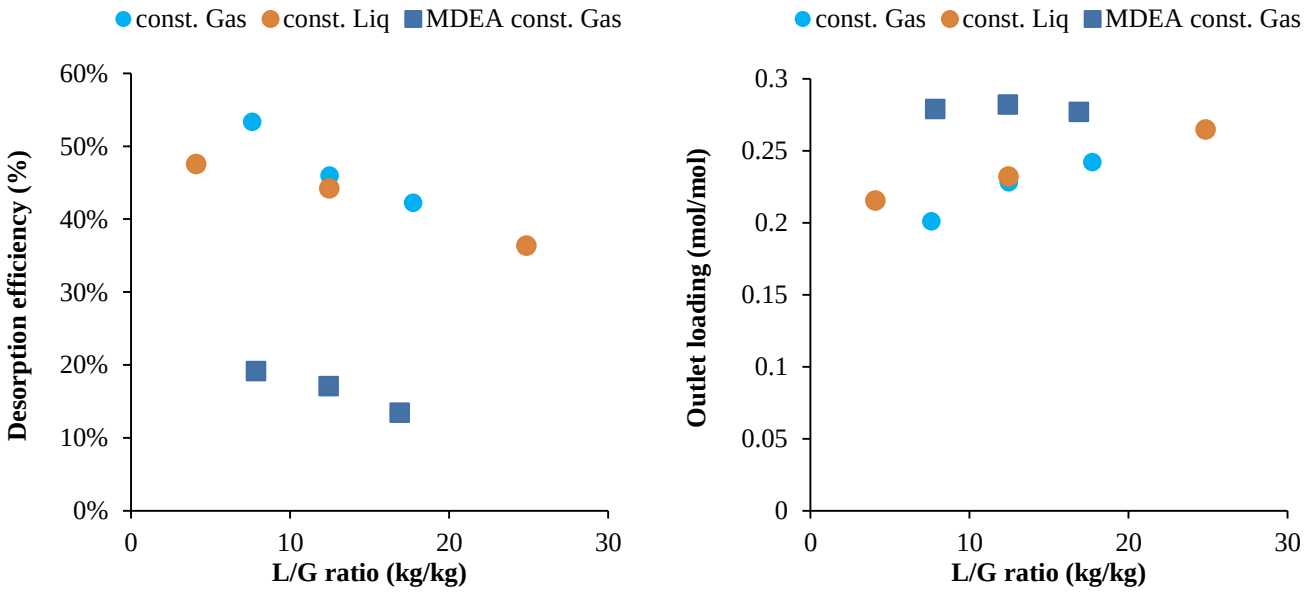

Figure 107: Desorption efficiency (left) and liquid outlet loading (right) from strip gas desorption experiments at 10 m column height for different L/G ratios.

The purpose of the desorption process is to reduce the solvent loading. The desorption efficiency[7], as well as the outlet loading of the solvents from the desorption experiments at 10 m column height are compared in Figure 107. For enzyme enhanced solvents (circles) the experiments are distinguished between being carried out at constant gas load (blue) or at constant liquid load (orange). The desorption efficiency was decreasing at higher L/G ratios. For low L/G ratio there was a disparity in trends between the experiments at constant gas and at constant liquid loads. The highest desorption efficiency (54 %) as well as the lowest solvent outlet loading (0.2) was achieved for the experiments with at constant gas load for the lowest L/G ratio. Even though the L/G ratio of one experiment at constant liquid loads was even lower it did not result in a higher desorption efficiency. A low L/G ratio is achieved by either a low liquid load, or a high gas load. Changing the gas and the liquid flow affected the mass transfer of CO_2 in stripgas desorption differently as shown in Figure 106. After a certain level there is will be just very little effect on the mass transfer by increasing the gas load. Changing the L/G through the gas load in that region will just slightly affect the desorption efficiency. A change in liquid load affected the mass transfer to a greater extent, this explains why the desorption efficiency increased more when the L/G ratio was decreased by increasing the liquid load.

Stripgas desorption should be carried out at a high L/G ratio, as the stripping gas has to be evaporated which requires energy. The stripgas desorption process is just feasible if the enzyme is not harmed during the process. In order to test the activity of the enzyme after one regeneration cycle similar absorption experiments were carried. The results from these experiments are shown in Figure 108.

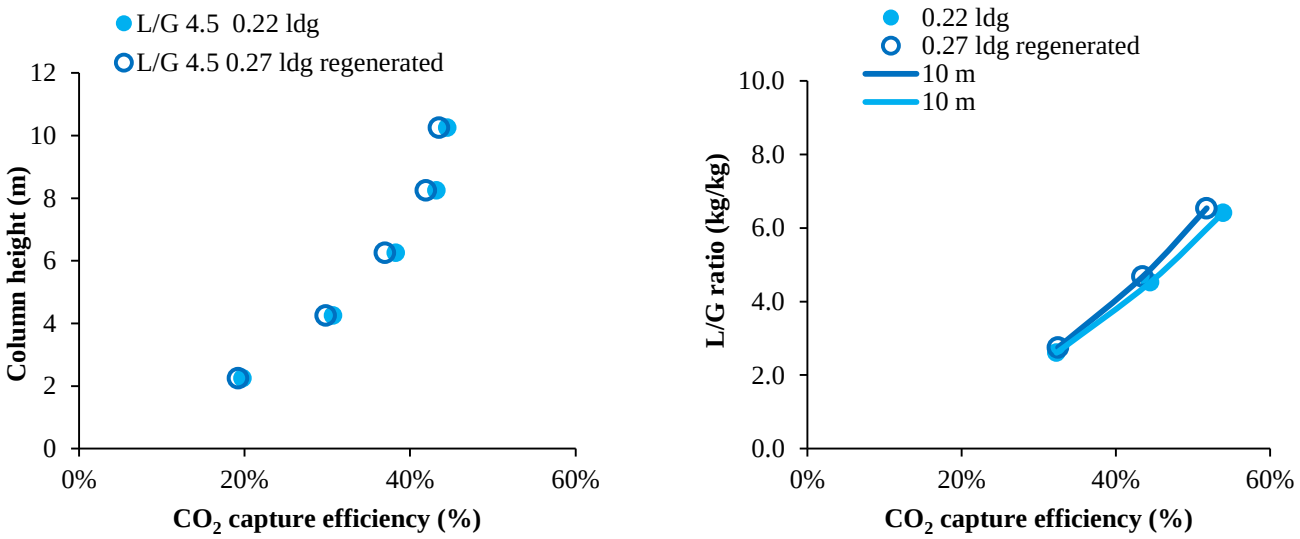

Figure 108: Checking enzyme activity after regeneration with stripgas desorption.

[7] calculated as difference in solvent loading between in and outlet in reference to the inlet loading

The regenerated solvent had a slightly higher loading than the previous experiment, 0.27 vs. 0.22. The capture efficiency of the regenerated solvent was also slightly lower than in the experiment before the regeneration. The enzyme has thus not lost activity in the regeneration process. A stripgas desorption at slightly elevated temperature might be a feasible process option for a temperature sensitive enzyme. Further test concerning the long term stability are needed for a final conclusion on this technology. Besides that the influence of temperature for this technology should be investigated in future.

BIBLIOGRAPHY

[1] M. Leimbrink, T. Limberg, A.-K. Kunze, and M. Skiborowski, "Different strategies for accelerated CO_2 absorption in packed columns by application of the biocatalyst carbonic anhydrase," *Energy procedia*, 2017.

[2] M. T. Gundersen, A. Gladis, P. L. Fosbøl, N. von Solms, and J. M. Woodley, "Operating windows for enzyme enhanced PCCC," *Energy Procedia*, 2017.

[3] M. T. Gundersen, N. Von Solms, and J. M. Woodley, "Enzymatically Assisted CO_2 Removal from Flue-Gas," *Energy Procedia*, vol. 63, pp. 624–632, 2014.

[4] L. Fradette, S. Lefebvre, and J. Carley, "Demonstration Results of Enzyme-Accelerated CO_2 Capture," *Energy Procedia*, vol. 0, pp. 14–18, 2017.

[5] A. Mersmann, M. Kind, and J. Stichlmair, *Thermal separation Technology*, 1st ed. Springer_Verlag, 2011.

[6] P. Masango, "Cleaner production of essential oils by steam distillation," *J. Clean. Prod.*, vol. 13, no. 8, pp. 833–839, 2005.

[7] F. A. Tobiesen and H. F. Svendsen, "Study of a modified amine-based regeneration unit," *Ind. Eng. Chem. Res.*, vol. 45, no. 8, pp. 2489–2496, 2006.

[8] A. Kossmann, S. Rehfeldt, P. Moser, and H. Klein, "Process study for stripping components in absorption-desorption processes for CO_2-removal from power plant flue gases," *Chem. Eng. Res. Des.*, vol. 99, pp. 236–247, 2015.

[9] F. A. Tobiesen, H. F. Svendsen, and K. A. Hoff, "Desorber Energy Consumption Amine Based Absorption Plants," *Int. J. Green Energy*, vol. 2, no. 2, pp. 201–215, 2005.

[10] Y. Le Moullec, T. Neveux, and L. Moullec, "Process modifications for CO_2 capture," in *Absorption-Based Post-Combustion Capture of Carbon Dioxide*, 2016.

[11] Q. Xiang, Y. Le Moullec, M. Fang, J. C. Valle-Marcos, J. Lu, W. Jiang, X. Zhou, G. Chen, and Z. Luo, "Novel solvent regeneration process through direct steam stripping," *Energy Procedia*, vol. 63, pp. 1392–1398, 2014.

[12] A. Gladis, M. T. Gundersen, P. L. Fosbøl, J. M. Woodley, and N. von Solms, "Influence of temperature and solvent concentration on the kinetics of the enzyme carbonic anhydrase in carbon capture technology," *Chem. Eng. J.*, 2017.

12. Conclusions and recommendations

Enzyme enhanced CO_2 capture is a novel technology in the field of CCS that still has to deal with a lot of uncertainties especially about process performance and enzyme stability due to the enzyme's temperature sensitivity. Many studies have shown great potential of this technology with mass transfer performance tests in lab scale and pilot scale. Enzyme stability could be maintained over a long time frame at higher temperatures, although the temperature range for enzyme handling solvent systems will never be the same as for conventional solvent systems with desorber temperatures up to 120-150 °C. Innovative process development considering the process limitations is needed for a successful application of the enzyme enhanced CO_2 capture technology; therefore precise process models are required.

12.1. Final conclusions

This work presents the first predictive process model for the enzyme enhanced CO_2 capture process that accurately describes the CO_2 mass transfer of pilot scale experiments in a very wide range of process conditions. It showcases a successful scale up of the enzyme enhanced CO_2 capture process. This process was evaluated in lab and pilot scale. For process model validation this work also offers experimental pilot plant data, such as temperature and solvent loading profiles as well as mass transfer rates on 71 absorption experiments with enzyme enhanced MDEA, 27 absorption experiments with the industrial standard 30 wt% MEA, as well as 37 stripgas desorption experiments.

First the mass transfer performance of several solvent types at different temperatures and solvent concentrations was investigated in lab scale on a wetted wall column. The different solvent types were: the industrial standard 30 wt% MEA representing a conventional solvent, a tertiary amine with a secondary amine as chemical promoter (MDEA/PZ mixture), as well as a carbonate salt (K_2CO_3), a tertiary amine (MDEA) and a sterically hindered amine (AMP) promoted by the biocatalyst CA.

Enzyme enhanced solvents showed a different temperature dependency on the CO_2 mass transfer than conventional solvents and chemically promoted solvents, as for the enzyme enhanced solvents MDEA and K_2CO_3 the CO_2 mass transfer decreased at higher temperatures, whereas for the other solvents an increase was observed. As the solvents CO_2 solubility as well as the mass transfer rates are higher at lower temperatures, an optimal absorption temperature could be identified for enzyme enhanced solvents. For conventional solvents and chemically promoted solvents the absorption temperature always represented a trade-off, between high solvent capacities and high mass transfer rates.

Chemically promoted solvents and conventional solvents, whose reaction kinetics are dependent on the concentrations of the active solvent/promoter, showed a significant decrease in mass transfer at higher solvent loadings. In enzyme enhanced solvents mass transfer just slightly decreased upon solvent loading. Even though the chemically promoted as well as the conventional solvents were faster

absorbing at unloaded conditions, enzyme enhanced MDEA solutions with 8.5 g/L CA at 298 K could compete with the best solvents available in literature in terms of solvent capacity and average mass transfer over the column.

The mass transfer of CO_2 into enzyme enhanced MDEA solutions could be described with mechanistic enzyme kinetic models. The kinetic model that incorporated the reversible enzyme reaction mechanism (MR) could describe the effects of solvent concentration, temperature, enzyme concentration, solvent loading and CO_2 gas partial pressure on the mass transfer of CO_2 in absorption and desorption very well in the range of tested process conditions. A simplified version of this model (SP), which neglected the substrate saturation by aqueous CO_2 but still accounted for the product saturation, was also able to describe all the effects of the different process conditions except the CO_2 partial pressures. This model was suitable for CO_2 partial pressures below 15 kPa and capable to simulate CCS from coal fired power plants. The other models tested failed to describe the effect of solvent loading on the mass transfer, which was found to be a very crucial parameter in mass transfer modelling of enzyme enhanced MDEA solutions.

In pilot scale absorption experiments enzyme enhanced 30 wt% MDEA solutions were benchmarked against the industrial standard for CCS 30 wt% MEA at different column heights and different liquid to gas ratios (L/G). The experiments with 30 wt% MDEA carried out at 0, 0.85 and 3.5 g/L CA proved the positive effect of CA in pilot scale, where the CO_2 capture could be increased from 23 % (0 g/L CA) to 56 % (0.85 g/L CA) and 83 % (3.5 g/L). The enzyme enhanced MDEA did not exceed the mass transfer of the industrial standard at similar L/G ratios and column heights, although more than 80 % of the capture performance could be achieved with 3.5 g/L CA. A further increase in L/G ratio as well as column height might even increase the capture performance of 30 wt% MDEA with 3.5 g/L CA compared to 30 wt% MEA.

Mass transfer analysis revealed, that the mass transfer of CO_2 in enzyme enhanced MDEA is much more equally distributed over the height of the column compared to MEA. This behavior could be explained by the different temperature influence on the mass transfer between enzyme enhanced solvents and conventional solvents. The exothermic reaction between solvent and CO_2 increases the temperature; in case of conventional solvents this sparks the mass transfer as the kinetics are increasing and creates hotspots inside the column. In case of enzyme enhanced solvents the temperature increment decreases the mass transfer which prevents hot spots.

The implemented enzyme kinetic model into the in-house absorber column model CAPCO2 could accurately predict the mass transfer in the pilot absorption experiments with enzyme enhanced MDEA solutions. The absorber model was capable to describe the influence of enzyme concentration between 0 and 3.5 g/L, solvent temperature, lean loading and L/G ratio on the capture efficiency correctly. The experimentally determined solvent loading profiles over the height of the column as well as the temperature profiles were in very good agreement with the simulation, showing that the mass transfer

inside the column could be accurately simulated. The absorber model was also very accurately predicting the trend of different L/G ratios as well as different column height. Hence this model can be used to identify the ideal process conditions and to determine the energy requirement for the process for a proper benchmark with conventional technologies.

The issue with the enzyme's temperature sensitivity in desorption could be circumvented with a new invented low temperature strip gas desorber. The use of a volatile stripping compound which is immiscible with the liquid phase facilitates a regeneration process at lower temperatures without a reboiler and enables the use of low-value heating sources below 100 °C. The technical process feasibility was tested in pilot plant scale with air as a stripping compound. The effects of the stripping gas flow and the liquid flow as well as the column height have been investigated. The enzyme clearly enhanced the desorption in these experiments and it was possible to reduce the CO_2 loading of a 30 wt% MDEA solution from 0.42 to 0.2 at around 50 °C for a low liquid flow and a high striping gas flow. An additional absorption study revealed that the enzyme's activity was not changed during the regeneration process.

Overall the work performed in this study clearly proved CA's justified existence in CCS. However enzyme enhanced solvent technology comes with both, opportunities as well as restrictions. The main restriction lies in a temperature limitation. This issue can be approached by a higher a higher maximum temperature level through protein engineering or by a regeneration process utilizing a stripping compound. The main advantage of enzyme enhanced solvents is the high enzyme activity at low temperatures, which enables rich solvent loadings that cannot be achieved with chemical promoters or conventional solvents.

12.2. Future recommendations

The work conducted in this PhD thesis aimed to demystify the topic of enzyme enhanced CO_2 capture and to provide a process model that is validated against pilot plant experiments in wide range of process conditions. The model can just be validated in the range where experiments were conducted therefore future work should focus on providing more experiments in pilot scale.

Even though the solvent concentration influence on CO_2 mass transfer into MDEA solutions has been determined on the wetted wall column and this influence implemented into CAPCO2 was able to predict the mass transfer into 30 wt% MDEA accurately, a model validation with pilot scale experiments conducted at another MDEA concentration is needed. This value might be chosen lower than 30 wt%, as the sensitivity analysis predicted higher capture efficiencies in that range.

Another focus of experimental research which might be even more impactful is the stripgas desorption. Especially the influence of higher desorption temperature should be investigated. These experiments should always be carried out with continuous absorption campaigns following a desorption campaign to monitor the enzyme's activity afterwards.

The presented process model in CAPCO2 should be applied to find ideal process conditions for enzyme enhanced MDEA and to optimize the process in regard to the energy requirement. In such a study focus should be put on a low temperature desorption, as a membrane filtration unit for the enzyme will be unlikely unless it is immobilized on bigger particles. Values for the temperature maximum might be unlikely above 100 °C in the desorber; temperatures of 85 °C are very realistic.

As the enzyme enhanced solvent technology is not linked to CCS from coal fired power plants, simulation studies on other industrial gas mixtures should be conducted. Especially mass transfer operations with high CO_2 partial pressures might be of interest. Conventional solvent technologies undergo overall reactions with CO_2 so fast that the Enhancement factor is at its maximum and the mass transfer shifts from reaction-controlled to diffusion-controlled regime. As the enzyme reacts with water which is abundant in the solvent a diffusion limitation of water will hardly affect the mass transfer of CO_2. Therefore mass transfer of CO_2 into enzyme enhanced solvents at high CO_2 partial pressure might be worth a look, although substrate limitation of CA according to Michaelis Menten kinetics could be a show-stopper.

The CAPCO2 model should be used to validate the stripgas desorption experiments. In that way an optimization of this process will become much easier. Besides that, heat integration, as well as utilizing the latent heat of the stripping compound as an additional energy source for heating up the solution before the stripper might reduce the energy requirement a lot.

Appendix

A: Wetted wall column experiments

Table 12: Physical properties of the solvents MEA (30 wt%), AMP (30 wt%), MDEA (30 wt%), K_2CO_3 (15 wt%) at 298 to 328 K

Property (unit)	Temperature	MEA 30 wt%	AMP 30 wt%	MDEA 30 wt%	K_2CO_3 15 wt%
$D_{CO_2}^{sol}$	298 K	1.29E-09 [3]	1.67E-09 [3]	9.33E-10 [3]	1.32E-09 [4]
(m^2 s^{-1})	313 K	1.97E-09 [3]	2.35E-09 [3]	1.40E-09 [3]	1.93E-09 [4]
	328 K	2.87E-09 [3]	3.20E-09 [3]	2.03E-09[3]	2.70E-09 [4]
$H_{CO_2}^{sol}$	298 K	3.55E+03 [5]	3.55E+03 [6]	2.96E+03 [1]	6.08E+03 [7]
(Pa m^3 mol^{-1})	313 K	4.50E+03 [5]	4.84E+03 [6]	4.11E+03 [1]	8.08E+03 [7]
	328 K	5.58E+03 [5]	6.41E+03 [6]	5.54E+03 [1]	1.04E+04 [7]
k_2	298 K	5.94E+00 [1]	5.55E-01 [8]	1.22E-02 [1]	1.54E+01 [9]
(m^3 mol^{-1} s^{-1})	313 K	1.42E+01 [1]	1.28E+00 [8]	2.77E-02 [1]	3.71E+01 [9]
	328 K	3.12E+01 [1]	2.72E+00 [8]	5.82E-02 [1]	8.26E+01 [9]
$k_{CO_2}^{liq\ '}$	298 K	1.74E-06	4.95E-07	5.05E-08	7.42E-08
(mol Pa^{-1} m^{-2} s^{-1})	313 K	2.60E-06	6.51E-07	7.73E-08	1.05E-07
	328 K	3.75E-06	8.34E-07	1.29E-07	1.43E-07

Table 13: Liquid side mass transfer coefficient k_{liq} (mol Pa^{-1} m^{-2} s^{-1}) of 30 wt% MDEA with 5 wt% PZ at different temperatures and solvent loadings (mol CO_2 /mol MDEA)

Solvent loading	0.08	0.16	0.21	0.21	0.28	0.34	0.4	0.45
298 K	1.35E-06	1.06E-06	7.76E-07	7.76E-07	6.45E-07	6.15E-07	3.75E-07	2.45E-07
313 K	1.92E-06	1.49E-06	1.11E-06	1.11E-06		5.96E-07	3.50E-07	2.03E-07
328 K	2.26E-06	1.81E-06	1.66E-06	1.66E-06	1.02E-06	6.05E-07	6.13E-07	5.90E-07

Table 14: Liquid side mass transfer coefficient k_{liq} (mol Pa^{-1} m^{-2} s^{-1}) of 30 wt% MDEA at different temperatures and solvent loadings (mol CO_2 /mol MDEA)

Solvent loading	0.03	0.10	0.26	0.30	0.36	0.42	0.53
298 K	6.11E-08	8.31E-08	6.22E-08	-	5.36E-08	4.37E-08	3.05E-08
313 K	9.70E-08	-	-	8.93E-08	0.00E+00	6.57E-08	4.41E-08
328 K	1.52E-07	9.01E-08	-	8.00E-08	7.70E-08	6.50E-08	3.33E-08

Table 15: Liquid side mass transfer coefficient k_{liq} (mol Pa^{-1} m^{-2} s^{-1}) 20 wt% K_2CO_3 solutions with 1.5 g/L CA Batch (I) at different temperatures and solvent loadings

Solvent loading	0.00	0.20	0.35	0.50	0.65
298 K	5.18E-07	4.76E-07	4.08E-07	3.70E-07	3.26E-07
313 K	5.37E-07	4.83E-07	4.03E-07	2.62E-07	2.41E-07
328 K	4.07E-07	3.66E-07	2.91E-07	2.44E-07	2.58E-07

Table 16: Liquid side mass transfer coefficient k_{liq} (mol Pa^{-1} m^{-2} s^{-1}) of enzyme unloaded enhanced solvent with 2 g/L CA Batch (I) at different temperatures and solvent concentrations

Solvent	MDEA			AMP		K_2CO_3			
Conc.	15 wt%	30 wt%	50 wt%	15 wt%	30 wt%	5 wt%	10 wt%	15 wt%	20 wt%
298 K	6.8E-07	5.4E-07	3.4E-07	8.0E-07	7.3E-07	8.3E-07	7.2E-07	6.2E-07	6.3E-07
313 K	6.0E-07	4.6E-07	3.3E-07	8.2E-07	9.2E-07	7.9E-07	6.8E-07	6.0E-07	6.4E-07
328 K	5.5E-07	4.2E-07	3.7E-07	8.6E-07	1.1E-06	7.8E-07	6.6E-07	5.5E-07	7.2E-07

Table 17: Liquid side mass transfer coefficient k_{liq} (mol Pa^{-1} m^{-2} s^{-1}) of enzyme enhanced unloaded MDEA with CA Batch (II) at different temperatures and CA concentrations

CA conc.	0.85 g/L	0.85 g/L	0.85 g/L	1.35 g/L	1.75 g/L	2.75 g/L	8.5 gL/
Solvent conc.	15 wt%	30 wt%	50 wt%	30 wt%	30 wt%	30 wt%	30 wt%
298 K	5.61E-07	3.78E-07	2.14E-07		5.13E-07		1.05E-06
313 K	5.04E-07	3.52E-07	2.14E-07	4.24E-07	4.59E-07	5.87E-07	9.19E-07
328 K	4.02E-07	3.16E-07	2.12E-07		3.51E-07		7.70E-07

Table 18: Liquid side mass transfer coefficient k_{liq} (mol Pa^{-1} m^{-2} s^{-1}) of enzyme enhanced loaded 30 wt% MDEA with 0.85 g/L CA Batch (II) at different temperatures

loading	0.03	0.03	0.10	0.14	0.16	0.22	0.23	0.32	0.45
298 K	3.72E-07	3.42E-07	3.39E-07	3.05E-07	2.79E-07	2.70E-07	2.68E-07	2.61E-07	1.88E-07
loading	**0.03**	**0.03**	**0.09**	**0.15**	**0.23**	**0.30**	**0.36**	**0.45**	
313 K	3.22E-07	3.26E-07	3.11E-07	2.69E-07	2.56E-07	2.28E-07	2.20E-07	1.61E-07	
loading	**0.03**	**0.14**	**0.30**	**0.45**					
328 K	3.02E-07	2.37E-07	2.53E-07	1.72E-07					

Table 19: Liquid side mass transfer coefficient k_{liq} (mol Pa^{-1} m^{-2} s^{-1}) of enzyme enhanced loaded 30 wt% MDEA with 8.5 g/L CA Batch (II) at different temperatures

loading	0.03	0.19	0.38
298 K	1.05E-06	9.24E-07	7.63E-07
313 K	9.19E-07	8.49E-07	7.11E-07
328 K	7.70E-07	5.77E-07	-

Table 20: Liquid side mass transfer coefficient kliq (mol Pa-1 m-2 s-1) of enzyme enhanced 15 and 50 wt% MDEA with 0.85 g/L CA Batch (II) at different solvent loadings and temperatures.

Solvent	**15 wt% MDEA**				**50 wt% MDEA**				
loading	**0.001**	**0.24**	**0.31**	**0.44**	**0.01**	**0.09**	**0.1**	**0.17**	**0.3**
298 K	5.61E-07	4.87E-07	3.86E-07		2.14E-07	1.67E-07	1.43E-07	1.77E-07	1.18E-07
313 K	5.04E-07	4.30E-07	3.42E-07	2.99E-07	2.14E-07	1.85E-07	1.69E-07	1.59E-07	9.43E-08
328 K	3.87E-07	2.72E-07	2.85E-07	3.69E-07	2.12E-07	1.75E-07	1.50E-07	1.83E-07	1.19E-07

Table 21: Solvent loading and solvent capacity for MDEA solutions at different temperatures, representing lean and rich solutions with a CO_2 equilibrium partial pressure of 5 kPa (rich) and 0.5 kPa (lean), cyclic loading and capacity represents difference between rich and lean solution. Results calculated with extended UNIQUAC model.

Solvent / Temperature		**15 wt%**		**30 wt%**		**50 wt%**	
		loading	capacity	loading	capacity	loading	capacity
		mol CO_2/ mol MDEA	mol CO_2/ kg solution	mol CO_2/ mol MDEA	mol CO_2/ kg solution	mol CO_2/ mol MDEA	mol CO_2/ kg solution
298 K	0.5 kPa (lean)	0.18	0.23	0.12	0.29	0.06	0.26
	5 kPa (rich)	0.54	0.68	0.41	1.04	0.26	1.08
	Δ (cyclic)	0.36	0.45	0.29	0.75	0.2	0.82
313 K	0.5 kPa (lean)	0.11	0.14	0.06	0.16	0.03	0.13
	5 kPa (rich)	0.36	0.45	0.25	0.62	0.14	0.58
	Δ (cyclic)	0.25	0.31	0.19	0.46	0.11	0.45
328 K	0.5 kPa (lean)	0.06	0.08	0.04	0.09	0.02	0.07
	5 kPa (rich)	0.22	0.28	0.14	0.35	0.07	0.3
	Δ (cyclic)	0.16	0.2	0.1	0.26	0.05	0.23

B: Pilot plant experiments

Table 22: Comparison of capture efficiencies of 30 wt% MEA to 30 wt% MDEA with varying enzyme concentrations the different solvents at column heights between 2 and 8 m

Solvent	Loading (mol/mol)	T (^{o} C)	L/G (kg/kg)	2.25 m	4.25 m	6.25 m	8.25 m
30 wt% MEA		28	3.2	45%	60%	52%	65%
30 wt% MEA	0.24 (2-4 m)	28	5.4	53%	74%	77%	85%
30 wt% MEA	0.29 (6-8 m)	28	7.8	58%	79%	84%	95%
30 wt% MDEA 0.85 g/L CA	0.1	28	4.0	21%	29%	35%	39%
30 wt% MDEA 0.85 g/L CA	0.1	28	9.6	24%	36%	46%	53%
30 wt% MDEA 0.85 g/L CA	0.27	40	4.0	16%	18%	19%	20%
30 wt% MDEA 0.85 g/L CA	0.27	40	9.6	18%	21%	24%	27%
30 wt% MDEA 3.5 g/L CA	0.07	28	4.5	25%	40%	51%	60%
30 wt% MDEA 3.5 g/L CA	0.22	28	4.5	20%	31%	38%	43%

Experimental setpoints, temperature and solvent loading profiles:

Table 23: Temperature profile for first MEA campaign

height	R1	R2	R3	R4	R5	R6	R7	R8	R9
in	25.7	25.7	25.7	25.5	26.3	26.2	26.2	24.0	24.0
10.25	25.3	25.4	25.6	25.5	26.7	25.7	25.6	43.5	23.9
9.25	25.7	25.8	26.1	25.7	28.4	26.1	26.1	56.7	24.6
8.25	25.9	26.0	26.4	26.0	32.5	26.2	26.2	55.0	25.0
7.25	25.5	25.7	26.5	25.8	55.0	25.9	25.8	48.1	25.6
6.25	25.6	25.9	27.1	26.1	65.1	26.0	25.8	43.7	26.5
5.25	25.7	26.2	28.2	26.7	65.8	26.4	25.7	39.8	28.5
4.25	26.2	27.2	30.4	27.8	64.0	27.5	26.0	37.1	31.2
3.25	26.7	28.1	32.5	28.9	61.1	28.9	26.2	35.1	34.7
2.25	28.3	30.7	36.6	31.5	56.9	33.8	28.1	33.1	42.5
1.25	31.1	34.3	41.2	34.5	49.4	39.3	31.7	31.0	49.9
0.25	32.1	34.6	38.0	34.1	34.7	37.7	34.7	28.4	39.5
0	32.1	34.5	38.4	35.0	35.4	37.4	33.7	27.2	41.2

Table 24: Loading profile for first MEA campaign

height	R1	R2	R3	R4	R5	R6	R7	R8	R9
in	0.23	0.23	0.23	0.23	0.23	0.23	0.23	0.23	0.23
9.25	0.23	0.23	0.23	0.23	0.23	0.23	0.23	0.29	0.23
8.25	0.23	0.23	0.23	0.23	0.24	0.23	0.23	0.36	0.23
7.25	0.23	0.23	0.23	0.23	0.24	0.23	0.23	0.42	0.24
6.25	0.23	0.23	0.24	0.23	0.25	0.23	0.23	0.44	0.24
5.25	0.23	0.23	0.25	0.23	0.29	0.23	0.23	0.46	0.25
4.25	0.23	0.23	0.25	0.24	0.31	0.23	0.23	0.47	0.26
3.25	0.23	0.23	0.26	0.25	0.35	0.25	0.23	0.48	0.27
2.25	0.24	0.24	0.29	0.26	0.39	0.27	0.24	0.48	0.30
1.25	0.26	0.28	0.32	0.28	0.42	0.30	0.26	0.49	0.34
0.25	0.28	0.30	0.34	0.30	0.44	0.34	0.29	0.49	0.37
0	0.28	0.31	0.35	0.31	0.45	0.35	0.31	0.50	0.39

Table 25: Setpoints and measured mass transfer in first MEA campaign

		Run	**R1**	**R2**	**R3**	**R4**	**R5**	**R6**	**R7**	**R8**	**R9**
	height	m	10.25	10.25	10.25	10.25	10.25	10.25	10.25	10.25	10.25
Liquid	Mass flow	kg hr^{-1}	198.8	197.5	196.6	299.4	99.5	99.8	98.2	50.0	150.0
	T	°C	25.7	25.7	25.7	25.5	26.3	26.2	26.2	24.0	24.0
	MEA	wt%	28.0	28.0	28.0	28.0	28.0	28.0	28.0	28.0	27.0
	CO_2	wt%	4.6	4.6	4.6	4.6	4.6	4.6	4.6	4.6	4.5
Gas	Mass flow	kg hr^{-1}	16.2	21.7	31.7	31.4	31.1	16.2	10.3	32.1	32.1
	T	°C	24.4	24.7	26.4	25.8	23.5	22.5	22.7	22.8	22.8
	p	kPa	100.7	101.0	101.3	100.7	102.0	100.0	99.9	102.3	102.3
	CO_2	vol%	10.1	10.3	10.1	10.1	10.2	10.0	10.1	10.4	10.1
	H_2O	vol%	3.0	3.1	3.4	3.3	2.8	2.7	2.8	2.7	2.7
Mass transfer CO_2		kg hr^{-1}	2.45	3.37	4.82	4.79	4.78	2.44	1.57	3.37	4.85

Table 26: Temperature profiles in second MEA campaign part 1

height	R10	R11	R12	R13	R14	R15	R16	R17	R18
in	25.9	25.2	24.8	25.8	25.1	24.8	24.9	24.2	23.7
10.25									
9.25									
8.25									
7.25									
6.25							28.5	25.1	24.5
5.25							46.7	28.3	26.2
4.25				30.6	25.9	25.2	51.4	31.9	28.1
3.25				48.4	31.3	28.1	50.9	37.2	31.3
2.25	31.5	27.3	25.9	56.0	40.6	32.4	46.4	45.4	36.2
1.25	47.5	36.3	31.0	50.8	48.6	36.9	41.1	47.7	40.6
0.25	35.6	35.7	32.7	35.8	41.1	36.0	29.9	33.6	34.1
0	35.1	35.9	33.5	36.3	41.4	38.0	31.4	39.7	38.4

Table 27: Loading profiles in second MEA campaign part 1

height	R10	R11	R12	R13	R14	R15	R16	R17	R18
in	0.25	0.25	0.25	0.26	0.26	0.26	0.30	0.30	0.30
9.25									
8.25									
7.25									
6.25									
5.25							0.33	0.31	0.31
4.25							0.37	0.33	0.31
3.25							0.41	0.35	0.33
2.25							0.45	0.38	0.36
1.25							0.47	0.41	0.39
0.25							0.49	0.44	0.40
0	0.41	0.35	0.32	0.46	0.41	0.37	0.49	0.45	0.41

Table 28: Setpoints and measured mass transfer in second MEA campaign part 1

		Run	R10	R11	R12	R13	R14	R15	R16	R17	R18
	height	m	2.25	2.25	2.25	4.25	4.25	4.25	6.25	6.25	6.25
Liquid	Mass flow	kg hr^{-1}	72.2	122.3	175.0	72.8	122.1	177.0	71.5	123.0	175.4
	T	°C	25.9	25.2	24.8	25.8	25.1	24.8	24.9	24.2	23.7
	MEA	wt%	29.5	29.5	29.5	29.5	29.5	29.5	29.2	29.2	29.2
	CO_2	wt%	5.2	5.2	5.2	5.4	5.4	5.4	6.2	6.2	6.2
Gas	Mass flow	kg hr^{-1}	26.5	26.2	26.2	26.4	26.5	26.6	29.2	28.4	28.7
	T	°C	22.4	22.8	23.0	23.0	23.2	23.1	24.3	26.4	24.5
	p	kPa	101.7	101.5	102.0	102.7	102.5	102.5	103.6	104.1	103.5
	CO_2	vol%	14.1	12.4	12.4	12.8	12.7	12.6	13.1	11.8	12.1
	H_2O	vol%	2.7	2.7	2.8	2.7	2.8	2.8	2.9	3.3	3.0
Mass transfer CO_2		kg hr^{-1}	2.67	2.71	2.92	3.16	3.83	4.02	3.13	3.99	4.42

Table 29: Temperature profiles in second MEA campaign part 2

height	R19	R20	R21	R22	R23	R24	R25	R26	R27
in	24.9	24.2	23.8	25.8	25.0	24.5	24.2	24.0	23.9
10.25				36.9	34.6	28.2	23.9	23.1	23.0
9.25				48.3	48.3	38.3	26.0	24.7	24.5
8.25	38.0	24.8	23.5	51.4	58.0	53.9	27.5	25.2	24.7
7.25	63.3	28.2	24.9	49.6	61.3	67.3	35.4	26.5	25.4
6.25	63.4	31.5	25.9	45.7	58.5	66.6	57.4	28.1	26.3
5.25	59.0	43.7	28.0	41.8	54.4	63.4	68.8	32.0	28.6
4.25	56.3	60.4	30.5	39.8	51.8	61.2	68.2	37.2	30.8
3.25	52.5	64.4	33.5	38.4	48.5	57.8	65.5	44.9	33.6
2.25	48.4	62.7	38.1	36.8	44.9	54.5	62.4	55.3	37.9
1.25	42.9	56.2	42.6	33.8	40.9	48.5	55.3	55.6	42.5
0.25	29.7	38.3	38.4	29.5	33.0	35.5	40.2	40.2	37.0
0	35.7	43.1	39.8	29.7	33.6	37.7	41.7	44.4	39.1

Table 30: Loading profiles in second MEA campaign part 2

height	R19	R20	R21	R22	R23	R24	R25	R26	R27
in	0.29	0.29	0.29	0.30	0.30	0.30	0.30	0.30	0.30
9.25				0.33	0.31	0.30	0.30	0.30	0.30
8.25				0.36	0.33	0.32	0.31	0.30	0.30
7.25	0.32	0.31	0.30	0.43	0.36	0.34	0.32	0.31	0.30
6.25	0.35	0.32	0.30	0.46	0.41	0.38	0.33	0.31	0.31
5.25	0.40	0.34	0.32	0.49	0.44	0.41	0.35	0.32	0.32
4.25	0.43	0.36	0.32	0.50	0.45	0.43	0.37	0.34	0.32
3.25	0.45	0.39	0.34	0.50	0.47	0.45	0.40	0.37	0.35
2.25	0.47	0.42	0.37	0.51	0.48	0.46	0.42	0.39	0.37
1.25	0.48	0.44	0.40	0.51	0.49	0.48	0.44	0.42	0.40
0.25	0.49	0.47	0.41	0.52	0.50	0.49	0.46	0.44	0.43
0	0.50	0.47	0.43	0.52	0.50	0.49	0.47	0.45	0.43

Table 31: Setpoints and measured mass transfer in second MEA campaign part 2

		Run	**R19**	**R20**	**R21**	**R22**	**R23**	**R24**	**R25**	**R26**	**R27**
	height	m	8.25	8.25	8.25	10.25	10.25	10.25	10.25	10.25	10.25
Liquid	Mass flow	kg hr^{-1}	75.4	123.6	176.0	49.6	75.1	99.3	126.1	150.8	175.8
	T	°C	24.9	24.2	23.8	25.8	25.0	24.5	24.2	24.0	23.9
	MEA	wt%	29.2	29.2	29.2	29.2	29.2	29.2	29.2	29.2	29.2
	CO_2	wt%	6.2	6.2	6.2	6.2	6.2	6.2	6.2	6.2	6.2
Gas	Mass flow	kg hr^{-1}	27.6	28.3	28.4	28.3	27.2	27.4	27.7	27.7	27.8
	T	°C	26.2	25.8	24.5	26.5	28.1	26.7	23.9	23.9	24.4
	p	kPa	104.8	105.6	105.0	106.6	104.5	104.3	103.6	103.0	103.2
	CO_2	vol%	12.2	13.1	12.5	14.4	12.1	13.3	12.6	12.1	11.6
	H_2O	vol%	3.3	3.2	2.9	3.3	3.7	3.4	2.9	2.9	3.0
Mass transfer CO_2		kg hr^{-1}	3.40	4.75	5.04	2.92	3.45	4.28	4.68	4.83	4.72

Table 32: Temperature profile for first MDEA campaign without CA

height	M1	M2	M3	M4	M5	M6	M7	M8	M9	M10	M11	M12
in	30.6	29.8	29.3	29.2	29.4	29.8	41.5	43.4	43.3	43.5	42.9	42.1
10.25	29.4	29.1	28.8	28.8	28.8	28.9	39.9	41.3	40.9	41.2	41.4	40.8
9.25	30.2	29.7	29.4	29.5	29.5	29.7	40.9	42.2	41.7	42.5	42.7	42.1
8.25	30.4	30.0	29.6	29.8	29.8	30.2	41.1	42.2	41.7	42.7	43.1	42.5
7.25	30.1	29.7	29.3	29.6	29.7	30.2	40.6	41.4	41.0	42.2	42.7	42.1
6.25	30.0	29.8	29.4	29.7	29.9	30.4	40.4	41.1	40.6	42.0	42.7	42.2
5.25	29.9	29.8	29.4	29.9	30.1	30.7	40.2	40.8	40.4	41.8	42.8	42.2
4.25	30.0	30.1	29.6	30.2	30.4	31.1	40.5	40.8	40.4	41.7	43.1	42.7
3.25	29.8	30.0	29.5	30.2	30.4	31.2	40.3	40.6	40.0	41.4	43.0	42.7
2.25	29.7	30.2	29.8	30.5	30.8	31.4	40.4	40.4	39.6	40.8	43.1	42.9
1.25	28.8	29.8	29.5	30.3	30.5	30.7	40.2	40.0	38.8	40.0	42.7	42.8
0.25	26.1	27.7	27.9	28.5	28.2	27.1	37.2	36.7	35.1	35.5	38.0	39.2
0	25.6	26.9	27.2	27.8	27.3	26.0	37.6	37.2	36.5	37.0	38.9	39.9

Table 33: Loading profile for first MDEA campaign without CA

height	M1	M2	M3	M4	M5	M6	M7	M8	M9	M10	M11	M12
in	0.02	0.02	0.03	0.03	0.04	0.04	0.06	0.06	0.07	0.07	0.08	0.09
9.25	0.02	0.03	0.03	0.04	0.05	0.05	0.06	0.06	0.07	0.08	0.09	0.10
8.25	0.03	0.03	0.03	0.04	0.05	0.06	0.06	0.07	0.07	0.09	0.09	0.10
7.25	0.03	0.03	0.03	0.05	0.06	0.07	0.06	0.07	0.08	0.10	0.10	0.11
6.25	0.03	0.03	0.03	0.05	0.06	0.08	0.06	0.07	0.08	0.11	0.11	0.11
5.25	0.04	0.04	0.04	0.05	0.07	0.08	0.06	0.07	0.09	0.12	0.11	0.12
4.25	0.04	0.04	0.04	0.06	0.07	0.09	0.07	0.08	0.09	0.13	0.11	0.12
3.25	0.05	0.05	0.04	0.07	0.08	0.10	0.07	0.08	0.09	0.14	0.12	0.13
2.25	0.05	0.05	0.05	0.07	0.08	0.11	0.07	0.08	0.10	0.15	0.12	0.13
1.25	0.05	0.05	0.05	0.07	0.09	0.12	0.08	0.09	0.10	0.16	0.13	0.14
0.25	0.05	0.05	0.05	0.07	0.09	0.12	0.08	0.09	0.11	0.17	0.14	0.15
0	0.06	0.05	0.05	0.08	0.09	0.12	0.08	0.09	0.11	0.17	0.15	0.15

Table 34: Setpoints and measured mass transfer in first MDEA campaign without CA

		Run	M1	M2	M3	M4	M5	M6	M7	M8	M9	M10	M11	M12
	Height	m	10.25	10.25	10.25	10.25	10.25	10.25	10.25	10.25	10.25	10.25	10.25	10.25
Liquid	Mass	kg hr^{-1}	70.3	124.1	176.0	176.0	124.2	73.8	175.6	125.3	71.2	74.3	126.5	175.4
	T	°C	30.6	29.8	29.3	29.2	29.4	29.8	41.5	43.4	43.3	43.5	42.9	23.7
	MEA	wt%	30.0	30.0	30.0	30.0	30.0	30.0	30.0	30.0	30.0	30.0	30.0	29.2
	CO_2	wt%	0.3	0.3	0.3	0.4	0.5	0.4	0.6	0.7	0.8	0.8	0.9	6.2
	Cenz	g/L	0.0	0.0	0.0	0.0	0.0	0.0	0.0	0.0	0.0	0.0	0.0	
Gas	Mass	kg hr^{-1}	20.8	20.6	20.0	21.2	21.1	21.0	19.1	18.3	19.2	20.1	20.2	28.7
	T	°C	22.8	22.8	22.8	22.8	22.8	22.8	33.8	33.8	33.8	33.8	33.8	24.5
	p	kPa	103.1	103.1	103.1	103.7	103.1	103.1	101.4	101.6	101.5	101.4	101.4	103.5
	CO_2	vol%	4.9	5.4	5.2	14.4	12.6	11.7	4.4	4.4	5.2	13.7	11.9	12.1
	H_2O	vol%	2.7	2.7	2.7	2.7	2.7	2.7	5.2	5.2	5.2	5.2	5.2	3.0
Transfer CO_2		kg hr^{-1}	0.30	0.35	0.35	1.11	0.83	0.68	0.31	0.27	0.29	0.82	0.76	0.93

Table 35: Temperature profile for first MDEA campaign with 0.85 g/L CA

height	M13	M14	M15	M16	M17	M18	M19	M20	M21	M22	M23	M24
in	27.3	27.7	28.5	28.6	28.0	28.2	40.4	39.7	39.2	25.6	26.7	28.1
10.25	26.8	27.1	27.6	28.7	27.9	27.8	38.4	38.0	37.7	26.0	26.9	28.3
9.25	27.3	27.8	28.3	30.8	29.4	29.1	40.2	39.8	39.3	26.6	27.8	29.8
8.25	27.5	28.0	28.7	31.9	30.3	29.6	40.8	40.3	39.7	26.9	28.1	30.4
7.25	27.4	27.8	28.7	33.3	31.4	30.0	41.1	40.3	39.5	27.2	28.6	31.2
6.25	27.5	28.0	29.0	34.2	32.6	30.6	41.4	40.6	39.8	27.7	29.2	31.9
5.25	27.7	28.1	29.3	34.8	33.7	31.4	41.6	40.9	40.0	28.2	29.7	32.4
4.25	28.1	28.5	29.6	34.9	35.0	32.4	41.8	41.4	40.5	29.0	30.4	32.8
3.25	28.2	28.5	29.7	35.1	35.6	32.8	41.5	41.3	40.4	29.3	30.6	32.8
2.25	28.6	28.9	30.1	34.8	36.5	33.8	41.1	41.5	40.8	29.9	31.2	32.8
1.25	28.9	28.9	29.9	33.9	36.4	34.2	39.7	40.8	40.5	30.0	31.1	32.0
0.25	28.3	28.2	28.1	30.0	32.1	31.9	35.5	37.5	37.5	28.1	28.9	28.8
0	28.2	27.7	27.6	29.1	31.7	32.0	34.8	36.3	37.4	28.7	29.2	28.9

Table 36: Loading profile for first MDEA campaign without CA with 0.85 g/L CA

height	M13	M14	M15	M16	M17	M18	M19	M20	M21	M22	M23	M24
in	0.17	0.17	0.17	0.18	0.21	0.22	0.28	0.30	0.31	0.32	0.35	0.37
9.25	0.17	0.18	0.18	0.21	0.22	0.24	0.30	0.31	0.32	0.34	0.37	0.38
8.25	0.18	0.18	0.19	0.23	0.23	0.25	0.31	0.31	0.32	0.35	0.38	0.40
7.25	0.18	0.19	0.20	0.26	0.26	0.26	0.32	0.33	0.33	0.36	0.39	0.42
6.25	0.18	0.19	0.21	0.29	0.27	0.27	0.34	0.33	0.33	0.37	0.41	0.43
5.25	0.19	0.20	0.22	0.32	0.30	0.29	0.35	0.34	0.34	0.39	0.41	0.44
4.25	0.19	0.20	0.23	0.34	0.31	0.30	0.36	0.35	0.35	0.40	0.43	0.46
3.25	0.19	0.21	0.24	0.35	0.31	0.31	0.36	0.35	0.35	0.41	0.44	0.46
2.25	0.20	0.22	0.25	0.37	0.34	0.33	0.37	0.36	0.36	0.42	0.45	0.47
1.25	0.20	0.22	0.26	0.39	0.35	0.34	0.38	0.36	0.36	0.43	0.45	0.47
0.25	0.21	0.23	0.27	0.41	0.36	0.35	0.39	0.37	0.36	0.43	0.46	0.47
0	0.20	0.23	0.27	0.41	0.36	0.35	0.40	0.40	0.37	0.43	0.46	0.47

Table 37: Setpoints and measured mass transfer in first MDEA campaign with 0.85 g/L CA

		Run	M13	M14	M15	M16	M17	M18	M19	M20	M21	M22	M23	M24
	Height	m	10.25	10.25	10.25	10.25	10.25	10.25	10.25	10.25	10.25	10.25	10.25	10.25
Liquid	Mass	kg hr^{-1}	174.6	125.8	74.2	72.7	125.1	175.8	73.2	125.1	175.7	175.6	125.7	70.8
	T	°C	27.3	27.7	28.5	28.6	28.0	28.2	40.4	39.7	39.2	25.6	26.7	28.1
	MEA	wt%	29.5	29.5	29.5	29.5	29.5	29.5	29.5	29.5	29.5	29.5	29.5	29.5
	CO_2	wt%	1.8	1.8	1.9	2.0	2.2	2.4	3.0	3.1	3.3	3.4	3.7	3.9
	Cenz	g/L	0.85	0.85	0.85	0.85	0.85	0.85	0.85	0.85	0.85	0.85	0.85	0.85
Gas	Mass	kg hr^{-1}	21.2	21.3	21.4	22.4	22.3	22.5	21.6	21.5	21.4	21.1	21.4	21.6
	T	°C	25.0	25.2	25.4	25.6	25.6	25.4	38.4	38.0	37.7	26.7	27.2	27.7
	p	kPa	100.0	100.0	100.0	100.2	100.0	100.1	100.1	100.0	100.0	100.5	100.5	100.6
	CO_2	vol%	3.7	3.9	4.5	13.3	12.5	13.4	12.8	12.5	12.4	13.6	13.5	13.8
	H_2O	vol%	3.2	3.2	3.2	3.3	3.3	3.2	6.8	6.6	6.5	3.5	3.6	3.7
Transfer CO_2		kg hr^{-1}	0.64	0.64	0.62	1.72	1.91	2.32	0.90	1.02	1.11	1.87	1.47	0.96

Table 38: Temperature profile for first MDEA campaign with 0.85 g/L CA

height	M25	M26	M27	M28	M29
in	39.1	37.1	39.2	38.7	38.4
10.25	42.7	39.4	42.1	40.5	39.6
9.25	48.4	41.8	45.1	42.8	41.2
8.25	50.9	42.9	46.5	43.9	41.9
7.25	53.3	44.7	46.7	44.7	42.3
6.25	53.2	46.6	46.4	46.0	43.0
5.25	52.1	48.5	45.6	46.8	43.7
4.25	51.5	50.9	45.2	47.9	45.0
3.25	50.1	51.7	44.2	47.8	45.3
2.25	48.2	52.3	43.2	48.0	46.1
1.25	45.7	50.8	42.3	47.0	46.0
0.25	41.8	43.3	41.1	43.1	42.2
0	40.0	43.4	39.1	41.7	42.7

Table 39: Loading profile for first MDEA campaign with 0.85 g/L CA

height	M25	M26	M27	M28	M29
in	0.05	0.05			
9.25	0.07	0.05			
8.25	0.09	0.08			
7.25	0.13	0.10			
6.25	0.16	0.13			
5.25	0.19	0.15			
4.25	0.20	0.18			
3.25	0.22	0.19			
2.25	0.25	0.21			
1.25	0.26	0.22			
0.25	0.29	0.23			
0	0.30	0.24			

Table 40: Setpoints and measured mass transfer in first MDEA campaign with 0.85 g/L CA

		Run	M25	M26	M27	M28	M29
	Height	m	10.25	10.25	10.25	10.25	10.25
Liquid	Mass	kg hr^{-1}	73.3	127.0	73.0	125.1	172.4
	T	°C	39.1	37.1	39.2	38.7	38.4
	MEA	wt%	29.5	29.5	29.5	29.5	29.5
	CO_2	wt%	0.5	0.5	3.3	1.2	1.2
	Cenz	g/L	0.85	0.85	0.85	0.85	0.85
Gas	Mass	kg hr^{-1}	20.9	20.7	22.1	22.4	21.6
	T	°C	39.1	37.1	39.2	38.7	38.4
	p	kPa	101.8	101.3	102.6	101.5	100.1
	CO_2	vol%	13.4	12.2	13.2	13.0	12.0
	H_2O	vol%	6.9	6.2	6.9	6.7	6.7
Transfer CO_2		kg hr^{-1}	1.80	2.19	1.47	1.76	1.98

Table 41: Temperature profile for first MDEA campaign with 0.85 g/L CA

height	M30	M31	M32	M33	M34	M35	M36	M37	M38	M39
in	25.5	24.9	26.1	25.2	26.4	25.6	26.8	26.1	25.5	24.9
10.25									26.6	26.7
9.25									28.2	27.9
8.25							27.8	27.3	27.5	27.3
7.25							28.5	27.5	28.5	27.9
6.25					27.2	26.7	30.0	28.3	27.7	27.2
5.25					28.7	27.3	31.2	29.4	28.6	27.7
4.25			27.3	26.3	30.3	28.7	31.9	30.8	27.7	27.0
3.25			28.8	26.9	31.4	29.6	32.8	31.7	28.3	27.0
2.25	26.0	25.3	31.3	28.4	32.8	30.6	33.5	32.9	26.0	25.3
1.25	29.0	26.7	32.3	29.8	32.8	32.1	33.3	33.8	29.0	26.7
0.25	26.1	26.7	28.0	28.5	28.0	30.7	28.5	31.2	26.1	26.7
0	26.1	26.4	27.6	28.7	28.1	30.3	28.6	31.0	26.1	26.4

Table 42: Loading profile for first MDEA campaign with 0.85 g/L CA

height	M30	M31	M32	M33	M34	M35	M36	M37	M38	M39
in	0.05	0.06	0.07	0.08	0.09	0.10	0.11	0.12	0.13	0.14
9.25										
8.25							0.11	0.12		
7.25										
6.25					0.09	0.10				
5.25										
4.25			0.07	0.08						
3.25										
2.25	0.05	0.06								
1.25										
0.25										
0	0.17	0.14	0.27	0.26	0.33	0.33	0.39	0.37	0.40	0.40

Table 43: Setpoints and measured mass transfer in first MDEA campaign with 0.85 g/L CA

		Run	M30	M31	M32	M33	M34	M35	M36	M37	M38	M39
	Height	m	2.25	2.25	4.25	4.25	6.25	6.25	8.25	8.25	10.25	10.25
Liquid	Mass	kg hr^{-1}	73.3	175.4	74.9	175.3	72.4	176.5	72.7	174.2	73.7	174.7
	T	°C	25.5	24.9	26.1	25.2	26.4	25.6	26.8	26.1	27.2	26.6
	MEA	wt%	29.5	29.5	29.5	29.5	29.5	29.5	29.5	29.5	29.5	29.5
	CO_2	wt%	0.5	0.7	0.8	0.9	1.0	1.1	1.2	1.3	1.4	1.5
	Cenz	g/L	0.9	0.9	0.9	0.9	0.9	0.9	0.9	0.9	0.9	0.9
Gas	Mass	kg hr^{-1}	22.7	22.6	22.8	22.6	22.6	22.6	22.5	22.3	22.3	22.2
	T	°C	22.5	23.5	23.8	24.0	24.2	24.4	24.5	24.6	24.7	24.8
	p	kPa	99.9	99.9	100.1	99.9	100.0	99.9	100.0	100.0	99.9	99.9
	CO_2	vol%	12.8	13.0	13.8	12.8	12.9	13.0	12.8	12.3	12.5	12.3
	H_2O	vol%	2.7	2.9	2.9	3.0	3.0	3.0	3.1	3.1	3.1	3.1
Transfer CO_2		kg hr^{-1}	1.00	1.16	1.47	1.69	1.63	2.16	1.80	2.28	1.81	2.39

Table 44: Temperature profile for first MDEA campaign with 0.85 g/L CA

height	M40	M41	M42	M43	M44	M45	M46	M47	M48	M49
in	39.4	40.1	41.1	41.6	41.7	41.6	41.6	40.9	40.4	39.2
10.25									38.4	37.7
9.25									40.2	39.3
8.25							39.3	39.5	40.8	39.7
7.25							40.9	40.9	41.1	39.5
6.25					39.9	40.1	41.0	41.2	41.4	39.8
5.25					41.7	41.5	42.0	41.4	41.6	40.0
4.25			39.5	40.1	42.0	42.2	42.4	42.0	41.8	40.5
3.25			41.5	41.7	42.2	42.2	42.3	42.0	41.5	40.4
2.25	38.1	38.7	41.5	42.2	41.9	42.7	42.1	42.4	41.1	40.8
1.25	38.8	40.3	40.0	42.0	40.3	42.4	40.4	42.1	39.7	40.5
0.25	30.8	36.7	34.3	38.6	35.0	39.6	35.8	39.3	35.5	37.5
0	32.1	36.4	33.9	37.8	34.8	38.2	35.8	38.1	34.8	37.4

Table 45: Loading profile for first MDEA campaign with 0.85 g/L CA

height	M40	M41	M42	M43	M44	M45	M46	M47	M48	M49
in	0.24	0.25	0.26	0.26	0.27	0.27	0.28	0.28	0.29	0.31
9.25										
8.25							0.28	0.28		
7.25										
6.25					0.27	0.27				
5.25										
4.25			0.26	0.26						
3.25										
2.25	0.24	0.25								
1.25										
0.25										
0	0.35	0.31	0.34	0.33	0.36	0.36	0.38	0.35	0.40	0.37

Table 46: Setpoints and measured mass transfer in first MDEA campaign with 0.85 g/L CA

		Run	M40	M41	M42	M43	M44	M45	M46	M47	M48	M49
	Height	m	2.25	2.25	4.25	4.25	6.25	6.25	8.25	8.25	10.25	10.25
Liquid	Mass	kg hr^{-1}	71.4	174.8	72.9	175.3	74.2	175.7	74.6	172.7	73.2	175.7
	T	°C	39.4	40.1	41.1	41.6	41.7	41.6	41.6	40.9	40.4	39.2
	MEA	wt%	29.5	29.5	29.5	29.5	29.5	29.5	29.5	29.5	29.5	29.5
	CO_2	wt%	2.6	2.6	2.7	2.8	2.8	2.9	2.9	3.0	3.0	3.3
	Cenz	g/L	0.85	0.85	0.85	0.85	0.85	0.85	0.85	0.85	0.85	0.85
Gas	Mass	kg hr^{-1}	22.4	22.1	21.8	21.8	21.8	21.7	21.7	21.6	21.6	21.4
	T	°C	25.6	28.5	30.2	30.8	31.4	31.8	32.0	32.2	32.4	32.3
	p	kPa	100.0	100.2	100.0	100.2	99.9	100.0	100.2	100.3	100.1	100.0
	CO_2	vol%	12.6	13.3	12.0	13.0	12.5	12.9	13.4	12.9	13.1	12.6
	H_2O	vol%	3.3	3.9	4.3	4.4	4.6	4.7	4.7	4.8	4.9	4.8
Transfer CO_2		kg hr^{-1}	0.68	0.82	0.73	0.93	0.80	1.05	0.94	1.20	0.92	1.13

Table 47: Temperature profile in second MDEA campaign with 3.5 g/L CA

height	C1	C2	C3	C4	C5	C6	C7	C8
in	25.9	25.9	25.9	25.8	26.4	25.9	25.7	25.5
10.25					26.5	25.5	25.1	24.9
9.25					29.3	27.5	26.7	26.3
8.25				25.3	30.4	28.1	27.0	26.6
7.25				27.6	33.0	29.3	27.6	26.7
6.25			25.7	28.3	35.1	30.4	28.3	27.2
5.25			28.0	29.8	37.6	32.4	29.2	27.8
4.25		25.6	29.2	30.9	39.1	34.4	30.5	28.8
3.25		28.0	30.7	32.2	39.8	35.8	31.4	29.2
2.25	26.4	29.6	32.1	33.6	39.9	37.6	32.5	30.3
1.25	29.3	31.1	33.3	34.6	38.0	38.4	33.6	31.0
0.25	27.1	28.1	29.1	30.2	30.5	33.2	30.9	28.9
0	28.0	28.9	30.0	31.0	30.3	33.3	31.7	30.6

Table 48: Loading profile in second MDEA campaign with 3.5 g/L CA

height	C1	C2	C3	C4	C5	C6	C7	C8
in	0.08	0.08	0.08	0.07	0.07	0.07	0.07	0.04
9.25					0.10	0.08	0.08	
8.25				0.07	0.12	0.10	0.09	
7.25					0.16	0.12	0.10	
6.25			0.08		0.21	0.15	0.12	
5.25					0.25	0.18	0.14	
4.25		0.08			0.28	0.20	0.16	
3.25					0.30	0.22	0.18	
2.25	0.08				0.33	0.26	0.22	
1.25					0.35	0.29	0.24	
0.25					0.38	0.31	0.26	
0	0.20	0.24	0.29	0.31	0.39	0.32	0.27	0.22

Table 49: Setpoints and measured mass transfer in second MDEA campaign with 3.5 g/L CA

		Run	C1	C2	C3	C4	C5	C6	C7	C8
	Height	m	2.25	4.25	6.25	8.25	10.25	10.25	10.25	10.25
Liquid	Mass	kg hr^{-1}	122.7	124.5	126.7	126.3	72.0	126.1	176.0	122.7
	T	°C	25.9	25.9	25.9	25.8	26.4	25.9	25.7	25.9
	MEA	wt%	31.0	31.0	31.0	31.0	31.0	31.0	31.0	31.0
	CO_2	wt%	0.9	0.9	0.9	0.9	0.8	0.8	0.8	0.9
	Cenz	g/L	3.5	3.5	3.5	3.5	3.5	3.5	3.5	3.5
Gas	Mass	kg hr^{-1}	28.0	27.5	27.6	27.4	27.2	27.1	27.1	28.0
	T	°C	20.9	21.3	21.6	21.9	22.7	22.9	22.7	20.9
	p	kPa	102.8	102.4	102.9	102.6	102.8	102.1	102.4	102.8
	CO_2	vol%	15.5	12.4	13.4	12.3	12.6	11.9	11.5	15.5
	H_2O	vol%	2.4	2.5	2.5	2.6	2.7	2.7	2.7	2.4
Transfer CO_2		kg hr^{-1}	1.78	2.17	2.96	3.17	2.62	3.24	3.60	3.82

Table 50: Temperature profile in second MDEA campaign with 3.5 g/L CA

height	C9	C10	C11	C12	C13	C14	C15
in	28.7	28.7	28.7	28.7	27.7	27.6	28.0
10.25					28.3	27.4	27.1
9.25					31.0	29.2	29.0
8.25				28.1	32.1	29.8	29.4
7.25				30.1	33.9	30.8	29.8
6.25			28.5	30.7	35.1	31.9	30.4
5.25			30.3	31.7	36.2	33.3	31.2
4.25		28.2	31.5	32.6	36.7	34.6	32.1
3.25		30.5	32.3	33.3	36.8	35.3	32.6
2.25	28.8	31.9	33.5	34.3	36.7	36.4	33.6
1.25	31.1	32.5	33.8	34.3	35.2	36.2	33.8
0.25	28.6	29.6	30.5	30.9	30.1	32.3	31.5
0	28.7	29.5	30.3	30.7	29.7	31.8	31.6

Table 51: Loading profile in second MDEA campaign with 3.5 g/L CA

height	C9	C10	C11	C12	C13	C14	C15
in	0.22	0.22	0.22	0.22	0.22	0.22	0.22
9.25							
8.25				0.22			
7.25							
6.25			0.22				
5.25							
4.25		0.22					
3.25							
2.25	0.22						
1.25							
0.25							
0	0.30	0.34	0.35	0.33	0.42	0.37	0.35

Table 52: Setpoints and measured mass transfer in second MDEA campaign with 3.5 g/L CA

		Run	C9	C10	C11	C12	C13	C14	C15
	Height	m	2.25	4.25	6.25	8.25	10.25	10.25	10.25
Liquid	Mass	kg hr^{-1}	123.9	122.5	124.6	123.5	72.1	124.0	175.8
	T	°C	28.7	28.7	28.7	28.7	27.7	27.6	28.0
	MEA	wt%	31.0	31.0	31.0	31.0	31.0	31.0	31.0
	CO_2	wt%	2.5	2.5	2.5	2.5	2.5	2.5	2.5
	Cenz	g/L	3.5	3.5	3.5	3.5	3.5	3.5	3.5
Gas	Mass	kg hr^{-1}	28.0	27.6	27.5	27.6	27.7	27.4	27.4
	T	°C	22.1	22.5	23.0	23.4	24.1	24.3	24.1
	p	kPa	102.2	102.1	102.2	102.5	101.9	101.3	102.3
	CO_2	vol%	13.4	11.9	11.9	12.4	14.3	12.5	11.9
	H_2O	vol%	2.6	2.7	2.7	2.8	2.9	3.0	2.9
Transfer CO_2		kg hr^{-1}	1.21	1.60	2.06	2.34	1.99	2.43	2.77

Table 53: Temperature profile in second MDEA campaign with 3.5 g/L CA

height	C16	C17	C18	C19	C20	C21	C22
in	21.2	21.3	21.3	21.4	22.1	21.5	21.1
10.25					22.7	21.9	21.4
9.25					24.2	23.0	22.2
8.25				22.0	25.1	23.7	22.7
7.25				23.1	26.4	24.7	23.3
6.25			21.8	24.0	27.4	25.7	23.9
5.25			23.2	25.1	28.3	26.7	24.8
4.25		21.9	24.5	26.3	29.0	28.0	25.7
3.25		23.3	25.3	26.9	29.5	28.7	26.3
2.25	22.0	24.9	26.5	28.0	30.0	29.8	27.3
1.25	23.5	25.8	27.2	28.4	29.5	30.0	27.8
0.25	22.1	23.9	25.5	25.8	25.6	27.0	26.1
0	23.0	24.4	25.4	26.1	25.8	27.5	26.7

Table 54: Loading profile in second MDEA campaign with 3.5 g/L CA

height	C16	C17	C18	C19	C20	C21	C22
in	0.33	0.33	0.34	0.34	0.27	0.27	0.27
9.25							
8.25				0.34			
7.25							
6.25			0.34				
5.25							
4.25		0.33					
3.25							
2.25	0.33						
1.25							
0.25							
0	0.40	0.45	0.47	0.50	0.48	0.44	0.42

Table 55: Setpoints and measured mass transfer in second MDEA campaign with 3.5 g/L CA

		Run	C16	C17	C18	C19	C20	C21	C22
	Height	m	2.25	4.25	6.25	8.25	10.25	10.25	10.25
Liquid	Mass	kg hr^{-1}	125.9	125.1	126.0	125.4	74.4	125.8	174.9
	T	°C	21.2	21.3	21.3	21.4	22.1	21.5	21.1
	MEA	wt%	30.6	30.6	31.1	31.1	30.9	30.9	30.9
	CO_2	wt%	3.7	3.7	3.9	3.9	3.1	3.1	3.1
	Cenz	g/L	3.5	3.5	3.5	3.5	3.5	3.5	3.5
Gas	Mass	kg hr^{-1}	27.5	27.2	27.0	27.0	27.0	26.9	26.8
	T	°C	20.4	20.9	21.3	21.7	21.9	22.1	22.2
	p	kPa	102.0	102.1	102.1	102.2	102.4	102.2	102.1
	CO_2	vol%	14.1	13.7	13.6	14.1	14.6	13.6	13.2
	H_2O	vol%	2.4	2.4	2.5	2.5	2.6	2.6	2.6
Transfer CO_2		kg hr^{-1}	1.28	1.84	2.22	2.44	2.01	2.47	2.82

C: CAPCO2 Sensitivity analysis:

Table 56: Results for the sensitivity analysis

Cenz	(g/L)	**0**	**0.1**	**0.2**	**0.4**	**0.7**	**1**	**1.5**	**2.5**	**3.5**	**5**	**10**	**50**
Capture	(%)	29.4	62.8	70.9	79.0	85.0	88.2	91.2	93.8	94.8	95.4	95.7	95.8
L/G	(kg/kg)	**1**	**2**	**3**	**4**	**5**	**6**	**7**	**8**	**9**	**10**	**15**	**20**
Capture	(%)	3.8	8.5	36.3	60.4	77.6	85.1	88.2	89.8	90.8	91.5	93.0	93.6
height	m	**10**	**12**	**14**	**16**	**18**	**20**	**22**	**24**	**26**	**28**	**30**	**40**
Capture	(%)	67.3	73.7	78.7	82.7	85.8	88.2	90.1	91.6	92.7	93.5	94.2	95.5
lean loading	(mol/mol)	**0.01**	**0.04**	**0.06**	**0.1**	**0.12**	**0.14**	**0.16**	**0.2**	**0.24**	**0.3**	**0.35**	**0.4**
Capture	(%)	96.7	95.1	93.7	90.2	88.2	86.0	83.6	78.2	72.1	61.5	51.4	40.4
Temperature	(°C)	**15**	**17**	**19**	**21**	**23**	**25**	**27**	**29**	**31**	**33**	**35**	**40**
Capture	(%)	96.1	95.0	93.7	92.1	90.3	88.2	85.8	83.1	80.1	76.6	72.8	61.5
solvent conc.	wt%	**5**	**10**	**15**	**20**	**25**	**30**	**35**	**40**	**45**	**50**	**55**	**60**
Capture	(%)	38.0	75.6	96.7	95.4	92.7	88.2	81.8	73.4	63.4	52.2	40.4	28.6

Table 57: Effect of L/G ratio and column height on capture efficiencies for different enzyme concentrations (CAPCO2 sensitivty analysis)

L/G	(kg/kg)	**1**	**2**	**3**	**4**	**5**	**6**	**7**	**8**	**9**	**10**	**15**	**20**
Cenz	0 g/L	3.6	5.2	21.7	25.0	27.0	28.3	29.4	30.3	31.0	31.6	33.9	35.4
	0.5 g/L	3.8	7.9	36.6	58.5	71.6	78.0	81.5	83.6	85.0	86.0	88.7	89.8
	1 g/L	3.8	8.5	36.3	60.4	77.6	85.1	88.2	89.8	90.8	91.5	93.0	93.6
	3.5 g/L	3.8	10.0	35.6	60.4	84.4	93.7	94.8	95.1	95.3	95.4	95.6	95.7
height	(m)	**10**	**12**	**14**	**16**	**18**	**20**	**22**	**24**	**26**	**28**	**30**	**40**
Cenz	0 g/L	11.8	15.6	19.3	22.9	26.2	29.4	32.5	35.3	38.1	40.7	43.2	54.0
	0.5 g/L	57.6	64.3	69.8	74.4	78.3	81.5	84.1	86.3	88.2	89.7	90.9	94.3
	1 g/L	67.3	73.7	78.7	82.7	85.8	88.2	90.1	91.6	92.7	93.5	94.2	95.5
	3.5 g/L	83.4	87.9	90.9	92.9	94.1	94.8	95.2	95.5	95.6	95.7	95.7	95.8

D: Stripgas desorption experiments

Table 58: Experimental results from Stripgas desorption experiments with air

		Run	D1	D2	D3	D4	D5	D6	D7	D8	D9	D10	D11
	Height	m	2.25	2.25	2.25	4.25	6.25	6.25	6.25	8.25	10.25	10.25	10.25
Liquid	Mass	kg hr^{-1}	76.5	125.2	176.2	124.0	74.0	126.4	173.4	125.7	76.6	126.0	176.8
	T	°C	51.9	50.4	51.7	52.2	50.4	51.2	52.2	53.3	52.5	51.3	53.4
	MEA	wt%	30.7	30.2	30.4	30.3	30.0	30.4	30.4	30.2	30.5	30.2	30.2
	CO_2 in	(mol/mol)	0.42	0.43	0.42	0.42	0.42	0.42	0.42	0.42	0.43	0.42	0.42
	CO_2 out	(mol/mol)	0.30	0.33	0.33	0.26	0.23	0.26	0.28	0.23	0.20	0.23	0.24
	Cenz	g/L	3.5	3.5	3.5	3.5	3.5	3.5	3.5	3.5	3.5	3.5	3.5
Gas	Mass	kg hr^{-1}	9.4	9.8	9.7	9.9	9.9	9.9	9.9	10.0	10.1	10.1	10.0
	T	°C	19.9	19.7	19.5	19.4	19.2	19.1	19.0	18.9	18.9	18.9	18.9
	p	kPa	103.0	103.0	103.0	103.0	103.0	103.0	103.0	103.0	103.0	103.0	103.1
Transfer CO_2		kg hr^{-1}	1.00	1.38	1.78	2.15	1.61	2.40	2.76	2.61	1.98	2.73	3.49

Table 59: Experimental results from Stripgas desorption experiments with air

		Run	D12	D13	D14	D15	D16	D17	D18	D19	D20	D21	D22
	Height	m	2.25	2.25	2.25	4.25	6.25	6.25	6.25	8.25	10.25	10.25	10.25
Liquid	Mass	kg hr^{-1}	123.8	124.5	125.3	125.0	124.5	123.2	125.1	126.2	126.8	126.2	125.8
	T	°C	52.0	52.3	51.6	52.3	52.3	51.6	50.7	50.5	50.7	50.3	51.2
	MEA	wt%	29.3	29.2	29.3	29.4	29.7	29.4	29.4	29.4	29.4	29.4	29.4
	CO_2 in	(mol/mol)	0.42	0.41	0.42	0.42	0.40	0.41	0.43	0.42	0.42	0.42	0.41
	CO_2 out	(mol/mol)	0.32	0.30	0.31	0.26	0.26	0.24	0.25	0.24	0.26	0.23	0.22
	Cenz	g/L	3.5	3.5	3.5	3.5	3.5	3.5	3.5	3.5	3.5	3.5	3.5
Gas	Mass	kg hr^{-1}	4.9	10.8	30.9	10.1	5.1	10.0	31.2	10.0	5.1	10.1	30.7
	T	°C	20.1	20.0	19.8	19.9	20.2	20.2	20.2	20.3	20.5	20.6	20.5
	p	kPa	101.0	101.0	101.7	101.0	101.0	101.0	101.8	101.1	101.0	101.1	101.8
Transfer CO_2		kg hr^{-1}	1.30	1.49	1.50	2.07	1.97	2.24	2.45	2.45	2.08	2.52	2.66

Table 60: Experimental results from Stripgas desorption experiments with air

		Run	D23	D24	D25	D26	D27	D28	D29	D30	D31
	Height	m	2.25	2.25	2.25	2.25	4.25	4.25	4.25	6.25	6.25
Liquid	Mass	kg hr^{-1}	76.2	123.8	171.4	76.0	126.4	173.8	75.2	126.6	175.7
	T	°C	51.1	51.1	51.5	51.1	51.0	51.5	50.2	53.2	51.4
	MEA	wt%	30.6	30.6	30.6	30.7	31.0	30.7	30.9	31.1	31.0
	CO_2 in	(mol/mol)	0.47	0.46	0.45	0.46	0.44	0.43	0.43	0.41	0.39
	CO_2 out	(mol/mol)	0.44	0.45	0.43	0.40	0.41	0.38	0.36	0.35	0.35
	Cenz	g/L	0	0	0	0	0	0	0	0	0
Gas	Mass	kg hr^{-1}	10.3	10.2	10.0	10.0	9.9	9.9	10.2	10.4	10.1
	T	°C	23.1	23.3	23.5	23.6	23.8	23.8	23.8	23.8	23.8
	p	kPa	101.5	101.4	101.4	101.4	101.4	101.4	101.4	101.3	101.3
Transfer CO_2		kg hr^{-1}	0.25	0.18	0.43	0.50	0.55	1.02	0.60	0.90	0.85

Table 61: Experimental results from Stripgas desorption experiments with air

		Run	D32	D33	D34	D35	D36	D37
	Height	m	8.25	8.25	8.25	10.25	10.25	10.25
Liquid	Mass	kg hr^{-1}	74.0	125.6	175.3	75.0	125.8	174.4
	T	°C	49.3	52.3	52.5	50.3	51.9	52.3
	MEA	wt%	31.2	31.2	31.2	31.2	31.4	31.7
	CO_2 in	(mol/mol)	0.39	0.37	0.35	0.35	0.34	0.32
	CO_2 out	(mol/mol)	0.31	0.31	0.30	0.28	0.28	0.28
	Cenz	g/L	0	0	0	0	0	0
Gas	Mass	kg hr^{-1}	9.9	9.8	9.6	9.5	10.1	10.3
	T	°C	23.8	23.8	23.7	23.7	23.7	23.7
	p	kPa	101.3	101.3	101.3	101.3	101.3	101.3
Transfer CO_2		kg hr^{-1}	0.68	0.84	0.99	0.57	0.84	0.88

E: PhD Contributions

Conferences:

Maria T. Gundersen, Arne Gladis, Nicolas von Solms, John M Woodley, "Reaction enhancement of post-combustion carbon capture using carbonic anhydrase" 8th Trondheim CCS conference (TCCS-8), Trondheim, Norway, June 2015. (Oral)

Jozsef Gaspar, Arne Gladis, John B Jørgensen, Kaj Thomsen, Nicolas von Solms, Philip L Fosbøl' "Dynamic Operation and Simulation of Post-Combustion CO_2 Capture" 8th Trondheim CCS conference (TCCS-8), Trondheim, Norway, June 2015. (Oral)

Arne Gladis, Maria T Gundersen, Philip L Fosbøl, John M Woodley, Nicolas von Solms, "Carbon dioxide absorption rate intensification by carbonic anhydrase for different solvent types" 8th Trondheim CCS conference (TCCS-8), Trondheim, Norway, June 2015. (Poster)

Arne Gladis, Maria T Gundersen, Philip L Fosbøl, John M Woodley, Nicolas von Solms, "Kinetics of Carbonic Anhydrase in Promoted Chemical Solvents for Carbon Dioxide Absorption", 3rd Post-Combustion Capture Conference (PCCC3), Regina, Canada, September 2015. (Oral)

Maria T Gundersen, Arne Gladis, Nicolas von Solms, John M Woodley, "Technical evaluation of implementation of carbonic anhydrase in post-combustion carbon capture", 3rd Post-Combustion Capture Conference (PCCC3), Regina, Canada, September 2015. (Oral)

Philip L Fosbøl, Arne Gladis, Kaj Thomsen, Jozsef Gaspar; Nicolas von Solms, "Enzymes in CO_2 Capture" 3rd University of Texas Conference on Carbon Capture and Storage (UTCCS-3), Austin; USA, February 2016. (Oral)

Arne Gladis, Maria T Gundersen, Philip L Fosbøl, John M Woodley, Nicolas von Solms, "How to use carbonic anhydrase enzyme in carbon capture technology", 22nd International Congress of Chemical and Process Engineering (CHISA 2016), Prague, Czech Republic, August 2016. (Oral)

Arne Gladis, Niels F Lomholdt, Philip L Fosbøl, John M Woodley, Nicolas von Solms, "Pilot absorption experiments with carbonic anhydrase enhanced MDEA", 13th International Conference on Greenhouse Gas Control Technologies (GHGT13), Lausanne, Switzerland, November 2016. (Poster)

Philip L Fosbøl, Jozsef Gaspar, Bjartur Jacobsen, Jens Glibstrup, Arne Gladis, Kevin Milla Diaz, Kaj Thomsen, John M Woodley, Nicolas von Solms, "Design and simulation of rate-based CO2 capture processes using carbonic anhydrase (CA) applied to biogas", 13th International Conference on Greenhouse Gas Control Technologies (GHGT13), Lausanne, Switzerland, November 2016. (Poster)

Maria T Gundersen, Arne Gladis, Philip L Fosbøl Nicolas von Solms, John M Woodley, "Operating considerations of ultrafiltration in enzyme enhanced carbon capture", 13th International Conference on Greenhouse Gas Control Technologies (GHGT13), Lausanne, Switzerland, November 2016. (Poster)

Jozsef Gaspar, Arne Gladis, John M Woodley, Kaj Thomsen, Nicolas von Solms, Philip L Fosbøl, "Rate-based Modelling and Validation of a Pilot Absorber Using MDEA Enhanced with Carbonic Anhydrase (CA)" 13th International Conference on Greenhouse Gas Control Technologies (GHGT13), Lausanne, Switzerland, November 2016. (Poster)

Arne Gladis, Maria T Gundersen, Kaj Thomsen, Philip Fosbøl, John M Woodley, Nicolas von Solms, "Comparison of the kinetic promoters piperazine and carbonic anhydrase for CO_2 absorption", 13th International Conference on Greenhouse Gas Control Technologies (GHGT13), Lausanne, Switzerland, November 2016. (Oral)

Arne Gladis, Maria T Gundersen, Philip L Fosbøl, John M Woodley, Nicolas von Solms, "Carbonic Anhydrase Enhanced Carbon Capture: Kinetic Measurements and Pilot Plant Trials", 2016 AIChE Annual meeting (AIChE2016), San Francisco, USA, November 2016. (Oral)

Arne Gladis, Niels F Lomholdt, Sebastian Nelke, Philip L Fosbøl, John M Woodley, Nicolas von Solms, "Evaluation of alternative desorption process without reboiler for carbonic anhydrase enhanced MDEA", 9th Trondheim CCS conference (TCCS-9), Trondheim, Norway, June 2017. (Poster)

Articles:

Gladis, A., M.T. Gundersen, P.L. Fosbøl, J.M. Woodley, and N. von Solms. "Influence of Temperature and Solvent Concentration on the Kinetics of the Enzyme Carbonic Anhydrase in Carbon Capture Technology." Chemical Engineering Journal 309 (2017). doi:10.1016/j.cej.2016.10.056.

Gladis, Arne, Maria T Gundersen, Randi Nerup, Philip Loldrup Fosbøl, John M Woodley, and Nicolas von Solms. "CO_2 Mass Transfer Model for Carbonic Anhydrase Enhanced MDEA Solutions." Chemical Engineering Journal (Submitted) (2017).

Gladis, Arne, Maria T Gundersen, Kaj Thomsen, Philip L Fosbøl, John M Woodley, and Nicolas von Solms. "Comparison of the Kinetic Promoters Piperazine and Carbonic Anhydrase for CO2 Absorption." Energy Procedia, 2016. doi:10.1016/j.egypro.2017.03.1214.

Gladis, Arne, Niels F. Lomholdt, Philip L. Fosbøl, John M Woodley, and Nicolas von Solms. "Pilot Absorption Experiments with Carbonic Anhydrase Enhanced MDEA." Energy Procedia, 2016. doi:10.1016/j.egypro.2017.03.1278.